



Trento Institute for  
Fundamental Physics  
and Applications

# ACTIVITY REPORT 2019





## **TIFPA Activity Report 2019**



**TIFPA**  
**Activity Report 2019**



Typeset in the Bitstream Charter typeface using the  $\text{\LaTeX} 2_{\epsilon}$  document formatting system and markup language

Editor: Piero Spinnato (TIFPA)

Cover and overall graphics design: Francesca Cuicchio (Ufficio Comunicazione INFN, Rome)

First print, July 2020

Printed and bound at Rotooffset Paganella, Trento

[www.rotooffset.it](http://www.rotooffset.it)

# Contents

Foreword	1	FOOT	49
Virtual Labs	3	<b>Theoretical Physics</b>	<b>51</b>
Space Research	5	BELL	53
Sensors and Detectors	11	BIOPHYS	55
INFN Experiments	17	FBS	58
Particle Physics	19	FLAG	59
ATLAS	21	MANYBODY	61
FASE2_ATLAS	23	NEMESYS	63
Astroparticle Physics	25	TEONGRAV	65
ADHD	27	<b>Technological Research</b>	<b>67</b>
AMS	29	3D-SiAm	69
DarkSide	31	ARCADIA	70
FISH	33	ARDESIA	72
HUMOR	35	ASAP	74
LIMADOU	37	DEEP_3D	76
LISA Pathfinder and LISA	39	DRAGoN	78
Quax	41	GLARE-X	80
Virgo	43	HDM	82
Nuclear Physics	45	Isolpharm Ag	84
AEgIS	47	KIDS_RD	86
		MoVe IT	88
		Redsox2	90

<b>SiCILIA</b>	<b>92</b>	<b>FIRE</b>	<b>107</b>
<b>Simp</b>	<b>93</b>	<b>FOOT DC detector</b>	<b>109</b>
<b>THEEOM-RD</b>	<b>95</b>	<b>HERMES</b>	<b>111</b>
<b>TIMESPOT</b>	<b>97</b>	<b>LIDAL</b>	<b>113</b>
		<b>MoVeIT-TO</b>	<b>115</b>
<b>Outreach</b>	<b>99</b>	<b>MoVe IT-WP3</b>	<b>117</b>
<b>OCRA</b>	<b>101</b>	<b>SEUP</b>	<b>119</b>
		<b>SUN_MEYER</b>	<b>121</b>
<b>Proton Beam-based R&amp;D</b>	<b>103</b>	<b>TIFPA Publications</b>	<b>125</b>
<b>4DPhantom</b>	<b>105</b>	<b>Seminars</b>	<b>145</b>



# Foreword

Giuseppe Battistoni

Direttore,  
TIFPA

The 2019 Annual Report of the Trento Institute for Fundamental Physics and Applications (TIFPA), has been prepared during the unprecedented difficult situation caused by the COVID-19 pandemics. Precisely because we are living this particular moment in which we are suffering from many limitations to our scientific activity, it is indeed source of genuine satisfaction to review the large amount of scientific and technological activity that has been carried out at TIFPA in the last year.

All the partners of TIFPA, the Italian National Institute for Nuclear Physics (INFN), Trento University (UniTn), Bruno Kessler Foundation (FBK) and the Health-care Agency of Trento (APSS), are proud to have contributed to these achievements, together with all our external collaborators and users. Our hope for the future is to keep this pace in scientific production, always continuing to stimulate new ideas and projects and to improve our infrastructures. This will be possible, as in the past, thanks to the strong commitment of TIFPA partners, to the fundamental support from the government of Trento Province and to the efforts of all staff and associates.

Unfortunately, because of the overwhelming effort required to tackle the COVID-19 crisis at the Protontherapy centre, it was impossible to prepare the contribution from the Medical Technologies Virtual Lab.

Once again I wish to express my sincere gratitude all collaborators, reserving a special thanks to the administrative and technical services that were essential for all the achievements of our Center. A particular acknowledgment is due to Dr. Piero Spinnato for editing this publication.





# Virtual Labs



# Space Research

Roberto Iuppa<sup>1,2†</sup>

roberto.iuppa@unitn.it

with contributions by

Pierluigi Bellutti,<sup>3,2</sup> Chiara La Tessa,<sup>1,2</sup> William Joseph Weber<sup>1,2</sup>

Space activities always played a preminent role at TIFPA. Experiments carried out within space missions characterised activities at TIFPA since its very foundation, in 2015. Many activities at TIFPA start as developments for INFN experiments, but they often grow until becoming independent initiatives. This is the case for the development of space-compliant Monolithic Active Pixel Sensors. The last two editions of the Activity Report told us about the HEPD-02 project or the ARCADIA project. This year these activities are well described in dedicated reports (see pp. 37 and 70), demonstrating how important is the space virtual lab at TIFPA. This year, we decided to focus on new activities, leaving apart developments now described in dedicated contributions.

**HIGH-TEMPERATURE SUPERCONDUCTING MAGNETS** TIFPA collaborates with ASI, CERN and University of Trento on the HDMS project, which aims to increase the technological readiness level of High-temperature superconducting magnets for space applications. The scientific case taken as benchmark is a magnetic spectrometer to measure high-energy cosmic rays up to hundreds of TeV of energy. HDMS focuses on YBCO superconductive tapes, making it possible to operate magnets up to 40 K, avoiding complex cryogenic systems based on liquid Helium. The design of a compact high-field high-precision spectrometer was the main

responsibility of TIFPA and University of Trento, which defined the scientific requirements of the project. The second phase of the HDMS project, developed mainly by the CERN team, was the conceptual design of the magnet, accounting for all issues related to the spatialisation of the high-temperature technology. The work of the magnet lab at CERN included the design of a small scale demonstrator coil, to be manufactured in the later stage of the HDMS project and to be used as benchmark to increase the technology readiness level of superconducting magnets. The status of the HDMS project is described in Dam et al. (2020).<sup>1</sup> Fig. 1 reports a sketch of the mechanical structure of one coil of the toroidal magnet system.

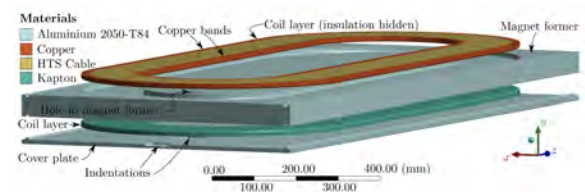


Figure 1: The mechanical structure of one coil pack of the toroidal magnet system. The insulation and cover plate are hidden for the upper part. The shapes of the coil layers are machined into the magnet former. Cover plates hold the coil layers in place. The two coil layers are electrically connected with a braided copper connector going through a hole in the magnet former. The current inlet and outlet are connected through indentations in the cover plate.<sup>1</sup>

The coil sketched in Fig. 1 can be used in a configuration like the one of Fig. 2. The magnet

<sup>2</sup>INFN TIFPA, Trento, Italy

<sup>3</sup>FBK, Trento, Italy

<sup>1</sup>Dam, M. et al. (2020), Superconductor Science and Technology **33**(4), Art. no.: 044012.

<sup>†</sup>Roberto Iuppa is warmly acknowledged for having volunteered to preparing this contribution, being the position of Space Research Virtual Lab coordinator currently vacant.

<sup>1</sup>University of Trento, Italy

features fields as high as 11 T, with an average bending strength of 3 Tm.

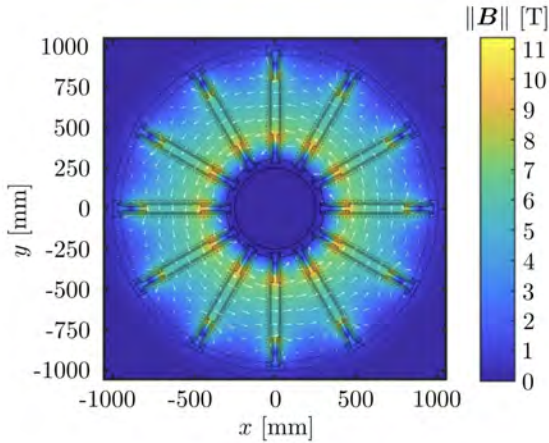


Figure 2: The boundaries of the coils and mechanical structure of the toroidal magnet system sketched on top of the magnetic field strength in the  $xy$ -plane.<sup>1</sup>

The potential impact of the high-temperature superconducting magnet technology for space applications is shown in Fig. 3, where the maximum attainable engineering current  $J_e$  is represented as a function of the effective field.

The HDMS project just entered the last phase of its program and the demonstrator coil is under construction.

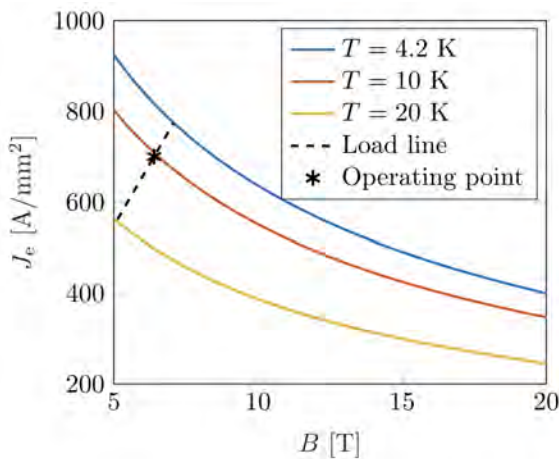


Figure 3: The engineering critical current density,  $J_e$ , as a function of the magnetic field strength at different temperatures if  $J_e = 400 \text{ A mm}^{-2}$  at 4.2K in a 20T magnetic field. This  $J_e$  is assumed as a minimum requirement for the HTS tape used for the demonstrator coil.<sup>1</sup>

**SPACE IN FBK** FBK (Fondazione Bruno Kessler) approaches space technology related

activities in the middle of the 90s with two specific developments of sensors and devices, featuring the main activity sectors of the silicon microtechnologies carried out in FBK labs: radiation sensors and MEMS (micro electromechanical systems). More precisely, the radiation sensors are large area ( $30 \text{ cm}^2$ ) double side microstrips for the AMS-02 project (from 2001 to 2003 FBK produced several hundreds of these sensors) and a microswitch (MEMS) for payload redundancy applications. The experience acquired with the AMS-02 project took FBK to produce even larger microstrip sensors (about  $100 \text{ cm}^2$ ) for the Limadou payload (CSES mission), in collaboration with TIFPA. In the following years, the space technology related activities grew slowly but constantly. Ten years after the conclusion of the AMS-02 production, among MEMS activities it is worth mentioning the development and qualification of a mass flow sensor to be used as controller of satellite thrusters, now operating on GAIA and Lisa-Pathfinder. From the radiation sensors side, relevant activities are focused on two solutions: an optical receiver for encoders and sensors for X-ray spectroscopy.

The first was developed in collaboration with a local company, Opto-I Microelectronics, starting from a device dating back to 1995 and sold on the worldwide market for industrial applications. The space compliant version was promoted by an initial direct interest of CNES, then supported by ASI and ESA, due to the absence of a European solution for such optical receivers.

The technology for X-ray sensors starts in FBK in 2010 for industrial applications. The excellent performances shown by the first devices attracts the interest of scientists of INFN and INAF eager to find specific solutions for their space (and not only) research programs. With the Silicon Drift Detector technology of FBK, the worldwide largest SDD was realized and it was the core of the experiment of the LOFT (Large Observatory For X-ray Timing) mission proposal, participating to the M3 call of ESA which went through the selection process up to the three final candidate missions. The encouraging results of the development opened

the way to another mission, now in phase B1, named eXTP (enhanced X-ray Timing and Polarimetry).

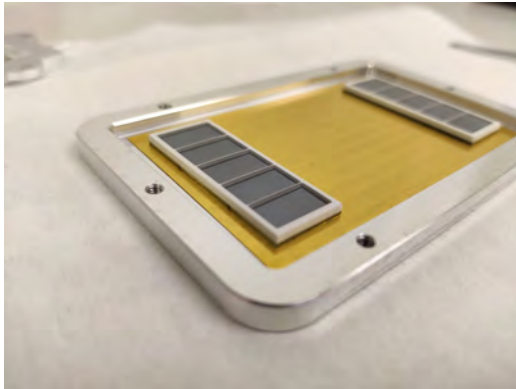


Figure 4: SDD sensors ready to be coupled with scintillators.

In the meantime, two other challenging satellite missions are taking advantage of the FBK-SDD technology. The former is a segmented SDD version as large as  $16\text{ cm}^2$ , a key component of the payload of the Theseus (Transient High-Energy Sky and Early Universe Surveyor) mission, one of the three selected by ESA for the M6 call; the latter is a smaller version of the detector to equip the Hermes-SP constellation (High Energy Rapid Modular Ensemble of Satellites, Scientific Pathfinder), an H2020 funded project. Both programs belong to the field of X ray astronomy with special focus on the study of the GRB (Gamma Ray Burst) phenomena.

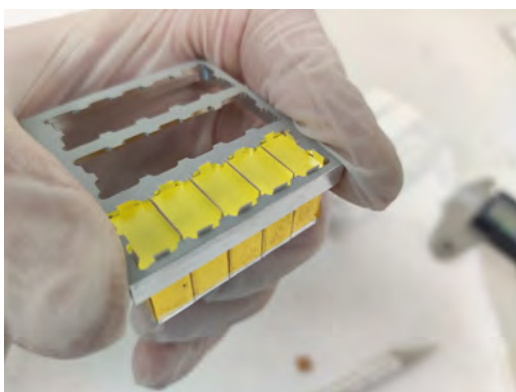


Figure 5: Integration of the scintillator wrapped with antireflective coating for Hermes Payload.

More recently, FBK started to further increase its effort in space technologies. Among the latest activities it is worth mentioning the development of components for a new generation of

optical encoders and a mini star tracker as well as the ongoing experience on payload integration (for the Hermes satellite), this last being an activity widening FBK expertise far beyond the development of components. In this way FBK follows and contributes to the expected goal of the national program named “space economy”: promoting space technologies as a driver for technological solutions and services for everyday life.

**RADIATION IN SPACE** The TIFPA-INFN experimental room situated inside the Trento Protontherapy center has been used to perform a variety of space research experiments by national and international teams. In 2016, it has been selected among the core facilities for the project “ASI supported Irradiation Facilities - ASIF”, whose goal is to create a collaboration among several Italian radiation centers. This network provides a platform for promoting space research with technological and scientific standard competitive with other European facilities. Furthermore, since 2018, the European Space Agency (ESA) has included the facility in the CORA-IBER project, financing experimental activities in different fields of space exploration.

**DEVELOPMENTS FOR THE LISA GRAVITATIONAL WAVE OBSERVATORY** In 2019, the LISA orbiting gravitational wave observatory, described at p. 39, successfully completed the midterm milestone review for the “phase A” and is on track for an early 2030’s launch as the L3 mission of ESA’s Cosmic Vision program.

The group has several key responsibilities in LISA development:

- PI for the gravitational reference sensor (GRS) that is the Italian (ASI) hardware contribution, including the test mass (TM) and surrounding hardware for electrostatic position sensing and force actuation, TM discharge, and launch lock / release
- participating in the coordination of the “Consortium” of ESA member states that will provide the metrology instrument
- providing metrology expertise in the ESA-appointed LISA “system engineering of-

“fice” that leads the mission definition and development.

The LISA “antenna” is a constellation of orbiting free-falling test masses, with a gravitational tidal acceleration resolved against a background noise of accelerations from stray forces. Achieving this constellation of geodesic reference TM is the focus of the Trento group, and the GRS – first designed and tested with LISA Pathfinder<sup>2</sup> and now under study for application in LISA – is the key hardware for this measurement science.

**GRAVITATIONAL REFERENCE SENSOR DEVELOPMENT.** The Trento group is leading development of the GRS and in general the design, performance modeling and testing for the system of LISA free-falling test masses. We briefly cite here several highlights of the work in 2019.

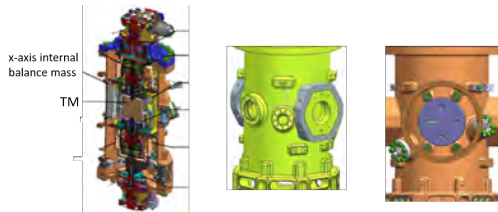


Figure 6: LISA Pathfinder GRS vacuum chamber at left, with additional y and x axis balance mass strategies external to the vacuum chamber. Illustrations courtesy of OHB-Italia.

**DC forces and spacecraft “self-gravity”** DC forces acting on the LISA test masses, largely produced by the local “self-gravity” from the distribution of mass on board the spacecraft, enter the LISA TM acceleration noise budget in various ways. This includes the force noise from the electrostatic actuation forces needed to compensate any differential DC force on the two TM inside a LISA spacecraft, by the force gradient coupling to the noisy spacecraft motion, direct gravitational fluctuations from thermal-mechanical deformation and mass loss, and by the noisy projection of DC forces onto

<sup>2</sup>Armano, M. et al. (2018), Physical Review Letters 120, Art. no.: 061101.

the inertial space axes due to spacecraft rotational noise. Gravitational balancing and high precision mass trimming, first demonstrated in LISA Pathfinder,<sup>3</sup> is needed at the level of several hundred pm/s<sup>2</sup> in LISA, with the GRS system balancing residual gravitational fields from the surrounding apparatus of up to 25-35 nm/s<sup>2</sup>. Various solutions are under study for achieving this with the required precision, minimum mass, and residual gradients.

**Vacuum and forces related to thermal and molecular impact effects** LISA relies on achieving a residual pressure of 10<sup>-6</sup> Pa around the TM to limit force noise from residual gas impacts, including equilibrium Brownian motion noise, thermally-activated pressure gradients, and possible “gas burst” events, the latter being a possible explanation for the impulse-like Poissonian “glitch” events observed in LISA Pathfinder.<sup>2</sup> Work is under way to understand the details of the gas loads inside the GRS, their possible role in non-equilibrium molecular impact forces, and the hardware and ground handling techniques necessary to limit pressure and mitigate the resulting forces in LISA.

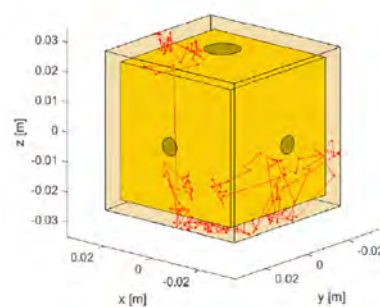


Figure 7: Molecular dynamics simulation<sup>4</sup> aimed at evaluating the compatibility of  $\Delta v \approx 10$  pm/s momentum exchange impulses with “gas bursts” from within the GRS.

**Stray electrostatic forces, TM charging and charge management** Electrostatic forces, and the interaction between stray electrostatic fields and residual TM charging from cosmic ray events, are an important source of force noise

<sup>3</sup>Armano, M. et al. (2016), Physical Review Letters 116, Art. no.: 231101.

<sup>4</sup>Rizzotti, D. (2019), Bachelor thesis.

for LISA. Discharging the TM is performed with a dedicated UV-light photoelectric discharge system, activated either periodically or continuously, to remove the roughly  $+25 e/s$  cosmic ray charging.

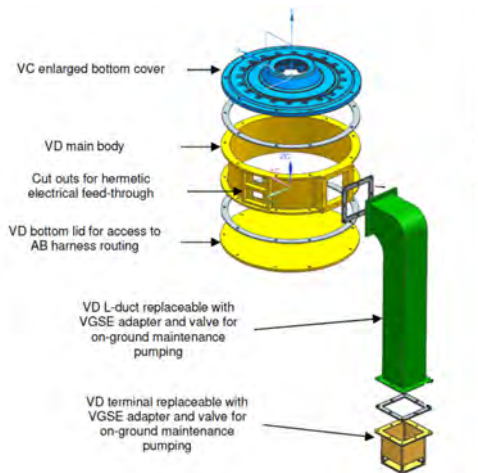


Figure 8: Possible implementation of a vent duct connecting the GRS vacuum chamber to space, with a vacuum interface for ground handling, under analysis for gas loading as well as thermal-mechanical considerations. Illustration courtesy of OHB-Italia.

Analysis and simulation of the discharge process – for the interesting physics of gold surface UV photoemission and electron motion in the complicated geometry and electrostatic field environment of the GRS, and for the resulting time evolution of the TM charge and its impact on the TM forces (see Fig. 9)– is a key activity for designing the UV light source and understanding the related surface requirements. In parallel, the group is testing the discharge system in lab with representative GRS hardware,

as part of an extensive torsion pendulum test campaign sponsored by the INFN (see p. 39).

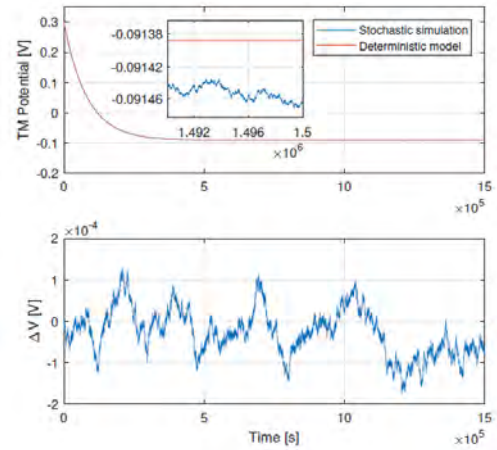


Figure 9: Simulation of TM charge evolution, both deterministic and – in zoom on fluctuations in the bottom figure – stochastic for a LISA TM in the presence of both UV photoelectric processes and cosmic ray charging.

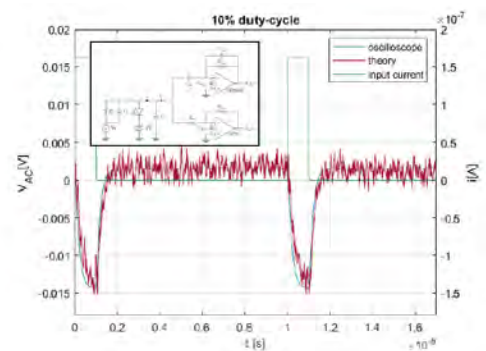


Figure 10: Illustration of the 100 kHz pulsed LED technique envisioned for UV discharge in LISA, with a measurement employing a fast photodiode readout.<sup>5</sup>

<sup>5</sup>Zavarise, M. (2019), Bachelor thesis.



# Sensors and Detectors

Maurizio Boscardin<sup>1,2</sup>  
boscardi@fbk.eu

The TIFPA Virtual Lab for Sensors and Detectors is a sum of skills and facilities focused on the realization of silicon radiation particles detectors that have their applications in different contexts such as high energy physics both in-ground facility and in space experiments than in biology and medicine.

In these contexts, the virtual laboratory of TIFPA aims to build a large technological platform that makes available to the Italian and international scientific community a set of skills and infrastructures that allow the development of silicon sensors. The presence in the same Institute of researchers that deal with detectors with the capability to realize silicon devices for various fields of application allows to be innovative and to be able to respond quickly to the technological challenges that the research activity requires.

The main contributions to the Virtual Lab for Sensors and Detectors are given by the Center for Materials and Microsystems (CMM) of FBK, the Department of Industrial Engineering of the University of Trento and TIFPA. These groups provide the Virtual Lab more than 20 years experience in the development of radiation sensors exploiting the microelectronics technology.

The key to the success of the laboratory is the presence inside FBK of a large technological facility that adds two main infrastructures:

- More than 500 mq of clean room fully equipped to process silicon devices
- a microanalysis capability based on the

availability of various physical/chemistry characterization technologies.

Whereby the Virtual Lab thanks to the presence of an internal silicon foundry combined with the use of external state-of-the-art CMOS foundries, has the capability to simulate, design, produce and test semiconductor sensors. The operating model, therefore, allows the access to a large number of competencies/technologies that allow both to develop new devices but also to realize a pre-production of custom devices. The technologies/skills available are described in the following sections.

**Simulation and design** In case of full-custom technology, we start from physics-based TCAD simulation of the device. It is possible to evaluate numerically both the electrical parameters inside the device and the measurable quantities at the electrodes. The device can also be stimulated with light or ionizing particles to model the induced electrical signal. Furthermore, to emulate as close as possible a real device, we simulate also the fabrication technology. The tools used are commercial ones (SILVACO or SENTAURUS). This software can be used both to predict the functioning of a device as well as to understand anomalous behavior or failures of existing ones. The output of the simulations is used to design the geometry of all the sensor components (layers) with the proper CAD software and to define the technology process flow. Geometry and process sequence are used

<sup>1</sup>FBK, Trento, Italy

<sup>2</sup>INFN TIFPA, Trento, Italy

to build the device(s) on the silicon wafers in the internal foundry.

In case of the standard CMOS approach, usually, there is limited access to fabrication technology. So our competencies are mainly on circuit simulations and Integrated Circuit (IC) design. We have dedicated software tools to this purpose: CADENCE and MENTOR GRAPHICS. We design both analog and digital architectures. Quite important in this case is the capability of firmware design based on FPGA to control and read the ASIC.



Figure 1: In line inspection area.

**FBK technological Facility** The Microfabrication Area runs two separate cleanrooms that process 6-inch wafers: the Detector Cleanroom (500m<sup>2</sup> ISO 3-4 class) dedicated to the development of radiation sensors and the MEMS cleanroom (100m<sup>2</sup> ISO 4-5 class) where microdevices and sensors for different applications are developed. The Detectors cleanroom is a fully equipped CMOS like pilot line with lithographic capabilities down to a few hundred nanometers with a rather strict list of materials to be processed to avoid cross-contamination. The MEMS cleanroom a much more flexible laboratory devoted to the development of devices where the integration of different materials with silicon is needed. Strategic, in the sensor field, is the capability to perform low leakage and double-side processing.



Figure 2: Litho area.

Main equipment include:

- Ion implanter Varian Exitron 220, with energy range up to 200 KeV; Ions As75, B11, 49, P31, N, Ar40
- Deep reactive ion etching Alcatel AMS200 for silicon deep etching based on Bosch process
- Plasma etching of silicon oxide, silicon nitride, polysilicon dry and metal.
- Magnetron sputter (Eclipse MRC Mark II) for Al, AlSi1%, Ti/TiN deposition
- Stepper Nikon with a resolution of 350nm
- Mask aligner Karl Suss with backside alignment (2.5  $\mu$ m resolution)
- PECVD system (STS - MPS CVD) for deposition of Si Oxide, Si Nitride, SiON, Si-rich Oxide and Amorphous Si
- 5 Atmospheric Furnaces Centrotherm for dry and wet oxidation, N<sub>2</sub> annealing, doping from BBr<sub>3</sub> or POCl<sub>3</sub> and H<sub>2</sub> alloying/sintering
- 3 LPCV furnaces Centrotherm for TEOS doped and undoped, SiN standard and low stress - SiN, PolySi doped and undoped deposition.
- Isotropic silicon wet etching based on TMAH Bulk Si Wet
- Wet bench for wet etch process
- Wafer bonding AML for anodic and adhesive bonding
- Metrology in line: Interferometer, mechanical and optical profilometer, 4 point probe, Lifetime Sinton system, ellipsometer, SEM.

The packaging lab has been recently upgraded to a clean environment. It is dedicated to the development of prototype packages for mounting the silicon devices. It is equipped with ball and wedge wire bonders, die bonder, stencil screen printer, and tools necessary for encapsulation in resins and hermetic packaging.



Figure 3: Wet etching area.

**Device Characterization** Finally, there is a transversal know-how on device characterization. This includes competencies in parametric testing which is usually done at the wafer level contacting it with probes. It is mostly used to evaluate the functionality of the device measuring current and impedance. The testing labs are divided in wafer-level parametric testing and functional characterization. The first consists of 2 manual and 4 automatic probe-stations. The automatic ones allow a full wafer characterization to identify functional devices and to monitor the uniformity of electrical parameters. Two of that feature also a temperature-controlled chuck that allows setting the wafer temperature from  $-40$  to  $100$  °C.

The functional testing laboratories are equipped with state-of-the-art instrumentation for a variety of characterizations. In particular: the electro-optical testing, that includes measurement of sensor efficiency/noise in the controlled environment and of time-of-flight with fast lasers and a test with radioactive sources. It includes coupling the photosensor with scintillators to measure energy and timing resolution in case of X-ray/Gamma radiation. Main

instruments are : multi-channel semiconductor analyzers; high-speed, four-channel digitizing oscilloscopes (600 MHz - 2.5 GHz; up to 40 GS/s); 3 PC-controlled thermostatic chambers; cooled CCD cameras for emission microscopy; fast lasers for time-of-flight measurements; integrating sphere and optical bench; pyroelectric detector; THz kit with drive synthesizer; radioactive sources of different energies; digital pattern generator; logic and network analyser and NI acquisition boards.

In addition, a range of skills and equipment are available within the FBK facility for the physical-chemical characterization of materials, techniques that allow an in-depth analysis on technological aspects of the devices created, such as the possibility of measuring doping profiles using SIMS techniques. The techniques available include Secondary Ion Mass spectrometry (SIMS), Proton Transfer Mass Spectrometry (PTRMS), X-Ray Fluorescence (XRF), X-ray Diffraction (XRD), X-Ray Photoelectron spectroscopy (XPS), Scanning Electron Microscopy (SEM) with Energy Dispersive Spectroscopy (EDS) and Electron Back Scatter Diffraction (EBSD), Scanning Probe Microscopy (SPM) with Atomic Force Microscopy (AFM), Scanning Spreading Resistance Microscopy (SSRM), Kelvin Probe Force Microscopy (KPFM), Scanning Capacitance Microscopy (SCM).



Figure 4: PE-CVD equipment.



Figure 5: Testing area

Within the virtual lab, a series of technological platforms have been developed that have allowed the realization of detectors for various applications/experiments. The main available technologies are described below.

**Low-Gain Avalanche Diodes and Ultra-Fast Silicon Detectors** Low gain avalanche diodes (LGADs) are a particular type of silicon detectors characterized by an internal structure engineered to linearly multiply the charge generated by ionizing radiation. Usually, these detectors are designed to provide a low, controlled gain in the order of  $\sim 10$ . This low gain differentiates them from standard APDS, which have a gain several order of magnitude higher, and is beneficial in several applications in which electronic noise from front-end electronics is not negligible, since it makes possible to increase the signal-to-noise ratio (SNR) without introducing significant shot-noise. A particular type of LGADs are the ultra-fast silicon detectors (UFSDs), which are LGADs specifically developed for timing applications in high-energy physics experiments, such as the end-cap timing layer in CMS and ATLAS experiments. Over the last few years, Fondazione Bruno Kessler, in col-

laboration with the universities of Trento and Turin, have been involved in developing an internal and original UFSD technology.

The first production batch (completed in 2016) was fabricated on  $275\ \mu\text{m}$  thick Silicon substrates. It was aimed at testing both the functionality and the reliability of the new proposed fabrication technology, showing excellent results in terms of gain and timing resolution.

A second pilot batch (completed in late spring 2017) was produced on Silicon-on-Silicon wafers with an active thickness of  $50\ \mu\text{m}$ , in order to improve the timing performance. In this production, new techniques to improve the radiation hardness of the devices were also tested. Two different dopant elements (Boron and Gallium) were used to realize the multiplication junction, as well as carbon co-implant was introduced on some wafers. The measurements obtained on irradiated samples demonstrated very promising, which showed the possibility to use such detectors for equivalent doses beyond the  $10^{15}\ \text{n}_{\text{eq}}/\text{cm}^2$ .

A third batch (completed in summer 2018) was then produced on Silicon-on-Silicon and epitaxial wafers: this batch was dedicated to optimize the carbon co-implantation technique to further improve the radiation hardness and to demonstrate the capability of producing large-area detectors using stepper lithography, which makes possible to reduce the dimension of the inter-pixel dead-border regions. The sensors produced in this batch demonstrated the capability of FBK to produce sensors that can achieve the timing performance and the radiation hardness required for CMS and ATLAS applications. Further batches have been made in 2019 and are currently under production in order to define a stable production technology and to experiment some additional improvements, especially to further increase the radiation hardness.

Besides the final optimization of the UFSD technology dedicated to the next upgrade of CMS and ATLAS timing layer, FBK is also now working on new LGAD and UFSD technologies which can combine fast timing and radiation-

hardness with reduced dead-borders, in order to produce LGADs with high granularity. Such technologies would make possible to develop 4-D tracking detectors, which could provide both accurate positioning and timing information in high-energy physics experiments.

Currently, two different technologies are under development: the first one, called Resistive Silicon Detectors (RSD), is based on an unsegmented multiplication structures in which the signal readout is obtained with AC coupled metal pads d,e. The second one, instead, uses deep trench isolation to provide electrical isolation between pixels. For both these technologies, test batches had been produced in 2019 and they both showed promising results in terms of dead-border reduction. Further developments are expected in 2020.

**Silicon Drift Detectors** The Silicon Drift Detectors (SDD) are currently mainly used for X-ray spectroscopy, thanks to the outstanding energy resolution that they can achieve.

The most common application for SDD is in the field of analytical instrumentation, where they are employed in many different techniques such as X-ray fluorescence (XRF) analysis, energy dispersive x-ray spectroscopy (EDS) combined with electron microscopy, x-ray reflectivity (XRR), etc. Besides these applications, SDDs are also used for x-ray spectroscopy in astrophysics experiments and particle physics experiments and they are also considered as photosensors for scintillation detectors in gamma-ray spectroscopy, thanks to their high quantum efficiency for visible light. By dealing with this kind of detectors, FBK has developed the following internal technologies:

- realization of devices with a really low leakage current, in order to achieve the best energy resolutions and to reduce the requirements for the sensor cooling.
- process to obtain a thin entrance window, which makes possible to extend the SDD energy detection range to low energy X-rays (few hundreds of eV).
- adaptation of the SDD technology to many different applications, creating sen-

- sors with dedicated layouts and geometries, also including monolithic arrays;
- producing the largest SDD sensor ever made, with an active area of  $\sim 1 \times 7 \text{ cm}^2$  for astrophysics applications;
- developing custom multi-pixel detectors, which are of the utmost importance to cover large areas in high-count-rate experiments at high luminosity facilities such as synchrotrons and x-ray free electron lasers (XFELs).

The most recent developments include:

- extensive characterization of the SDD-based ARDESIA detector system developed in the previous years at two different synchrotron beamlines, with state-of-the-art performances in terms of energy resolution and counting rates (Hafizh et al. 2019b);
- design and realization of the first prototypes of SDD arrays targeted at the THESEUS and HERMES (F. Fuschino et al. 2019b) space experiments;
- first spectroscopic results from SDDs realized on thicker substrates, showing good energy resolution and enhanced efficiency at higher X-ray energies;
- preliminary spectroscopic characterization of the low-leakage version of the large area SDD sensor;
- realization of SDD prototypes with a protective layer on the SDD entrance window to improve the reliability of the coupling with scintillator crystals without deteriorating the system performances in terms of electronic noise.

**Si-3D and Active Edge** First introduced by Sherwood Parker in 1997, 3D silicon detectors consist of an array of columnar electrodes of both doping types, oriented perpendicularly to the wafer surface and penetrating entirely through the substrate. This unique structure enables to decouple the active sensor thickness from the electrode distance, offering important advantages in terms of low operation voltage, fast time response and high radiation tolerance. Additionally, 3D technology allows for “active

edges”, i.e., deep trenches heavily doped to act as ohmic terminations of the sensors, able to reduce the insensitive edge region to a few micrometers. Obviously this is gained at the expense of a complex and expensive technology, due to the use of several non standard techniques, such as Wafer Bonding (WB) and Deep Reactive Ion Etching (DRIE).

The first Si-3D technology developed in FBK is a two-sided process, where the junction columns are engraved from the front side, the ohmic columns from the back side, without the presence of a wafer support. The columns are completely passing through the thickness of the wafer. We used this approach in the production of sensors for ATLAS IBL. In terms of functional characteristics, remarkable performance has been demonstrated for IBL 3D sensors: in particular, they have demonstrated a reconstruction efficiency of  $>98\%$  for  $15^\circ$  slopes inclined to 160 V bias after  $5 \times 10^{15} n_{eq}/cm^2$ .

As an alternative, a single-sided 3D technology with handle wafer has been proposed by FBK with modifications allowing for back-side sensor bias. The wafers is composed by two parts: a device layer of high quality and High resistivity silicon and a support wafers with low resistivity material.

The ohmic columns are etched deep enough to reach the highly doped handle wafer, so that a good ohmic contact is achieved on the sensor

back-side and the junction column has a lower depth than the thickness of the device layer.

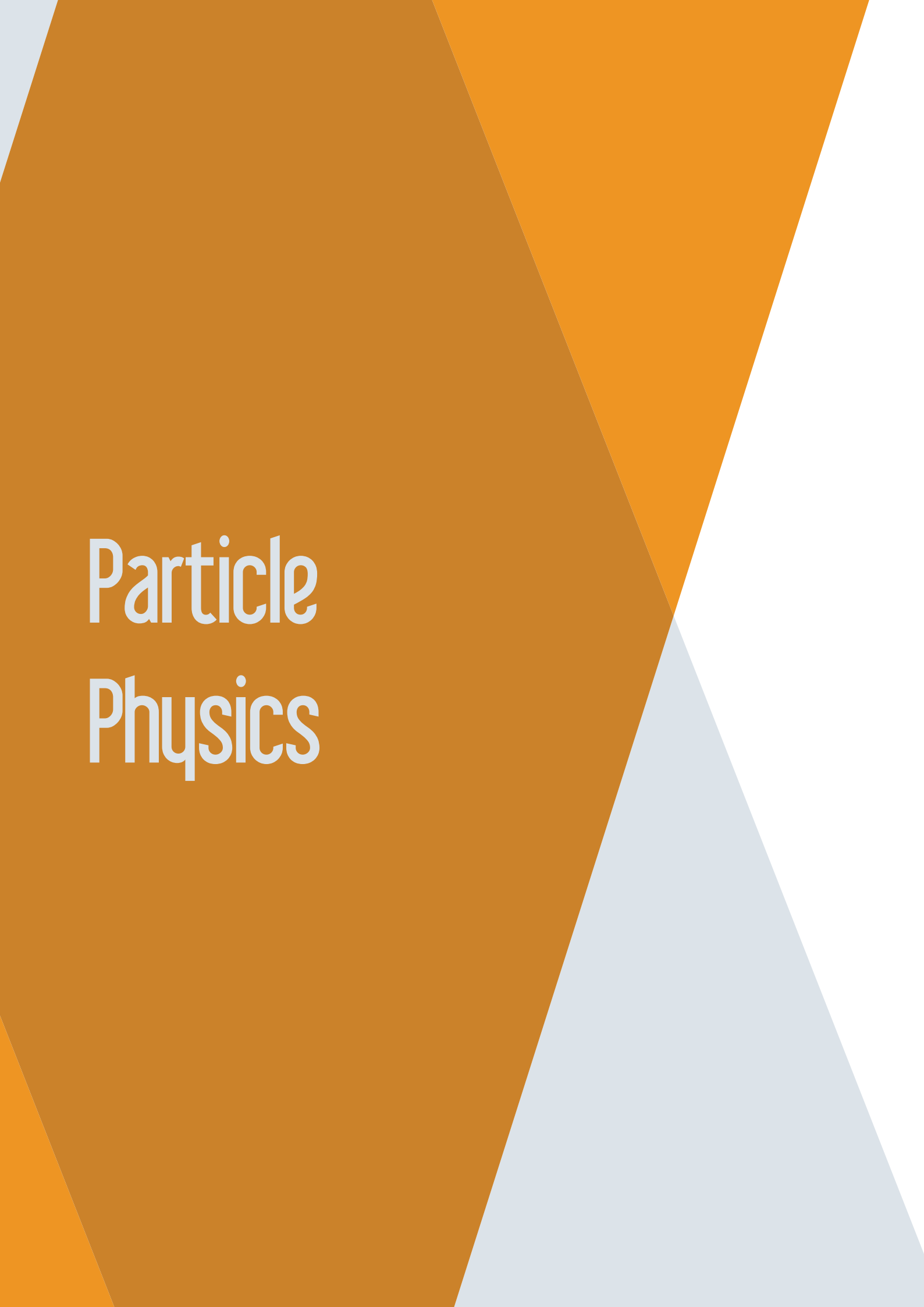
FBK also demonstrated the feasibility of this technology with Silicon on Insulator (SOI) wafers: to this purpose, it was proved that the p+ columns can be etched by DRIE also through the bonding oxide, thus reaching the heavily doped handle wafer. Among the advantages offered by the single-sided solutions are the mechanical robustness provided by the thick handle wafer, which is also compatible with active edges; moreover, the active layer thickness can be tailored to the desired value. With a thin active layer ( $\sim 100 \mu m$ ), narrow columns can be etched even though the aspect ratio is not improved, and all the device dimensions can be more easily downscaled.

FBK is also involved in TIMESLOT INFN project that has the aim to develop silicon 3D sensors with geometries optimized for high time resolution. The final detectors must have a time resolution in the order of 10 ps and suitable to be used in very harsh radiation environments (up to  $10^{17}$  1 MeV neutron-equivalent per  $cm^2$ ).

The Si-3D technology is be used also to increase the detector geometrical efficiency, by reducing as much as possible the dead area at the border. In FBK has been optimized a technique based on the realization of a deep-trench, filled by polysilicon as edge of the sensors.

# INFN Experiments





# Particle Physics



# ATLAS

Marco Cristoforetti, Andrea Di Luca, Francesco Maria Follega, Gian-Franco Dalla Betta, Roberto Iuppa<sup>†</sup>

In 2019 the ATLAS group at TIFPA continued to progress on the application of automatic learning strategies to the analysis of LHC collision data. We consolidated our expertise on flavour tagging and used it to study the  $J(b\bar{b})J$  event topology, i.e. collisions where two recoiling large-radius jets are produced, one of which containing a pair of small-radius  $b$ -jets.

**Flavour tagging.** The identification of jets containing a  $b$  or  $c$  hadron, typically referred to as  $b$ - and  $c$ -tagging respectively, plays a vital role for the ATLAS experiment. It is important for Standard Model measurements as well as for exploring new physics scenarios. The identification of  $b$ -quark jets in ATLAS is based on several low-level  $b$ -tagging algorithms that exploit complementary information from charged particle tracks reconstructed in the inner detector and muon system. This information is then combined by a high-level  $b$ -tagging algorithm into a single discriminant, which is used in physics analyses to identify the flavour of a jet.<sup>1</sup>

New high-level taggers based on Deep Neural Networks have been introduced recently. They are grouped within the DL1 algorithm, that the group at TIFPA contributed to validate with particular attention on jet-feature selections and performance reproducibility. The group evaluated the impact of the reduction of the number of jet features given as input to DL1. It was found that some impact parameter-based taggers are redundant and can be removed without affecting the performance of flavour tagging. The validation of DL1 within the analysis pipeline of the experiment made it also necessary to develop a new platform for quick comparison between data and Monte Carlo input of the taggers. In this context the group developed

<sup>†</sup>Contact Author: roberto.iuppa@unitn.it

a framework to quantify and possibly reduce systematic uncertainties associated to the training of taggers. Since the very design stage, the framework has been integrated in the infrastructure used for calibration. The tool allows to cross-check and assess mismodelling in new taggers *without* running the full data-derivation chain needed for calibration.

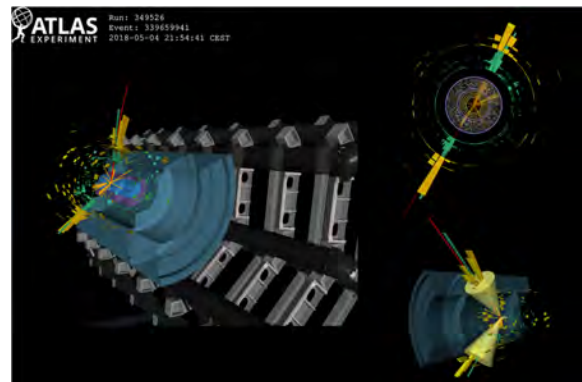


Figure 1: Display of a  $Z^0$ +jet event (2018). On the right the radial (top) and the longitudinal (bottom) views are shown. The green/yellow rectangles represent the energy deposits in the electromagnetic/hadronic calorimeter, while the red line indicates the flight direction of a muon.

**$pp \rightarrow J(b\bar{b})J$  analysis.** The search for events where two large-R jets  $J$  recoil against each other is particularly important at the LHC, as large-R jets likely come from collision products with high  $p_T$  and consequently large boost factors. In such a context, if one of the large-R jets contains a pair of small-R  $b$ -tagged jets, it is a good candidate to be a  $Z^0$  boson, a Higgs boson or an exotic particle. The last two cases are both sensitive to new Physics, the Higgs one because of possible contributions from hidden sectors to the production cross section at high- $p_T$  (ATLAS Collaboration 2019). A collision recorded

<sup>1</sup>ATLAS Collaboration (2017), ATL-PHYS-PUB-2017-013, <https://cds.cern.ch/record/2273281> tech. rep.

with the ATLAS detector showing the  $Z^0$  boson decaying to  $b$ -quarks, is shown in Fig. 1.

Data collected by the ATLAS and CMS experiments in 2015-2018 constitute the largest high-energy physics dataset ever existed, approximately 140/fb. Such an increase of statistics made it worth to repeat most analyses conducted so far, exploiting the occasion to increase also the sensitivity. The ATLAS group at TIFPA greatly contributed to the search for boosted Higgs decaying to  $b$ -quarks, produced in association with a large- $R$  jet. The upgrades of the analysis mostly targeted the increase of the signal acceptance, by introducing:

- *the use new triggers with a mass cut on the large- $R$  jet.* This additional requirement on the jet substructure allows to relax the cut on the reconstructed large- $R$  jet  $p_T$  and to lower the previous  $p_T$  threshold from 480 to 450 GeV ( $2\times$  gain in acceptance);
- *the inclusion of the second highest  $p_T$  jet in the event.* The event selection and cate-

- gorisation have been modified to take in account this case, since there is no *a priori* reason to have the Higgs boson to be the highest  $p_T$  object in the event;
- *suitable corrections for muons inside the jet.* We take into account the energy carried away by the muon when the  $b$ -quark decays semileptonically. This correction provides up to 10% improvement to the Higgs mass resolution.

The other improvement that the ATLAS group at TIFPA introduced in the analysis regarded the modelling of the multi-jet background. Since Monte Carlo simulations are not sufficiently accurate in reproducing QCD collisions, a functional form was tuned to data to model the QCD contribution to the selected dataset. This modelling has been validated on a dataset built on purpose, deigned not to contain Higgs bosons, but enriched of vector bosons. As shown in Fig. 2 the agreement of the of the prediction with data is good in both the validation region and the signal region.

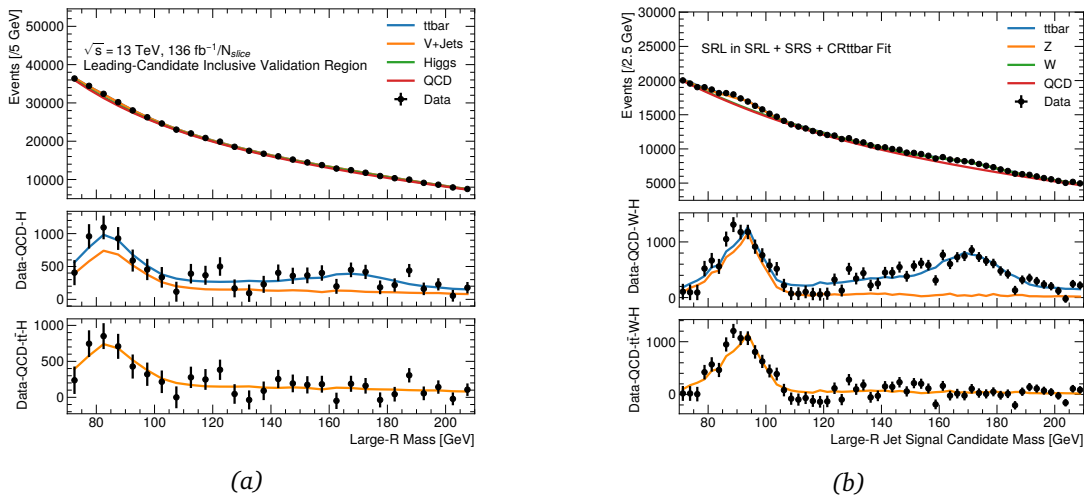


Figure 2: Post-fit plot for a validation region (a) and signal region (b) data slice analysed with a complete fit model. The Higgs candidate is associated to the leading jet in  $p_T$  ordering. In the right plot the expected Higgs boson contribution has been subtracted not to unblind the analysis.

## Selected Papers

ATLAS Collaboration (2019). *Search for light resonances decaying to boosted quark pairs and produced in association with a photon or a jet in proton-proton collisions at  $\sqrt{13}$  TeV with the ATLAS detector.* Physics Letters B **788**, pp. 316–335.

# FASE2\_ATLAS

Gian-Franco Dalla Betta,<sup>†</sup> Giacomo Baldi, Maurizio Boscardin, Francesco Ficorella, Roberto Iuppa, David Macii, Roberto Mendicino, Giulio Monaco, Neha Neha, Giovanni Paternoster, Sabina Ronchin, Giovanni Verzellesi, Nicola Zorzi

The project is aimed at completing the R&D activities previously started in the RD-FASE2 project, with a more focused approach aimed at solving some specific remaining issues in view of the construction of the new ATLAS detector for High-Luminosity LHC.

Within the Inner Tracker sub-project (ITk), TIFPA is responsible for the development and optimisation of 3D pixel sensors for the innermost layer. This application requires very high hit-rate capabilities, increased pixel granularity (e.g.,  $50 \times 50$  or  $25 \times 100 \mu\text{m}^2$  pixel size) and extreme radiation hardness (up to  $2 \times 10^{16} n_{eq} \text{cm}^{-2}$  fluence). New 3D sensors are made at FBK with a single-sided process with thin active regions ( $150 \mu\text{m}$ ), narrow columnar electrodes ( $\sim 5 \mu\text{m}$ ) with reduced inter-electrode spacing ( $\sim 30 \mu\text{m}$ ), and very slim edges ( $\sim 100 \mu\text{m}$ ).

In 2019, the focus of the activity was twofold: on one hand, the characterization of modules from sensors belonging to the second batch continued, including beam tests on irradiated samples. On the other hand, the third batch of sensors was fabricated at FBK using the stepper lithography for the first time. The main results of both these activities are summarized in the following.

Selected RD53A modules were irradiated with protons up to a fluence of  $1 \times 10^{16} n_{eq} \text{cm}^{-2}$ , and measured in a beam test (Meschini et al. 2019a). The hit efficiency with perpendicular incident particles was found to be about 97% for both the  $50 \times 50$  and  $25 \times 100$  -1E pixel layouts (see Fig. 1). Similar results were obtained from other modules tested at DESY, and comparable to those previously obtained from small-pitch 3D modules based on the FEI4 readout chip (Oide et al. 2019b).

<sup>†</sup>Contact Author: gianfranco.dallabetta@unitn.it

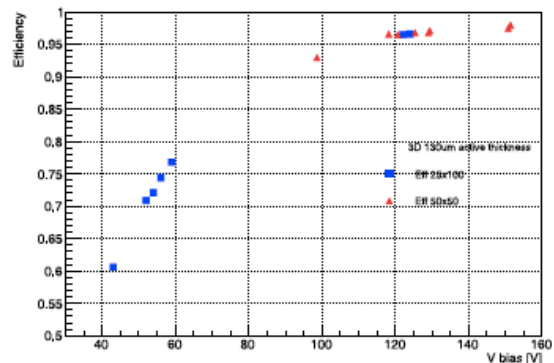


Figure 1: Hit detection efficiency as a function of the bias voltage for irradiated 3D sensors up to a fluence of  $1 \times 10^{16} n_{eq} \text{cm}^{-2}$  for  $50 \times 50$  (red triangles) and  $25 \times 100$  -1E (blue squares), with perpendicular incident particles.

After the fabrication of the second batch, the technology was revised in order to improve the yield, especially for the  $25 \times 100 \mu\text{m}^2$  -2E layout (i.e., with two read-out electrodes). In particular, for lithography, it was decided to pass from the mask aligner to the stepper, so as to better control the small feature sizes and have a higher alignment accuracy. As can be appreciated in Fig. 2, the very small distance

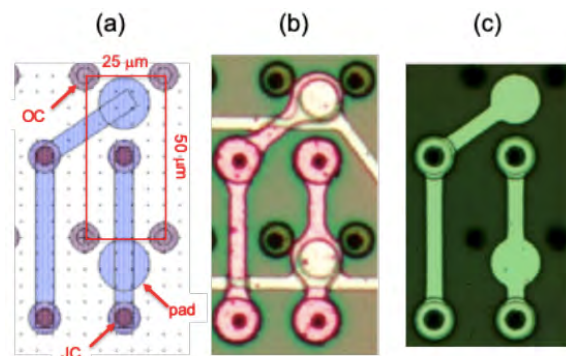


Figure 2: (a) Layout detail of a  $25 \mu\text{m} \times 100 \mu\text{m}$  -2E 3D pixel and corresponding micrographs of this pixel fabricated at FBK with (b) mask aligner, and (c) stepper lithography.

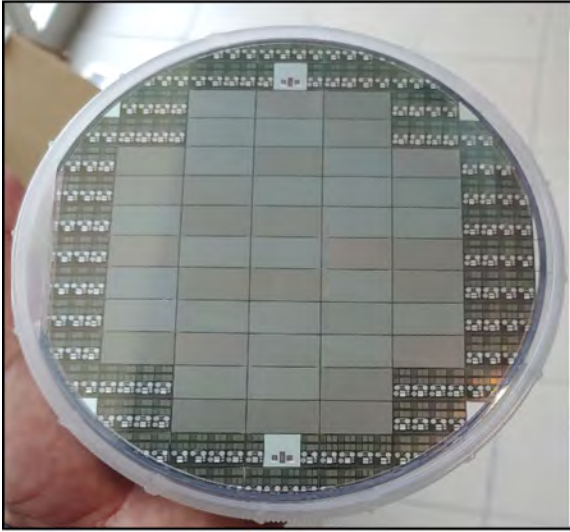


Figure 3: Photograph of a wafer from batch 3 fabricated with stepper lithography.

between the pads and the ohmic columns (OC) in the layout cannot be preserved by mask aligner lithography, whereas a much better control is achieved by stepper lithography.

The wafer layout of the third batch was designed to comprise 47 sensors compatible with the RD53A readout chip with different pixel versions, including  $50 \times 50$  and  $25 \times 100 \mu\text{m}^2$  (both 1E and 2E), and test structures at the periphery (see Fig. 3). Despite some problems occurred during the process, the batch was completed in July 2019.

From the electrical tests carried out at wafer level using the temporary metal, it was possi-

ble to appreciate the good quality of the sensors. As an example, Fig. 4 shows the I-V plots of all sensors from wafer 38. It can be seen that most sensors are working with low leakage currents and breakdown voltage larger than 50 V (the maximum bias applied).

Based on the electrical characterisation results, the four best wafers were sent for bump bonding to IZM and Leonardo. Several pixel modules were assembled with RD53A read-out chips, and tested in laboratory and in beam tests at DESY and Fermilab. Preliminary results confirm the high hit efficiency obtained from sensors of previous batches up to  $1 \times 10^{16} \text{ n}_{eq} \text{ cm}^{-2}$ . An irradiation campaign to larger fluences is under way to qualify the sensors for the ITk maximum fluence of  $2 \times 10^{16} \text{ n}_{eq} \text{ cm}^{-2}$ .

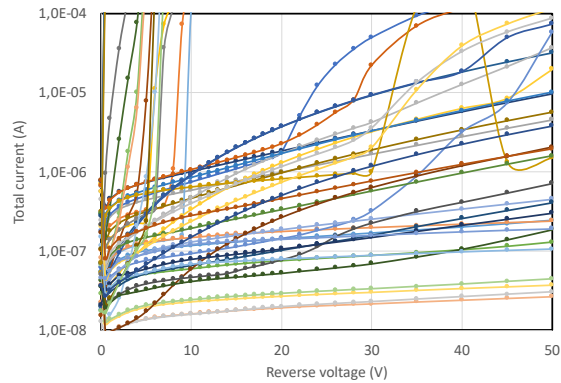
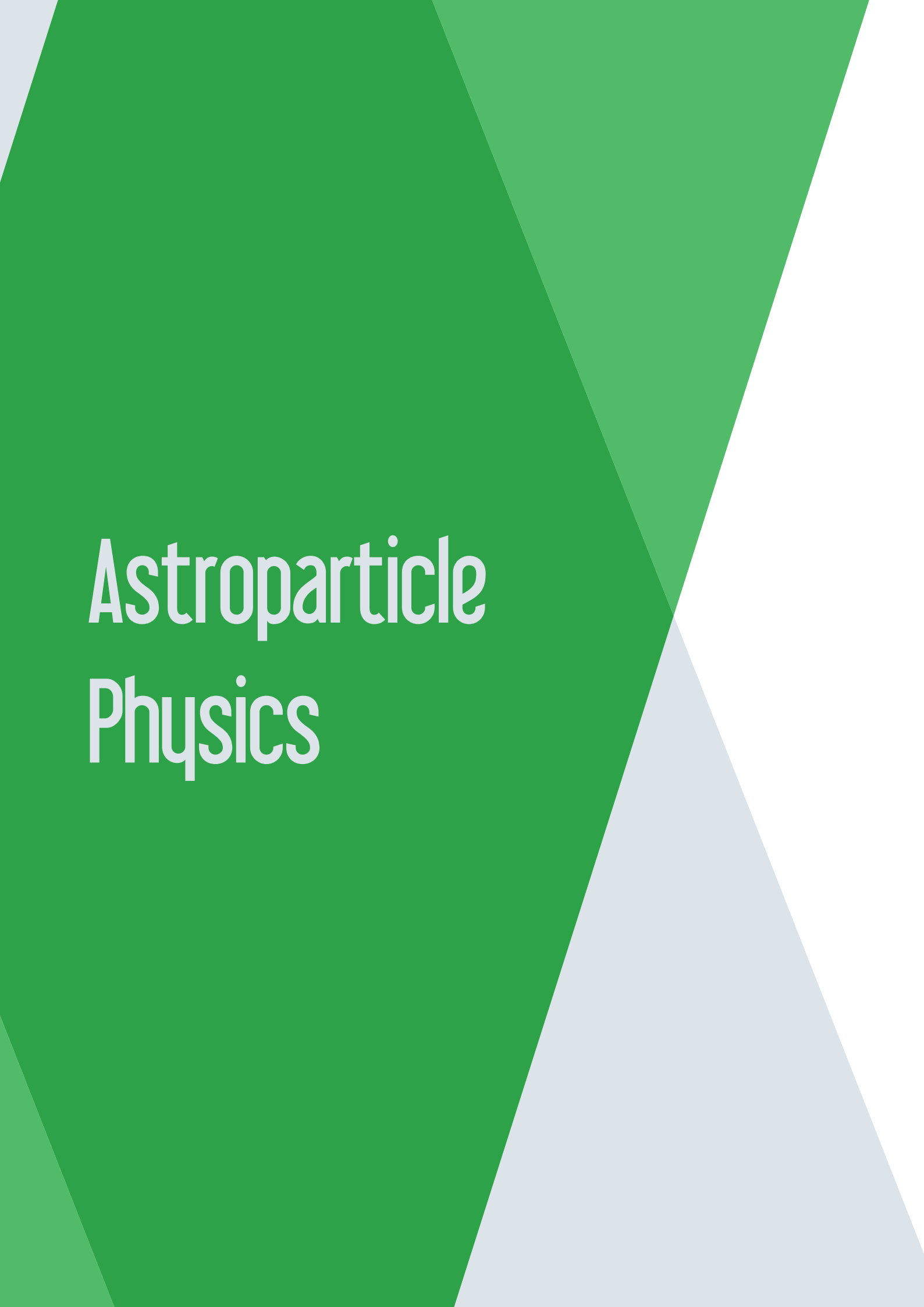


Figure 4: I-V curves of all RD53A sensors from wafer 38 of batch 3.

## Selected Papers

- Meschini, M., Ceccarelli, R., Dinardo, M., Gennai, S., Moroni, L., Zuolo, D., Demaria, L., Monteil, E., Gaioni, L., Messineo, A., Curràs, E., Duarte, J., Fernández, F., Gómez, G., Garía, A., González, J., Silva, E., Vila, I., Dalla Betta, G.-F., Mendicino, R., and Boscardin, M. (2019a). *First results on 3D pixel sensors interconnected to the RD53A readout chip after irradiation to  $1 \times 10^{16} \text{ n}_{eq} \text{ cm}^{-2}$* . *Journal Instrum.* **14**. Art. no.: C06018.
- Oide, H., Alimonti, G., Boscardin, M., Dalla Betta, G., Darbo, G., Ficorella, F., Fumagalli, E., Gariano, G., Gaudiello, A., Gemme, C., Meschini, M., Messineo, A., Mendicino, R., Ronchin, S., Rovani, A., Ruscino, E., Sultan, D., Zorzi, N., and Vazquez Furelos, D. (2019b). *INFN-FBK developments of 3D sensors for High-Luminosity LHC*. *Nuclear Instrum. Methods A* **924**, pp. 73–77.



# Astroparticle Physics



# ADHD

Francesco Dimiccoli, Francesco Nozzoli,<sup>†</sup> Paolo Zuccon

The predicted antideuteron ( $\bar{d}$ ) flux resulting from secondary interactions of primary cosmic rays (CR) with the Inter-Stellar medium is expected to be very small and in particular it is kinematically suppressed at low energy (sub-GeV). Well motivated theories beyond the Standard Model contain viable dark matter candidates, which could lead to a significant enhancement of  $\bar{d}$  flux in the CR due to annihilation of dark matter (DM) particles. This flux contribution is believed to be relatively large at low energies, where the secondary background is naturally suppressed, this leads to a high interest in the development of new detection techniques for low energy  $\bar{d}$ . Current search of  $\bar{d}$  in cosmic rays are based on the well established technique of magnetic spectrometry. A new different experimental approach must be used to detect  $\bar{d}$  with kinetic energy below 0.2 GeV/n that is the region of interest for indirect search for Dark Matter.

Anti Deuteron Helium Detector (ADHD) project is aiming to study a new signature offered by an high pressure He target for the identification of  $\bar{d}$  in space.<sup>1,2,3</sup>

The typical lifetime for stopping  $\bar{d}$  (like stopping  $\bar{p}$ ) in matter is of the order of picoseconds, however, since 1991, the existence of long-living ( $\sim \mu\text{s}$ ) metastable states for stopping  $\bar{p}$  in helium target was measured. These metastable states in helium have also been measured for other heavy negative particles, such as  $\pi^-$  and  $K^-$ . The theoretical description of the effect is predicting that the metastable state lifetimes increase as the reduced mass squared, i.e. a slightly larger delay is expected for  $\bar{d}$  capture in helium with respect to the measured  $\bar{p}$  case. This characteristic delayed annihilation signal in He is a distinctive signature to identify the antimatter nature of the stopping particle

that can be used to detect  $\bar{d}$  in space.

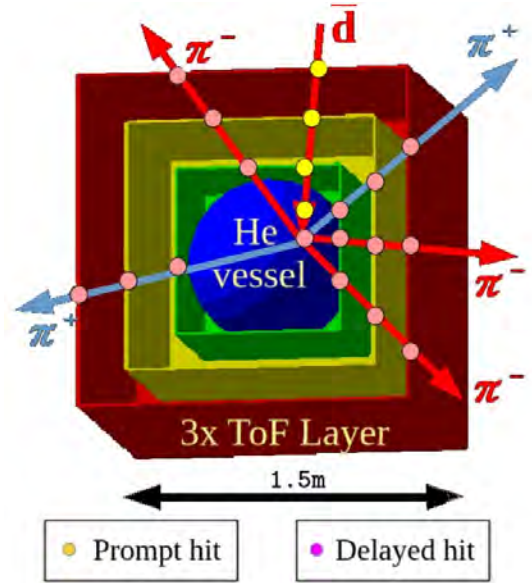


Figure 1: The ADHD detector is made of a 400 bar helium-gas calorimeter (HeCal) surrounded by a Time-of-Flight system with three scintillator layers. Antideuterons are detected as a single in-going prompt track (yellow points) followed by several out-going delayed pions (light-red points).

A possible layout for ADHD (Fig. 1) has been simulated with the Geant4 10.5 package. The inner portion contains the helium calorimeter (HeCal), which consists of an approximately 90-cm diameter spherical thermoplastic vessel filled with 20 kg of scintillating helium (300 liters at 400 bar pressure). The vessel wall thickness of about 3 cm (mass about 100 kg) ensures a burst pressure larger than 800 bar; a similar system is already considered for helium transportation in space or for  $\text{H}_2$  tanks. Helium gas is a fast UV scintillator, having a light yield similar to other fast plastic or liquid scintillators and capable of providing nanosecond timing performance.

The HeCal is surrounded by a Time-of-

<sup>†</sup>Contact Author: francesco.nozzoli@unitn.it

<sup>1</sup>Nozzoli, F. et al. (2019), Journal of Physics: Conference Series 10th Young Researcher Meeting (in press on JoP), pp. 1–6.

<sup>2</sup>Dimiccoli, F. et al. (2019), Journal of Instrumentation 15th Topical Seminar on Innovative Particle and Radiation Detectors (in press on JINST), pp. 1–10.

<sup>3</sup>von Doetinchem, P. et al. (2020),

Flight system consisting of three layers of 4 mm-thick plastic scintillator bars, which provides velocity and charge measurements via ionization energy loss. It is assumed that with current technology such a system can deliver velocity resolution of 5% and energy-loss resolution of 10%, implying a timing resolution on the order of 100 ps and position resolution of the order of a few centimeters. Considering energy loss in the TOF and vessel, a minimum kinetic energy of approximately 60 MeV/n is necessary for  $\bar{d}$  to reach the helium target. On the other hand,  $\bar{d}$  with kinetic energy larger than 150 MeV/n would typically cross the active helium region without stopping inside. Combining information on the velocity and energy depositions measured by the TOF, the prompt and delayed energy measured by the HeCal, and the reconstructed event topology, it is possible to identify a single  $\bar{d}$  over  $10^3$  background  $\bar{p}$ . The expected acceptance for ADHD, in this configuration, is about 0.2 m<sup>2</sup>sr in the energy region 60-150 MeV/n for  $\bar{d}$  and 100-300 MeV for  $\bar{p}$ . Fig. 3 shows the expected sensitivity for this ADHD layout as compared with current Dark Matter models and planned experiments.

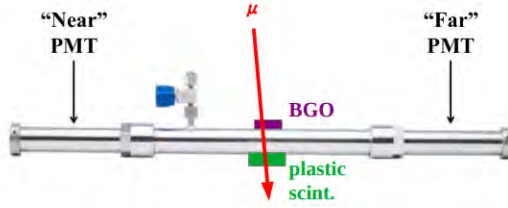


Figure 2: Preliminary test of ADHD performances detecting muons with Arktis B470 prototype.

Tests of ADHD approach using an helium scintillator prototype (200 bar Arktis Radiation Detectors B470, see Fig. 2) are ongoing at INFN-TIFPA to validate the expected ADHD performances.

Beam test in the Trento Proton-therapy center are planned for 2020. Preliminary data collected in 2019 by using cosmic muons, provide a time resolution of  $\sim 3$ ns and an energy resolution of  $\sim 15\%$  for the Arktis B470 prototype. Cosmic rays muons are minimum ionizing particles (MIPs), therefore they are expected to release 2-3 MeV cm<sup>2</sup>/g in He gas. Much larger deposited energy is expected for  $\sim 60 - 150$  MeV/n protons (or  $\bar{d}$ ). This implies a much larger photoelectron yield with an expected improvement of at least 1 order of magnitude of the timing and energy resolution in the energy range of interest for ADHD project.

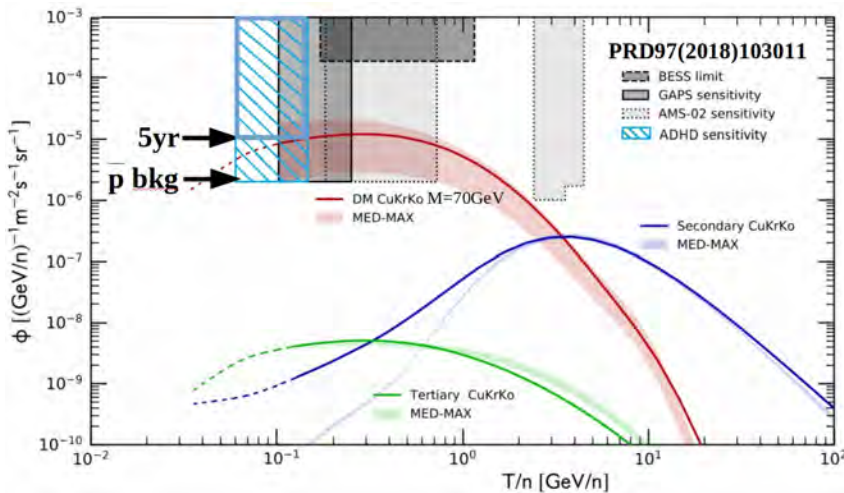


Figure 3: The expected sensitivity of ADHD approach is compared with current Dark Matter models and planned experiments.

# AMS

Roberto Battiston, William Jerome Burger, Cinzia Cernetti, Francesco Dimiccoli, Konstantin Kanishev, Ignazio Lazzizzera, Francesco Nozzoli,<sup>†</sup> Paolo Zuccon

AMS-02 is a state-of-the-art particle physics detector (see Fig. 1) designed to operate as an external module on the International Space Station (ISS).

AMS-02 goal is to study the universe and its origin by searching for antimatter and dark matter, while performing precision measurements of cosmic ray composition and flux. The measurements high accuracy along with the large collected statistic allow to study cosmic ray component flux variations with rigidity and time. This is important to understand the origin, acceleration and propagation of cosmic rays in our galaxy.

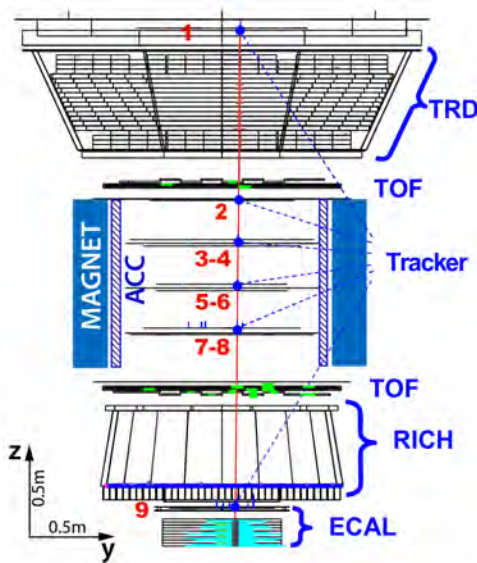


Figure 1: The AMS detector with an example of a measured 868 GeV positron event. Tracker planes 1-9 measure the particle charge, sign and momentum. The TRD identifies the particle as an electron/positron. The TOF measures the charge and ensures that the particle is downward-going. The RICH measures the charge and velocity. The ECAL independently identifies the particle as an electron/positron and measures its energy.

During 2019 AMS published an update of measured flux of Positrons up to TeV (Aguilar et

al. 2019c) and Electrons up to 1.4 TeV (Aguilar et al. 2019b).

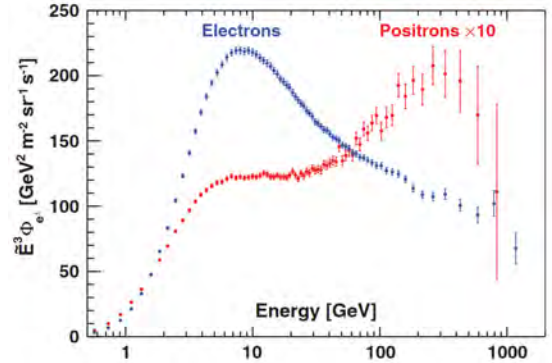


Figure 2: The AMS electron (blue) and positron (red, multiplied by 10) spectra ( $E^3\Phi_{e^\pm}$ ). The electron spectrum has distinctly different magnitude and energy dependence compared to that of positrons.

In particular there is a clear evidence that high energy positrons originate from an unexpected source (astrophysical or exotic) and different sources must be invoked for high energy electrons. Contrary to the positron flux, which has an exponential energy cutoff of  $810^{+310}_{-180}$  GeV, at the  $5\sigma$  level the electron flux does not have an energy cutoff below 1.4 TeV. AMS-02 data collected up to ISS end-life will provide further updates, allowing  $e^+$  measurements above TeV (disentangling different models for exotic or astrophysical sources) and electron measurements above 1.4 TeV testing the presence of high energy cutoff in the spectrum.

Moreover the Helium isotopic composition measurement up to 10 GeV/n (Aguilar et al. 2019a) has been published in 2019.

Below 4 GV, the  $^3\text{He}/^4\text{He}$  flux ratio shows a significant long-term time dependence. Different from the B/C and B/O flux ratios, which show a maximum around 4 GV, the  $^3\text{He}/^4\text{He}$  flux ratio was found to be decreasing with rigidity; below 4 GV, the ratio is well described by a single power law  $R^\delta$  with  $\langle\delta\rangle_t = -0.21 \pm 0.02$  and a time variation of  $\pm 0.05$ .

<sup>†</sup>Contact Author: francesco.nozzoli@unitn.it

Above 4 GV, the  $^3\text{He}/^4\text{He}$  flux ratio was found to be time independent, and its rigidity dependence is well described by a single power law  $R^\Delta$  with  $\Delta = -0.294 \pm 0.004$ . This last value is in noticeable agreement with the B/O and B/C spectral indices at much higher energies allowing interesting insight about propagation properties of cosmic rays at large distance from our galactic neighborhood.

Finally from nov. 2019 to jan. 2020, NASA and ESA have accomplished a series of four spacewalks (EVA-59, EVA-60, EVA-61 and EVA-64) to upgrade the AMS-02 Tracker cooling system. The upgrade was successfully and Tracker is now fully operative allowing AMS-02 to collect high quality data up to the endlife of International Space Station.

The AMS/TIFPA group is currently finalizing the measurement of Deuteron flux and flux ratio as a function of Rigidity and time. Similarly to  $^3\text{He}/^4\text{He}$ , the Deuteron/Proton flux ratio measurement is very important, because it is a flux ratio between exclusively secondary and primary produced CR particles giving important constraints to the propagation models of CR in the Galaxy.

Moreover, analysis of  $^{10}\text{Be}/^9\text{Be}/^7\text{Be}$  abundances in cosmic rays, being a very important cosmic-ray radioactive clock, is started as the next goal of the AMS/TIFPA group.

## Selected Papers

- Aguilar, M. et al., AMS collaboration (2019a). *Properties of Cosmic Helium Isotopes Measured by the Alpha Magnetic Spectrometer*. Phys. Rev. Lett. **123**(18). Art. no.: 181102.
- AMS collaboration (2019b). *Towards Understanding the Origin of Cosmic-Ray Electrons*. Phys. Rev. Lett. **122**(10). Art. no.: 101101.
- AMS collaboration (2019c). *Towards Understanding the Origin of Cosmic-Ray Positrons*. Phys. Rev. Lett. **122**(4). Art. no.: 041102.

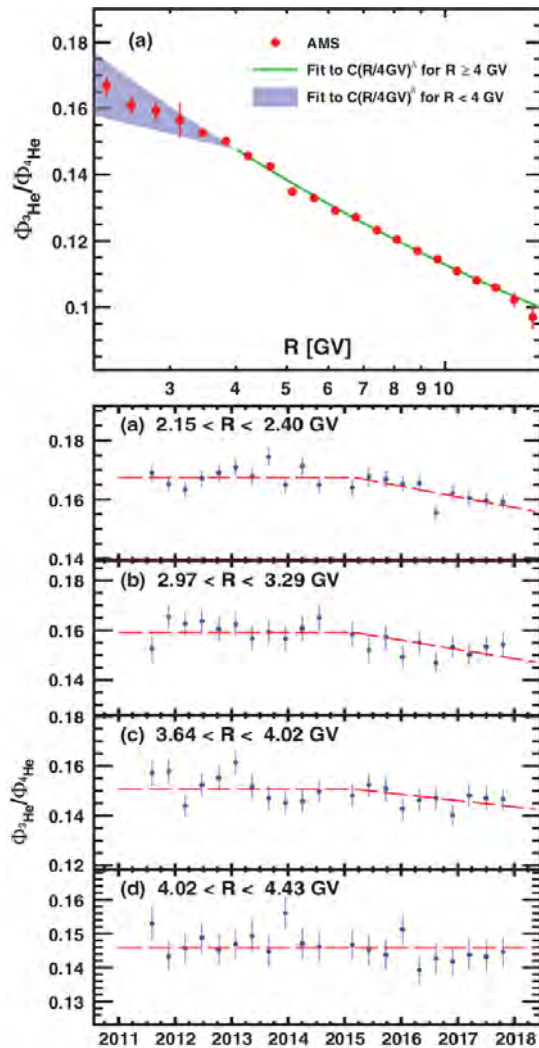


Figure 3:  $^3\text{He}/^4\text{He}$  flux ratio as a function of Rigidity and time. Above 4 GV it can be described as a time independent single power law.

# DarkSide

Fabio Acerbi, Alberto Gola,<sup>†</sup> Marco Marcante, Alberto Mazzi, Stefano Merzi, Giovanni Paternoster, Veronica Regazzoni

The existence of dark matter in the Universe is commonly accepted as the explanation of many phenomena, ranging from internal motions of galaxies to the large-scale inhomogeneities in the cosmic microwave background radiation and the dynamics of colliding galaxy clusters.

A favored hypothesis that explains these observations is that dark matter is made of weakly interacting massive particles (WIMPs). However, no such particles exist in the Standard Model and none has been observed directly at particle accelerators or elsewhere. Hence, the nature of the dark matter remains unknown.

DarkSide-20k experiment (DS-20k) is a direct dark matter detection experiment based on a shielded underground detector, with 20 tons of liquid argon target mass. It will be based on a two-phase time projection chamber (TPC) filled with low-background, depleted argon (DAr) and will be deployed in the underground Hall C at Gran Sasso National Laboratory (LNGS), inside a newly constructed, two-chamber veto, filled with atmospheric Argon, and a cryostat, as shown in Fig. 1. DS-20k constitutes an expanded version of the DS50 experiment, which finished taking data at LNGS in October 2017.

**DS-20k Time Projection Chamber** In the TPC, events in the liquid argon (LAr) result in electron or nuclear recoils that deposit energy in the argon, resulting in excitation and ionization. The direct excitation, and that due to recombining ions, results in a prompt scintillation signal, called S1. LAr scintillation has a wavelength of 128 nm, in the far UV, thus a wavelength shifter will cover all surfaces that the UV light hits. Ionization electrons escaping recombination are drifted by an applied electric field to the top of the LAr, where a stronger applied field extracts the electrons into the argon gas above the liquid. Here the strong field accelerates the electrons enough for them to excite (but not ionize) the argon gas, producing a secondary scintillation signal, S2, that is propor-

tional to the initial ionization. Photosensors at the top and bottom of the TPC read out both scintillation signals in each event.

S1 is used for energy determination and pulse-shape discrimination. S2 is used for energy and 3D position measurement of the event, obtaining the vertical coordinate from the drift time between S1 and S2, and the horizontal coordinates from the pattern of light in the top photosensors.

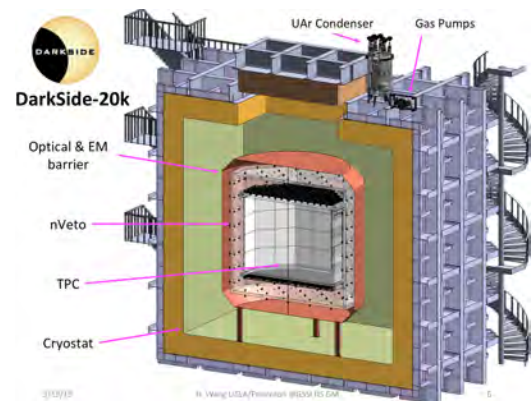


Figure 1: Cross sectional view of the DS20k experiment through its center plane, showing the inner TPC, the inner and outer active veto chambers, and the cryostat.

**Silicon Photomultipliers** The use of Silicon Photomultipliers (SiPMs) instead of Photo Multiplier Tubes as photodetectors in both TPC and Veto is one of the main technological challenges of the experiment, the other being the production of ultra-low-background depleted argon. There are several advantages in using these detectors in DS-20k, among them: low bias voltage (30 - 45 V), efficient integration into tiles to cover large areas, customizable size and performance, excellent photon counting capabilities and high Photon Detection Efficiency (PDE). The most important one, however, is that SiPMs are virtually radioactivity free (silicon is very radio pure material). SiPMs will be grouped in tiles and integrated in several photo-detection modules, to cover a total area of approximately 10 m<sup>2</sup>.

<sup>†</sup>Contact Author: gola@fbk.eu

**DS-20k Activity at TIFPA** The use of SiPMs at cryogenic temperatures is innovative and very few studies have been carried out on their characterization and optimization at cryogenic temperatures. Furthermore, the readout of such large active areas poses several challenges in the design and optimization of both SiPMs and front-end electronics, developed at LNGS, and in packaging techniques. In this context, TIFPA started the DS-20k activity in 2016, collaborating mainly with Fondazione Bruno Kessler (FBK), LNGS and Naples INFN section and Princeton University. The activity was focused on the cryogenic characterization of different SiPMs technologies developed by FBK to verify and characterize their functionality at cryogenic temperatures and, in particular, at 87 K, to select the most suitable one for DS-20k, and to provide information to optimize the SiPM parameters and layout for the best possible performance in DS-20k.

In this context, the most important results demonstrated are:

- (i) exceptionally low Dark Count Rate (DCR) at 87 K;
- (ii) Suppression of the increase of the after-pulsing previously observed at cryogenic temperatures;
- (iii) Increased temperature stability of SiPM quenching resistor.

These features are combined in the NUV-HD-Cryo SiPM technology, exceeding the performance specifications of the experiment. The SiPMs feature a  $1\text{ cm}^2$  active area,  $30\ \mu\text{m}$  cell size, and show a PDE of 50% at 420 nm, DCR of  $10\ \text{mHz}/\text{mm}^2$  at 77 K, after-pulsing probability lower than 8%, crosstalk probability lower than 25%, at 6 V of bias above breakdown.

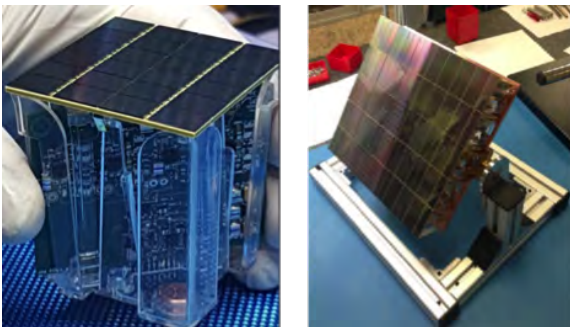


Figure 2: Left:  $24\text{ cm}^2$  PDM, composed of 24 NUV-HD-Cryo SiPMs connected to a single readout channel. Right:  $600\text{ cm}^2$ , fully functional motherboard, containing 25 PDMs.

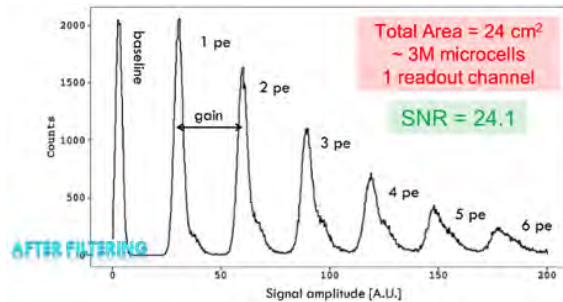


Figure 3: Few-photon spectrum recorded with a whole PDM, after optimized digital filtering. The spectrum demonstrates, among other things, the excellent gain uniformity of the 3M microcells composing the PDM.

Four SiPM lots commissioned by TIFPA to FBK from 2017 to 2019, in the context of the INFN-FBK agreement, were used by the Dark-Side collaboration to build large-area,  $24\text{ cm}^2$  SiPM tiles and mount them in the first batch of photo-detection modules (PDMs) (Fig. 2, left). The PDMs were then assembled on the first test motherboard with a total sensitive area of  $600\text{ cm}^2$  (Fig. 2, right).

Using cryogenic electronics developed at LNGS for the PDM readout, remarkable few-photon counting capability was demonstrated at 77 K, with S/N in excess of 20, using a  $24\text{ cm}^2$  SiPM array coupled to a single analog readout channel (Fig. 3).

During 2019, activities at TIFPA and FBK were focused on the transfer of the NUV-HD-Cryo technology to an external CMOS foundry (LFoundry), capable of mass production for the DS-20k experiment. After microfabrication process definition and the validation of a first, explorative SiPM run, composed of  $1 \times 1\text{ mm}^2$  SiPMs, the final,  $11.7 \times 7.9\text{ mm}^2$  SiPMs layout was designed by FBK, fabricated by LFoundry and delivered in November 2019. Characterization of the run, carried out by TIFPA and FBK, showed SiPM parameters in line with previous productions at FBK, with the exception of one electrical parameter at 87 K, which is under investigation to complete the SiPM technology transfer. Finally, development of a customized Through Silicon Via (TSV) technology, applied to NUV-HD-Cryo SiPMs, compatible with cryogenic operation and meeting DS-20k requirements in terms of radio-purity is under development at LFoundry, with the support of FBK and TIFPA and is expected to be available in 2020.

# FISH

Arturo Farolfi, Dimitrios Trypogeorgos, Carmelo Mordini, Albert Gallemí, Iacopo Carusotto, Salvatore Butera, Alessio Recati, Sandro Stringari, Alessandro Zenesini, Giacomo Lamporesi, Gabriele Ferrari <sup>†</sup>

FISH, Fundamental Interaction Simulations with quantum gases, focuses on the dynamics of quantum gases of ultracold atoms with the aim to model interactions and mechanisms at the basis of high energy physics. This research field belongs to the domain of quantum simulation, where physical systems difficult to address experimentally are studied through analogies with simpler systems. In particular we focus on the study of vortices in a system made of two Rabi-coupled atomic Bose-Einstein condensates to simulate quark confinement.

The activity of last year was devoted to the finalization and characterization of the novel experimental setup, and to the first scientific measurements with the novel apparatus. More specifically we focused on:

**Magnetic shield:** was integrated with the experimental apparatus, including the electromagnets and antennas devoted to the production of the atomic sample and the manipulation of the spin degrees of freedom. The experimental sequence to produce the sample was redefined in the context of the novel experimental setting where the fields applied to produce the atomic sample and the magnetic screen are coupled.

**Theory of Rabi-coupled BECs:** we numerically simulated the generation of bound states of vortices and their fragmentation. This allowed us to identify the experimental conditions to induce confinement and to generate bound states of vortices (Gallemí et al. 2019). This work also provided the experimental strategy for the production of bound states of vortices through the decay of the relative phase discontinuity (domain wall) featuring a sufficiently long extension through the sample. The

phase discontinuity will be experimentally created through a non-homogeneous and spin-selective optical-dipole potential.

**Optical trapping:** in order to achieve the experimental conditions described above, we realized a specific optical dipole trap where we transfer the atomic sample once it is condensed. This additional dipole trap is based on two highly elliptical laser beams at 1064 nm and power of several Watts per beam, which are orthogonally arranged. The optical setup allows to modify the confinement conditions with good flexibility in order to vary the ratio of the axes of the sample distribution.

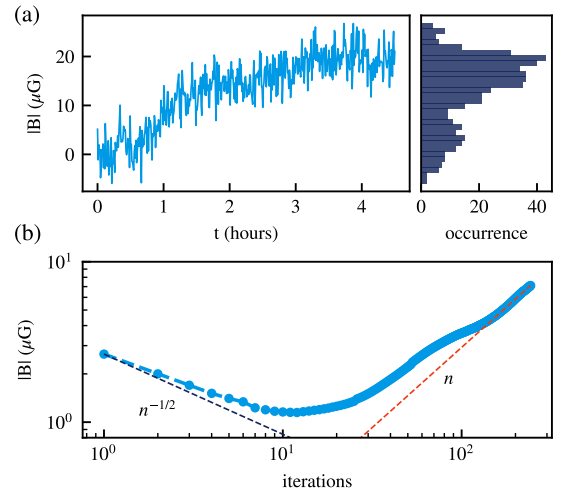


Figure 1: (a) Typical measurement of the magnetic field drift within the magnetic shield; spectroscopic signal on the 2-photon Raman-coupled system; (b) Allan variance of the magnetic field drift on 3 hours.

**Spin manipulation:** the spin state control system, which is based on the hyperfine two-photon Raman transition at 1.8 GHz, is now available and features the real-time control of

<sup>†</sup>Contact Author: gabriele.ferrari@unitn.it

the amplitude, frequency and phase of the coupling. It allows to implement both adiabatic rotations to initialize the spin state in eigenstates of  $\sigma_x$ , and to drive Rabi flopping with population transfer between the two eigenstates of  $\sigma_z$ . Spectroscopic measurements of coherent dynamics between spin states made it possible to characterize the stability of the magnetic field inside the screen with resolution at the microgauss level, see Fig. 1 (Farolfi et al. 2019a).

**Magnetic soliton:** The study of excitations in the Rabi-coupled BEC requires the prior characterization of the properties of the system in the absence of Rabi coupling. Of particular relevance in this regard are solitonic excitations with a magnetic character, see Fig. 2. These have been the subject of a campaign of measures in an effective 1-dimensional geometry using a multiple-images technique to extract all the relevant components of the wave function (Fig. 2c), allowing us to fully characterize the individual properties of these novel excitations (Farolfi et al. 2019b).

**Current activity:** we are further advancing the experimental apparatus by implementing optical phase imprinting, that will be used to produce topological excitations on the Rabi-coupled spinor BEC system. Such excitations will be studied as a function of the accessible

experimental parameters (e.g. the intensity of the coupling, or the confining external potential) within the FISH project framework.

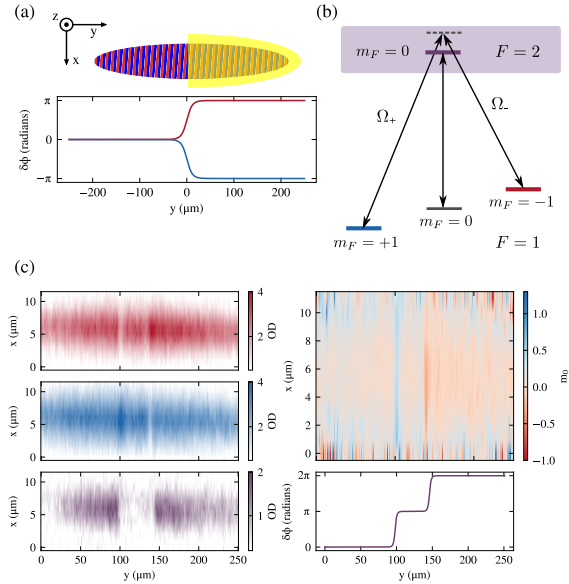


Figure 2: (a) A spin-selective optical potential generates a pair of MSs. The overall imparted phase of  $2\pi$  is dealt symmetrically on the two spin components. (b)  $\Lambda$ -coupling scheme showing all the hyperfine transitions that are used for preparation of the mixture. (c) Full tomography of a pair of MSs 15 ms after their creation. Left column: Optical densities (OD) of  $|1, -1\rangle$  (red) and  $|1, +1\rangle$  (blue), and relative phase (purple). Right column: The measured apparent magnetisation (top) and the expected relative-phase profile (bottom).

## Selected Papers

- Farolfi, A., Trypogeorgos, D., Colzi, G., Fava, E., Lamporesi, G., and Ferrari, G. (2019a). *Design and characterization of a compact magnetic shield for ultracold atomic gas experiments*. Review of Scientific Instruments **90**(11). Art. no.: 115114.
- Farolfi, A., Trypogeorgos, D., Mordini, C., Lamporesi, G., and Ferrari, G. (2019b). *Observation of magnetic solitons in two-component Bose-Einstein condensates*. arXiv:1912.10513.
- Gallemí, A., Pitaevskii, L. P., Stringari, S., and Recati, A. (2019). *Decay of the relative phase domain wall into confined vortex pairs: The case of a coherently coupled bosonic mixture*. Phys. Rev. A **100** (2). Art. no.: 023607.

# HUMOR

Enrico Serra,<sup>†</sup> Michele Bonaldi, Antonio Borrielli, Giovanni Andrea Prodi

Different approaches to quantum gravity, such as string theory and loop quantum gravity, as well as doubly special relativity and gedanken experiments in black holes physics, all indicate the existence of a minimal measurable length of the order of the Planck length, about  $10^{-35}$  m. A common feature of these theories is that the space-time changes nature, become “granular” at a very small length, called “Planck scale” ( $L_P = \sqrt{\hbar G/c^3} = 10^{-35}$  m). The emergency of a minimal length scale can originate relevant consequences also for low-energy quantum mechanics experiments. In fact the Heisenberg relation states that the position and the momentum of a particle cannot be determined simultaneously with arbitrarily high accuracy. However, an arbitrarily precise measurement of only one of the two observables, say position, is still possible at the cost of our knowledge about the other (momentum), a fact which is obviously incompatible with the existence of a minimal observable distance. This consideration motivates the introduction of generalized Heisenberg uncertainty principles (GUPs), such as

$$\Delta q \Delta p \geq \frac{\hbar}{2} \left( 1 + \beta_0 \left( \frac{L_P \Delta p}{\hbar} \right)^2 \right), \quad (1)$$

that implies indeed a nonzero minimal uncertainty  $\Delta q_{min} = \sqrt{\beta_0} L_P$ . The dimensionless parameter  $\beta_0$  is assumed to be around unity, in which case the corrections are negligible unless lengths are close to the Planck length. Any experimental upper limit for  $\beta_0 > 1$  would constrain new physics below the length scale  $\sqrt{\beta_0} L_P$ . This GUP implies two relevant effects with respect to a harmonic oscillator: the appearance of the third harmonic and a dependence of the oscillation frequency on the amplitude. Therefore, to set a limit on the value of  $\beta_0$ , we can measure the frequency of highly isolated oscillators at different oscillation amplitudes. As a consequence, an alternative way to check quantum gravitational effects would

be to perform high-sensitivity measurements of the uncertainty relation, in order to reveal any possible deviation from predictions of standard quantum mechanics. In the experiment we measure the Heisenberg uncertainty relation on the momentum position variables of a micro- and nano-resonators probed by a laser readout system.

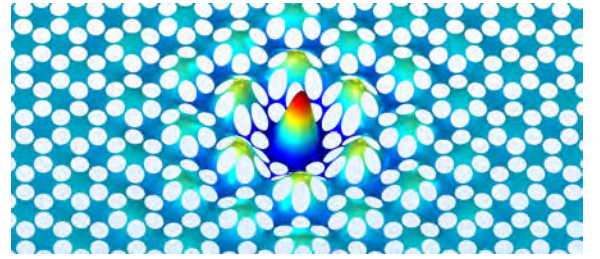


Figure 1: Mode-shape function evaluated by a FEM analysis for the Band-gap mode A. Defect mode evanescently couples to the frame.

Freestanding silicon nitride ( $\text{Si}_3\text{N}_4$ ) nano-membranes provide an ideal platform for realising ultra-coherent harmonic oscillator thanks to the dissipation dilution produced by an internal pre-stress (1 GPa). Two membranes oscillators were developed: a round-shaped membrane endowed with an on-chip shield for rejecting the clamping losses and a rectangular-shaped resonator endowed with a phononic band-gap crystal. The latter implements the novel soft-clamping concept, that is a design strategy that reduce intrinsic dissipation at the edge. Introduced by Tsaturyan et al. in 2017, it relays on the fact that the phononic crystal modal shape function matches the vibrational defect vibrational mode (shown in Fig. 1) leading to a clamp-free resonator. In fact, the defect mode evanescently couples to the frame that eliminates the extra curvature at the edge imposed by the boundary conditions. For some band-gap modes, soft-clamping results in a Q-factor of  $5 \times 10^7$  in case of a 100 nm thick membrane.

<sup>†</sup>Contact Author: [enrico.serra@tifpa.infn.it](mailto:enrico.serra@tifpa.infn.it)

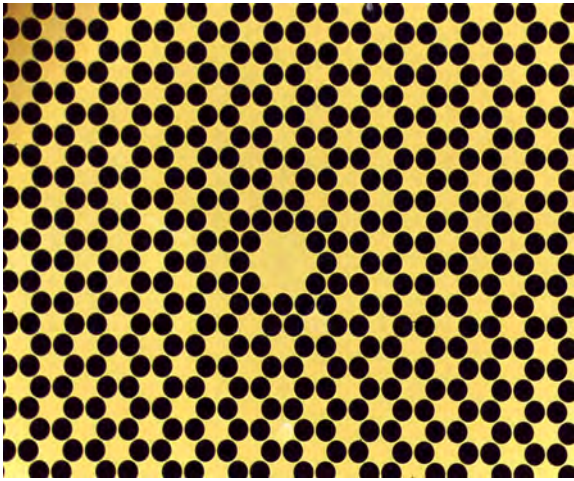


Figure 2: Micro-fabricated membrane with the phononic reticle.

The resonators are fabricated exploiting M-/NEMS technologies based on bulk micromachining (Fig. 2) and they have an effective mass in the range of ng - pg and a working bandwidth up to 2 MHz as shown in Fig. 2. Combining the advantages of both configurations we were able to realize state-of-the-art resonators for quantum optomechanical experiments.

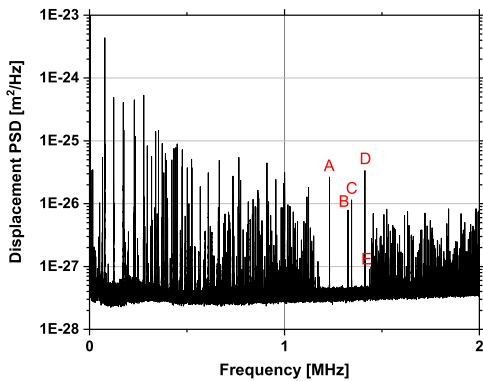


Figure 3: Displacement Power Spectral Density for a rectangular-shaped membrane showing the band-gap with ultra-high Q-factor modes.

Membranes resonators were used for observation of peculiar quantum features in the behavior of macroscopic mechanical oscillators. Most relevant indicator of the achieved mechanical quantum domain is the so-called motional sidebands asymmetry that is a powerful index to deduce the oscillator occupation number. In Fig. 4 the Stokes peak is on the right while anti-Stokes peak is on the left-side. The asymmetry leads to a  $3.87 \pm 0.21$  occupation number.

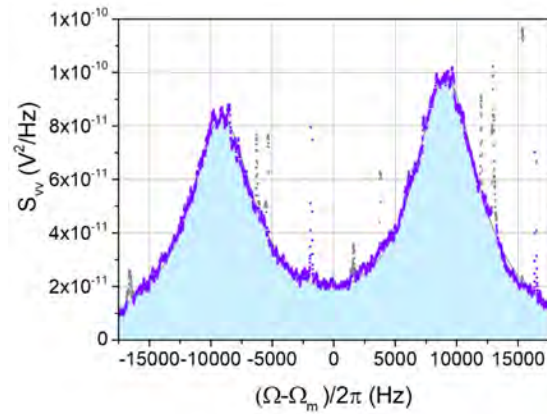


Figure 4: Stokes (right) and anti-Stokes (left) spectral peaks of the (1,1) membrane's mode using the heterodyne detection scheme.

# LIMADOU

Roberto Battiston, William Jerome Burger, Marco Cristoforetti, Francesco Dimiccoli, Benedetto Di Ruzza, Francesco Maria Follega, Giuseppe Gebbia, Roberto Iuppa,<sup>†</sup> Ignazio Lazzizzera, Christian Manea, Francesco Nozzoli, Irina Rashevskaya, Ester Ricci, Enrico Serra and Paolo Zuccon

The CSES mission was launched on February 2<sup>nd</sup>, 2018 and the commissioning lasted until November of that year. 2019 has been the first year of nominal operation for all payloads, including the High Energy Particle Detector (HEPD), designed and constructed by INFN, in collaboration with ASI. The Limadou collaboration focussed on the optimisation of the performance of HEPD and on science, exploiting the multi-messenger sensitivity of the CSES mission to perturbations of the ionosphere and Van Allen belts.

**HEPD performance optimisation.** When measuring the dynamics of 1-100 MeV particles trapped in the Earth's magnetic field, the measurement of the arrival direction is of crucial importance. It allows to backtrace the trajectory of the particle, revealing whether observed fluxes are consistent with the background hypothesis or significantly deviate from that. HEPD has a particle tracker made of two planes of double-sided silicon micro-strip technology, 300  $\mu\text{m}$  thick and fabricated by FBK-CMM. To improve the quality of the measurement and to be in condition of facing potential inefficiencies of the tracker, the Limadou group at TIFPA explored the possibility of reconstructing the arrival direction by using just signals from HEPD scintillators. A set of fully connected neural networks was used to determine the nature of the impinging particle, and to measure its energy and arrival direction. Fig. 1 shows that single-event resolution below 10 degrees can be achieved for protons, a remarkable result if one considers that plastic scintillators have light attenuation length as large as 3.8m and almost no sensitivity on the impact position of the charged particle. The result is under validation, with high- $\Psi$  relative weight in data being 10% larger than in Monte Carlo simulation.

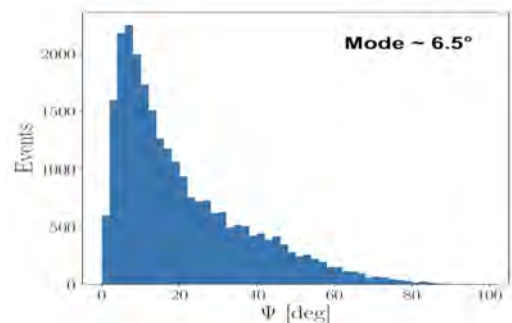


Figure 1: Angle between the reconstructed direction and the true one, for Monte Carlo proton events uniformly sampled in the energy range 30-300 MeV. From (Proc. 15th Topical Seminar on Innovative Particle and Radiation Detectors (Siena, Italy, October 2019) 2020).

**Low-energy cosmic rays.** In 2019, HEPD has been the most sensitive experiment to observe charged cosmic rays at low energy (3-100 MeV electrons and 30-300 MeV/n nuclei). With an effective area as large as 400  $\text{cm}^2$ , HEPD collects more than 20 times the statistics of its competitors, making it possible to measure flux variations even on a daily base. Fig. 2 clearly demonstrates such sensitivity: one month of data taking suffices to HEPD to measure the flux of galactic protons and precisely position the baseline between the maximum and the minimum expectations from solar activity.

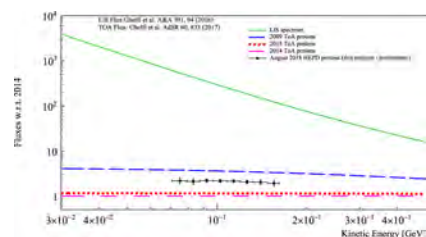


Figure 2: HEPD galactic proton flux (black squares) compared to TOA theoretical fluxes for 2009 (blue dashed line), 2014 (magenta dashed-dotted line), 2015 (red dotted line), and LIS spectrum (green solid line). From Picozza et al. (2019a).

<sup>†</sup>Contact Author: roberto.iuppa@unitn.it

**Seismic phenomena.** CSES stands for “China Seismo-Electromagnetic Satellite” and the study of possible ionosphere-lithosphere interactions correlated with seismic phenomena is one of the main scientific objectives of the mission. To this purpose, CSES has payloads measuring electric field, magnetic field, plasma density and temperature, X-rays, electrons and nuclei. Such an ensemble of instruments provides a unique opportunity for a multi-messenger approach to the problem of seismo-induced ionosphere perturbations, as demonstrated in Fig. 3. An anomaly in the East-Y component of the magnetic field was found on August 14<sup>th</sup>, 2018 on the area of the  $M_W = 7.5$  earthquake occurred in Indonesia

on September 28<sup>th</sup>, 2018 hinting at phenomena possibly linked to the earthquake preparation phase.

**Limadou-02.** On December 16<sup>th</sup>, 2019, ASI, INFN and other partners kicked-off the Limadou-02 project, devoted to the construction of the HEPD and EFD (Electric Field Detector) payloads for the second satellite of the CSES constellation. The group at TIFPA is in charge of the construction of the HEPD tracker, to be realised with ALPIDE sensors, as well as of the simulation of the HEPD response to electrons and nuclei.

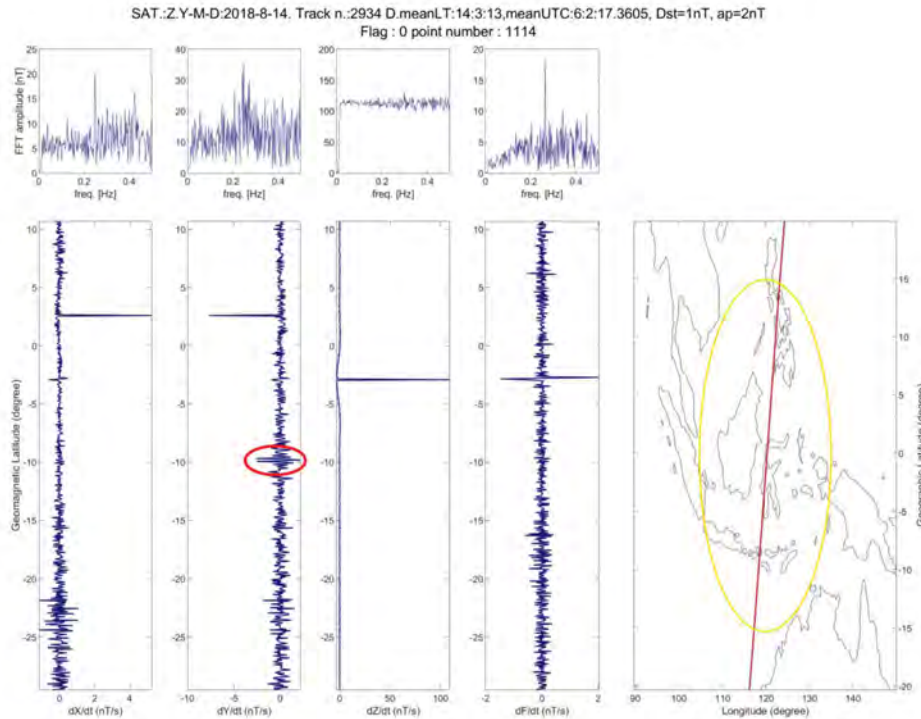


Figure 3: CSES High Precision Magnetometer track crossing the Dobrovolsky area and future  $M_W = 7.5$  Indonesia epicenter on August 14<sup>th</sup>, 2018. The red circle underlines an anomaly in the East-Y component of magnetic field. The map at the right presents the projection of the CSES track on ground with a brown line and the Dobrovolsky’s area by a yellow circle. See Marchetti et al. (2020) for details.

## Selected Papers

Marchetti, D. et al. (2020). Possible Lithosphere-Atmosphere-Ionosphere Coupling effects prior to the 2018  $M_W = 7.5$  Indonesia earthquake from seismic, atmospheric and ionospheric data. *Journal of Asian Earth Sciences* **188**, p. 104097.

Picozza, P. et al. (2019a). Scientific Goals and In-orbit Performance of the High-energy Particle Detector on Board the CSES. *The Astrophysical Journal Supplement Series* **243**(1), p. 16.

*Proc. 15th Topical Seminar on Innovative Particle and Radiation Detectors (Siena, Italy, October 2019)* (2020). Vol. C05014. JINST. Trieste, Italy: Sissa.

# LISA Pathfinder and LISA

Daniele Bortoluzzi, Eleonora Castelli, Antonella Cavalleri, Davide Dalbosco, Rita Dolesi,<sup>†</sup> Valerio Ferroni, Martina Muratore, Francisco Rivas Garcia, Giuliana Russano, Lorenzo Sala, Daniele Vetrugno, Davide Vignotto, Stefano Vitale, William Joseph Weber

Our current image of the Universe is essentially based on the observation of electromagnetic waves in a broad frequency spectrum. Much of the Universe, however, does not emit electromagnetic radiation, while everything interacts gravitationally. Despite being the weakest of the fundamental interactions, it is gravity that dominates the Universe on a large scale and regulates its expansion since the Big-Bang. As predicted by Einstein's General Relativity, gravity has its messenger: gravitational waves produced by massive accelerating bodies, such as coalescing black holes binaries or violent phenomena like stellar core collapse. Gravitational waves propagate at the speed of light, essentially undisturbed, bringing often not otherwise accessible information about events across all cosmic ages, from Cosmic Dawn to the present. The observation of gravitational waves promises to open new extraordinary perspectives for investigation of crucial issues like the nature of gravity in weak and in strong field regime, the nature of black holes, the formation and evolution of stellar binary system, the formation and evolution of cosmic structures since the earliest stages of the Universe.

While the ground-based observatories of the LIGO-VIRGO collaboration in 2019 are performing a long joint observation run, the project of LISA is rapidly progressing toward the implementation of the first space-based observatory devoted to the low-frequency sources that can not be detected from ground. Einstein's theory describes gravity in terms of the curvature of space-time that is deformed by the passing of gravitational waves. These effect can be detected in space by measuring with great precision the relative acceleration of masses in free fall, i.e. reference masses subject to gravity field but well-isolated from other types of disturbing forces. The precursor space mission LISA

Pathfinder measured the relative acceleration of two 2 kg test masses in near-perfect geodesic motion, and its outstanding performance provided an experimental benchmark demonstrating the ability to realize the low-frequency science potential of the LISA mission. LISA consists of three identical satellite in a triangular constellation, with arms of several million km, orbiting around the Sun, shown in Fig. 1 with its strain sensitivity. It should allow for the observation of thousands of gravitational wave sources with high signal-to-noise, and in many cases very well characterized in terms of frequency, position in the sky, and luminosity distance. It targets massive sources emitting in the 0.1 mHz to 1 Hz band not accessible from ground due to the gravitationally noise terrestrial environment, ranging from stellar mass binaries in our own Galaxy to the merger of two galactic-core black holes, from  $10^5$  to  $10^7$  solar masses, from the recent Universe back to the epoch of the first galaxies.

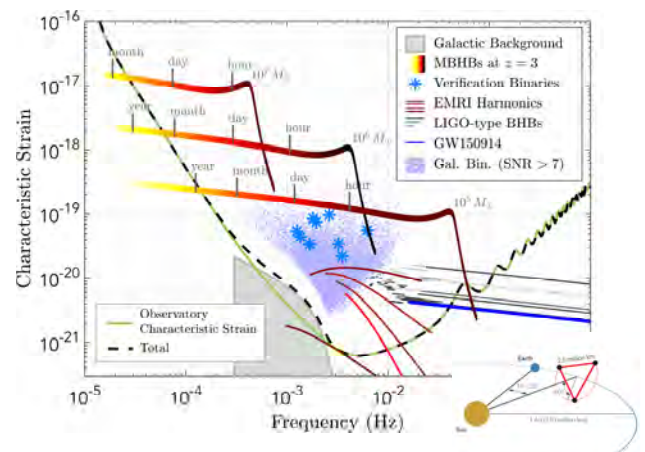


Figure 1: LISA's sensitivity curve plotted with the signal levels for several GW sources. In the insert a schematic of the LISA-concept.

The Trento Group, led by the Principal In-

<sup>†</sup>Contact Author: rita.dolesi@unitn.it

investigator prof. Stefano Vitale, has contributed in a leadership role in all phases of the LISA PF mission, including hardware design and prototyping, laboratory torsion pendulum testing, scientific guidance of the industrial aerospace contractors, and finally to the design and operation of the flight measurement campaign.

LISA Pathfinder legacy consists in a LISA Gravitational Reference Sensor at TRL 9, a detailed physical model for parasitic forces close to quantitative demonstration at sub-femto-g level down to  $20 \mu\text{Hz}$ , a demonstration of local interferometry on free falling test-masses at tens of femto-m level down to mHz, the demonstration of drag-free satellite down to femto-g, the demonstration of gravitational balance, of test mass charge management system and of an in flight test mass releasing mechanism. Several papers documenting these performances has been published in 2019 (see p. 132) and others are still in preparation.

As internationally recognized leader in development and realization of systems of free-falling geodesic reference test masses for space based gravitational wave detector, the group TIFPA is currently working on the definition of the measuring instrument and guides the ASI development of the Gravitational Reference Sensor (GRS) system to guarantee the free fall of the geodetic reference masses that are at the heart of the instrument (for more information about LISA see <https://www.elisascience.org/>).

In 2019 LISA passed the MCR (Mission Consolidation Review), with the Trento Group supporting the review of the documents provided by the two competitive studies of the system (Thales Alenia and AIRBUS).

Important support was given also in defining the MOSA by writing and reviewing the doc-

umentation provided by the LISA Consortium for the instrument. No showstoppers for the system nor for the instrument have been identified. We are now in the second half of phase A of the mission, working towards the mission baseline review (Mission Formulation Review, MFR in the mid 2020) for a mission adoption in the mid-2023 and launch in 2033-2034.

In parallel, the activity in the laboratory proceeded successfully with a measurement campaign performed with a torsion pendulum apparatus. This facility is a high sensitivity force noise instrument at mHz frequencies, that is integrated with copy of the capacitive sensor for LISA, and is successfully employed in verifying the functioning principle of the Test Mass discharge strategy with synchronized UV pulses (see Fig. 2).

As with LPE, the Trento torsion pendulum facility will be a vital instrument for targeted and representative tests that will validate the implementation of the LISA flight hardware from the design phase to the commissioning phases.

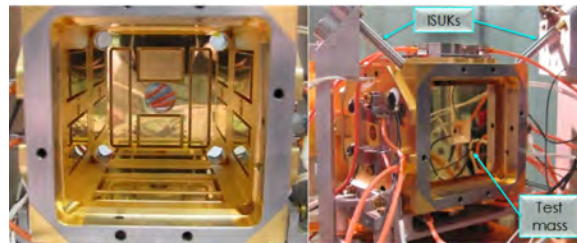


Figure 2: On the left, the capacitive sensor without one face to show its inner electrodes configuration (by OHB-Italy); on the right, a LISA-like test mass, which is part of the torsion pendulum inertial member, inside the capacitive sensor integrated with the UV ISUKs (Inertial Sensor UV Kit), that inject the UV light extracting photoelectrons needed to neutralize the Test Mass charged in space by cosmic rays

# Quax

Paolo Falferi,<sup>†</sup> Renato Mezzena

The axion is a pseudoscalar particle predicted by S. Weinberg and F. Wilczek as a consequence of the mechanism introduced by R.D. Peccei and H. Quinn to solve the “strong CP problem”. Axions are also well-motivated dark-matter (DM) candidates with expected mass laying in a broad range from pico-electron-volts to few milli-electron-volts. Post-inflationary scenarios restrict this range to  $10 - 10^3 \mu\text{eV}$ . To probe the existence of axion some running and planned experiments use a haloscope, i.e., a detector composed of a resonant cavity immersed in a strong magnetic field. When the resonant frequency of the cavity  $\nu_c$  is tuned to the corresponding axion mass the DM axions are converted into microwave photons whose very tiny amount of power (less than a yoctowatt) scales with the volume of the cavity, its quality factor, its frequency and the square of the magnetic field.

One of the experimental limitations is the anomalous skin effect that reduces the copper cavities quality factor at high frequencies (at 10 GHz,  $Q \leq 10^5$ ) while the optimum value of the Q-factor for haloscopes is approximately  $10^6$ . A “natural” solution is represented by the superconducting cavity but the strong magnetic fields in which it is operated weakens superconductivity and is in part screened by the superconducting material.



Figure 1: One of the two halves of the superconducting cavity. The cylindrical body is 50 mm long with diameter 26.1 mm, while the cones are 19.5 mm long.

To overcome both these limitations, we designed, realized and tested a cavity (Di

Gioacchino et al. 2019) divided in two halves, each composed by a type II superconducting body (NbTi sputtered copper) and copper end caps (see Fig. 1). We have facilitated the penetration of the magnetic field in the inner cavity volume by interrupting the screening supercurrents with the insertion of a thin ( $30 \mu\text{m}$ ) copper layer between the two halves. At 4.2 K and no applied external magnetic field, we measured  $Q = 1.2 \times 10^6$  in agreement with the maximal expected value. For  $B = 2 \text{ T}$ , the nominal field used in our axion search, we measured  $Q = 4.5 \times 10^5$ , a factor of approximately 5 better than a bulk copper cavity; at 5 T we measured  $Q = 2.95 \times 10^5$ .

The cavity was mounted in the experimental site at Laboratori Nazionali di Legnaro which hosts an apparatus capable of searching for galactic axions. The scheme of the apparatus is shown in Fig. 2. The cavity is inside a vacuum chamber inserted in a 2 T superconducting magnet. The magnet and the vacuum chamber are immersed in a LHe bath at the temperature of 4.2 K. The cavity is instrumented with two antennas. A weakly coupled one is used to inject probe signals. The second one, with a variable coupling, is connected to a low noise cryogenic amplifier (A1). Before reaching the amplifier, the coaxial cable is connected to a cryogenic switch and then to an isolator. The switch, used for calibration purposes, allows the replacement of the cavity output with the output of a resistor ( $R_J$ ). The setup is completed by a second amplifier (A2) at room temperature and a down-converter mixer referenced to a local oscillator (LO). The in-phase (I) and quadrature (Q) components of the mixer output are further magnified by two identical room temperature amplifiers ( $A3_I$  and  $A3_Q$ ).

With this setup we performed the first search for galactic axions using a superconducting cavity. The frequency of the TM010 cavity mode,  $\nu = 9.07 \text{ GHz}$ , was in good agreement with the simulated value.

<sup>†</sup>Contact Author: [paolo.falferi@unitn.it](mailto:paolo.falferi@unitn.it)

Operating this setup, we set the limit  $g_{a\gamma\gamma} < 1.03 \times 10^{-12} \text{ GeV}^{-1}$  on the axion photon coupling in a frequency band of 45 kHz at  $\nu_c$  corresponding to a mass range of approximately 0.2 neV around the axion mass  $m_a \simeq 37.5 \mu\text{eV}$  (Alesini et al. 2019). This result is limited by the low magnetic field, the high system temperature, and the small cavity volume. A new experimental setup is now in preparation and consists of a dilution refrigerator, a quantum limited Josephson parametric amplifier (JPA), and an 8 T superconducting magnet. At 50 mK, with a quantum limited JPA and a 20-cm-long NbTi cavity in a 5 T magnetic field, we expect, from our measurements, a quality factor  $Q = 3.54 \times 10^5$ , a factor 4 better than a copper cavity. With this setup, the expected exclusion limit would be  $g_{a\gamma\gamma} < 4 \times 10^{-14} \text{ GeV}^{-1}$  for  $m_a \simeq 37.5 \mu\text{eV}$  a value that touches the region expected for the Kim-Shifman-Vainshtein-Zakharov (KSVZ) axions.

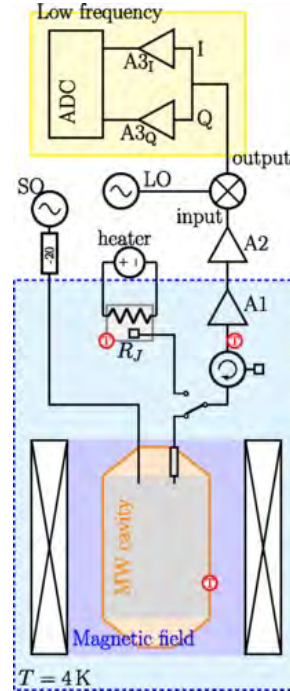


Figure 2: QUAX- $\alpha\gamma$  setup: the blue dashed line encloses the liquid helium temperature part of the apparatus, the yellow rectangle stands for the low-frequency electronics, and the red circled T's represent the thermometers. See the text for further details.

## Selected Papers

- Alesini, D., Braggio, C., Carugno, G., Crescini, N., D'Agostino, D., Di Gioacchino, D., Di Vora, R., Falferi, P., Gallo, S., Gambardella, U., Gatti, C., Iannone, G., Lamanna, G., Ligi, C., Lombardi, A., Mezzena, R., Ortolan, A., Pengo, R., Pompeo, N., Rettaroli, A., Ruoso, G., Silva, E., Speake, C. C., Taffarello, L., and Tocci, S. (2019). *Galactic axions search with a superconducting resonant cavity*. PHYSICAL REVIEW D **99**, pp. 101101–101106.
- Di Gioacchino, D., Gatti, C., Alesini, D., Ligi, C., Tocci, S., Rettaroli, A., Carugno, G., Crescini, N., Ruoso, G., Braggio, C., Falferi, P., Gallo, C. S., Gambardella, U., Iannone, G., Lamanna, G., Lombardi, A., Mezzena, R., Ortolan, A., Pengo, R., Silva, E., and Pompeo, N. (2019). *Microwave Losses in a DC Magnetic Field in Superconducting Cavities for Axion Studies*. IEEE TRANSACTIONS ON APPLIED SUPERCONDUCTIVITY **29**, pp. 1–5.

# Virgo

Albino Perego, Antonio Perreca, Giovanni Prodi,<sup>†</sup> Matteo di Giovanni, Andrea Grimaldi, Andrea Miani, Michele Valentini, Anna Puecher

The main recent achievement of LIGO-Virgo collaborations has been the successful joint observation run O3.<sup>1</sup> This gravitational wave (GW) survey lasted about one calendar year, from April 2019 to March 2020. The Advanced Virgo detector fully participated from its start, ensuring its science quality data for more than 75% of the time. At the same time, Virgo collaboration entered the preparatory phase for the next detector upgrade, Advanced Virgo + (AdV+), which is planned to be completed in time for the next joint observation run with LIGO.

**INSTRUMENT SCIENCE** Among the ongoing upgrades, Trento group focused on the implementation of the Signal Recycling (SR) technique and on the injection of Frequency Dependent Squeezed (FDS) vacuum state. Those will allow to broaden the detector bandwidth and to further reduce the shot noise contribution to GWs. Moreover, Trento group participated to the October 2019 commissioning, half way during O3.

**Interferometer Sensing and Control (ISC) for AdV+** The main contribution to the ISC activities has been towards the design and validation of the AdV+ lock acquisition strategy. Since the upgrade involves substantial modifications to the interferometer optical layout, such as the addition of the SR mirror, a complete review of the interferometer control system was needed.

The first step of this review focused on finding new accuracy requirements, i.e. residual noise thresholds needed to ensure a linear behaviour of the interferometer and its controls. Additionally, using modal simulation techniques, the interferometer has been studied both in the stable “steady state” configura-

tion, representing the state of the interferometer in the optimal working point, and in other steps of the “lock acquisition” procedure. This allowed to choose the error signals needed for the longitudinal control of the main interferometer and to study their behaviour and robustness against interferometer non-idealities, such as mirror misalignments.

**FDS activities for AdV+** One of the main changes connected to the implementation of FDS source is the installation of a new optical cavity, named Filter Cavity (FC). This new resonator adds a frequency dependent phase shift to the squeezed vacuum field and requires the design of a new optical interface between the Squeezing source, the interferometer and this new cavity. During the design of FDS, Trento focused on the issues caused by the optical losses generated by the mismatch between the squeezed vacuum field and those three systems. In particular, we collaborated with the Quantum Noise Reduction (QNR) group in order to include the mode-matching sensor into the optical design of FDS as well as with the Virgo Padua group to install the experimental setup for testing and validation.

**Commissioning activities** The commissioning activities aim to achieve an optimal interplay of the various interferometer subsystems, to maximise reliability and the duty cycle of the detector. Trento contributed to the ISC subsystem activities, with the aim of increasing the robustness of the interferometer longitudinal and angular controls and therefore to allow an increase of the injected power from 18W to 24W. The success of these activities allowed to reach 60 Mpc of BNS range sensitivity during the second part of the O3 observation run.

<sup>†</sup>Contact Author: giovanniandrea.prodi@unitn.it

<sup>1</sup>see [www.gw-openscience.org](http://www.gw-openscience.org)

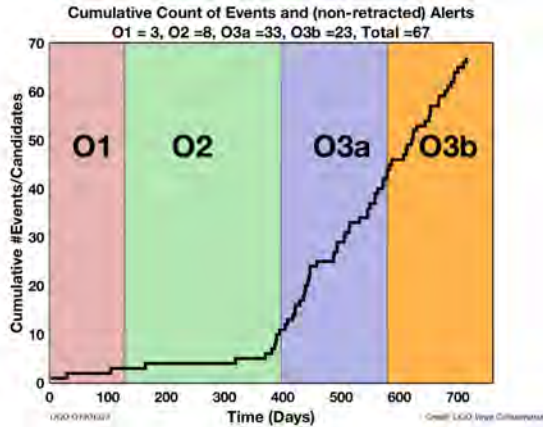


Figure 1: Number of low latency alerts for gravitational wave transients issued by LIGO-Virgo in the recent observation runs since 2015. Up to the O2 run the alerts were shared with selected partners under confidentiality agreements, while from the O3 run the alerts has been publicly released. The increased rate of alerts of O3 is a proxy of the large increase of surveyed volume of the universe.

**OBSERVATIONAL SCIENCE** Trento involvement in observational science included the coordination of Virgo data analysis activities until Nov.2019, as well as specific achievements on the search and interpretation of transient GWs.

**LIGO-Virgo observation run O3.** The main novelty deployed in the O3 observation run has been the public release of GW alerts, to enable the widest possible followup across different messengers. Fig. 1 summarizes the number of alerts which were issued by LIGO-Virgo since the first gravitational wave detection, and highlights the GW factory production reached in O3 thanks to the improved detector performances with respect to O1 and O2. Each

O3 GW alert includes: a broad classification of the source, its significance in terms of false alarm rate, the reconstructed sky position and, for compact binary coalescences, the distance. The target average purity of the alerts related to compact binary coalescences is  $\sim 90\%$ . For all other transient sources, whose astrophysical rate is yet unmeasured, the threshold for public alerts was set to a false alarm rate of  $\sim 1$  per year.

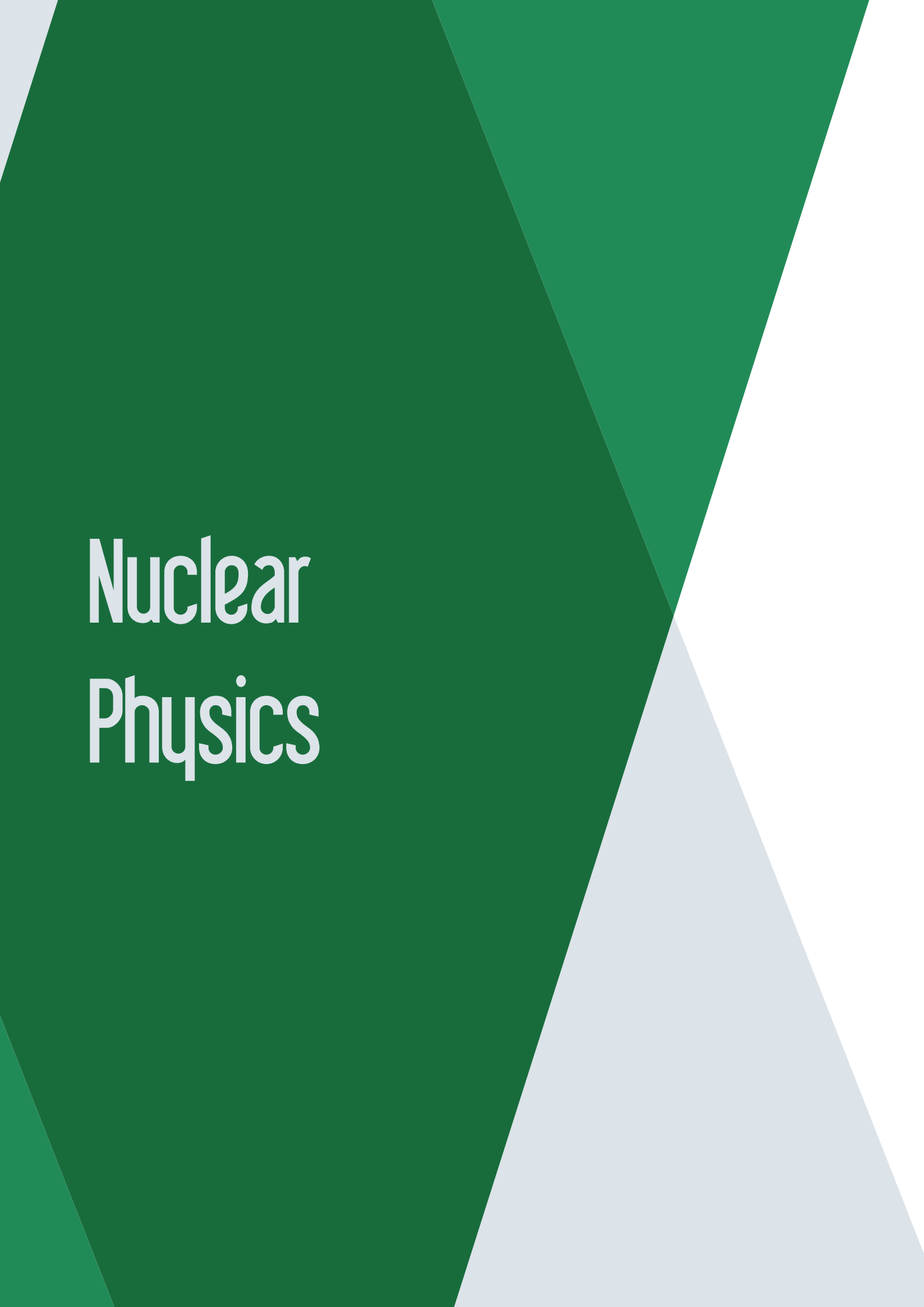
**Contribution to the study of compact binary coalescences.** Trento has been deeply involved in the low-latency and off-line analyses of the compact binary mergers detected in O3, when at least two detectors were in simultaneous observation. We developed and used the coherent WaveBurst pipeline (cWB) (Salemi et al. 2019), which provides a waveform-agnostic reconstruction of the GW events. This allows to extend the detection and interpretation capabilities of GWs beyond what is accomplished by means of accurate theoretical models of the emission. For instance, cWB can extend the LIGO-Virgo search to eccentric binary BH coalescences (Abbott et al. 2019h).

On the interpretation side, cWB enables to check for the presence of possible weak physical features over-imposed to the main GW. Some performances have been demonstrated on the published catalog of binary compact coalescences, GWTC-1 (Salemi et al. 2019). A more recent development is related to the search for possible signals closely following a binary black hole coalescence, as they may hint to unexpected remnant properties (even to violations of General Relativity) or to an-isotropic effects of the merger emission.

## Selected Papers

Abbott, B. P. et al., LIGO Scientific, Virgo (2019h). *Search for Eccentric Binary Black Hole Mergers with Advanced LIGO and Advanced Virgo during Their First and Second Observing Runs*. The Astrophysical Journal **883**(2), p. 149.

Salemi, F., Milotti, E., Prodi, G., Vedovato, G., Lazzaro, C., Tiwari, S., Vinciguerra, S., Drago, M., and Klimenko, S. (2019). *Wider look at the gravitational-wave transients from GWTC-1 using an unmodeled reconstruction method*. Physical Review D **100**(4). Art. no.: 042003.



# Nuclear Physics



# AEgIS

Sebastiano Mariazzi, Ruggero Caravita, Luca Povolo, Luca Penasa, Roberto S. Brusa<sup>†</sup>

AEgIS (Antimatter Experiment: Gravity, Interferometry, Spectroscopy) is an experiment aiming to answer the question of whether antimatter falls in the Earth's gravitational field with the same acceleration  $g$  as ordinary matter. The eventual existence of an asymmetry, in the free fall of matter and antimatter, could help to explain the apparent absence of antimatter in our world (baryonic asymmetry).

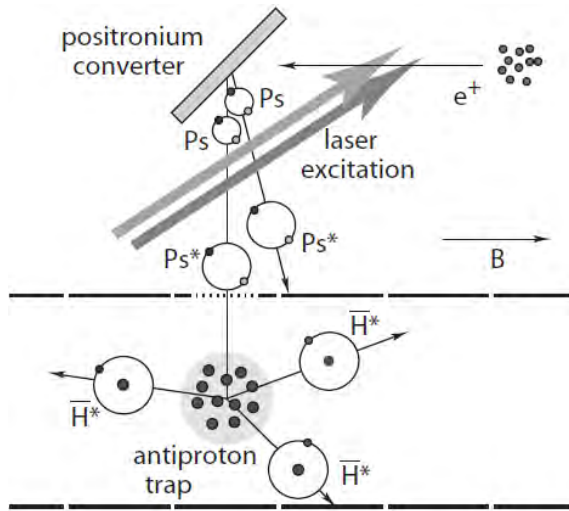


Figure 1: Scheme of the  $\bar{H}$  formation in AEgIS. The method builds on the charge exchange reaction between a burst of  $\text{Ps}^*$  and trapped  $\bar{p}$ . A cloud of Ps is formed by  $e^+$  implantation in a  $e^+/\text{Ps}$  converter. Ps emitted by the converter is laser excited to Rydberg level before reacting with trapped  $\bar{p}$ .

AEgIS is based at the antiproton decelerator (AD) at CERN and it is designed to produce an antihydrogen ( $\bar{H}$ ) pulsed beam. The gravitational acceleration  $g$  on  $\bar{H}$  will be investigated by measuring the vertical displacement of each  $\bar{H}$  after its crossing of a moire deflectometer. Antiprotons ( $\bar{p}$ ) delivered by AD are caught in a Penning-Malmberg trap in the 1 T magnet where  $\bar{H}^*$  is formed. Positrons ( $e^+$ ), produced by a  $^{22}\text{Na}$  source, are stored in a Penning-Malmberg accumulator delivering  $e^+$  bunches that are transferred to the 1 T magnet where they are injected in a  $e^+/\text{Ps}$  (positron-

ium) porous silica converter. Ps emitted by the converter are laser excited to Rydberg states by a two step-procedure. Ps is firstly excited to  $n=3$  level by an UV laser pulse and then to the final Rydberg state by an IR laser pulse.  $\text{Ps}^*$  fly into the  $\bar{p}$  trap, where  $\bar{H}$  is formed in an excited state via charge exchange reaction:  $\text{Ps}^* + e^+ \rightarrow \bar{H}^* + e^-$  (Fig. 1). After formation,  $\bar{H}^*$  is Stark accelerated to produce a beam.  $\bar{H}$  will decay to ground state along its path towards the moire deflectometer. Over the main apparatus, a chamber for R&D and experiments with Ps is connected to the  $e^+$  accumulator.

**Antihydrogen formation** In 2018, we have optimized the  $\text{Ps}^*$  production in the 1 T field. A new detection technique of Ps based on laser or field ionization of Ps emitted by the converter has been developed (Amsler et al. 2019a).  $e^+$  detached by Ps ionization have been guided with the magnetic field lines and are imaged onto an MCP (multichannel plate). The obtained spatial resolution was  $\sim 90 \mu\text{m}$ . The diagnostic technique allowed measuring the average Ps velocity along the laser direction by scanning the wavelength of the UV laser exciting the  $n=3$  level and the velocity distribution normal to the target by scanning the time delay between the  $e^+$  implantation in the target and the laser shot (Fig. 2a). Moreover, it permitted to study the self-ionization of  $\text{Ps}^*$  due to motional Stark effect in the 1 T field where the converter is installed (Fig. 2b).

On the light of the results of this study, Ps with a velocity of  $\sim 10^5 \text{ m/s}$  has been selected to be excited to  $n=17$  level (IR wavelength  $\sim 1690 \text{ nm}$ ) and employed for charge exchange reaction with  $\bar{p}$ . Measurements, running the protocol for  $\bar{H}$  formation by charge exchange, were performed at the end of 2018 before the two-year stop of AD. Pions produced by  $\bar{p}$  and  $\bar{H}$  annihilations have been detected by plastic scintillating slabs placed around the  $\bar{p}$  trap.

<sup>†</sup>Contact Author: robertosennen.brusa@unitn.it

In 2019 the acquired data have been analyzed and an excess of signal with a statistical significance larger than  $4\sigma$  has been observed within  $25\ \mu\text{s}$  from the implantation of  $e^+$  in the converter (Fig. 3).

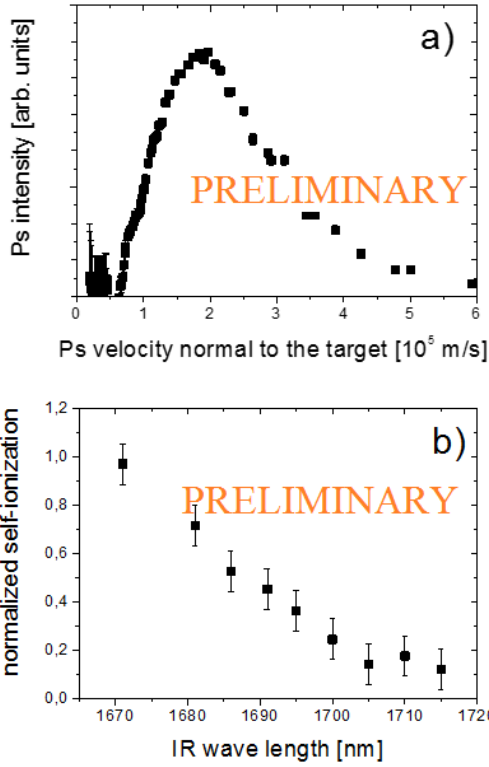


Figure 2: Ps velocity distribution normal to the target (a). Ps\* self-ionization due to motional Stark effect in 1 T as a function of the waveleth of the IR pulse used to excite Ps from  $n = 3$  to the Rydberg level (b).

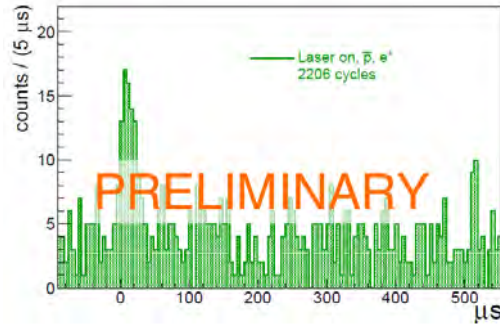


Figure 3: Time distribution of signals detected by the plastic scintillating slabs around the  $\bar{p}$  trap. The data are the result of 2206  $\bar{H}$  production cycles.

This excess is ascrivable to the  $\bar{H}^*$  escaping from the trap being no more radially confined by the magnetic field and it is consistent with the formation of around  $0.07\ \bar{H}$  per production cycle.

**$2^3S$  Ps beam** In parallel with this activity on  $\bar{H}$ , we have performed studies of production of Ps in the metastable state  $2^3S$ , in the chamber for R&D experiments on Ps (Amsler et al. 2019b; Antonello et al. 2019). A monochromatic source of  $2^3S$  with tunable velocity in the range of  $7 \cdot 10^4 - 10^5\ \text{m/s}$  has been demonstrated. By introducing an iris, a beam expanding within a solid angle of  $\sim 17\ \text{msterad}$  has been selected. The possibility to use this neutral matter/antimatter leptonic system for tests of deflectometry and measurements of forces is under investigation.

## Selected Papers

- Amsler, C. et al., AEGIS collaboration (2019a). *A  $\sim 100\ \mu\text{m}$ -resolution position-sensitive detector for slow positronium*. NIMB **457**, pp. 44–48.
- AEGIS collaboration (2019b). *Velocity-selected production of  $2^3S$  metastable positronium*. Phys. Rev. A **99**. Art. no.: 033405.
- Antonello, M. et al., AEGIS collaboration (2019). *Efficient  $2^3S$  positronium production by stimulated decay from the  $3^3P$  level*. Phys. Rev. A **100**. Art. no.: 063414.

# FOOT

Francesco Tommasino<sup>†</sup> on behalf of the FOOT Collaboration

The aim of the FOOT (FragmentatiON Of Target) experiment is the measurement of double-differential target fragmentation cross-sections in proton therapy, thus allowing improving the accuracy of proton therapy cancer treatments. In fact, target fragments originating from nuclear inelastic interactions can have high charge (i.e. high biological effectiveness) and low residual range. Thus, a biological effect might be associated to target fragments, especially in terms on normal tissue damage in the entrance channel before reaching the tumour. Due to the lack of cross section data to describe the production of target fragments, these aspects are not explicitly taken into account in current treatment planning systems. From the experimental point of view, the detection of target fragments is hindered by their low residual range, which is in order of tens of micrometers. For this reason, FOOT will adopt an inverse kinematic approach, studying the fragmentation of different ions beams (e.g. C, O, Ca) onto hydrogen enriched target, such as C<sub>2</sub>H<sub>4</sub>.<sup>1</sup> Secondary fragments will have boosted energy and longer range, making the detection easier. The choice of the inverse kinematics forces the measurement of the beam momentum in each direction: for this reason a Beam Monitor (BM) detector has been adopted in the pre-target region, which will allow the determination of the Lorentz boost to be applied to the produced fragments. The final goal of the FOOT experiment will be the measurement of the heavy fragment ( $Z > 2$ ) cross section with maximum uncertainty of 5% and the fragment energy spectrum with an energy resolution of the order of 1-2 MeV/u. The charge and isotopic identification (at the level of 3% and 5% respectively) are also important goals of this measurement. Performing the analysis in terms of direct kinematics, FOOT will also contribute

to extend and complete the measurements of projectile fragmentation cross sections induced by C and O beams. Such measurements are needed to improve the projectile fragmentation description of these beams in ion therapy as well as for shielding applications in space.



Figure 1: The exposure of one emulsion chamber at GSI in 2019.

The activities of the Collaboration during 2019 have been dedicated to the development of the experimental setup as well as to extensive testing activity on the FOOT sub-detectors (Montesi et al. 2019a; Morrocchi et al. 2019). In this context, the contribution of the TIFPA Unit was focused on the calibration of the drift chamber (i.e. the FOOT beam monitor) space-time relations by means of an external tracker (i.e. the Microstrip Silicon Detector provided by the Perugia Unit). The calibration took place in Trento based on the data acquired with a 80 and 200 MeV proton beam. This activity was important to understand the actual tracking potential of the drift chamber, which is related to the possibility to reject events affected by fragmentation events occurring before the target. A more detailed report of this activity can be found in the Section dedicated to the Experimental Area.

Remarkably, the first FOOT experimental shift took place at GSI in April 2019 in the framework of the ESA-IBER program. This was the chance to acquire the first data with

<sup>†</sup>Contact Author: francesco.tommasino@unitn.it

<sup>1</sup>Dudouet, J. et al. (2013), Phys Rev C **88**, Art. no.: 064615.

Webber, W. et al. (1990), Phys Rev C **41**, p. 547.

the Emulsion Setup by exposing the emulsion chambers to either a 200 or 400 MeV/u Oxygen beam (see Fig. 1). The analysis of the emulsion data is currently on-going and the first results are expected in 2020. In parallel, the GSI shift gave the opportunity to test the global data acquisition software on a partial electronic setup with a 400 MeV/u Oxygen beam (Fig. 2). The partial electronic setup was composed by the Start Counter detector and the Beam Monitor, the Vertex Detector and the TOF wall. The data acquired during the test beam will be used to optimize both the hardware and software performances of the FOOT sub-detectors. Additional test beam are scheduled for 2020.

Finally, during 2019 the TIFPA unit started

## Selected Papers

Montesi, M. et al. (2019a). *Ion charge separation with new generation of nuclear emulsion films*. *Open Physics* **17**(1), pp. 233–240.

Morrocchi, M. et al. (2019). *Development and characterization of a  $\Delta E$ -TOF detector prototype for the FOOT experiment*. *NIM-A* **916**, pp. 116–124.

to be involved in the FOOT global analysis, especially for what concerns the study of the global reconstruction performances and the sensitivity of the cross section estimation on TOF, momentum and kinetic energy resolution.

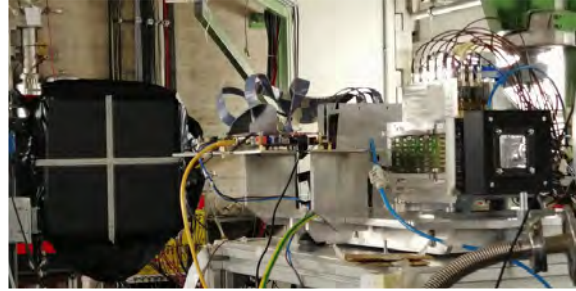
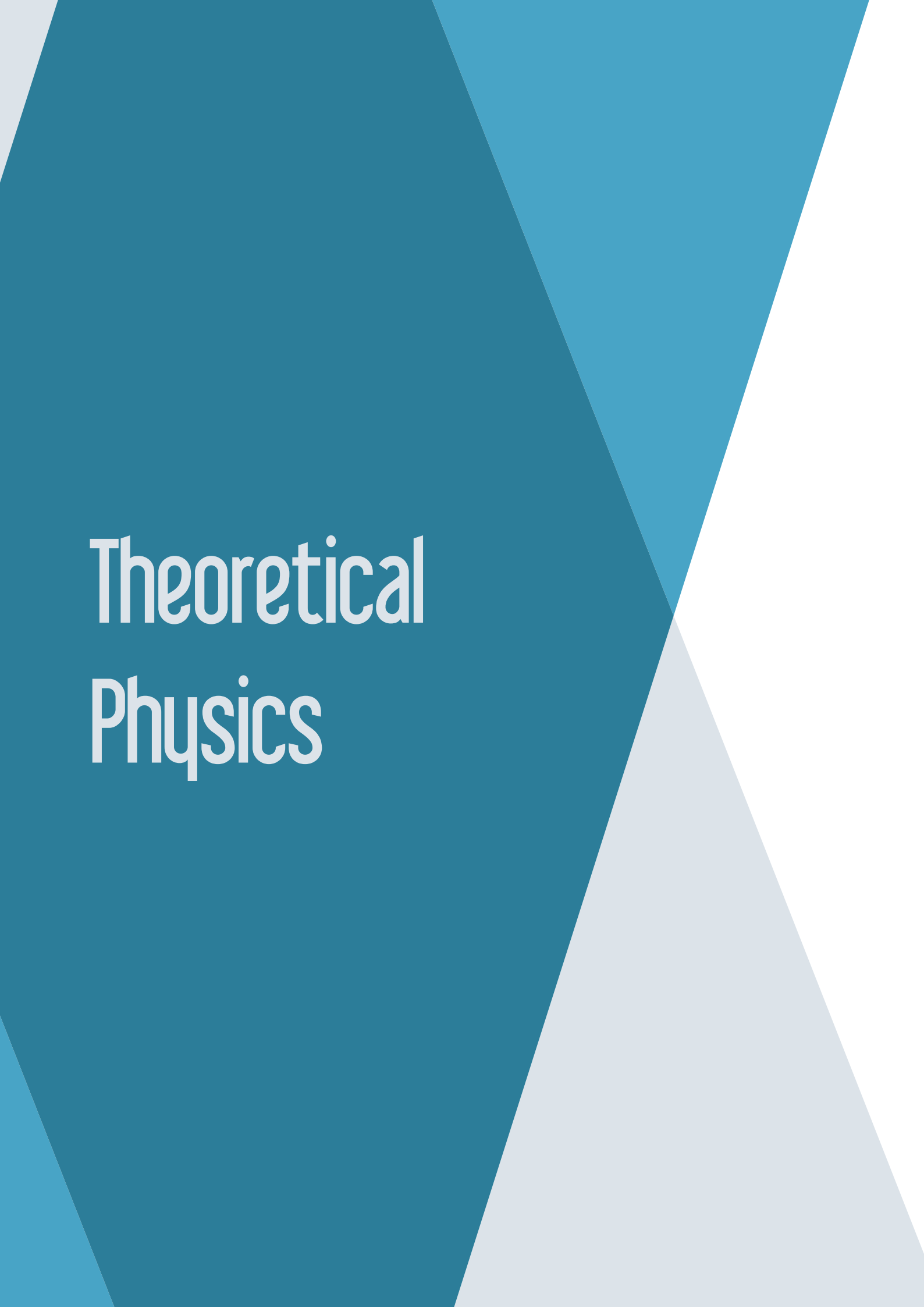


Figure 2: The partial FOOT electronic setup during the test beam at GSI in 2019.



# Theoretical Physics



# BELL

Valter Moretti,<sup>†</sup> Riccardo Ghiloni, Sonia Mazzucchi, Alessandro Perotti, Davide Pastorello, Niccolò Cangini, Chris van de Ven

BELL research group at TIFPA studies various foundational, axiomatic and mathematical topics of Quantum Theories, also in relation with quantum field theory and quantum gravity. Mathematical advanced technologies are exploited to solve difficult problems of theoretical physics or to construct physically significant, non-trivial, mathematical models, completely solvable which can be used as starting points for physical applications. During 2018-2019 we published several research papers on international research journals, two monographies. Just to have a (not exhaustive) look of our intensive production we focus attention on four relevant papers about four corresponding topics of mathematical methods for physics.

**Functional Integration Methods for Physical Theories** In the paper (Albeverio et al. 2020) by S. Albeverio, N. Cangini and S. Mazzucchi, in press in *Communications in Mathematical Physics*, a Feynman path integral formula for the Schrödinger equation with magnetic field is rigorously mathematically realized in terms of infinite dimensional oscillatory integrals. The work proves (by the example of a linear vector potential) that the requirement of the independence of the integral on the approximation procedure forces the introduction of a counterterm to be added to the classical action functional. This provides a natural explanation for the appearance of a Stratonovich integral in the path integral formula for both the Schrödinger and heat equation with magnetic field.

**Quantum Field Theory in algebraic approach** N. Drago and V. Moretti addressed in (Drago and Moretti 2020) some usually overlooked issues concerning the use of  $*$ -algebras in quantum theory and their physical interpretation. If  $A$  is a  $*$ -algebra describing a quantum system

and  $\omega$  a state, they focus in particular on the interpretation of  $\omega(a)$  as expectation value for an algebraic observable  $a = a^* \in A$ , studying the problem of finding a probability measure reproducing the moments  $\omega(a^n)$ . This problem enjoys a close relation with the self-adjointness of the (in general only symmetric) operator  $\pi_\omega(a)$  in the GNS representation of  $\omega$  and thus it has important consequences for the interpretation of  $a$  as an observable. The paper provides physical examples (also from QFT) where the moment problem for  $\omega(a^n)$  does not admit a unique solution. To reduce this ambiguity, we consider the moment problem for the sequences  $\omega_b(a^n)$ , being  $b \in A$  and  $\omega_b(\cdot) := \omega(b^* \cdot b)$ . Letting  $\mu_{\omega_b}^a$  be a solution of the moment problem for the sequence  $\omega_b(a^n)$ , we introduce a consistency relation on the family of the said measures. We prove a 1 – 1 correspondence between consistent families  $\mu_{\omega_b}^a$  and positive operator-valued measures (POVM) associated with the symmetric operator  $\pi_\omega(a)$ . In particular there exists a unique consistent family of  $\mu_{\omega_b}^a$  if and only if  $\pi_\omega(a)$  is maximally symmetric. This result suggests that a better physical understanding of the notion of observable for general  $*$ -algebras should be based on POVMs rather than projection-valued measure (PVM).

**Foundational Aspects of Quantum Theories** The paper (Landsman et al. 2020), by K. Landsman, Valter Moretti and C. van de Ven, in press in *Reviews in Mathematical Physics*, concerns some open problems with the notion of quantization procedure in a rigorous sense (strict quantization procedure). In the paper below the problem of strict quantization of matrix models has been investigated in any dimension discovering a new quantization map which associates quantum observables to classical observables defined on a suitable Poisson manifold preserving the Poisson structure in par-

<sup>†</sup>Contact Author: [valter.moretti@unitn.it](mailto:valter.moretti@unitn.it)

ticular. That map has been next exploited to study the classical limit of the so-called Curie-Weiss model (a mean-field approximation of the quantum Ising model) proving that the classical limit exists (for a large number of the sites) and it is characterized by the spontaneous breaking of the  $Z_2$  symmetry. The analysis has been performed either from a purely theoretical point of view and also using computational procedures.

**Quantum Information** In the paper (Blanzieri and Pastorello 2019), by E. Blanzieri and D. Pastorello, a novel strategy to solve optimization problems within a hybrid quantum-

classical scheme based on quantum annealing is presented, with a particular focus on QUBO problems. The proposed algorithm implements an iterative structure where the representation of an objective function into the annealer architecture is learned and already visited solutions are penalized by a tabu-inspired search. The result is a heuristic search equipped with a learning mechanism to improve the encoding of the problem into the quantum architecture. We prove the convergence of the algorithm to a global optimum in the case of general QUBO problems. Our technique is an alternative to the direct reduction of a given optimization problem into the sparse annealer graph.

## Selected Papers

- Albeverio, S., Mazzucchi, S., and Cangioni, N. (2020). *A rigorous mathematical construction of Feynman path integrals for the Schrödinger equation with magnetic field*. Commun. Math. Phys. **374**.
- Blanzieri, E. and Pastorello, D. (2019). *Quantum Annealing Learning Search for solving QUBO problems*. Quantum Information Processing **18**, p. 303.
- Drago, N. and Moretti, V. (2020). *The notion of observable and the moment problem for \*-algebras and their GNS representations*. Lett. Math. Phys.
- Landsman, K., Moretti, V., and Ven, C. van de (2020). *A Strict Deformation Quantization Map on the state space of  $M_k(\mathbb{C})$  and the Classical Limit of the Curie-Weiss model*. Reviews in Mathematical Physics **32**. Art. no.: 1950013.

# BIOPHYS

Gianfranco Abrusci, Pietro Faccioli,<sup>†</sup> Giovanni Garberoglio, Marco Giulini, Gianluca Lattanzi, Roberto Menichetti, Lorenzo Petrolli, Raffaello Potestio, Thomas Tarenzi, Luca Tubiana, Marta Rigoli, Michele Turelli, Luigi Zanovello

The BIOPHYS unit of TIFPA focuses on developing, testing and applying advanced theoretical methods to investigate dynamics in complex molecular systems, by combining advanced statistical mechanics, data modeling and large scale computer simulations. While our main focus is on biological and biomimetic molecular systems, we are also involved in a number of cross disciplinary scientific collaborations focusing on diverse topics, ranging from theory of open quantum systems to material science, network dynamics and, more recently, to data science and machine learning. All our projects are carried out in direct contact with experimental teams, operating in physics, chemistry and molecular biology laboratories, within the framework of international collaborations.

**Multiscale resolution modeling and multiple-coarse-graining methods**

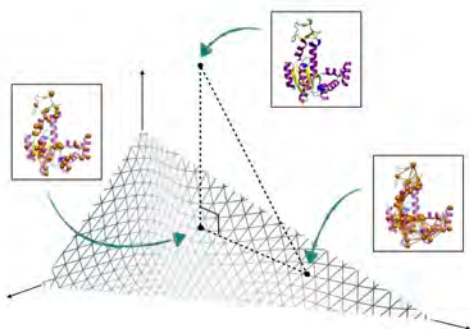


Figure 1: Example of variable resolution modeling

One of the core activities of this unit is the development of various methods to coarse-grain proteins retaining different levels of resolution in different regions, in order to provide the highest detail only where necessary. This is the overarching objective of ERC VARIAMOL project, which combines fundamental statisti-

cal mechanics methods and advanced molecular modelling approaches to improve our understanding of the underpinnings of coarse-graining on the one hand, and of the relationship between structure, dynamics and function of biomolecules on the other. During the year 2019 the TIFPA unit has published 4 papers on this topic, tackling different aspects of the problem.

**Self-entangled polymers and topologically non-trivial materials** Another research line of the group focuses on the relation between the topological entanglement of a protein in the native state and its folding process. A work on this topic, resulted in a publication on the Biophysical Journal, has shown, by means of a simple coarse-grained model, that different pH conditions, affecting the opening or closure of cysteine bonds in a protein featuring a lasso topology, shift the relative population of alternative folding pathways. Still on the topic of knotted and self-entangled proteins, this unit has published a review on the computational methods employed to investigate these systems.

**Enhanced path sampling for macromolecular transitions** A number of results obtained in 2019 contributed to build confidence that the enhanced path sampling techniques developed in our group over the last decade provide a realistic representation of the sequence of microscopic events involved in rare conformational transitions of proteins. In particular, we performed a direct and accurate comparison with the results of protein folding simulations generated by plain MD on the largest special purpose supercomputing and by direct comparison with experimental results obtained by means of different ensemble and single-molecule spec-

<sup>†</sup>Contact Author: [pietro.faccioli@unitn.it](mailto:pietro.faccioli@unitn.it)

troscopy, in collaboration with the experimental team led by Prof. B. Schuler at U. Zurich. These results are being finalized in a manuscript to be shortly submitted for publication. We then applied these methods, along with plain MD simulations, to study different problems at the interface between biophysics and molecular biology. These projects involved the study of ion transport in aquaporin membrane proteins and the study of incorporation of cellular prions (PrP<sup>c</sup>) into aberrant and toxic prions (PrP<sup>Sc</sup>) responsible for pathogenic fibrils.

**Target searching by active matter** Active particles represent a prototype of intrinsically out of equilibrium systems. On the one hand, they can be used as platform to develop and test theoretical and computational tools to study statistical mechanics of systems in far from equilibrium conditions. On the other hand, modeling active systems can bring important insight into many biological problems including, e.g. bacterial motion. In 2019 the TIFPA group started a collaboration with the Theoretical Physics Department of Innsbruck University aiming at adapting the enhanced sampling techniques developed in Trento to study rare transitions undergone by active particles. This project is completed and a manuscript is being sent for publication.

**Data science for molecular simulations** The huge amount of data emerging from molecular simulations must be reduced in order to extract the relevant information, in particular the sequence of metastable state which are visited during conformational changes, such as e.g. protein folding. Within a collaboration with SISSA, we have developed and tested an unsupervised scheme to perform reliable data reduction of molecular simulation based on combining elements of statistical mechanics of activated processes, differential geometry and theory of stochastic processes.

**Pharmacological applications of protein folding simulations** The computational techniques developed by the TIFPA unit of BIOPHYS enables us to accurately predict the structure

of protein folding intermediates, for chains of size of several hundred amino-acids and folding times as long as minutes. This technological advancement enabled us to envision, apply and experimentally validate an entirely new approach to Rational Drug Discovery denominated Pharmacological Protein Inactivation by Folding Intermediate Targeting (PPI-FIT). This approach has been filed for international patent led to the discovery of pharmacologically active small molecules able to inhibit the cellular expression of a protein previously considered undruggable.

**Allosteric networks and conformational changes in membrane proteins** The BIOPHYS group has constantly applied atomistic molecular dynamics simulations to the investigation of several membrane proteins. Within this year 2019, the focus has definitely shifted towards the development of analysis tools aimed at elucidating the complex network of interactions within a protein structure (allosteric networks) and, in particular, how lipid molecules within the membrane take part into the network. The new tool will be made freely available within the PyIntergraph framework, in collaboration with the University of Verona. In addition, different biasing strategies have been explored to obtain and validate conformational changes in membrane proteins.

**Radiation damage** The BIOPHYS group has recently started a new research line aimed at characterizing radiation damage from small structures (molecular level) to entire cells. In particular, we have challenged the widely employed software suite Geant4 to track radiation damage at the level of single nucleosomes. The insights obtained. within this analysis have contributed to shed light on how radiation damage is usually hypothesized in the context of radiation biophysics. In addition, we have challenged another software package, CellSim3D, which was originally developed to investigate cell replication. In collaboration with the Western University (Canada) and the Institute of Macromolecular Compounds, Russian Academy of Science, we successfully contributed to im-

plement in CellSim3D a novel feature that simulates cell death after radiation exposure. The results of our simulations were compared with experimental results from tumor treatments.

**Dynamics in mixed classical-quantum systems** In the past years, the BIOPHYS unit has developed a theoretical framework to investigate the non-equilibrium dynamics of open systems composed by a mixture of classical and quantum degrees of freedom. This method is based on combining quantum field theory and theory of stochastic processes and enables to obtain quantitative predictions by combining analytical methods with numerical simulations. In the past, this scheme was applied to study exciton transport in photosynthetic complexes

and diffusion of heavy quarks and anti-quarks in super hot strongly interacting matter (Quark-Gluon Plasma). We have started a collaboration with the BEC centre in which these methods are applied to investigate the dynamics of heavy impurities in fermionic ultracold atomic baths.

In 2019 the BIOPHYS unit has also developed a path-integral method to calculate the second dielectric virial coefficient of non-degenerate quantum gases. This approach was validated by comparing the results with more traditional wavefunction-based methods. We also developed a time-dependent density-functional approach to investigate the dynamics of an impurity (polaron) in a one-dimensional Fermi gas interacting with contact potential and subject to external trapping.

# FBS

Giuseppina Orlandini<sup>†</sup>, Paolo Andreatta, Elena Filandri, Winfried Leidemann

In 2019 we have devoted our attention to three research projects. The results of all three lines have been presented at the biennial 2019 European Few-body conference EFB24 (Filandri et al. 2020).

In continuation of our research line that mainly consists of application of the Lorentz integral transform (LIT) method,<sup>1</sup> in (Efros et al. 2019) we have studied a specific inversion problem discussed in the literature.<sup>2</sup> It concerns the  $^3\text{He}$  photodisintegration, where the nucleon-nucleon interaction is described by a hypercentral potential plus a Coulomb force between the two protons. As a matter of fact in their work the authors came to the conclusion that the inversion of the LIT leads to unreliable results. In our work (Efros et al. 2019) we have pointed out that certain rules have to be obeyed in the inversion process, rules that were not taken into account and that consequently, led to such unreliable results. We have proved that also in this case the LIT inversion can be made in a reliable way.

Another direction of our research, initiated a few years ago, concerns the physics of cluster nuclei described within the so-called “halo-EFT”. It consists in considering  $\alpha$ -particles and neutrons as effective degrees of freedom. The  $\alpha - \alpha$  and the  $\alpha - n$  interactions are described in effective field theory (EFT), where in both cases, the experimental values for scattering length and effective range are reproduced for a given cutoff. Since our EFT potentials are defined in momentum space, a computer code had to be developed, based on a non-symmetrized

hyperspherical harmonics (NSHH) expansion in momentum space. Such a code has been realized by Paolo Andreatta (PhD in 2019). In his thesis, after checking its validity in various benchmark tests, he considered the Borromean nucleus  $^9\text{Be}$  and could show a large cutoff dependence (see Fig. 1) that suggests the necessity of three-body forces. A new PhD student (Elena Filandri) is continuing the work in such a direction.

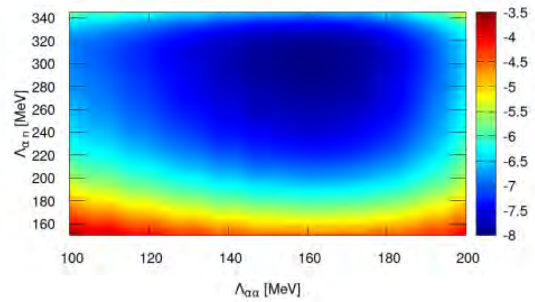


Figure 1: Heatmap showing the ground state energy of  $^9\text{Be}$  with the cluster EFT potential for different cutoffs  $\Lambda_{\alpha\alpha}$  and  $\Lambda_{\alpha n}$

The  $^9\text{Be}$  system is the object of particular interest in nucleosynthesis studies. In fact the inverse of the photodisintegration of  $^9\text{Be}$  in two  $\alpha$  particles and one neutron ( $\alpha + \alpha + n \Rightarrow ^9\text{Be} + \gamma$ ) could represent a way for a possible explosive nucleosynthesis of  $^{12}\text{C}$ . The LIT approach allows to tackle this reaction and this project has started with an MSc thesis (Francesca Bonaiti).

Our interest has not been restricted to  $^9\text{Be}$ . In fact we can tackle also alpha-nuclei with up to six  $\alpha$  particles with a possible further increase of the particle number in future.

## Selected Papers

Efros, V. D., Leidemann, W., and Shalamova, V. Y. (2019). *On Calculating Response Functions Via Their Lorentz Integral Transforms*. *Few-Body Systems* **60**, 35a–35g.

Filandri, E., Andreatta, P., Manzata, C. A., Ji, C., Leidemann, W., and Orlandini, G. (2020). *Beryllium-9 in cluster effective field theory*. *SCiPost Phys. Proc.* **3**, pp. 34.1–34.9.

<sup>†</sup>Contact Author: giuseppina.orlandini@unitn.it

<sup>1</sup>Efros, V. D. et al. (1994), *Physics Letters B* **338**, pp. 130–133.

<sup>2</sup>Suzuki, Y. et al. (2010), *Prog. Theor. Phys.* **123**, pp. 547–568.

# FLAG

Luciano Vanzo,<sup>†</sup> Massimiliano Rinaldi, Alessandro Casalino, Silvia Vicentini, Simon Boudet, Samuele Marco Silveravalle

Most of the research activity 2018 focussed on the research areas described below.

## Quantum corrections to scale invariant models of inflation

We resolved the question of one-loop quantum corrections to a scale invariant inflationary model previously investigated by Vanzo and Rinaldi. In this model, quadratic gravity plays along a scalar field in such a way that inflation begins near the unstable point of the effective potential and it ends at a stable fixed point, where the scale symmetry is broken and a fundamental mass scale naturally emerges. We computed the one loop corrections to the classical action on the curved background of the model and we report their effects on the classical dynamics with both analytical and numerical methods (M. Rinaldi et al. 2019). Fig. 1 illustrates the general behaviour we founded by solving numerically the equations and the renormalization group equation.

## The theory of regular Black holes and the echoes

We presented a unified approach for the study of idealized gravitational compact objects like wormholes and horizon-less stars, here simulated by the presence of boundary conditions at a deeply inner wall. At the classical level, namely neglecting quantum effects, the presence of the wall leads to characteristic echoes following the usual ringdown phase, such that it can discriminate black holes from other horizon-less, and probably exotic, compact objects. With regard to this issue, an analytical though approximated expression for the complex frequencies of the quasi-normal echoes is found and discussed. At the quantum level, we showed that static wormholes do not radiate (Sebastiani et al. 2019).

## Horndeski theories, mimetic gravity and applications

In the work (Casalino et al. 2019), the near-simultaneous multi-messenger detection of the gravitational wave (GW) event GW170817 and its optical counterpart, the short  $\gamma$ -ray burst GRB170817A, implies that deviations of the GW speed from the speed of light are restricted to being of  $\mathcal{O}(10^{-15})$ . We have studied the implications of this bound for mimetic gravity and confirmed that in the original setting of the theory, GWs propagate at the speed of light, hence ensuring agreement with the recent multi-messenger detection. A higher-order extension of the original mimetic theory, appearing in the low-energy limit of projectable Hořava-Lifshitz gravity, was then considered. Performing a Bayesian statistical analysis where we compared the predictions of the higher-order mimetic model for the speed of GWs against the observational bound from GW170817/GRB170817A, we derived constraints on the three free parameters of the theory. Imposing the absence of both ghost instabilities and superluminal propagation of scalar and tensor perturbations, we found very stringent 95% confidence level upper limits of  $\sim 7 \times 10^{-15}$  and  $\sim 4 \times 10^{-15}$  on the coupling strengths of Lagrangian terms of the form  $\nabla^\mu \nabla^\nu \phi \nabla_\mu \nabla_\nu \phi$  and  $(\square \phi)^2$  respectively, with  $\phi$  the mimetic field. We discussed implications of the obtained bounds for mimetic theories. This work presents the first ever robust comparison of a mimetic theory to observational data.

## The nature of dark energy (and possibly of dark matter)

We considered a model of dark matter fluid based on a sector of Horndeski gravity. The model is very successful, at the background level, in reproducing the evolution of the Universe from early times to today. However, at the perturbative level the model fails.

<sup>†</sup>Contact Author: [luciano.vanzo@unitn.it](mailto:luciano.vanzo@unitn.it)

To show this, we used the code *hi class* and we computed the matter power spectrum and the cosmic microwave background spectrum. Our results confirm, in a new and independent way, that this sector of Horndeski gravity is

not viable, in agreement with the recent constraints coming from the measurement of the speed of gravitational waves obtained from the observation of the neutron star merger event GW170817 (Casalino and M. Rinaldi 2019).

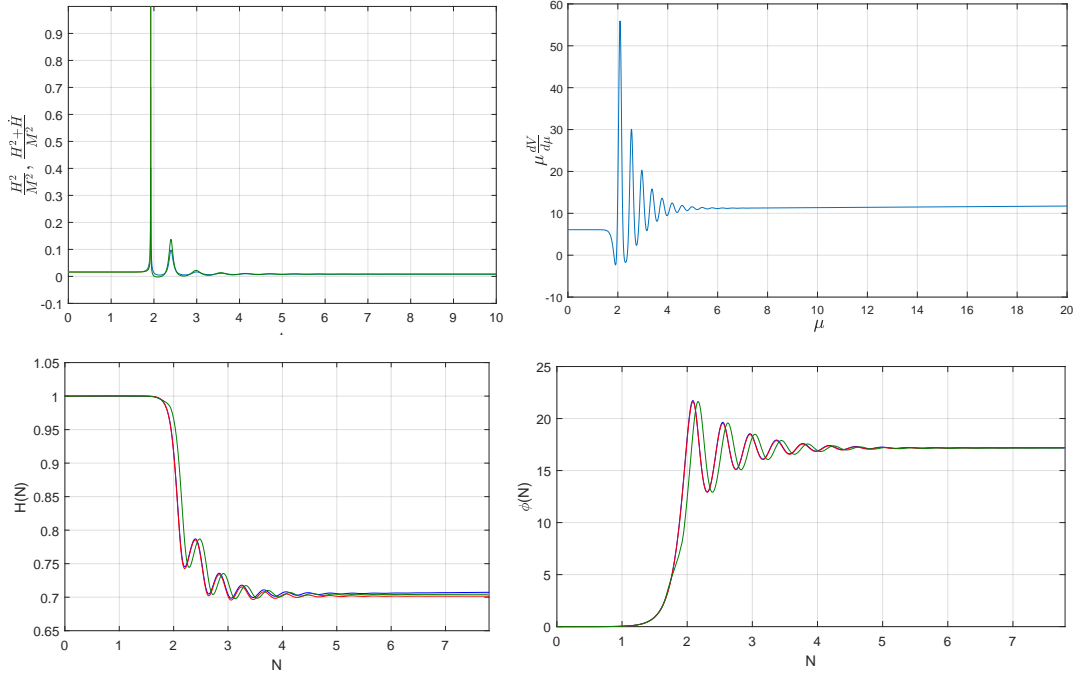


Figure 1: **Top left:** validity of the adiabatic approximation. The peak around  $N = 2$  denotes that the approximation fails. **Top right:** plot of  $\mu \frac{d\Gamma}{d\mu}$  in the pseudo-optimal energy scale choice as a function of the number of  $e$ -foldings. **Bottom left:** evolution of  $H(N)$  from the unstable point to the stable one. The blue line is the classical evolution, the green line is the one-loop corrected one, and the red line is the one-loop corrected one implemented with the pseudo-optimal energy scale. In the classical numerical solution, couplings are chosen as  $\xi = 15$ ,  $\lambda = 0.1$  and  $\alpha = \frac{\xi^2}{\lambda}$  and these are the initial values to solve the renormalization group equations. **Bottom right:** evolution of  $\phi(N)$ , with the same conventions as in the bottom left plot.

## Selected Papers

- Casalino, A. and Rinaldi, M. (2019). *Testing Horndeski gravity as dark matter with hi-class*. Phys. Dark Univ. **23**. Art. no.: 100243.
- Casalino, A., Rinaldi, M., Sebastiani, L., and Vagnozzi, S. (2019). *Alive and well: mimetic gravity and a higher-order extension in light of GW170817*. Class. Quant. Gravity **36**. Art. no.: 017001.
- Rinaldi, M., Vanzo, L., and Vicentini, S. (2019). *Scale-invariant inflation with 1-loop quantum corrections*. PHYS. REV. D **D99**. Art. no.: 103516.
- Sebastiani, L., Vanzo, L., and Zerbini, S. (2019). *On a WKB formula for echoes*. Int. J. of Geom. Methods in Physics **16**. Art. no.: 1950181-1.

# MANYBODY

Francesco Pederiva,<sup>†</sup> Alessandro Lovato, Maurizio Dapor, Simone Taioli, Hilla de Leon, Piero Luchi, Luca Riz, Francesco Turro

The TIFPA unit of the MANYBODY collaboration pursues development and applications of quantum many-body techniques to both systems of interest for nuclear physics and nuclear astrophysics (Lovato, Taioli, de Leon, Luchi, Riz, Turro, Pederiva), and applications to condensed matter physics and nuclear medicine (Dapor, Taioli). The methods toolbox is quite diverse, ranging from Quantum Monte Carlo and transport Monte Carlo to density functional theory and direct diagonalization of the Hamiltonian. Recently a particular emphasis has been given to the development application of quantum computing techniques for the quantum many-body problem (Turro, Luchi, Taioli, Pederiva).

The proper interpretation of neutrino-oscillation experiments requires accurate theoretical calculations of neutrino-nucleus scattering cross sections. We carried out GFMC calculations of the charged-current response functions of  $^{12}\text{C}$ , based on realistic treatments of nuclear interactions and currents, for momentum transfer ranging from  $q = 100$  MeV to  $q = 700$  MeV. We then computed the flux-folded neutrino-nucleus scattering cross sections relevant for MiniBooNE and T2K experiments. We found that both nuclear correlations and two-body currents are crucial in providing an accurate description of experimental data in the quasi-elastic regime. A paper in this work is in preparation and will soon be submitted.

The charged-changing currents used above, are constrained to the empirical value of the Gamow-Teller matrix element in tritium.

To validate them at larger values of momentum transfer, we have devised a quantum Monte Carlo framework to compute the muon-capture rate of light nuclei, focusing initially on  $^3\text{H}$  and  $^4\text{He}$ . At first, we compute the charged-current responses on a fine grid of momentum transfers, ranging from  $q = 10$  MeV to  $q = 110$  MeV.

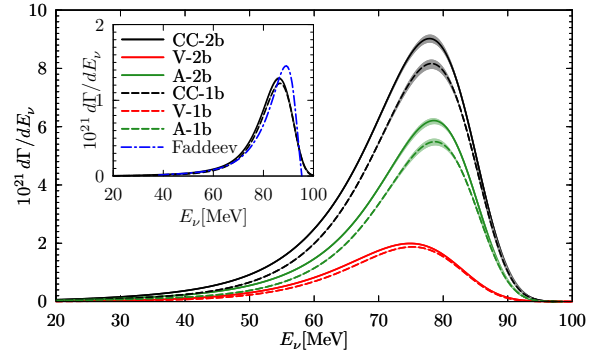


Figure 1: The  $^4\text{He}$  differential rates obtained with one-body (1b) only and both one- and two-body (2b) terms in the vector (V) and axial (A) components of the charge-changing (CC) weak current, and full CC current, are displayed as function of the neutrino energy  $E_\nu$ . The theoretical uncertainties resulting from combining statistical errors in the GFMC calculation with errors associated with the maximum-entropy inversion of the imaginary time data are shown by the bands. The full CC 1b and 2b results for  $^3\text{H}$  are compared to the Faddeev CC 1b results in the inset.

The differential capture rate is estimated by interpolating them at energy transfer  $\omega = m_p - m_n - E_\nu$  and momentum transfer  $q = E_\nu$ , with  $m_n$  ( $m_p$ ) being the neutron (proton) mass and  $E_\nu$  the energy of the outgoing neutrino.

Results for  $^4\text{He}$  obtained by considering only the vector (V) or axial (A) components of the charge-changing (CC) weak current and by including one-body (1b) terms only or both one- and two-body (2b) terms in these currents are shown separately in Fig. 1. For  $^3\text{H}$ , only the full CC 1b and 2b GFMC, and full CC 1b Faddeev differential rates are displayed in the inset.

The total capture rate  $\Gamma$  is obtained by integrating the differential energy over  $E_\nu$ . Note that because of the interference between the matrix elements of the V and A currents it turns out that  $\Gamma(\text{CC}) > \Gamma(\text{V}) + \Gamma(\text{A})$ . We find that two-body currents increase the total inclusive capture rate by about 15%, bringing its value from  $265 \pm 9 \text{ s}^{-1}$  to  $306 \pm 9 \text{ s}^{-1}$ . On the other hand, we explicitly checked that the total rate

<sup>†</sup>Contact Author: francesco.pederiva@unitn.it

is only marginally affected (at a fraction of a 1% level) by changes in the parametrization of the nucleon axial form factor. Our predicted value is consistent with the lower range of available experimental determinations. However, these measurements from bubble chamber experiments of the late 60's have large errors, making it impossible to establish, at a quantitative level, the validity of the model for the nuclear charge-changing weak current we have adopted here. As for  ${}^3\text{H}$ , the 1b GFMC and Faddeev integrated rates are in excellent agreement with each other: the GFMC 1b result is  $32.4(6) \text{ s}^{-1}$ , to be compared to the  $32.6 \text{ s}^{-1}$ . Two-body currents increase the total rate to  $35.1(9) \text{ s}^{-1}$ . A paper describing this work has been published on Physical Review C (Lovato et al. 2019)

The GFMC is not ideally suited to describe neutrino-nucleus reaction mechanisms occurring at much larger energy transfers than those corresponding to quasi-elastic kinematics. To tackle this challenge, over the past years, we have extended the factorization scheme, based on the impulse approximation and the spectral function formalism, to allow the description of electromagnetic nuclear interactions driven by two-nucleon currents. This year, we included two-body weak charged and neutral currents, and carried out calculations of the double-differential neutrino-carbon and neutrino-oxygen cross sections using two different models for the spectral function of the target nucleus. Our results, showing a moderate dependence on the input spectral function, confirm that our approach provides a consistent treatment of all reaction mechanisms contributing to the signals detected by accelerator-based neutrino experiments (Rocco et al. 2019[a]). We have then further extended the factorization

scheme to investigate electroweak pion production on  ${}^{12}\text{C}$ , one of the main reaction mechanisms for neutrinos with energies of a few GeV, such as those expected in the DUNE beam. The ANL-Osaka amplitudes are used to generate the matrix elements of current operators relevant to pion-production off the nucleon. Medium effects on the  $\Delta(1232)$  component of meson-exchange current are included by using a  $\Delta$ -nucleus potential determined from the previous  $\Delta$ -hole model studies of pion-nucleus reactions. Nuclear correlations in the initial target state and in the spectator system(s) are modeled using realistic hole spectral functions. As a first step, we show that inclusive electron scattering data of  ${}^{12}\text{C}$  up to the  $\Delta(1232)$  region can be described reasonably well. We also made predictions for neutrino —  ${}^{12}\text{C}$  inclusive cross sections that are immediately relevant for the analysis of the MiniBooNE and MINER $\nu$ a accelerator-neutrino experiments. A paper on this work has been published on Physical Review C (Rocco et al. 2019[b]).

One of the important activities that have been ramping up in the MANYBODY group in the last year is related to the application of quantum computing techniques to study of nuclear reactions, in collaboration with the Quantum Coherent Device and Nuclear Theory groups at LLNL (USA). In particular, in Trento we are pursuing two research lines. The first concerns the possibility to exploit unitary transformations to study the ground state of a many-body system (Turro, Pederiva). The second aims to find an efficient procedure, based on machine learning techniques, to implement the control pulses to generate arbitrary, parametrized unitary transformations (reconfigurable gates) used on the LLNL quantum testbed (Luchi, Taioli, Turro, Pederiva).

## Selected Papers

- Lovato, A., Rocco, N., and Schiavilla, R. (2019). *Muon capture in nuclei: An ab initio approach based on Green's function Monte Carlo methods*. PHYSICAL REVIEW C **100**(3). Art. no.: 035502.
- Rocco, N., Barbieri, C., Benhar, O., De Pace, A., and Lovato, A. (2019[a]). *Neutrino-nucleus cross section within the extended factorization scheme*. PHYSICAL REVIEW C **99**(2). Art. no.: 025502.
- Rocco, N., Nakamura, S. X., Lee, T.-S. H., and Lovato, A. (2019[b]). *Electroweak pion production on nuclei within the extended factorization scheme*. PHYSICAL REVIEW C **100**(4). Art. no.: 045503.

# NEMESYS

Simone Taioli,<sup>†</sup> Maurizio Dapor

The research topics carried out in 2019 moved along three different lines. First, we proposed an analogue gravitational system to study the behaviour of quantum systems in curved space-time (Morresi et al. 2019). Typically, setups are based on ultracold quantum gases, which have been recently harnessed to explore the thermal nature of Hawking’s and Unruh’s radiation that was theoretically predicted almost 50 years ago. For solid state implementations, a promising structure is graphene, in which a link between the Dirac-like low-energy electronic excitations and relativistic quantum field theories has been unveiled soon after its discovery. In this work we show that this link extends to the case of curved quantum field theory when the graphene sheet is shaped in a surface of constant negative curvature, known as Beltrami’s pseudosphere (see Fig. 1). Thanks to large-scale simulations, we provide numerical evidence that energetically stable negative curvature graphene surfaces can be realized; the ratio between the carbon-carbon bond length and the pseudosphere radius is small enough to allow the formation of an horizon; and the associated Local Density Of States evaluated at horizon’s proximity has a thermal nature with a characteristic temperature of few tens of Kelvin. Such findings pave the way to the realization of a solid-state analogue in which the curved spacetime dynamics of quantum many body systems can be investigated.

The very same approach to tile the hyperbolic membrane by a defected graphene sheet has been used also to propose a few novel energetically and dynamically stable all-carbon-based architectures with low density (Morresi et al. 2020). The latter are obtained by augmenting planar three-coordinated uniform tessellations. Using geometrical packing arguments, we show that such arrangements satisfy the locally-jammed packing condition and represent some of the least dense structures

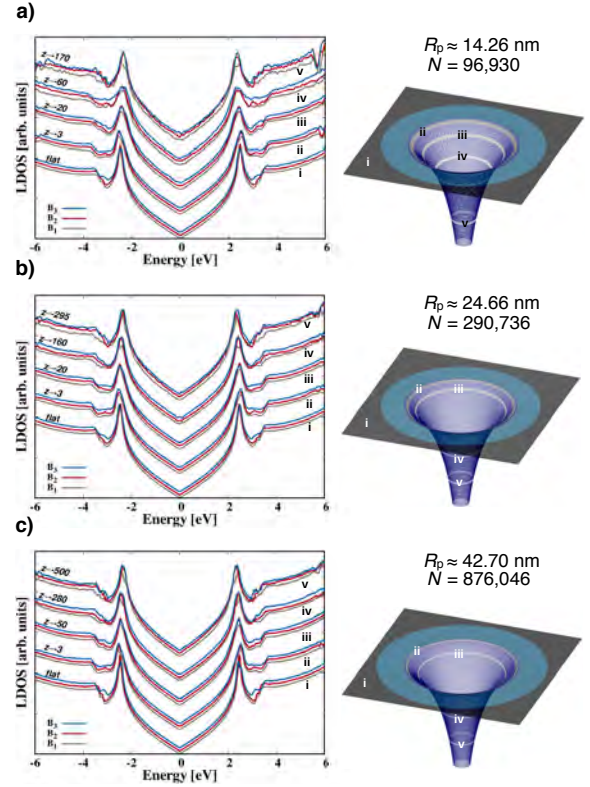


Figure 1: Evaluation of the LDOS through a multi-orbital TB approach implementing the Kernel Polynomial Method. Panels a) through c): LDOS projected onto five regions at different depth along the revolution axis  $z$  (i through v) for various pseudospheres characterized by three different values of the number of atoms  $N$  and radius  $R_p$ . For each case of  $N$  and  $R_p$  we report the LDOS for three pseudosphere realizations  $B_{1-3}$  differing by the configurations of SW defects, of which a representative is shown on the right of each panel. The Fermi energy is set equal to zero in all cases.

of all-bonded carbon allotropes that could ever be synthesised. We fully characterize from first principles these new architectures, by assessing:

- (i) the electronic properties, such as the band structure and the density of states;
- (ii) the dynamical characteristics, such as the phonon dispersion;
- (iii) the mechanical properties, such as the elastic constants and the stress-strain relationships.

<sup>†</sup>Contact Author: taioli@ectstar.eu

We compare our findings with already synthesised carbon-based materials, in particular graphene, and we find that in the lowest-density structures the mechanical rigidity is considerably depleted, while other specific mechanical characteristics, such as toughness and strength, are comparable to the relevant specific values of graphene. Furthermore, a flat band at the Fermi level emerges in the electronic band structure of the augmented geometries, which is a feature similarly appearing in Kagome lattices and strongly correlated materials.

A second research area is the development of a computational method, based on the Monte Carlo statistical approach, for calculating electron energy emission and yield spectra of metals, such as copper, silver and gold. The calculation of these observables proceeds via the Mott theory with a Dirac–Hartree–Fock spherical potential to deal with the elastic scattering processes, and by using the Ritchie dielectric approach to model the electron inelastic scattering events. In the latter case, the dielectric function, which represents the starting point for the evaluation of the energy loss, is obtained from both ab-initio and experimental reflection electron energy loss spectra. The generation of secondary electrons upon ionization of the samples was implemented, obtaining a remarkable

agreement between theoretical and experimental electron emission spectra and yield curves.

Finally, we further developed our relativistic approach to the simulation of beta-decay processes along two directions, that is first to investigate the possibility of determining the electron neutrino mass by electron capture of a bound electron in  $^{163}\text{Ho}$ , which relies on a precise understanding of the deexcitation of a core hole after a beta-decay event. In this regard the decay spectra of Ho, including shake-up and shake-off excitations, was calculated. Second, we applied our method in astrophysical scenario, in particular to estimate the solar neutrino fluxes from electron-capture on  $^7\text{Be}$ , which is the main production channel for  $^7\text{Li}$  in several astrophysical environments (Vescovi et al. 2019a). Theoretical evaluations have to account for not only the nuclear interaction, but also the processes in the plasma in which  $^7\text{Be}$  ions and electrons interact. In recent decades several estimates were presented, pointing out that the theoretical uncertainty in the rate is in general of a few percent. In particular, we analyzed the effects of our new rate on standard solar models (SSMs) and compared the results obtained by adopting the revised  $^7\text{Be}+e^-$  rate to those obtained by that reported in a widely used compilation of reaction rates (ADE11).

## Selected Papers

- Morresi, T., Binosi, D., Simonucci, S., Piergallini, R., Roche, S., Pugno, N. M., and Taioli, S. (2019). *Exploring Event Horizons and Hawking Radiation through Deformed Graphene Membranes*. arXiv preprint:1907.08960.
- Morresi, T., Pedrielli, A., Beccara, S., Gabbrielli, R., Pugno, N. M., and Taioli, S. (2020). *Structural, electronic and mechanical properties of all-sp<sup>2</sup> carbon allotropes with density lower than graphene*. Carbon **159**, pp. 512–526.
- Vescovi, D., Piersanti, L., Cristallo, S., Busso, M., Vissani, F., Palmerini, S., Simonucci, S., and Taioli, S. (2019a). *The effects of a revised  $^7\text{Be} e^-$ -capture rate on solar neutrino fluxes*. Astronomy & Astrophysics **623**(A126), p. 7.

# TEONGRAV

Bruno Giacomazzo,<sup>†</sup> Federico Cipolletta

The main research activity of the TEONGRAV group in Trento concerned fully general relativistic simulations of compact binaries, either neutron stars (NSs) or black holes (BHs). We here very briefly summarize the main results from two representative papers published by our group in 2019. The first one discusses the very long evolution of a long-lived neutron star formed after the merger of a magnetized binary neutron star (BNS) system. The second one presents instead our new fully general relativistic magnetohydrodynamic (GRMHD) code Spritz.

**First 100 ms of a long-lived magnetized NS formed in a BNS merger** Neutron stars are the remnants of supernova explosions (the spectacular deaths of massive stars) and the densest objects in the universe besides black holes. A typical neutron star concentrates more than the mass of the Sun within a radius of only around 10 km. Because of their extreme gravity a proper description of neutron stars requires Einstein’s theory of General Relativity. Investigating neutron star properties can shed light on the behavior of matter at very high densities, which is not yet understood well by nuclear physics. Two neutron stars can also bind together in a binary system, and orbit around each other for millions of years with a smaller and smaller separation. Eventually, the two merge together in an instant (just a few milliseconds) resulting either in a black hole or in a rapidly rotating neutron star, which can still collapse to a black hole later on.

On August 17 2017 the first gravitational wave (GW) signal from a BNS merger was detected by the LIGO and Virgo collaboration. This event was also observed in all bands of the electromagnetic spectrum and it included also the observation of a short gamma-ray burst (SGRB). This provided the first evidence that, at least some, SGRBs are produced by BNS merg-

ers. Due to the low sensitivity of GW detectors to the post-merge phase, it was not possible to say if a BH or a long-lived NS was formed after the merger. There are indeed two main scenarios for the production of an SGRB: an accretion disk around a spinning BH or a strongly magnetized NS (a magnetar). In both cases magnetic fields could provide the energy to power a relativistic jet and give rise to the gamma-ray emission.

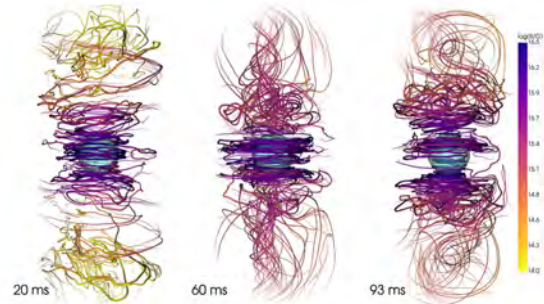


Figure 1: Magnetic field structure 20, 60, and 93 ms after merger. To give a scale reference, we added a (cyan) sphere of 10 km radius placed at the remnant center of mass. Field line colors indicate the magnetic field strength. Figure and caption are taken from Ciolfi et al. (2019)

In Ciolfi et al. (2019) we performed the longest GRMHD simulation of an NS formed after a BNS merger and covered up to  $\sim 100$  ms after merger. This allowed us to study the emerging structure and amplification of the magnetic field (see Fig. 1). We also followed the magnetically supported expansion of the outer layers of the remnant NS and found no torus formation and no sign of jet launching by the end of the simulation. This provided evidence that relativistic jets may not be formed unless the post-merger remnant collapses to a BH. We also examined the rotation profile of the remnant, the conversion of rotational energy associated with differential rotation, the overall energy budget of the system, and the evolution of the GW frequency spectrum. Finally,

<sup>†</sup>Contact Author: [bruno.giacomazzo@unimib.it](mailto:bruno.giacomazzo@unimib.it)

we also investigated what would happen if the NS collapsed to a BH  $\sim 70$  ms after merger. In this case we found the formation of a BH surrounded by a magnetized disk with enough mass to possibly power a SGRB. It seems therefore that in order to produce an SGRB the post-merger remnant needs to collapse to a BH.

**Spritz: a new fully GRMHD code** As briefly pointed out in the previous section, magnetic fields can have an important role in the post-merger evolution of a BNS system and in powering relativistic jets and SGRBs. Almost all GRMHD simulations nowadays are still limited to the use of simple equations of state and do not take into account the effects of neutrino emission. Our *WhiskyMHD* code, the one used in the previous section, shares these same limitations. We decided therefore to develop a new GRMHD code, named *Spritz*, that can handle both finite temperature tabulated equations of state (that model NS matter much more accurately) and neutrino emission. In Cipolletta et al. (2019) we presented the first tests of this new code, focusing in particular on the new algorithms used to evolve the magnetic field. As in *WhiskyMHD* we evolve the vector potential and then compute the magnetic field from it. This guarantees that the magnetic field has zero divergence as required by Maxwell's equations. There are two formulations that can be used to evolve the vector potential: one in which the vector potential is stored at the center of numerical cells, together with the other MHD variables (e.g., as done in *WhiskyMHD*), and one in which it is instead staggered, i.e.,

stored on cells' edges (as done in our new code *Spritz*). We showed for the first time that a staggered formulation of the vector potential is more robust in handling the propagation of shock waves (see Fig. 2). In our paper we also presented a number of tests in 1D, 2D and 3D, including the evolution of magnetized NSs. All tests show the robustness of our new GRMHD code and in a future paper we will also present our first GRMHD simulations which take into account neutrino emission. We will also make the *Spritz* code publicly available.

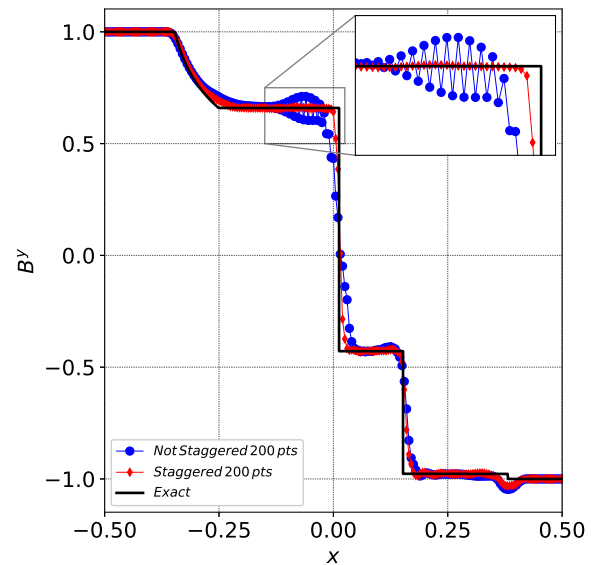


Figure 2: Comparison of results for a shock tube test, obtained via a staggered (red diamonds) and a non-staggered (blue dots) vector potential formulation. Post-shock oscillations are clearly visible in the blue curve, while the new *Spritz* code (red diamonds) provides an accurate solution. The black-solid line shows the exact solution. Figure published in Cipolletta et al. (2019)

## Selected Papers

- Ciolfi, R., Kastaun, W., Kalinani, J. V., and Giacomazzo, B. (2019). *First 100 ms of a long-lived magnetized neutron star formed in a binary neutron star merger*. *Phys. Rev. D* **100**(2). Art. no.: 023005.
- Cipolletta, E., Vijay Kalinani, J., Giacomazzo, B., and Ciolfi, R. (2019). *Spritz: a new fully general-relativistic magnetohydrodynamic code*. preprint, arXiv:1912.04794.



# Technological Research



## 3D-SiAm

Maurizio Boscardin,<sup>†</sup> Michele Crivellari

Hydrogenated amorphous silicon (a-Si:H) can be produced from growth by plasma-enhanced chemical vapor deposition (PECVD) of SiH<sub>4</sub> (Silane). The resulting material has remarkable radiation resistance at high fluencies; planar diodes made with a-Si:H increase only a factor 2 in leakage current after an irradiation at  $7 \cdot 10^{15}$  p/cm<sup>2</sup> and after 24 hours of annealing their leakage current comes back at the original value before the irradiation. A-Si:H based particle detectors have been built since mid-80s as planar p-i-n or Schottky diode structures; the thickness of this detectors ranged from 1 to 50  $\mu\text{m}$ . Planar a-Si:H detectors have been used also to detect different kind of radiation other than MIPs, namely: x-rays, neutron and ions as well as low energy protons and alphas. However MIP detection using planar structures has always been problematic due to the poor S/N ratio due to high depletion field and consequently high leakage current and the charge collection efficiency around 50% for a 30  $\mu\text{m}$  planar diode. In order to overcome these problems we propose to use a 3D detector geometry that allows to keep a small collection distance (the inter-electrode distance that may be kept around 20-30  $\mu\text{m}$ ) while having a larger detector space for charge generation since it is possible to grow the substrate up to about 100  $\mu\text{m}$  in thickness. The depletion voltage in this case can be kept as low as about 200 V - 400 V reducing the leakage current.

The starting process of the detector fabrication is PECVD of Silane at 200 °C. We would like to reach at least 100  $\mu\text{m}$  of a-Si:H thickness but some effort will be made to have a larger thickness because thickness is a key factor to increase signal-to-noise ratio. Once the a-Si:H substrate

is grown holes should be made in the substrate in order to prepare electrode manufacturing. The technique that will be used for this purpose is DRIE (Dry reactive ion etching). Once the holes are drilled, in order to build the basic p-i-n electrode structure of the detector, there is the necessity to dope the a-Si:H material in the surfaces the holes. Since commonly used techniques for planar structures (i.e. PECVD deposition of doped a-Si:H) are not available for this process, two options will be considered:

- a) Atomic layer deposition (ALD) of metallic oxides: Titanium oxide for n-type and Tungsten or Molybdenum oxide for p-type.
- b) Ion implantation of Phosphor ion for n-type doping and Boron for p-type doping and subsequent activation at low temperature (e.g. 250 °C).

Since these processes are not very common, a prototyping phase, where these two techniques will be used in the construction of planar p-i-n diodes, is foreseen, this prototype is current under construction and within March relevant testing of junction made with ion implantation and ALD will be performed. In parallel simulation of these detector is ongoing a model of the a-Si:H material has been developed and an article about this model is under publication Such a detector can be used for future hadron colliders for its radiation resistance and also for X-ray imaging for medical and structural analysis applications. The realization of a first batch of diodes structure on Hydrogenated amorphous silicon are carry on at MNF facility at Fondazione Bruno Kessler.

---

<sup>†</sup>Contact Author: boscardi@fbk.eu

# ARCADIA

Lucio Pancheri,<sup>†</sup> Coralie Neubüser, Thomas Corradino, Gian-Franco Dalla Betta, Andrea Ficorella, Majid Zarghami, Matteo Favaro, Roberto Iuppa, Paolo Zuccon, Francesco Nozzoli, Benedetto Di Ruzza, Ester Ricci

The purpose of ARCADIA project is to develop a novel CMOS platform tailored for the realization of pixel sensors with the following characteristics:

- Active sensor thickness in the range 50  $\mu\text{m}$  to 500  $\mu\text{m}$  or more;
- Operation in full depletion with fast charge collection only by drift;
- Small charge collecting electrode for optimal signal-to-noise ratio;
- Scalable readout architecture with ultra-low power capability;
- Compatibility with standard CMOS fabrication processes.

In the last years, fully depleted CMOS sensors have gained the attention of the scientific community. Novel designs exploiting commercial bulk technologies have been recently proposed, while the more traditional SOI-based process has been improved. Nevertheless, a technology incorporating all the characteristics listed above does not yet exist. Such a technology will allow to replace the more expensive standard hybrid pixel and silicon sensors in most applications. It is hence relevant for all those experiments that plan to use silicon detectors, including experiments at future colliders and space-born experiments. The project relies on the positive results achieved in the explorative research SEED, which led to the development of a patent-pending approach, validated on small scale sensors with an elementary readout.

A strict cooperation with the silicon foundry will allow to further improve the sensor performance in terms of signal-to-noise ratio and power consumption. By using the latest design integration and verification methodologies, large area sensors, indispensable for a

thorough validation of the concept will be deployed. A common readout framework makes it possible to characterise different sensor flavours by changing only the substrate material. The federation of a large number of INFN units provides the critical mass and allows to foster the expertise of the national community in the field of CMOS radiation imagers, improving the competitiveness of INFN in this critical field.

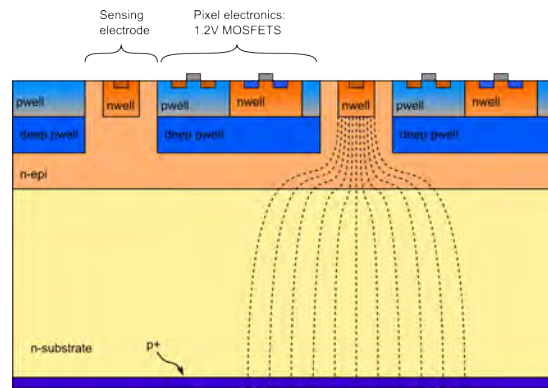


Figure 1: Simplified cross section of ARCADIA pixels

A simplified cross-section of ARCADIA sensor is shown in Fig. 1. The sensor is based on a commercial 110-nm CMOS process flow, with the addition of dedicated processing steps (Pancheri et al. 2019). The high-resistivity substrate is n-type, and a p+ implant on the backside forms a junction that is used to deplete the substrate when a suitable backside bias is applied.

During 2019, the collaboration has defined the characteristics of the substrates that will be used in the fabrication run. Further characterisation campaigns have been carried on the test structures produced in SEED project to fully assess the characteristics of the proposed sensors and to acquire additional data for the validation of the simulation models. TCAD simulations have been used to tune the process param-

<sup>†</sup>Contact Author: lucio.pancheri@unitn.it

eters by comparison with the characterisation results.

A full-chip MAPS demonstrator featuring a matrix of  $512 \times 512$   $25 \mu\text{m}$  pixels is under design, and the tape-in is due to mid-2020. The complete synthesis, place-and-route, post-layout simulation, timing and power analysis flows and scripts were developed by the collaboration during 2019. The pixel and matrix digital logic are complete, and the pixel analogue front-end is included as a macro.

The collaboration also studied the development of a data acquisition chain based on a commercial off-the-shelf board Z-turn. This solution will allow for readout rates up to 1.25 Gb/s per IO and features an ethernet port for interface with the data acquisition workstation.

In 2019, further characterisation activities have been carried out using the SEED prototypes, both pseudo-matrices (no embedded front-end electronics) and small area complete arrays, in different flavours. Investigation was pursued along three different lines:

- irradiation with  $^{55}\text{Fe}$  X-rays, in order to measure noise and gain, study the charge

diffusion, charge collection efficiency and clustering algorithms;

- micro-beam of single protons at low energy (a few MeV) and low rate at Zagreb RBI, in order to study the charge collection efficiency, the homogeneity of the response, and characterize the charge sharing at the boundary between the pixels and the guard ring;
- scan with red and IR focused lasers, complementing the studies reported above with an energy deposition comparable to a few m.i.p.

Radiation hardness studies were performed using the silicon produced with the 2nd run of the SEED project. The characterisation was done both using the pseudo-matrices test structures and the MATISSE MAPS featuring  $50 \mu\text{m}$  pixels and a correlated double-sampling readout scheme. The Collaboration generated characterisation data on the TID of the sensors, and a test campaign of neutron irradiated devices will be performed in 2020. The samples were irradiated with fluxes of neutrons up to  $10^{14} \text{cm}^{-2}$  at the TRIGA reactor facility (RIC), “Jozef Stefan” Institute (JSI) - Ljubana.

## Selected Papers

Pancheri, L., Olave, J., Panati, S., Rivetti, A., Cossio, F., Rolo, M., Demaria, N., Giubilato, P., Pantano, D., and Mattiazzo, S. (2019). *A 110 nm CMOS process for fully-depleted pixel sensors*. *Journal of Instrumentation* **14**. Art. no.: C06016.

# ARDESIA

Nicola Zorzi,<sup>†</sup> Giacomo Borghi, Francesco Ficorella, Antonino Picciotto

ARDESIA project aims at the realization of a versatile and high-performance X-ray Spectroscopy detection system for synchrotron experiments in the energy range between 0.2 keV and 25 keV. The basic detection module is built around a 2×2 monolithic array of Silicon Drift Detectors (SDDs) with 5 mm pitch and realized using the technology available at FBK (Trento). The readout chain is based on a monolithic version with four channels of the CMOS preamplifier CUBE developed by Politecnico di Milano. Both the analog and the digital processing systems are developed to be compatible with several filtering and data acquisition interfaces available in different synchrotron facilities.

The role of INFN-TIFPA in the project concerns simulation, design, development of the fabrication technology, production and preliminary characterization of the SDD array detectors in close collaboration with the FBK microfabrication laboratory. The other INFN units involved in the project are as follows: INFN-Milan (overall project coordination, detection module development and integration with electronics and DAQ) and INFN-LNF Frascati (detector module installation in the synchrotron facilities, characterization measurements at X-ray beamlines). ARDESIA project ended officially in 2018, however the last detector production with increased thickness suffered a considerable delay and was completed in January 2019. Therefore, the activity continued also in the last year and was mainly aimed at two different goals:

- (i) functional characterization of the spectrometer fabricated in the previous years;
- (ii) characterization of the new SDD devices produced in the last batch.

As already reported in the 2018 report, the ARDESIA spectrometer has been installed in two different synchrotron facilities: the LNF DAΦNE-Light DRX1 soft X-ray beamline

and the ESRF LISA BM-08 beamline. Results were obtained both in fluorescence analysis of trace elements at low energy (down to 277 eV) and XAFS experiments, demonstrating good energy resolution, high count rate capability and stability of the instrument over time. The achieved results represent an improvement with respect to state-of-the-art commercial instruments sharing the same detector technology and have been reported in two papers (Hafizh et al. 2019a; Hafizh et al. 2019c).

The TIFPA activity in 2019 was mainly focused to the characterization of SDD detectors with increased thickness realized in the last FBK-ARDESIA production with the specific aim to improve the X-ray detection efficiency in the energy range above 15 keV. The test structures for technology monitoring were first evaluated at wafer level and the measurement results confirmed that the characteristic parameters are within the expected typical ranges. With reference to the leakage current, which is a parameter depending on both the technology and the silicon substrates, the results obtained for the reference wafers with standard thickness (450 μm) demonstrated the good quality of the production, with values in the range of 500-800 pA/cm<sup>2</sup>. The corresponding values for the thicker wafers did not scale by a simple factor corresponding to the thickness ratio. In fact we obtained about 3 nA/cm<sup>2</sup> for 800 μm-thick substrates and about 4.5 nA/cm<sup>2</sup> for 1 mm-thick ones. A possible explanation of this observation can be ascribed to the quality (slightly worse) of the starting thick wafers. Anyway, these values are acceptable for the functional characterization. The other critical parameter of the thick substrates is the depletion voltage. The effective values of the depletion voltages obtained from the measurements are ~110 V and ~80 V for 800 μm and 1 mm thick wafers, respectively. These values are lower than expected, given the nominal substrate resistivity. The positive as-

<sup>†</sup>Contact Author: zorzi@fbk.eu

pect of this result is that no high voltage sources are required. On the other hand, the proper biasing of the SDD devices at the optimal condition is more critical, in particular for 1 mm thick wafers. The subsequent testing step involved the measurement of all the different SDD devices (single devices and arrays). The results confirmed the observations obtained from the test structures in terms of both leakage current and depletion voltage. In addition, these measurements allowed the ranking of the devices according to quality parameters, the selection of the best ones for the next functional tests and the identification of the defective ones. An example of the leakage current density measured at the anode terminal of all the SDD devices belonging to a 800  $\mu\text{m}$  thick wafer is reported in Fig. 1. The black squares correspond to defective devices or array elements.

Very preliminary functional tests have been made on thick SDD detectors after dicing and assembling with the readout electronics. A 800  $\mu\text{m}$  thick SDD irradiated with an  $^{55}\text{Fe}$  source showed an energy resolution of 137.3 eV (at 5.9 keV,  $-35^\circ\text{C}$ ), not far from the one achievable with the 450  $\mu\text{m}$  thick SDD. A comparison of the spectra from an  $^{241}\text{Am}$  source collected with the 800  $\mu\text{m}$  and 450  $\mu\text{m}$  SDDs demonstrated a clear improvement in the detection efficiency of the first one at energies larger than

10 keV up to 59.5 keV (Utica et al. To be published). A more in depth characterization is still under way, also involving the 1 mm thick detectors. A new version of the full spectrometer will be built using the thick  $2\times 2$  SDD arrays. Furthermore, the activity will continue to develop an instrument based on a  $4\times 4$  SDD array in order to enhance the count rate capability.

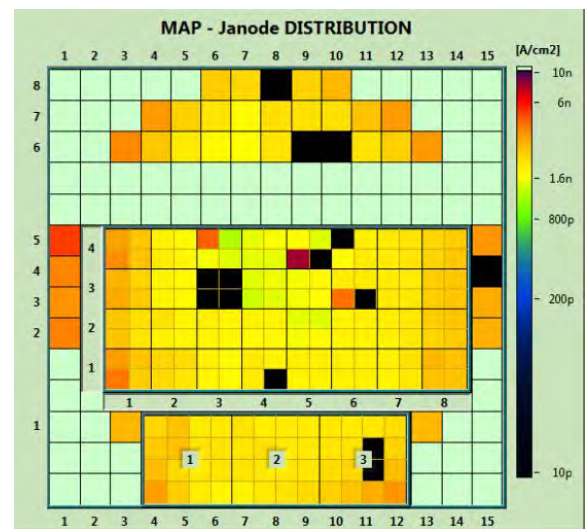


Figure 1: Spatial distribution of the anode current density measured at 1.5 times the depletion voltage. The map refers to a 800  $\mu\text{m}$  thick wafer. Single SDDs are located at top, left and right.  $2\times 2$  SDD arrays are in the center, while  $4\times 4$  arrays are placed at the bottom.

## Selected Papers

- Hafizh, I., Bellotti, G., Carminati, M., Utica, G., Gugiatti, M., Balerna, A., Tullio, V., Borghi, G., Picciotto, A., Ficarella, F., Zorzi, N., Capsoni, A., Coelli, S., Bombelli, L., and Fiorini, C. (2019a). *ARDESIA: a Fast SDD X-ray Spectrometer for Synchrotron Applications*. *X-Ray Spectrometry* **48**(5), pp. 382–386.
- Hafizh, I., Bellotti, G., Carminati, M., Utica, G., Gugiatti, M., Balerna, A., Tullio, V., Lepore, G., Borghi, G., Ficarella, F., Picciotto, A., Zorzi, N., Capsoni, A., Coelli, S., Bombelli, L., and Fiorini, C. (2019c). *Characterization of ARDESIA: a 4-channel SDD X-ray spectrometer for synchrotron measurements at high count rates*. *Journal of Instrumentation* **14**(6). Art. no.: P06027.
- Utica, G., Fabbrica, E., Gugiatti, M., Hafizh, I., Carminati, M., Balerna, A., Borghi, G., Ficarella, F., Zorzi, N., Capsoni, A., Coelli, S., and Fiorini, C. (To be published). “Towards Efficiency and Count-Rate Enhancement of X-ray ARDESIA Spectrometer”. *Conference Record of the 2019 IEEE Nuclear Science Symposium and Medical Imaging Conference*. IEEE.

# ASAP

Lucio Pancheri,<sup>†</sup> Gian-Franco Dalla Betta, Andrea Ficorella, Mahid Zarghami

The ASAP project aims at improving the technology demonstrated in the APiX2 project with the goal of building a buttable module of suitable area, of improving the efficiency and reducing the noise characteristics and the thickness of the sensor. As for the APiX2 demonstrator, the ASAP sensor is based on the concept of vertically-integrated avalanche pixels made of two layers, using coincidence to reject thermally-generated spurious signals. This approach offers several advantages in applications requiring low material budget and fine detector segmentation as, for instance, for tracking and vertex reconstruction in particle physics experiments and charged particle imaging in medicine and biology. A sensor based on this concept can have low noise, low power consumption and a good tolerance to electromagnetic interference. In addition, a timing resolution in the order of tens of picoseconds can be achieved thanks to the fast onset of avalanche multiplication in Geiger-mode regime.

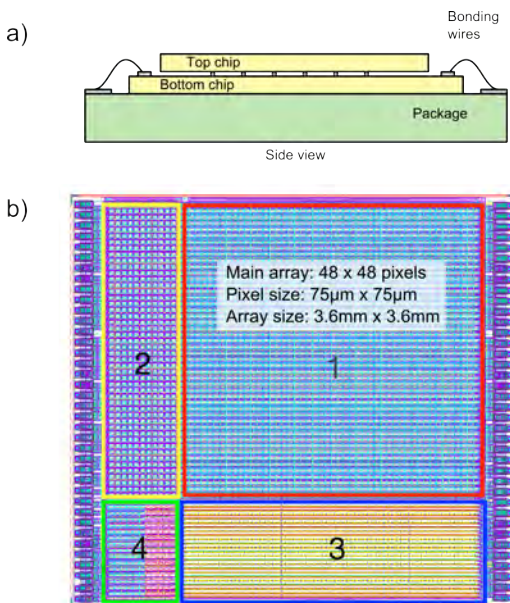


Figure 1: a) Schematic cross section of the vertically-integrated sensor assembly. b) Layout of the top chip.

To optimize the efficiency of the two-tier de-

tectors, that is basically determined by the sensor fill factor, a second design was submitted at the end of 2017 and fabricated in 2018 in a commercial 0.15 μm CMOS process, the same used in the design of APiX2 prototype. The design contains several subarrays with pixel size of 50×50 μm<sup>2</sup> and 75×75 μm<sup>2</sup> (Fig. 1).

The main array included in the design is made of 48×48 pixels, for a total size of 3.6×3.6 mm<sup>2</sup>. Each coincidence pixel is composed by 2 levels of detectors and electronics, with one interconnection used to deliver the digitized signal from the top to the bottom layer. The schematic diagram of the half pixel in the bottom layer is shown in Fig. 2. The detector front-end includes a quenching transistor, a low threshold inverter working as a comparator and a programmable monostable for pulse shortening. The coincidence resolution time depends on the monostable pulse width, that can be set to 400 ps, 750 ps or 2 ns. A latch included in each pixel can inhibit the recharge of the detector and the signal propagating from the comparator, and can thus be used to enable or disable the pixels with an arbitrary pattern. The bottom half-pixel also includes a coincidence detector, a memory latch for signal storage and an output latch in pipeline with the memory for the parallel readout of the array. Six fast outputs lines, shared by groups of 8×48 pixels and delivering trigger signals to the external electronics have also been included.

A few samples of top and bottom chips were wire-bonded for testing before proceeding to vertical integration. Electrical tests showed the correct functionality of both avalanche detectors and electronics in the two chips. The threshold voltage of each single cell was measured, and an excellent uniformity was found between all the pixels in the same array, with a standard deviation lower than 25 mV and a peak-to-peak maximum variation lower than 200 mV. It is worth mentioning that the mea-

<sup>†</sup>Contact Author: lucio.pancheri@unitn.it

sured non-uniformity is both due to variations in the detector breakdown voltage and in the threshold voltage of the inverters.

DCR statistics were acquired on several samples, yielding a median DCR ranging between 5 kHz and 13 kHz, for an excess bias voltage ranging from 2 V to 4 V. Cross-talk measurements were also conducted at different voltages, demonstrating an average optical cross-talk in the range of a few percent between neighboring pixels at 3 V excess bias.

Several vertically integrated assemblies are currently in production using bump bonding technique. An extensive measurement campaign is under way to characterize DCR, variability and cross-talk between pixels in different operating conditions.

In parallel, the design of a first test chip in 110nm project, aimed at implementing new avalanche detector structures in this process, is going on and will be completed and submitted for fabrication during 2020.

Further characterization and system activities have been conducted on the first APiX2 prototypes. Irradiation campaigns with both X-rays and neutrons have been carried out to investigate the effect of ionizing and non-ionizing ra-

diation damage. Radiation damage results have been analyzed and a predictive model has been implemented (Musacci et al. 2019; Ratti et al. 2019a; Ratti et al. 2019b).

An application case for the use of ASAP approach in radio-guided surgery has been studied using GEANT4 simulation, and a hand-held probe for the detection of beta-tracers has been designed and fabricated.

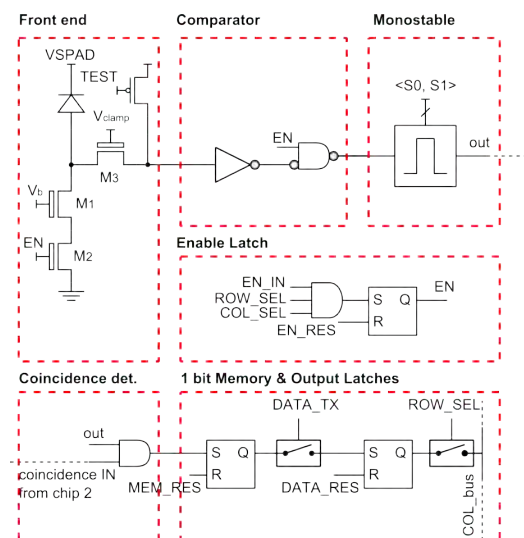


Figure 2: Simplified schematic of the 1-bit pixel in the bottom layer

## Selected Papers

- Musacci, M., Bigongiari, G., Brogi, P., Checchia, C., Collazuol, G., Dalla Betta, G.-F., Ficorella, A., Marrocchesi, P., Mattiazzo, S., Morsani, F., Noli, S., Pancheri, L., Ratti, L., Savoy Navarro, A., Silvestrin, L., Stolzi, F., Suh, J., Sulaj, A., Vacchi, C., and Zarghami, M. (2019). *Radiation tolerance characterization of Geiger-mode CMOS avalanche diodes for a dual-layer particle detector*. Nuclear Instruments and Methods in Physics Research, Section A **936**, pp. 695–696.
- Ratti, L., Brogi, P., Collazuol, G., Dalla Betta, G.-F., Ficorella, A., Lodola, L., Marrocchesi, P., Mattiazzo, S., Morsani, F., Musacci, M., Pancheri, L., and Vacchi, C. (2019a). *Dark Count Rate Degradation in CMOS SPADs Exposed to X-Rays and Neutrons*. IEEE Transactions on Nuclear Science **66**(2).
- Ratti, L., Brogi, P., Collazuol, G., Dalla Betta, G.-F., Ficorella, A., Marrocchesi, P., Pancheri, L., and Vacchi, C. (2019b). *Dark Count Rate Distribution in Neutron-Irradiated CMOS SPADs*. IEEE Transactions on Electron Devices **66**(12), pp. 5230–5237.

# DEEP\_3D

Roberto Mendicino,<sup>†</sup> Emanuele Tosi, Gian-Franco Dalla Betta, Alberto Quaranta, Matteo Perenzoni, Giacomo Borghi.

Different technologies for solid state thermal neutron detection have been developed with encouraging results. The most used system is composed by a light neutron-scintillator material and a CCD camera that use the emitted light for the image reconstruction. This system usually have an efficiency of the 10% but, in order to achieve good contrast in the images, it is necessary to have exposition times of 1 s, so that a low noise CCD is needed (in many cases they must be cooled down in order to maintain low values of dark current). Semiconductor detectors can offer good spatial resolution and very high gamma rejection ratio (similar to the system using CCD) but with an increase of temporal resolution and with a theoretical infinite dynamic range. The DEEP\_3D project addresses the most promising solutions for neutron imaging, with two main objectives:

- (i) to build a 2D neutron imager for artwork tomography, based on the interconnection of a Medipix-2 chip to a silicon 3D neutron detector,
- (ii) to develop a high performance neutron detector with a monolithic approach.

Since silicon is not sensitive to neutrons, a converter material is required, so that a silicon detector can easily detect the reaction products. In order to increase the detection probability, 3D geometries have been studied and developed.

The first part of the project uses a hybrid 3D detector filled with lithium fluoride as converter material and coupled with a Timepix chip (Fig. 1). The matrix is composed of  $256 \times 256$  pixels and different trenches dimensions have been proposed. In order to grant the possibility of being filled with *LiF* or *B* different filling tests have been studied at the Institute of Experimental and Applied Physics in Prague. Furthermore irradiation tests with Americium and

Uranium sources have been made and analyzed at the University of Trento.



Figure 1: *Fitpix* chip connected with the hybrid 3D Silicon neutron detector (not filled with *LiF*).

The second part is the development of a monolithic 3D detector for neutron imaging, that is highly innovative and can represent a turning point for this field. The demonstrator has smaller area and a less sophisticated electronics as compared to the hybrid detector, in order to maximize the flexibility in the testing, but it will have globally a better performance. Sensors are fabricated on high resistivity wafer that allows a full depletion of the volume, isolated from the electronics by a buried oxide layer (BOX). The device has been produced in 200 nm CMOS Silicon On Insulator (SOI) technology by *Lapis Semiconductor Co., Ltd.* in Japan. It is composed of a matrix of  $25 \times 25$  pixels ( $35 \times 40 \mu\text{m}^2$  each), one test structure composed of two pixels (one with the same electronic readout of those in the matrix and one with half of the structure) and the IO ring with all the analog and digital components on the edges, rounded by a guard ring, for a total dimension of  $2.9 \times 2.9 \mu\text{m}^2$  (Fig. 2). In the future trenches, the boron will be used as converter material on the backside, in order to test

<sup>†</sup>Contact Author: roberto.mendicino@unitn.it

the device under neutron irradiation.

The in-pixel electronics is composed by:

1. **Charge Pre-Amplifier** that is a cascade amplifier, with high gain that is used to amplify the charge injected on the pixel,
2. **Feedback capacitors** that define the charge-to-voltage conversion gain of the preamplifier,
3. **Mirror current generator**, in which the current flows in the opposite direction with respect to the current flow of the amplifier,
4. **A hysteresis comparator** that operate in a circuitry of analog time over threshold (TOT).
5. **IO ring and column/row readout.**

The analog signal coming out from the sensor is then converted into a digital signal through an Analog to Digital Converter (ADC) with 12 bit sensitivity built in a Field Programmable Gate Array (FPGA) used for the signal acquisition. After the conversion, the signal is processed and prepared in order to be memorized inside the

Random Access Memory (RAM) of the FPGA through the employment of the Digital Memory Access (DMA). After that the signal is stored within the RAM of the FPGA, it is then sent to the PC and analyzed with a MATLAB software.

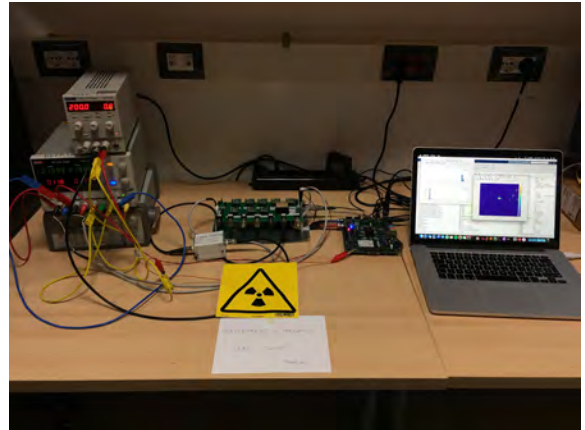


Figure 2: Setup used for irradiation tests with  $\alpha$ -particles on the monolithic 3D neutron detector. The sensor is placed on the motherboard with the proper current and voltage reference generators, the signal is acquired by a FPGA board and analyzed on the PC using a Matlab software.

# DRAGoN

Davide Brunelli,<sup>†</sup> Lucio Pancheri

Nuclear materials may compose a threat to public health and homeland security in the form of terrorism threats, lost orphan sources, nuclear accidents, or radioactive contamination.

The goal of the **Drone for Radiation detection of Gammas and Neutrons - DRAGoN** project is to design, develop, and characterize a mobile system composed of an Unmanned Aerial Vehicle (UAV). The UAV will be equipped with a detection system able to identify radioactive contamination spread over an area of a few to tens of square meters.

The type of radioactive sources that will be detected are gamma emitters and special nuclear materials (SNM). Moreover, it can be easily brought to the site rather than bringing the suspicious vector to the screening device. Being mounted on a UAV, the detection system and electronics shall be defined by size, weight, and power constraints. The proposed technology incorporates thermal and fast neutron detectors along with gamma-ray detectors.

These measurements are complementary, and their combined power is expected to improve the system performance. In particular, SNM (Highly Enriched Uranium and Plutonium) are challenging to detect, especially when masked or shielded: gamma rays and neutrons emitted by SNM have to be detected for increasing the sensitivity against natural background.

Unmanned aerial vehicles are mainly used in accident scenarios where the doses are too high for a manned survey or in areas of difficult access. They are also employed when the static radiation detector network is destroyed, as it happened at the Fukushima Daiichi Nuclear Power Plant in 2011 after the 15 m high tsunami hit.

There are several designs of UAVs, such as fixed-wing UV or single rotor helicopter-style aircraft. The role of a UAV is to provide a fast data acquisition to create an accurate mapping of the zone of interest. UAVs for gas or radiation mapping have been deployed on multiple occasions over the past decade.<sup>1,2,3</sup>

An ideal detector configuration would use a very high-density material for a high counting rate and a large volume. Such configuration guarantees a high stopping power of the radiation, in other words, a high chance of stopping and detecting radiation. While such a detector would not be suitable for deployment on a UAV due to its weight, a swarm of UAVs could be implemented to establish static monitoring points within a target zone. Using a number of these systems equipped with the traditional smaller volume detectors in a single target survey is a potential solution for the inherent loss of stopping power experienced by these detectors.

Detectors used in the studies detailed herein vary between a number of different types, including: scintillator detectors, Geiger-Muller (GM) tubes, and semiconductor detectors. Currently, the general applied solution for the gamma radiation mapping, alternative to scintillation-type detectors, are cadmium zinc telluride (CZT) detectors.

These are a type of semiconductor radiation detectors. A traversal characteristic, to the cited monitoring systems, is that they are mainly focused on detecting and identifying gamma sources and not neutron radiation.

The Dragon solution is characterized by its main capability of distinguishing between neutrons and gamma radiation types. The system compactness and mobility will give a practical instrument to picture of the surrounding en-

<sup>†</sup>Contact Author: [davide.brunelli@unitn.it](mailto:davide.brunelli@unitn.it)

<sup>1</sup>Rossi, M. and Brunelli, D. (2016), IEEE Transactions on Instrumentation and Measurement **65**(4), pp. 765–775.

<sup>2</sup>Tosato, P. et al. (2019), *2019 IEEE 20th International Symposium on "A World of Wireless, Mobile and Multimedia Networks" (WoWMoM)*, pp. 1–6.

<sup>3</sup>Facinelli, D. et al. (2019), *2019 IEEE 43rd Annual Computer Software and Applications Conference (COMPSAC)* vol. 1, pp. 463–468.

vironment. During the development and the characterization, the project considers the standards describing the requirements for mobile systems, including the ANSI N42.43. As the system will be intended to be used in potentially contaminated areas, experimental tests with relevant gamma and neutron sources will be done, to satisfy the IAEA requirements for safety and security in the field. For instance, one of the requirements is to detect a neutron source in a high gamma background. For this reason, the capabilities of distinguishing the two sources is an important added value.

**DRAGoN prototype description** An important aspect of Dragon project is finding miniaturized solutions both for the detection system and the electronics. The proposed Dragon system is presented in Fig. 1.

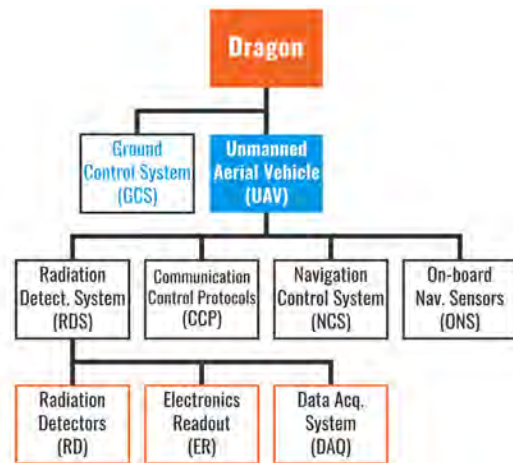


Figure 1: The Dragon project constituents scheme.

The Unmanned Aerial Vehicle has been realized as depicted in Fig. 2 and, at a functional level, provides both an autonomous real-time path planning, and a flight controller to allow manually pilot of the drone, guaranteeing safety with redundant input; and a telemetry communication using a dedicated 2.4 GHz radio link.

The Radiation Detection System (RDS) uses two detection solutions:

- Radioactivity counter monitor: Modern boron loaded liquid scintillator EJ-309B (high flash-point, low vapor pressure, low chemical toxicity).
- Radionuclide identification system: Gamma spectroscopic scintillator with neutron detection capability (Elpasolite crystal CLYC or CLLB).

For both the solutions, a standard Photomultiplier Tube is used to detect the scintillation light signal. An alternative readout channel based on large-area Silicon Photomultipliers is also being developed to reduce the overall weight, size, and power consumption of the detection system.

A digitizer with a sampling rate of 125 MHz and 14 bits of resolution will be then used and mounted on the UAV to complete real-time wireless measurement. The reduction of the sampling rate reduces energy consumption, which can be partially compensated by an increase in the number of bits of resolution.

The solutions are under design and are conceived to be interchangeable with the same electronics readout, thanks to a suitable mechanical design, to adapt the system to the requirements of a variety of threats in nuclear security.

The first detector will be employed as a radioactivity counter, whereas the second one will be used for a second-line identification system. Moreover, the second solution can be used also as a first-line inspection system for very high dose environments, like in catastrophic events involving high quantities of neutron emitting materials.



Figure 2: Tests with the assembled UAV.

# GLARE-X

William Jerome Burger,<sup>†</sup> Alvise Bagolini, Roberto Battiston, Pietro Battocchio, Nicola Bazzanella, Massimo Cazzanelli, Claudio Cestari, Riccardo Checchetto, Roberto Iuppa, Christian Manea, Antonio Miotello, Michele Orlandi and Jacopo Terragni

The research activity at the TIFPA in the field of the space applications of laser ablation started with the CSN5 experiment New Reflections (NR), 2016-2018, devoted to the development of laser technologies for space: geo-referencing, tracking, propulsion, and debris mitigation. The activity continues in the CSN5 experiment GLARE-X (Geo-referencing via LAsER Ranging and LAsER debris Redirection from space-X).

Laser ablation refers to the ejection of matter from the surface of a material heated to high temperatures by a laser beam. The thrust produced by the ejected matter may be used for the launch and propulsion of small satellites, and the orbital deflection of space debris.

The fundamental parameter common to the space applications is the momentum-coupling coefficient  $C_m$ , which relates the impulse produced by the ablated mass to the energy density of the incident laser beam. The combination of  $C_m$  and the specific impulse  $I_{sp} = v_E/g_0$ , i.e. the thrust generated by a unit mass of propellant, indicates the relative efficiency of the laser propulsion system. The exhaust velocity  $v_E$  is related to  $C_m$ , the areal mass loss density  $\mu$ , and the laser pulse energy density  $\Phi$  by the expression  $v_E = C_m \Phi / \mu$  ( $g_0 = 9.81 \text{ m/s}^2$ ).

The Pulsed Laser Deposition (PLD) facility of the IdEA Laboratory is devoted to the study of laser interactions in matter. The results obtained in the context of NR for aluminium, a common material employed in spacecraft and satellite construction, and two candidate propellant materials, at the PLD are reported in Fig. 1. The principle of the coupling coefficient measurement is shown in Fig. 2.

<sup>†</sup>Contact Author: william.burger@tifpa.infn.it

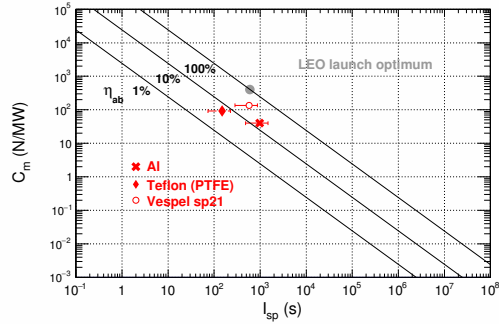


Figure 1: The peak value of the coupling coefficient and corresponding specific impulse are compared to the optimal combination for a LEO launch (gray point) and the ablation efficiencies  $\eta_{ab}$  reported in Phipps et al. (2000).<sup>1</sup>

The coupling coefficient is determined with a measurement of the angular deflection produced by the impulse delivered to the target material, mounted on a ballistic pendulum, by a KrF excimer laser ( $\lambda = 248 \text{ nm}$ ,  $\tau_{pulse} = 20 \text{ ns}$ ). The deflection angle is measured with a second laser beam, reflected vertically from the top of the pendulum, to a graduated scale located at a distance of  $\sim 4 \text{ m}$ .

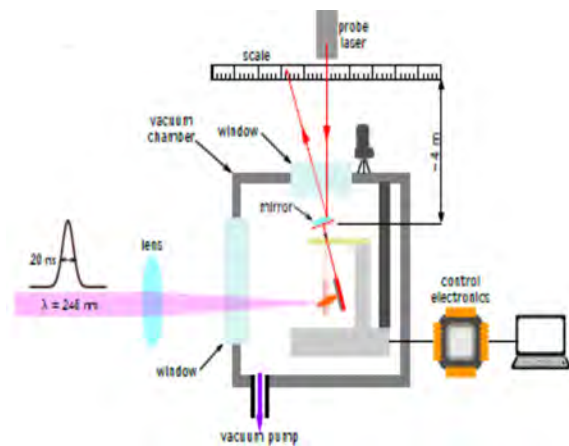


Figure 2: Schematic view of the ballistic pendulum used to measure the coupling coefficients at the PLD.

<sup>1</sup>Phipps, C. et al. (2000), Laser and Particle Beams **18**, pp. 661–695

A second vacuum chamber dedicated to the space application studies was installed at the PLD in 2019, with an optimized optical system to minimize energy losses and improve the precision of the beam spot on the target. The ballistic pendulum and supporting structures have been redesigned to reduce the systematic errors affecting the measurement of the coupling coefficient. The new ballistic pendulum and mechanical support, providing automated vertical and horizontal displacements with respect to the laser beam direction, are shown in Fig. 3.

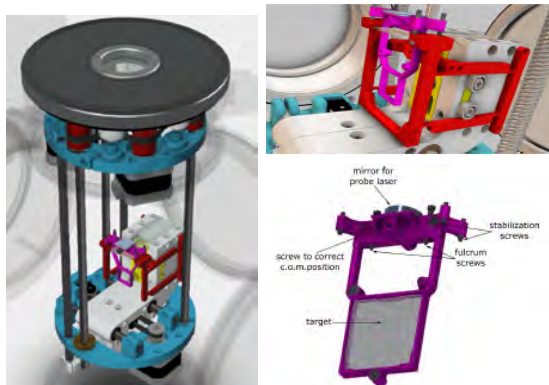


Figure 3: Views of the ballistic pendulum (magenta) mounted in its mechanical support (left), the support structures (red) designed to release the pendulum (upper right), and the positions of the target, reflecting mirror, stabilization and fulcrum screws of the pendulum (lower right).

The precision of the coupling coefficient measurement of the new pendulum is shown in Fig. 4. The average value and standard deviation of the aluminum  $C_m$  is  $20.60 \pm 0.25 \mu\text{N/W}$  @  $70 \text{ J/cm}^2$ .

The precise determination of the ablation mass loss per pulse is obtained from the mass loss generated by a large number of pulses. The target masses before and after the illumination

are measured on a balance scale (resolution  $\sim 10 \mu\text{g}$ ). An automated procedure has been developed to displace the target in the beam to control the temperature at the laser spot during the measurement.

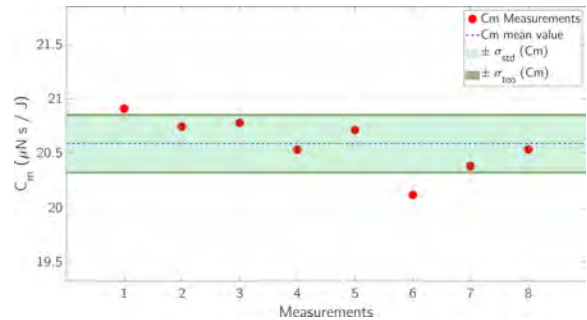


Figure 4: The average value and standard deviation of the aluminium  $C_m$  @  $70 \text{ J/cm}^2$  obtained with eight measurements.

The average and standard deviation of the ablated mass, obtained with a 3 Hz repetition rate and 12.6k pulses (70 min.), is  $0.761 \pm 0.002 \mu\text{g/pulse}$ . The corresponding aluminium specific impulse,  $I_{sp} = 930 \pm 8 \text{ s}$ , may be compared to the previous aluminium result presented in Fig. 1, 980 s. The horizontal error bars drawn in Fig. 1 represent a conservative error estimate of  $\sigma_{I_{sp}} = 0.5 \times I_{sp}$ .

The integration of the space application vacuum chamber at the PLD represents a major step forward for the research program, allowing systematic studies of propellant material candidates and enlarging the field of applications. For example, laser ablation is among the technologies considered for asteroid avoidance. The coupling coefficient of asteroid stimulant material of type C1 carbonaceous chondrite meteorites<sup>2</sup> as well as their chemical composition, were measured at the PLD in NR. Ablation also plays an important role in breakup of meteorites in the atmosphere where the observation of the visible light emitted is used to determine their chemical composition,<sup>3</sup> fundamental to our understanding of their origin.

<sup>2</sup>courtesy Dan Britt, Center for Lunar and Asteroid Surface Science, Physics Dept., University of Central Florida, FL, USA

<sup>3</sup>Loehle, S. et al. (2017), The Astrophysical Journal 837, pp. 112–121.

# HDM: a new hybrid detector for microdosimetry

Marta Missiaggia,<sup>1,2,3</sup> Enrico Pierobon,<sup>1,2</sup> Michele Castelluzzo,<sup>1</sup> Emanuele Scifoni,<sup>2</sup> Francesco Tommasino,<sup>1,2</sup> Matteo Centis Vignali,<sup>3</sup> Leonardo Ricci,<sup>1</sup> Vincenzo Monaco,<sup>4</sup> Maurizio Boscardin,<sup>2,3</sup> Chiara La Tessa<sup>1,2†</sup>

Microdosimetry provides information about radiation quality at a microscopic level, where the energy deposition follow a stochastic behavior. At this scale, the features of the radiation track structure have important implications on effects induced in biological targets.

To measure the energy deposition in a microscopic volume, dedicated detectors called *microdosimeters* have been developed. Currently, there are two types of microdosimeters: tissue equivalent proportional counters (TEPC) and silicon detectors. We use a commercial TEPC model type LET-1/2 from Far West Technology, Inc, with a spherical sensitive volume made of A-150 tissue-equivalent plastic and filled with propane gas. The physical size of the TEPC active volume is 12.7 mm diameter, but the gas is set to a density of  $1.08 \cdot 10^{-4} \text{ g}\cdot\text{cm}^{-3}$ , which makes the energy depositions of the particle equivalent to that in a  $2 \mu\text{m}$  diameter of tissue.

The fundamental microdosimetric quantity is the lineal energy transfer  $y$  (the equivalent of the Linear Energy Transfer (LET)) and its probability distribution. To measure  $y$ , the energy deposition  $\epsilon$  resulting from the gas ionization is divided by the particle track length  $l$ . The latter depends on the detector geometry and for a sphere is assumed to be equal to the mean chord length, i.e.  $\frac{2}{3}$  of the diameter (8.5 mm for our TEPC) (H. H. Rossi and Zaider 1996).

This approximation is adequate only if the TEPC is exposed to an isotropic and uniform radiation field and leads to significant uncertainties on the lineal energy. As many microdosimetry measurements are taken by placing the TEPC directly in water, we investigated the

validity of the mean chord length approximation for this setup. We used *Geant4* toolkit to simulate a uniform radiation field and transport it at different water depths before irradiating the TEPC. The results indicated that even after a few millimeters of water, the actual path length traversed by a particle deviated from the mean chord length with an average discrepancy of 10-15%. In addition, the whole path distribution is not well described by the mean value of 8.5 mm because the standard deviation is around 3 mm.

An example of the particle track distribution inside the TEPC placed at 3 cm water depth and irradiated with a uniform 160 MeV proton beam is shown in Fig. 1. The mean chord length value at 8.5 mm is marked with the red dashed line.

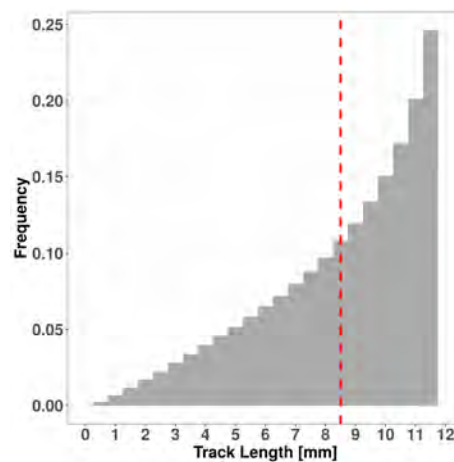


Figure 1: Track length distribution of particles traversing the TEPC. The red dashed line marks the mean chord length at 8.5 mm.

**Hybrid system** To overcome the  $y$  uncertainty stemming from the particle track length,

<sup>†</sup>Contact Author: chiara.latessa@unitn.it

<sup>1</sup>University of Trento, Italy

<sup>2</sup>INFN TIFPA, Trento, Italy

<sup>3</sup>FBK, Trento, Italy

<sup>4</sup>University of Turin, Italy

we are developing a hybrid microdosimeter, composed by the TECP and 4 layers of Low Gain Avalanche Diodes (LGADs) for particle tracking. In this way, the real track length of each particle traversing the TEPC can be obtained and used to calculate more accurate  $y$  values.

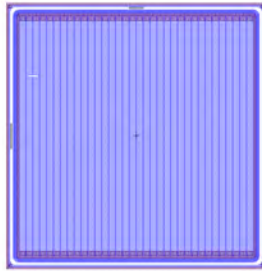


Figure 2: Design of an LGAD consisting of 34 strips.

LGAD is a recent technology in silicon detection systems. Using n-in-p silicon diodes, these detectors differ from the standard Avalanche Photodiodes (APDs) because of their low and controlled internal multiplication mechanism. LGADs have been optimized for fast timing and tracking of charged particles and their features make them an excellent candidate for applications in radiotherapy (Vignati et al. 2017).

The production details of the LGADs that we will employ for the microdosimeter can be found in (Sola et al. 2019b). In particular, the active region and the substrate are  $50\ \mu\text{m}$  and  $300\ \mu\text{m}$  thick, respectively. The substrate can be further thinned down to  $70\ \mu\text{m}$  post-

production.

An additional LGAD production with new sensor geometries is under development at the Bruno Kessler Foundation (FBK) of Trento and will include two types of doping in the active layer to achieve different gains. The new sensors will consist of 34 strips, each  $0.294\ \text{mm}$  wide and  $12.5\ \text{mm}$  long. Thus, the total height of the sensor will be equal to  $13.8\ \text{mm}$  and the total width to  $13.4\ \text{mm}$ , resulting in an area of  $\sim 4\ \text{mm}^2$ . The sensor layout is given in Fig. 2 while the microdosimeter design is shown in Fig. 3.

The signals generated by the LAGDs are read out with the ABACUS chip developed by the University of Turin in the framework of the INFN Move-it project (described at p. 115). The read-out of the hybrid microdosimeter will require a custom FPGA system and a dedicated Data Acquisition (DAQ) system.

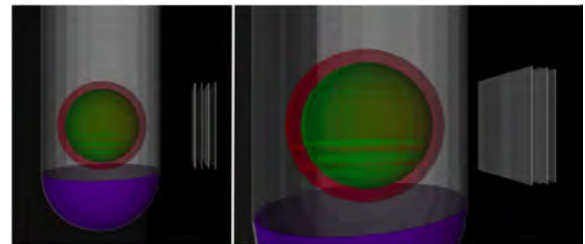


Figure 3: Hybrid microdosimeter layout consisting on a spherical TEPC (green) followed by 4 LGAD layers (grey planes).

## References

- Rossi, H. H. and Zaider, M. (1996). *Microdosimetry and its Applications*. Springer.
- Sola, V., Arcidiacono, R., Boscardin, M., Cartiglia, N., Dalla Betta, G.-F., Ficorella, F., Ferrero, M., Mandurrino, M., Pancheri, L., Paternoster, G., et al. (2019b). *First FBK production of  $50\ \mu\text{m}$  ultra-fast silicon detectors*. Nuclear Instruments and Methods in Physics Research Section A: Accelerators, Spectrometers, Detectors and Associated Equipment **924**, pp. 360–368.
- Vignati, A., Monaco, V., Attili, A., Cartiglia, N., Donetti, M., Mazinani, M. F., Fausti, F., Ferrero, M., Giordanengo, S., Ali, O. H., et al. (2017). *Innovative thin silicon detectors for monitoring of therapeutic proton beams: preliminary beam tests*. Journal of Instrumentation **12**(12). Art. no.: C12056.

# Isolpharm Ag

Devid Maniglio,<sup>†</sup> Antonella Motta, Alessandra Bisio, Walter Tinganelli, Alberto Quaranta

In targeted radiation therapy, a fundamental part of the radiopharmaceutical moiety is the targeting agent, i.e. the vector molecule. This portion is used for the molecular recognition between the drug and a biological entity, like a receptor, usually over-expressed on cancer cells. This moiety can be decorated with different chelators, opportunely spaced with a linker, depending on the radiometal to incorporate.

In this project two different biological targets are considered: calreticulin and cholecystokinin receptor. While for the second one the targeting strategies are quite well established, the focus in the first year of the project was mainly on finding a suitable targeting agent for calreticulin.

Calreticulin (CRT) is an endoplasmic chaperon molecule that can translocate from the cytosol to the cell surface, particularly during ER stress induced by e.g., drugs, UV irradiation and microbial stimuli. CRT is also exposed on the surface of many cancer cells and plays a role in recruiting macrophages thus promoting engulfment. Currently, CRT is recognized as a very promising molecular target for many anticancer immunotherapy protocols.

CRT can be considered then as a good and innovative target for the development of receptor targeting radiopharmaceuticals. The design and synthesis of a vector molecule with high affinity for CRT is crucial to deliver the radioactive payload selectively to tumor cells. As proof of concept, we aim at designing and synthesizing new molecules endowed with affinity towards CRT. For the development of a molecule with affinity for calreticulin, we set up several experiments to assess the targeting capability of different commercial CRT specific antibodies. Their performances have been compared with sugar-based molecules (oligosaccharides), among which, mannose resulted to have significant affinity for CRT.

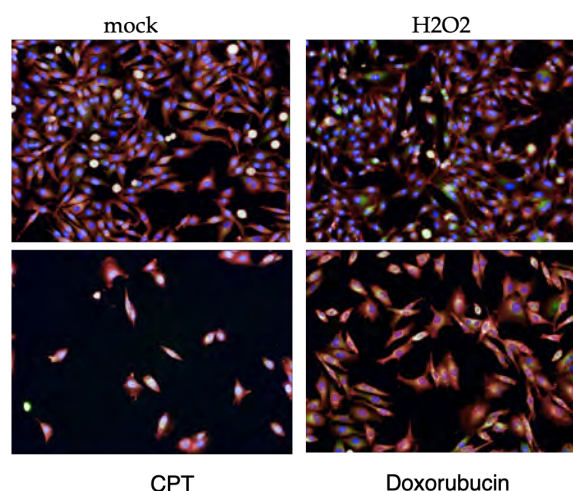


Figure 1: Confocal images of A375M cells after exposure to  $H_2O_2$ , Doxorubicin and CPT to induce CRT translocation, versus non treated cells (mock). CRT-specific antibodies (orange), nuclei (blue), cytoskeleton (red).

To verify targeting efficiency, we set up several in vitro cell experiments using B16F10 and A375M cell lines and testing CRT translocation with fluorescence tagged antibodies through confocal microscopy. Translocation was obtained exposing cells to different agents:  $H_2O_2$ , Doxorubicin, and Camptothecin (CPT) (see Fig. 1).

To ensure a better in vitro simulating system, we have started developing a gelatin based material suitable for cell incorporation. The commercial pig skin-derived gelatine underwent to chemical functionalization, to allow methacrilation of the polymer chains (GelMA). This allows, with the use of a suitable photoinitiator, the complete conversion of the liquid solution into a homogeneous crosslinked hydrogel.

Since the process is quite soft and can be performed in physiological conditions, cells can be incorporated in the liquid suspension to realize living constructs, or they can be seeded in a second time on the threedimensional scaffold.

<sup>†</sup>Contact Author: [devid.maniglio@unitn.it](mailto:devid.maniglio@unitn.it)

fold. The CRT overexpression in membrane have been successfully tested also on 3D matrices (see Fig. 2), confirming that they are a suitable platform to realize experiments on radiopharmaceutical targeting, mimicking a living tissue.

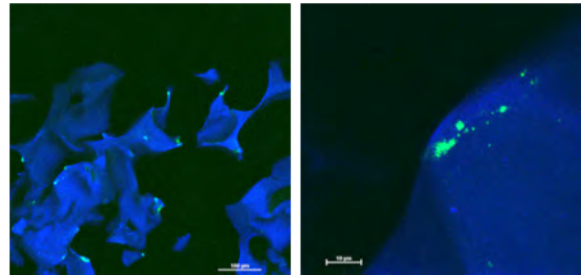


Figure 2: Confocal images of CT-26 colon on a 3D porous GelMA scaffold. Cell distribution (left), detail (right)

# KIDS\_RD

Renato Mezzena,<sup>†</sup> Benno Margesin

For the KIDS\_RD project, 2019 was the final year. Microwave Kinetic Inductance Detectors (MKIDs) fabricated by FBK have been extensively investigated in order to show the potentiality of these low temperature devices as electromagnetic radiation detectors (Fig. 1). Very encouraging and promising results have been obtained for the MKIDs especially designed as infra-red wavelengths photon number resolving detectors. We have employed the Ti/TiN multilayer film technology (Faverzani et al. 2020) to develop MKIDs capable to resolve single photons at 1550 nm. For the 0- and 1-photon peaks, we obtained a FWHM energy resolution of 0.44 eV and 0.56 eV, respectively; events up to 4 photons can be resolved (Mezzena et al. 2019). This result is within a factor of two from the best value published in the literature.

Further improvements are theoretically still expected. Since the energy resolution of MKIDs improves by reducing the volume of the resonator inductor, an effort was done to redesign the detector layout during 2019. A reduction of the resonator inductor volume leads to a reduction of the geometric inductance and consequently to an increase of the resonator resonance frequency. Due to the actual limitation in frequency range of our microwave equipment and particularly to the range 4-6 GHz for optimum noise temperature and gain of our cryogenic preamplifier, we had to ways for limiting the resonance frequency : increase the resonator capacitance and increase the surface inductance. The first requirement is obtainable by adding more fingers to the interdigital capacitors. As regards the film surface inductance, it turns out that it is proportional to the film sheet resistance and inversely proportional to the superconducting energy gap.

By reducing the film thickness we can at the same time increase the film sheet resistance and decrease the superconducting energy gap (Faverzani et al. 2020). Moreover, a lower su-

perconducting energy gap leads to a rise of the number of broken Cooper pairs per absorbed photon, therefore a further improvement of energy sensitivity is expected. Four different resonator layouts, each with many sub-variants have been designed. In order to foresee the resonance frequencies, the coupling with the feed line and the current density a software for electromagnetic modeling of planar circuits has been employed. The mask for the thin film lithography has been prepared during the last part of 2019 and the new fabrication is expected in 2020.

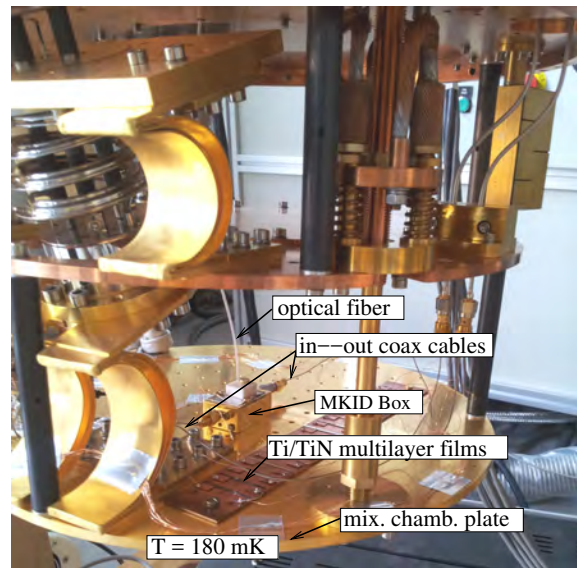


Figure 1: The picture displays the dilution refrigerator mixing chamber with the installed devices. The MKID detector is inside the gold plated copper shielding box. The in and out microwave signals are feeded by means of superconducting coaxial cables. A single mode optical fiber connected to a room temperature 1550 nm laser diode radiates the MKID. Multilayer Ti/TiN films are separately tested in order to measure the superconducting transition temperature

The other important target included in the KIDS\_RD project, i.e. the development of MKIDs for broad band high energy resolution X-ray spectroscopy, required further tests in order to address the unwanted dissipation effects. We

<sup>†</sup>Contact Author: [renato.mezzena@unitn.it](mailto:renato.mezzena@unitn.it)

discovered that this issue affects devices provided with a silicon nitride layer, which is included to obtain a suspended membrane. Such a membrane is deposited only for detectors designed for X-ray spectroscopy; it holds the gold radiation absorber ( about  $2.3\ \mu\text{m}$  thick) and the thermally coupled microresonator inductor. The membrane is required to avoid the escape of phonons from the film sensitive part to the substrate. For the detectors fabricated with silicon nitride layer deposited by PECVD, the signal transmitted through the feed line was found attenuated by about 30 dB and no resonances have been detected. The deposition of silicon nitride layer by LPCVD resulted in a significant improvement: the signal transmitted through the feed line showed the correct intensity and the resonances have been detected approximately in the expected frequency band. Nevertheless a residual dissipation determined a resonators quality factor about a factor 10 lower than what we expected. The next attempt was the deposition of the silicon nitride layer not on the whole wafer, but only in the region where it is really necessary for the membrane, i.e. around the absorber and the res-

onator inductor. Possible dissipations due to silicon nitride present below the capacitive resonator elements could it this way be avoided. This try resulted in a not valuable improvement. At that point, it was necessary to focus the investigations on other possible dissipative phenomena and we decided to study the presence of negative charges in the silicon nitride. Employing a mercury probe, capacitance-voltage measurements have been carried out on some test wafer with deposited silicon nitride. The results showed an high presence of negative charges inside the dielectric, a value around  $2 \times 10^{16}$  charges/cm<sup>3</sup> was estimated. To get rid of this charges a new device fabrication was done in which an oxide layer between the silicon wafer and silicon nitride was deposited. The quality factor of the resonators obtained with this configuration, improved about a factor of 2. This is non yet the desired target, but a further improvement could be obtained in a complete detector fabrication, where the silicon substrate is removed in the regions where the membrane is released. This new MKIDs production is planned for 2020.

## Selected Papers

- Faverzani, M., Ferri, E., Giachero, A., Giordano, C., Margesin, B., Mezzena, R., Nucciotti, A., and Puiu, A. (2020). *Characterization of the low temperature behavior of thin Titanium/Titanium Nitride multilayer films*. Supercond. Sci. Technol **33**. Art. no.: 045009.
- Mezzena, R., Faverzani, M., Ferri, E., Giachero, A., Margesin, B., Nucciotti, A., Puiu, A., and Vinante, A. (2019). *Development of Microwave Kinetic Inductance Detectors for IR Single-Photon Counting*. J. Low Temp. Phys. DOI: 10.1007/s10909-019-02251-1.

# MoVe IT

Elettra Bellinzona and Emanuele Scifoni<sup>†</sup> on behalf of the MoVe IT collaboration<sup>1</sup>

MoVe IT, Modeling and Verification for Ion beam Treatment planning is a Call project coordinated by TIFPA and supported by CSNV-INFN, starting in 2017, with the major aim of including in treatment planning for hadron therapy new physical and biophysical properties of particle beams. The project ran its third year in 2019, and got an extension for an additional year in 2020. Beside coordination (WP0), in 2019 TIFPA personnel was heavily involved in all the Scientific Workpackages (1-4), with some notes reported below.

**WP1 - Radiobiological Modeling for Treatment Planning** The analysis of RBE impact of nuclear fragmentation of the target nuclei was finalized. The proton spectra description has been obtained by Monte Carlo simulation performed with TOPAS (collaboration with Krakow University), and FLUKA thanks to INFN Milano (Embriaco et al. submitted to Phys Med). As Fig. 1(left) describes, all the secondary particles generated from a proton in water are scored.

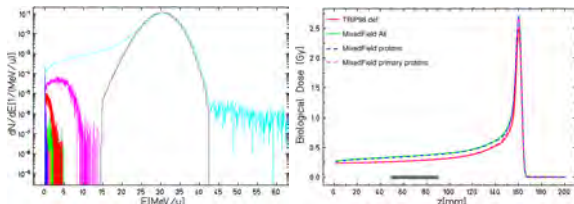


Figure 1: (Left) Fluence spectra of 150 MeV proton in water simulated with TOPAS; (Right) biological dose comparison calculated including only primary protons or all fragments.

Thanks to a conversion tool developed on purpose to create input files for TRIP98 TPS, the RBE description has been based on the mixed field theory, accounting for the radio-biological impact of all the secondary particles separately. The consequent biological dose is evaluated considering all fragments and compared with the one obtained considering only primary pro-

tons, as it is in the current TPS workflow; an example is shown in Fig. 1(right).

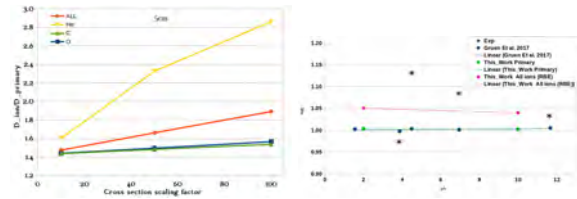


Figure 2: (Left) Biological dose for a proton beam with  $E_0 = 150 \text{ MeV/u}$  obtained by using modified fluence spectra in which selected ions i.e. Helium, Carbon, Oxygen,  $Z > 2$ , have been multiplied for a factor 10. (Right) RBE evaluated in LET region of 0-1  $\text{KeV}/\mu\text{m}$  at 50% of survival ( $RBE_{50}$ ) vs  $\alpha/\beta$  ratio, with and without fragments contribution, compared with experimental data and previous calculations (Bellinzona et al., in prep. for Phys. Med. Biol.).

Waiting for FOOT data, an analysis on the impact of the uncertainty on the fragment production cross section has been performed, varying manually the secondaries abundance; the more effective species are found to be protons and Helium as Fig. 2a shows.

RBE evaluated at 50% and 80% of survival are evaluated at different  $\alpha/\beta$  ratio and compared with experimental data and a previous only proton LEMIV calculation. The results obtained considering fragments contribution fits better the experimental points as Fig. 2b reports.

The TIFPA group started also the development of NTCP based optimization in TPS.

**WP2 - NTCP/TCP Modeling** The modeling package lead by Naples was succeeding to realize important translational studies on different effects of protons and photons on patient data from Trento Proton therapy center (Palma et al. 2020) and MD Anderson (Houston, TX, see Fig. 3 (Palma et al. 2019c)).

<sup>†</sup>Contact Author: emanuele.scifoni@tifpa.infn.it

<sup>1</sup>for full list of contributors see [www.tifpa.infn.it/projects/move-it/](http://www.tifpa.infn.it/projects/move-it/)

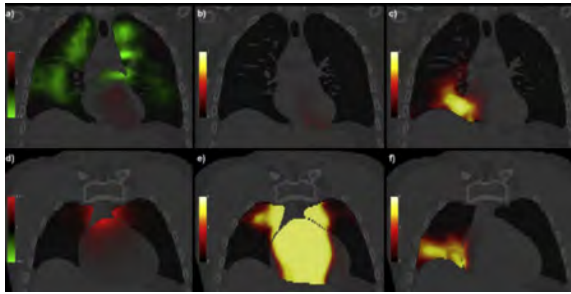


Figure 3: Impact of dose distribution difference between photon (IMRT) and protons (PSPT) plans on significance map in patients treated and developing Lung Pneumonitis (a) and (d) maps of mean differences in biologically effective dose (BED, in Gy) between patients treated with IMRT or PSPT. (b) and (e) significance maps ( $-\log p$ ) of such BED differences. (c) and (f) significance maps of differences in BED between patients developing or not radiation pneumonitis symptoms. See (Palma et al. 2019c) for details.

**WP3 - Biological Dosimetry** Among the advances in this part, TIFPA-CIBIO team together with BioTECH and Naples (Parthenope University) coworkers, succeeded to finalize the protocol for  $\gamma\text{H}_2\text{AIX}$  analysis of irradiated biophan-

tom, in order to obtain highly spatially resolved DNA damage images in the of a proton Bragg Peak (see X-ray test in Fig. 4). At the same time, in collaboration with GSI and LNS, the hypoxic chamber design was completed and is currently in construction.

#### WP4 - Facilities and beamline simulations

Beside new implementations in the TIFPA proton beam lab for radiobiological experiments, TIFPA team contributed to the development of a new beam profiler with LNS team (Catalano et al. 2020).

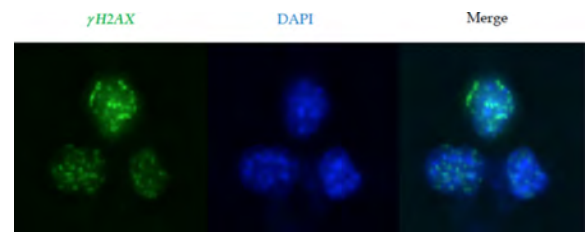


Figure 4: Results of X-ray irradiation on the last developed phantom, showing visualization of damaged nuclei (through the  $\gamma\text{H}_2\text{AIX}$  assay) superimposed to the total nuclei imaging (through DAPI).

## Selected Papers

- Catalano, R., Petringa, G., Cuttone, G., Bonanno, V., Chiappara, D., Musumeci, M., Puglia, S., Stella, G., Scifoni, E., Tommasino, F., and Cirrone, P. (2020). *Transversal dose profile reconstruction for clinical proton beams: A detectors inter-comparison*. *Physica Medica* **70**, pp. 133–138.
- Palma, G., Monti, S., Xu, T., Scifoni, E., Yang, P., Hahn, S. M., Durante, M., Mohan, R., Liao, Z., and Cella, L. (2019c). *Spatial dose patterns associated with radiation pneumonitis in a randomized trial comparing intensity-modulated photon therapy with passive scattering proton therapy for locally advanced non-small cell lung cancer*. *International Journal of Radiation Oncology\* Biology\* Physics* **104**(5), pp. 1124–1132.
- Palma, G., Taffelli, A., Fellin, F., D'Avino, V., Scartoni, D., Tommasino, F., Scifoni, E., Durante, M., Amichetti, M., Schwarz, M., and Cella, L. (2020). *Modelling the risk of radiation induced alopecia in brain tumor patients treated with scanned proton beams*. *Radiotherapy and Oncology* **144**, pp. 127–134.

## Redsox2

Irina Rashevskaya,<sup>†</sup> Pierluigi Bellutti, Giacomo Borghi, Francesco Ficorella, Giancarlo Pep-  
poni, Antonino Picciotto, Nicola Zorzi

In 2019 the TIFPA group in the REDSOX2 col-  
laboration continued the activities for the char-  
acterisation of a large number of silicon drift  
detectors.

The batch Sesame was produced by FBK  
in 2018. A test of a large number of Sesame  
sensors were performed with a probe card that  
optimise the test process and apply a bias on  
all eight cells of the structures simultaneously.  
Sensor testing revealed a large variation of dop-  
ing concentration from the center to the edge  
of the wafer. This fact introduced a further uni-  
formity parameter in the choice of the sensors,  
required some changes in the power supply and  
requires testing of sensors at two different bias  
voltages to define a sufficient number of sensors  
that can be mounted on the same system.

A 64-channel detector system has been spe-  
cially designed and developed by the ReDSOX  
Collaboration for the XRF-XAFS beamline of the  
SESAME Synchrotron light source in Jordan  
(Rachevski et al. 2019a). The detector system  
consists of 8 monolithic array of Silicon Drift  
Detectors each with 8 cells, with a total area  
of 570 mm<sup>2</sup>. Numerous tests both in the Optical  
X-ray laboratory and at the XAFS beam line, al-  
lowed characterisation and performance evalu-  
ation. The overall energy resolution achieves a  
result below 170 eV FWHM at the Mn 5.9 keV  
K $\alpha$  line at room temperature and an output  
count-rate (OCR) of  $15.5 \times 10^6$  counts/s. The  
work for the realisation of another “Sesame  
like” detectors with 64 readout channels for the  
ELETTRA synchrotron of Trieste is in progress.

For TwinMic experiment at ELETTRA syn-  
chrotron of Trieste 6 trapezoidal sensors with  
8 cells and area of 308 mm<sup>2</sup> of batch Sesame  
were tested and mounted for test beam.

The batch Redsox4 produced by FBK in  
2019 include several sensors for various experi-  
ments and applications. The first automatic test  
of test structures and all SDDs were performed

by FBK on the wafer. The total current of all  
SDD, measured by automatic test with “tree  
needles” provide the first very useful informa-  
tion on the production yield. After cutting a test  
of a large number of sensors were performed  
with optimised test process. This test defined  
the applicable voltage range, the value of inte-  
grated resistants of every sell and the anodes  
current of each cell of sensors. The selected  
and cataloged sensors were then mounted in  
the Theseus, Flares, HERMES (F Fuschino et al.  
2019a), and other experiments within the Red-  
sox2 project.

In addition to the sensor acceptance test for  
Hermes experiment, several studies were per-  
formed:

- (i) Radiation test. The irradiation test  
were performed on 4 single anode sen-  
sors. Two of them were mounted on  
board with connection to the bias sys-  
tem. The measurements of anodes cur-  
rent were performed during irradiation  
without bias, then immediately after ir-  
radiation by applying bias for 30'. The  
study of annealing of the current on all 4  
sensors were performed for 3 month (see  
HERMES contribution at p. 111).
- (ii) Epoxy process. The epoxy process were  
performed by FBK group. The sensors  
were tested again after each step of the  
process. Same additional test as hitting  
the sensor with Epoxy up to 80°C or  
cleaning the sensor were performed in  
laboratory. Two sensors were bent to  
study the effect of mechanical stress on  
electrical performance of the sensors (see  
Fig. 1). Stability tests were performed on  
this sensors, no negative effects were ob-  
served. The definition of Epoxy process is  
in progress.

<sup>†</sup>Contact Author: [irina.rashevskaya@tifpa.infn.it](mailto:irina.rashevskaya@tifpa.infn.it)

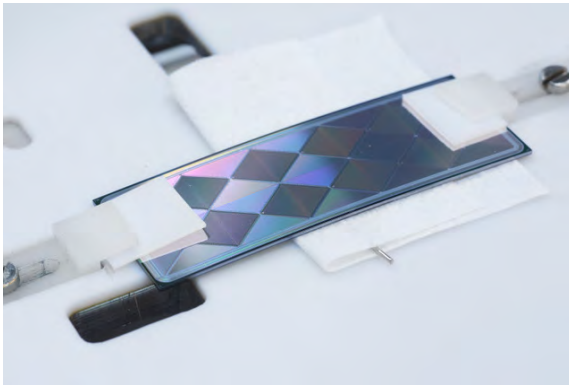


Figure 1: Mechanical stress on HERMES sensor.

The test and the study carried out on different structures were presented at the Collaboration Meeting in Rome 6-8 June 2019 and Hermes Meeting 22-23 January 2020.

The close collaboration between the RED-SOX project and FBK that jointly develop the SDD sensors has produced remarkable achievements in the design of very-large area, low leakage current, spectroscopy detectors for low X-ray measurements. This Large Area SDD for applications of X-ray Astrophysics will be used in two active projects:

- eXTP approved (Chinese-led international collaboration Chinese Academy of Science- ASI coordinates the consortium of non-Chinese space agencies) (Zhang et al. 2018a). EXTP is a space science mission designed to study fundamental physics under extreme conditions of density, gravity and magnetism. The mission aims to determine the equation of

state of matter at supra-nuclear density, to measure the effects of QED, and to understand the dynamics of matter in strong-field gravity. In addition to investigating fundamental physics, eXTP will be a very powerful observatory for astrophysics that will provide observations of unprecedented quality on a variety of galactic and extragalactic objects. In particular, its wide field monitoring capabilities will be highly instrumental to detect the electro-magnetic counterparts of gravitational wave sources.

- STROBE X ongoing development (NASA). Time-Resolving Observatory for Broadband Energy X-rays (STROBE-X), a Probe mission concept which utilises the significant recent advances in very large-area silicon detectors by combining two pointed instruments: the large-area collimated SDDs which formed the main instrument of EXTP mission and SDD-based wide-field monitor.

The batch of LOFT detectors with active area of  $76 \text{ cm}^2$  (LOFT2018) produced in FBK in September of 2018 showed a very promising results at preliminary test. The complete double-sided test of a few LOFT detectors were performed with a new probe card, that contacts all the anodes. The visual inspection of defects and the study of the yield of the production are in underway.

The opening of the new experimental group EXTP in CSN2 of INFN is expected during 2020.

## Selected Papers

- Fuschino, F. et al. (2019a). *HERMES: An ultra-wide band X and gamma-ray transient monitor on board a nano-satellite constellation*. Nuclear Instruments and Methods in Physics Research Section A: Accelerators, Spectrometers, Detectors and Associated Equipment **936**. Frontier Detectors for Frontier Physics: 14th Pisa Meeting on Advanced Detectors, pp. 199–203.
- Rachevski, A. et al. (2019a). *The XAFS fluorescence detector system based on 64 silicon drift detectors for the SESAME synchrotron light source*. Nuclear Instruments and Methods in Physics Research Section A: Accelerators, Spectrometers, Detectors and Associated Equipment **936**. Frontier Detectors for Frontier Physics: 14th Pisa Meeting on Advanced Detectors, pp. 719–721.
- Zhang, S. et al. (2018a). *The enhanced X-ray Timing and Polarimetry mission eXTP*. Science China Physics, Mechanics Astronomy **62**(2).

# SiCILIA

Maurizio Boscardin,<sup>†</sup> Giacomo Borghi, Michele Crivellari, Francesco Ficorella, Sabina Ronchin

SiCILIA (Silicon Carbide Detectors for Intense Luminosity Investigations and Applications) is an INFN project which aim to develop technologies for the construction of radiation hard detectors for next generation of nuclear physics experiments at high beam luminosity. Silicon Carbide technology offers today an ideal response to such challenges, since it gives the opportunity to cope the excellent properties of silicon detectors (resolution, efficiency, linearity, compactness) with a much larger radiation hardness (up to five orders of magnitudes for heavy ions), thermal stability and insensitivity to visible light. However, no commercial SiC detector exists and a significant upgrade of present devices is required in terms of thickness of the active region and detection area.

The aim of the project is to develop innovative processes, which allows the production of thick ( $>100\ \mu\text{m}$ ) and large area (about  $1\ \text{cm}^2$ ) SiC detectors with unprecedented level of defects; Schottky technology represents today the state of art for the manufacture of SiC devices. We propose to push forward the limits for this technology in relation to the thickness and the active area.

Starting in 2016, the first phase of the project has been totally dedicated to setting-up a processes flow in FBK, in order to produce different prototype devices. After this phase, a second step has required a complete characterization of the prototypes when these are irradiated by different kind of radiation (heavy-ions, electrons, neutrons and photons), in conjunction also with standard and customized low-noise electronics.

The fallout of the project is used and will be useful also for other fields of fundamental and applied research. The SiC Schottky diodes have been realized in the Fondazione Bruno Kessler Microfabrication Facility on 4H-SiC wafers sup-

plied by LPE, the epilayer is  $10\ \mu\text{m}$  thick and doped in  $5\times 10^{13}\ \text{cm}^{-3}$ . A Schottky diode is made of a thin metal layer (Au) to form the Schottky contact on the semiconductor surface. On the top of this metallization, we add  $1.2\ \mu\text{m}$  of AlSi in order to realize the bonding pads. A silicon oxide deposited at  $720\ ^\circ\text{C}$  (TEOS) but annealed at high temperature was used as a passivation. For the final back-side metallization, we used a Ti metallization layer. Devices have been made with different geometry and area:

- (i) circular diode  $300$  and  $500\ \mu\text{m}$  in diameter;
- (ii) square diodes with an area of about  $2.5\times 2.5\ \text{mm}^2$  and  $5\times 5\ \text{mm}^2$ .

Also, different types of terminations have been explored in particular:

- (i) The first is based on an annular Schottky contact surrounding the main diode that acts as guard electrode for collecting the surface currents, both singular and multiple ring structures have been realized;
- (ii) The second is based on junction termination extension (JTE) technique. The JTE is implemented through a boron implantation done at RT, followed by annealing step at  $1050\ ^\circ\text{C}$ .

All the diodes detectors have been characterized by an automatic probe station with an I-V scan from  $-200\ \text{V}$  to  $5\ \text{V}$  and with a C-V characterization up to  $40\ \text{V}$ .

Characterizations with ionic beams and radioactive sources are underway at the LNS and at the Milano INFN section. Furthermore, FBK has recently completed the realization of large area Schottky diodes ( $1\ \text{cm}^2$ ) on  $100\ \mu\text{m}$  epitaxial substrates.

---

<sup>†</sup>Contact Author: boscardi@fbk.eu

# Simp

Paolo Falferi,<sup>†</sup> Benno Margesin, Eugenio Monticone, Luca Oberto, Mauro Rajteri

The possibility to build electronic nanoscale devices operated at millikelvin temperatures has started the superconducting quantum technology. To the more traditional applications, that include for example cosmic background radiation and THz imaging, has been recently added the development of the circuit quantum electrodynamics, that is the realization of on-chip quantum optics circuits in the microwave frequency range. Axions were introduced to solve the so-called “Strong CP problem” and are expected to be light sub-eV particles weakly bound to ordinary matter and, for this reason, are good candidates for Dark Matter. An increasing number of experiments intends to exploit the conversion of Dark Matter axions by means of strong magnetic fields into microwave photons. All these activities will benefit from the development of ultrasensitive microwave photon detectors. For this purposes, INFN has financed the SIMP project which has the goal of developing two types of single microwave photon detectors: Transition Edge Sensor (TES) for the frequency range 30-100 GHz and Current Biased Josephson Junction (CBBJ) for the frequency range 10-50 GHz.

Transition Edge Sensors are thermometers based on the steep resistive transition of a superconducting material: superconducting films are biased within the transition region where the high slope of the resistance vs temperature curve enhances the sensitivity to temperature variations and makes them thermometers suitable either as bolometers or as microcalorimeters. TESs were developed for measurement of single photons from gamma and X-ray down to the visible and near infrared region where they demonstrated photon-number-resolving capability. TESs were also developed in array configuration to study the cosmic microwave background at millimeter wavelengths with ground-based telescopes, sub-orbital balloon-flights telescopes and (planned) space tele-

scopes.

The TES sensitivity is basically determined by the Johnson noise of the TES resistance and thermodynamic fluctuations associated with its thermal impedance (phonon noise). In this case the TES energy resolution can be shown to scale with the critical temperature of the TES superconductor, and the square root of its heat capacitance. In addition, a critical parameter is the sharpness of the superconducting transition (higher is better). This suggests lowering the operation temperature and the sensor volume as much as possible in order to detect the low-energy microwave photons and suppress the dark count. In order to finely tune the transition temperature in the range of tens of mK, we use of the proximity effect in the normal/superconductor bilayers made of Ti/Au or Al/Cu. As a reasonable example we consider a TiAu bilayer TES with  $V_{Ti} = 300 \times 80 \times 10 \text{ nm}^3$  and  $V_{Au} = 300 \times 80 \times 25 \text{ nm}^3$ , operating at a critical temperature of 40 mK with sharpness parameter of 20. In this case the expected energy resolution is 0.1 meV which corresponds to a frequency resolution of 24 GHz. To summarize, a photon-number-resolving TES, operating in the frequency range 30-100 GHz with negligible dark count, seems feasible. Our initial efforts are directed at finding the best TES materials.

Superconducting circuits based on Josephson junctions are fabricated by standard lithographic technologies and can be integrated in complex systems, with an extremely high flexibility and controllability. The nonlinearity of the Josephson junctions allows the realization of systems behaving as artificial atoms, with typical level spacing of the order of few GHz up to tens of GHz. All these characteristics make them interesting as detectors for microwave single photons. Non-destructive measurement of 6 GHz photons was performed in a coplanar resonator. Further improvements were obtained

<sup>†</sup>Contact Author: [paolo.falferi@unitn.it](mailto:paolo.falferi@unitn.it)

using two-cavity schemes and 3D cavities. The flexibility of Josephson elements makes possible a series of different approaches. For example, it is possible to consider a current biased Josephson junction operating in the phase regime, where the escape from the excited level causes a transition to the voltage state that can be easily read out, or a flux qubit based on a lambda-type three level system. In order to apply the CBJJ detector to an axion experiment, our aim is to drastically reduce the dark count

of this type of devices below the mHz rate.

We have presented the project Simp for the development of a single microwave photon detector for fundamental physics experiments and quantum technologies, its goals and the planned techniques to achieve them. The next steps will be the selection of the best practical superconducting materials for the TES detector and the achievement of a dark count rate of the order of magnitude of 10 kHz for the CBJJ detector.

# THEEOM-RD

Enrico Serra,<sup>†</sup> Michele Bonaldi, Antonio Borrielli, Giovanni Andrea Prodi

In Quantum Sensing and more generally in the Quantum Technologies context, High Efficiency Electro-Optic Modulators (EOM) based on RF/Optic bi-directional conversion are gaining momentum because of their unique behaviour of maintaining coherence of quantum states in the two frequency domains. Efficient up-conversion/down-conversion of RF signals to an optical carrier would enable their transmission through optical fibres instead of through copper wires, drastically reducing losses, and would give access to the set of established quantum optical techniques that are used in quantum-limited signal detection. This is of fundamental interest in quantum communications where qubits in a superconductive quantum computer in a cryogenic environment are transmitted to optical fibers networks at great distance in a quantum network at room temperature. The relevance of these devices is foreseen also in other fields like radio-astronomy, RF non-reciprocal switches and in medical imaging. EOM devices can efficiently work, in the classical domain, as ultra-low noise read-out systems for weak RF signals. For instance, in NMR (Nuclear Magnetic Resonance) a shot-noise limited read-out improves the image reconstruction process. The platform for the transduction consists of a high-quality nano-membrane resonator that can simultaneously be coupled to a the electric and optical degrees of freedom and therefore they can transduce signals at disparate frequencies with high efficiency. This is done by adding a conductive layer to the membrane's surface realising a capacitive coupling between the moving electrode and the fixed LC rf circuit. The fluctuations of the vibrating mode of the membrane links the rf-electromagnetic field to the optical field of a high finesse cavity. The EOM design we are developing is shown in Fig. 1 consists of membrane resonator with and on-chip shield for mechanical losses and the two electrodes

separated by a micron-scale gap. The moving electrode is under action of the fluctuation of the radiation pressure and the thermal noise coming from the environment. The coherence will be guaranteed by a high Q-factor of the membrane that is reachable applying advanced design techniques that reduces the mechanical dissipation and decouples the resonator from the thermal bath.

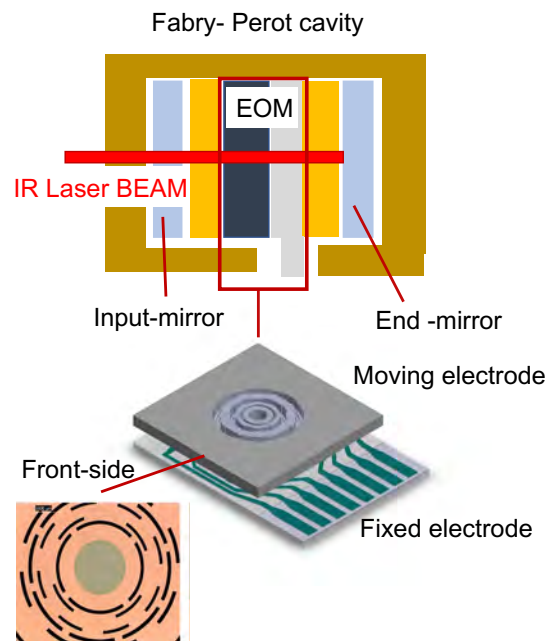


Figure 1: Schematic of a Fabry-Perot cavity with a membrane-in-the-middle setup configuration

Our membrane electrode design maximise the overlapping function between electrodes improving the electro-optical coupling rate. A TiN (Titanium Nitride) layer is RF-sputtered and was chosen as membrane's electrode, because it has a uniform thickness and resistivity, and shows the potential for yielding reproducible low-temperature devices with transition temperature of 5.6 K. On the other hand, TiN films are widely used for coplanar resonators and microwave kinetic inductance detectors (MKID). Besides the CMOS compatibility, the major advantage, is that it can be eas-

<sup>†</sup>Contact Author: [enrico.serra@tifpa.infn.it](mailto:enrico.serra@tifpa.infn.it)

ily integrated in the fabrication silicon nitride nano-membranes process previously developed (HUMOR). The fabricated electrode is ultra-thin (25 nm) deposited over a tensile (1 GPa) with an ultra-high aspect ratio: 100 nm membrane's thickness and 1.5 mm in diameter for reducing the mechechanical dissipation. The patterning of the electrode and the silicon structures was done by surface/bulk micromachining techniques used in M/N-MEMS processing.

A preliminary test on a nano-membrane was performed to see the membrane actuation via the trapped charge in the dielectric layer. Moreover, the membrane was located between two armatures of a capacitor and actuated with an external electric field. In the actuation scheme we feed back the Langevin thermal force to cool the resonator down to a low effective temperature. As result, we were able to see the feedback cooling of the resonator from room temperature

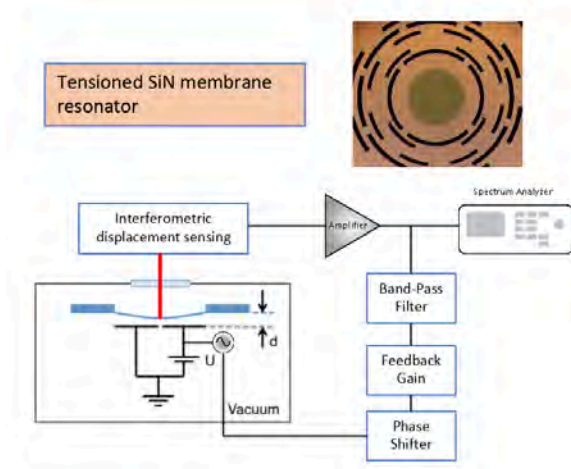


Figure 2: Simplified scheme for feedback cooling of a SiN membrane starting from room temperature.

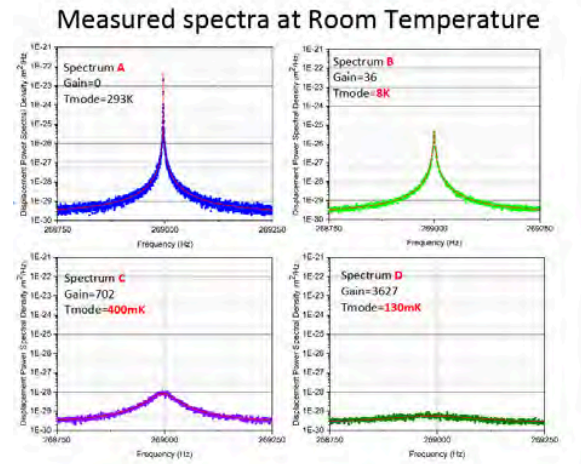


Figure 3: Displacement Spectral Density of the (0,1) membrane modes by varying the feedback gain and the corresponding effective temperature.

to 130 mK. A simplified scheme for the feedback cooling and the thermal noise displacement spectrum of mode (0,1) is shown in Fig. 2 and Fig. 3, respectively. In the experiment, the functionalized nano-membrane, will be embedded into a Fabry-Perot cavity and used to detect weak signals in the MHz bandwidth that are of interest in NMR imaging. Mapping the signal in the optical intracavity field with a shot-noise limited read-out will give us the platform for understanding devices behaviours and to study the electro-opto-mechanical interaction at room and cryogenic temperatures. Advanced measurement schemes based on quantum cavity optomechanics protocols will be used for observing state rf/Optical transfer when resonator is at low phonon occupation number.

# TIMESPOT

Gian-Franco Dalla Betta,<sup>†</sup> Maurizio Boscardin, Francesco Ficorella, Giulio Tiziano Forcolin, David Macii, Roberto Mendicino, Giovanni Paternoster, Giancarlo Pepponi, Sabina Ronchin, Giovanni Verzellesi, Nicola Zorzi

The project is aimed at the development and implementation of a complete integrated system for tracking having very high precision both in space ( $100\ \mu\text{m}$  or less) and in time (100 ps or less) per pixel. The main use and scope is in HEP experiments at high luminosity (e.g., upgrade of LHCb VELO), where the high density tracking, both in space and time, is an issue. The approach is based on 3D geometry Silicon and Diamond pixelated sensors, dedicated integrated front-end and pre-processing chip (time measurement electronics) in 28 nm CMOS, and real-time processors for data elaboration both at front-end and back-end level (fast tracking algorithms). TIFPA is responsible for WP1: 3D Si sensors development and characterisation, and is also involved in WP6: System integration and tests.

Following an intense design and TCAD simulation phase (Mendicino et al. 2019b), which allowed to identify the most promising layout options and trench geometries, the first batch of TIMESPOT sensors was produced at FBK in 2019 using a single-sided fabrication process. P-type Silicon-Silicon Direct Wafer Bonded wafers were used as starting material, consisting of a  $150\ \mu\text{m}$  thick, high-resistivity FZ active layer bonded to a  $500\ \mu\text{m}$  thick, low-resistivity handle wafer. The p-type (ohmic) trenches are etched deeper than the active layer and penetrate the highly doped handle wafer, so that the bias voltage can be applied from the back-side. On the contrary, the n-type (read-out) trench etching is stopped at  $15\ \mu\text{m}$  from the support wafer to avoid early breakdown. The thick handle wafer allows the production of thin active layers and active edges without compromising the mechanical stability of the wafers during fabrication. It could eventually be thinned to the desired thickness at the end of the process, and a metal layer could be de-

posited on the back-side in order to improve the contact and ease wire bonding.

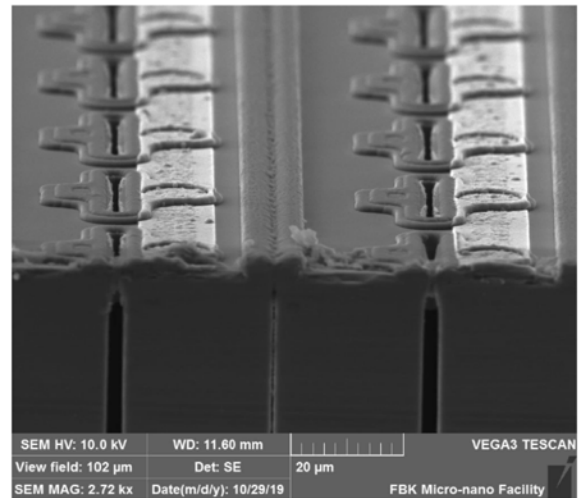


Figure 1: SEM cross section through one a processed wafer.

A Scanning Electron Microscope (SEM) cross section through one the wafers is shown in Fig. 1, where some details of the pixels (both types of trenches and surface topography) can be appreciated.

The reticle layout used in the first batch contains a full TIMEPIX compatible pixel sensor as well as a large number of different types of test devices (Forcolin et al. 2019b). Devices have been thoroughly tested, starting from an electrical characterization at wafer level.

The current-voltage (I-V) characteristics in reverse bias were measured on both the TIMEPIX compatible devices as well as the small ( $18 \times 18$ ) pixel devices, using a temporary metal on the wafer. Fig. 2 shows the I-V curves of groups of pixel shorted together by the temporary metal in a TIMEPIX sensor. The leakage current is very good: after normalization to the number of pixels, the measured values correspond to  $\approx 10\ \text{pA/pixel}$ . The breakdown volt-

<sup>†</sup>Contact Author: gianfranco.dallabetta@unitn.it

age of the devices was measured on test structures after the removal of the temporary metal and was found to be in the range from 150 and 200 V, which allows for a wide operational range.

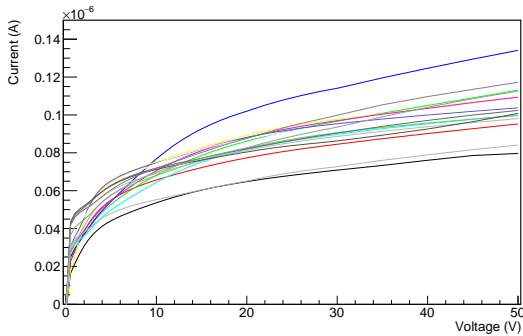


Figure 2: I-V plot of a pixel sensor: each curve represents a  $16 \times 256$  pixel section of the device.

Capacitance-voltage (C-V) measurements were subsequently carried out on the  $7 \times 10$  pixel strip devices, see Fig. 3. The curve shapes are not ideal due to the metal layer which connects rows of pixels and the pad: the measured capacitance is actually the sum of the pixel capacitance and of the MOS capacitance. This prevents from an accurate extraction of the depletion voltage, which, however, is likely associated with the first saturation plateau of the curves at just a few Volts (see also the I-V curves for comparison). The second saturation plateau at larger voltage indicates that the surface region beneath the metal layer is inverted. After removing the contribution to the capacitance from the metal connections and the pad, the opposite electrode capacitance per pixel was determined to be 70-75 fF/pixel at full depletion

and largely independent on trench dimensions and pixel geometry. This is in reasonable agreement with simulations which predicted the capacitance to be 80-85 fF/pixel, independent of the geometry used (Forcolin et al. 2019b).

Functional measurements have been performed in the laboratories of the TIMESPOT Collaboration, using laser and radioactive sources. The first test beam measurements carried out on these devices at PSI are very promising, showing a timing resolution below 30 ps. Further functional tests are under way, including radiation damage tests.

Meantime, the reticle layout for the second batch of sensors was designed at UniTN and submitted for fabrication to FBK. It contains twenty ( $5 \times 4$ ) pixel sensors, each consisting of an array of  $32 \times 37$  pixels, compatible with the new TIMESPOT read-out chip, as well as a large number of test devices and test structures for process monitoring.

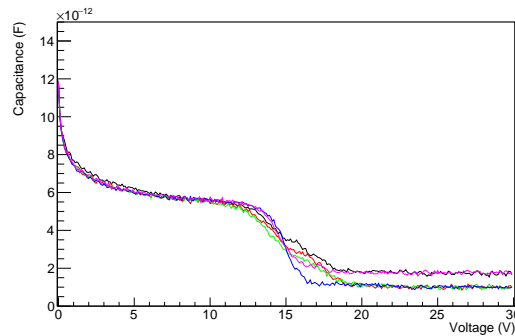


Figure 3: C-V plot of a  $7 \times 10$  pixel strip device, the three lines with a lower plateau are 10 pixel strips while the remaining two are from two pairs of connected 10 pixel strips.

## Selected Papers

- Forcolin, G., Mendicino, R., Boscardin, M., Lai, A., Loi, A., Ronchin, S., Vecchi, S., and Dalla Betta, G.-F. (2019b). *Development of 3D trenched-electrode pixel sensors with improved timing performance*. *Journal Instrum.* **14**. Art. no.: C07011.
- Mendicino, R., Boscardin, M., Ficorella, F., Forcolin, G., Lai, A., Loi, A., Ronchin, S., Vecchi, S., and Dalla Betta, G.-F. (2019b). *3D Trenched-Electrode Sensors for Charged Particle Tracking and Timing*. *Nuclear Instrum. Methods A* **927**, pp. 24–30.

The background consists of several overlapping triangles in shades of purple and light blue. A large, dark purple triangle is on the left side, pointing downwards. To its right, a medium purple triangle points upwards. Below these, a light blue triangle points upwards. The right side of the image is white.

Outreach



# OCRA - Outreach Cosmic Ray Activities

Elettra V. Bellinzona, Francesco Dimiccoli,<sup>†</sup> Christian Manea, Marta Missiaggia, Francesco Nozzoli, Ester Ricci

The phenomenon of cosmic radiation, invisible to human eyes, encompasses all the fundamental problems of modern physics: from the origins and evolution of the Universe to the current understanding of the behaviour of known forces up to the intimate structure of matter. From the study of this radiation all modern theories and knowledge of the world around us were born. On the other hand, cosmic radiation is easily intercepted and can easily be “made visible” through simple telescopes of particle detectors, therefore it represents in itself an excellent teaching laboratory to introduce non-experts, in particular students, to the study of physics and fundamental phenomena of nature. Through the use of a simple detector and with the guidance of the researchers of the center, the INFN project named “Outreach Cosmic Ray Activities” (OCRA) aims to make students participate in a real campaign of measurements of the cosmic ray phenomenon. OCRA’s program includes participation in the International Cosmic Day (ICD), a three-day internship for high school students and the development and production of instrumentation for educational activities. These activities are carried out at TIFPA and in 17 other locations around the world and coordinated internationally by the DESY collaboration. The experimental activity carried out at ICD regards one particularly interesting target of cosmic ray physics, the measurement of cosmic muon rate. The goal of the activities regards the measurements of atmospheric muons, which are copiously created in the interaction of energetic primary cosmic particles (mostly protons) with the Earth atmosphere, mainly by the decay of charged pions and kaons. While most of the soft component in the secondary radiation is absorbed by a relatively small thickness of material, muons have a large penetrating power, reaching the sea level and even passing through a large thickness of solid rock.

<sup>†</sup>Contact Author: francesco.dimiccoli@unitn.it



Figure 1: At ICD-2019, various experts from the TIFPA gave introductory speeches on Cosmic Ray Physics to the students, before involving them in a real cosmic muon flux measurement.

Apart from the low-energy region, the differential energy spectrum of the vertical secondary muons in a shower exhibits a power-law shape with an average value around a few GeV. The detailed shape and the average momentum of muons depend however on the orientation of the secondary muons with respect to the vertical. The 2019, 6th November the TIFPA center joined the initiative for the first time, proposing an afternoon dense of activities to 26 students coming from 3 different high schools of Trentino-Alto-Adige:

- Istituto di Istruzione “A. Degasperi”, Borgo Valsugana
- Istituto di Istruzione “Martino Martini”, Mezzolombardo
- Liceo Scientifico “L. da Vinci”, Trento

After an introduction on the cosmic ray physics from the various expert of TIFPA

(Fig. 1), they carried out their own measurements of the cosmic muon rate and got in contact with groups all over the world to compare and discuss their results, working like a real scientist in an international collaboration. Divided in groups, they collaborated with each other to measure the muon average velocity and the angular dependence of the cosmic muon flux.

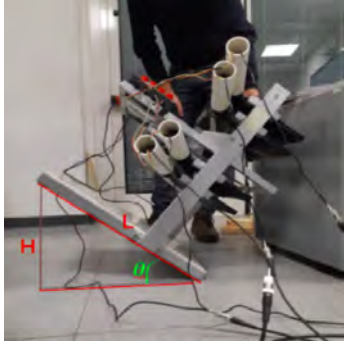


Figure 2: The TIFPA muon Telescope, inclined for the measurement of muon flux angular dependence

To do so they used an experimental set-up prepared by the experts of the centre, made up by a detector and an high performance oscilloscope for data read-out. The detector (TIFPA Muon Telescope) has a simple and solid structure that allows to perform the measurements at different angles (Fig. 2). It consists of 4 layers of scintillator, which we will number from 1 to 4. Layers 1 and 3 and layers 2 and 4 are both  $L = 24$  cm apart. For quantifying the muon velocity the average of the measurements of  $\Delta T_{1,3}$  and  $\Delta T_{2,4}$  was considered. Each measurement was taken with the detector in nominal working condition (N) and upside-down (U). This procedure allows to factorize eventual spurious delays given by the non-homogeneity of the wiring of the 4 planes. In-fact, the following relation is valid:

$$\Delta T_{1,3}^N - \Delta T_{1,3}^U = 2L/V$$

from which is possible to obtain the velocity  $V$  of the muons. Obtaining the value of  $V$  using the couple of planes (2,4), in line of principle virtually identical, gives an estimation of the error associated to the procedure. The values of  $V$  obtained are:  $V_{1,3} = 29.6$  cm/ns,  $V_{2,4} = 28.3$  cm/ns for a total estimation of  $V = 29.0 \pm 0.6$  cm/ns. The measurement of the angular dependence of the muon flux was obtained instead measuring the rate of events with a 3 out of 4 signal coincidence of the scintillation planes. The measurement was repeated multiple times at different inclination of the detector. The measurement confirmed very well the expected trend proportional to  $\cos^2(\theta)$  for an isotropic muon flux coming from above (Fig. 3). During the event, the students had also the opportunity to see the cosmic ray detectors of the centre and have a live virtual visit of the Control room of the AMS-02 experiment, sited at CERN in Geneva. Finally, they presented their results at the participants of other institutions from all-over the world, in a series of video-calls organized by the DESY collaboration.

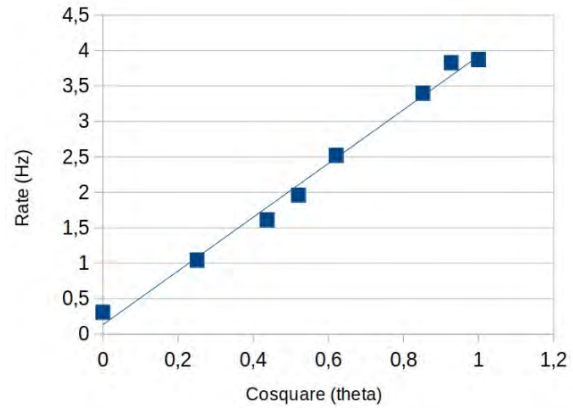
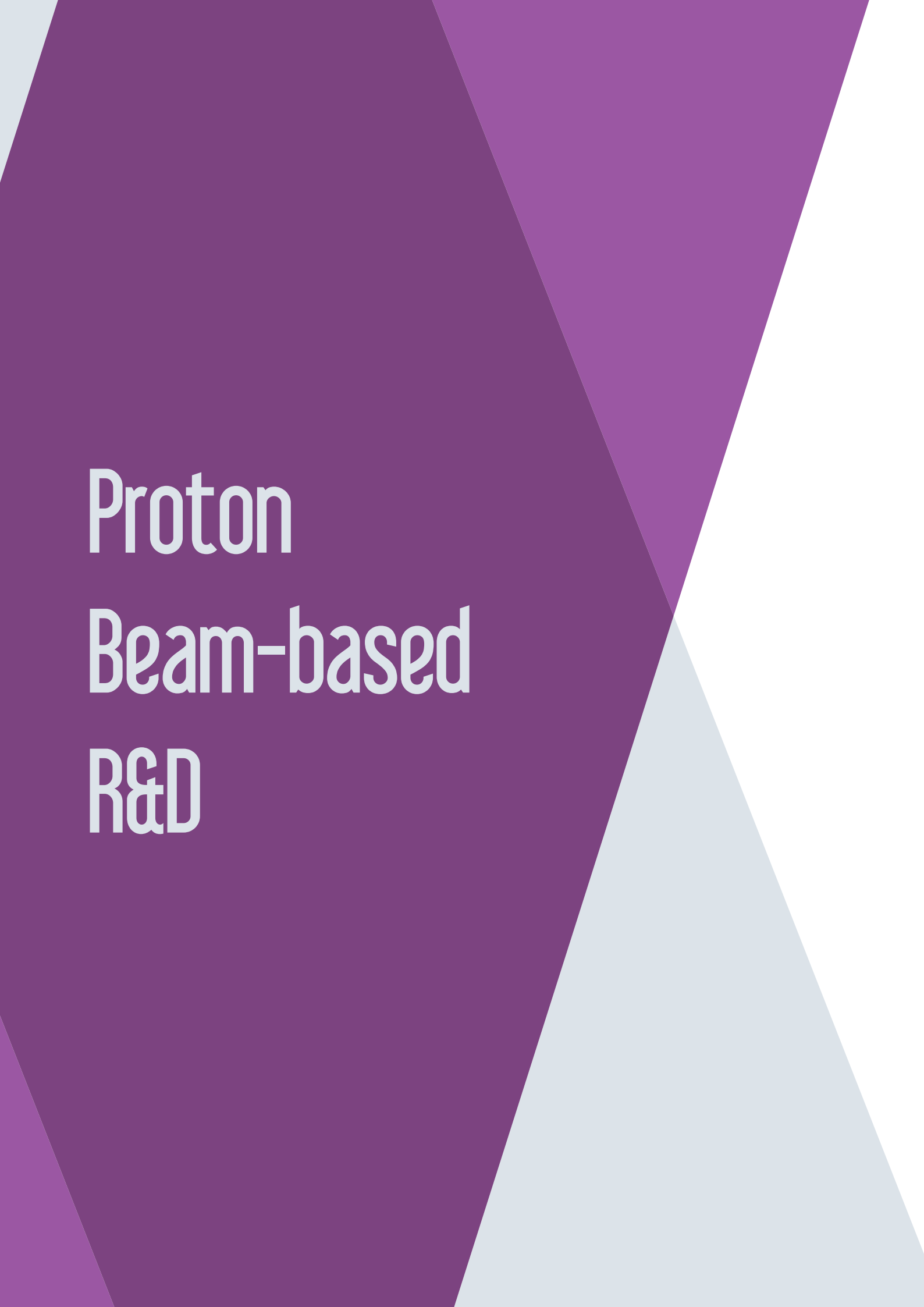


Figure 3: Cosmic muon rate measured by high school students with the TIFPA Muon telescope during ICD-2019 as a function of the square cosine of the inclination angle.



# Proton Beam-based R&D



# 4DPhantom

Franco Andreis,<sup>1</sup> Giuseppe Battistoni,<sup>2</sup> Edoardo Borghini,<sup>3</sup> Benedetto Di Ruzza,<sup>4†</sup> Francesco Fracchiolla,<sup>5</sup> Claudio Salomon,<sup>1</sup> Emanuele Scifoni,<sup>4</sup> Marco Schwarz,<sup>5</sup> Francesco Tommasino<sup>1,4</sup>

Proton therapy exploits the Bragg-peak depth-dose profile to obtain conformal treatments, while sparing healthy tissues and organs at risk surrounding the tumor. The high physical selectivity of protons makes them very sensitive to treatment-related uncertainties, one of them being related to organ motion that may induce significant distortion in the expected dose distribution. Organ motion is an issue especially for intensity-modulated proton therapy (IMPT) delivered with pencil beam scanning (PBS), since interplay effects between organ motion and beam delivery might combine together and affect treatment quality. In this context, it is important to include an evaluation of organ motion in the quality assurance (QA) workflow.

internal organ of a patient (e.g. lung or pancreas) during breathing. The software is able to reproduce analytical curves (such as  $\sin(t)$ ,  $\cos^4(t)$ ) to simulate a breathing signal and also real breathing patterns of patients acquired via infrared cameras (VisionRT<sup>1</sup>) during the radiotherapy treatment as illustrated in Fig. 2.

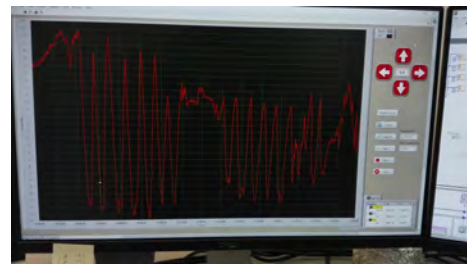


Figure 2: Real breathing signal

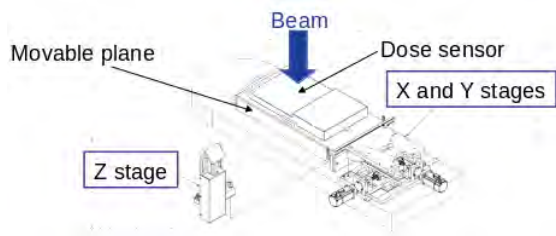


Figure 1: Overview of the 4DPhantom project

The goal of the project 4DPhantom (3D plus time) is to realize a moving plane reproducing the breathing signal of oncological patients in order to perform hadrontherapy dose measurement on a array of ionization chambers which is the most widespread detector for patient specific quality assurance in modern hadrontherapy facilities. A general overview of this project is described in Fig. 1.

The movement in each direction will be realized using three motors remotely controlled by a dedicated software. The software must be able to reproduce curves of pre-stored movement (X-t, Y-t and Z-t curve) that reproduce the 3D time dependent movement oscillation of an

The simulated (X-t) and (Y-t) curves are generally regular sinusoidal oscillations with max. amplitude greater than one cm and fundamental frequency of about 0.3 Hz. An independent plane, arranged in proximity of the fundamental plane will then reproduce a movement in the Z vertical direction in order to simulate the “Surrogate Movement”.



Figure 3: Gantry room

†Contact Author: benedetto.diruzza@tifpa.infn.it

<sup>1</sup>University of Trento, Italy

<sup>2</sup>INFN Milan, Italy

<sup>3</sup>Hypertech Solution S.R.L., Rovereto, Italy

<sup>4</sup>INFN TIFPA, Trento, Italy

<sup>5</sup>APSS, Trento, Italy

<sup>1</sup><https://visionrt.com/>



Figure 4: Therapy control room

The framework chosen to control all the movement system is the National Instruments LabVIEW<sup>2</sup> framework. To speed up movement control in the three independent directions a National Instruments FPGA (model NI MyRIO 1900) was added.

The first concluded part of the activity, has focused on the realization a prototype phantom able to reproduce the time dependent movement in the Y direction only.

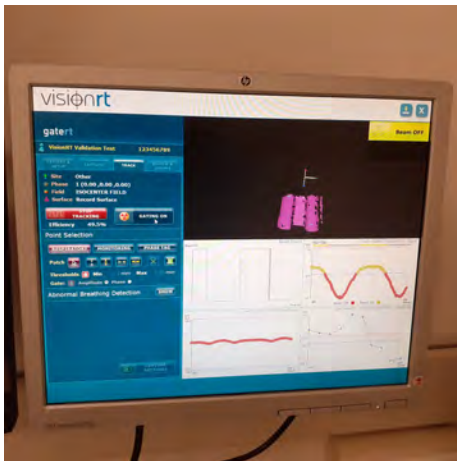


Figure 5: Optical tracking system (VisionRT)

The first successful tests of this Phantom prototype were performed on January and May 2020 in one of the two gantry rooms of the

Centro di Protonterapia di Trento (see Figs. 3 and 4).

During these tests a realistic treatment irradiation plan was delivered. A simulated movement was used for the phantom, while the standard infrared patient monitoring movement system was used to monitor the phantom position (Fig. 5). The delivered dose of the irradiation was measured using the clinical patient specific QA procedure monitor system (see Fig. 6).

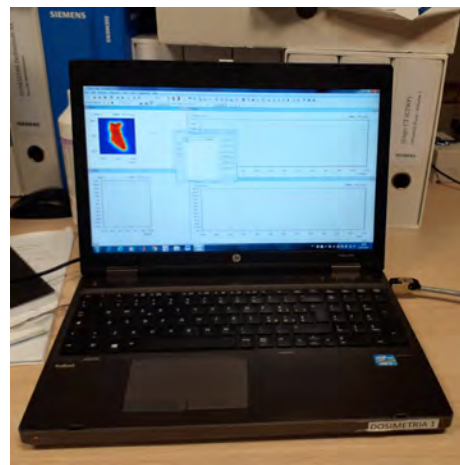


Figure 6: patient Specific QA software for dose measurement

The final goal of the project will be the delivery of a 4D phantom that is easy to use, allowing at the same time high flexibility. The phantom would then be adopted by the Centro di protonterapia di Trento for the evaluation of organ motion effects. This might contribute to enhance the spectrum of treated lesions, including patients with thoracic malignancies.

**Acknowledgements** This work was partially financed by the Caritro Foundation with the Call “Bando Ricerca e Sviluppo 2017”. The authors also thanks the Hypertec Solution S.R.L.,<sup>3</sup> Rovereto, (Italy) for the financial support, the suggestions and the useful discussions.

<sup>2</sup><https://www.ni.com/>

<sup>3</sup><https://www.hypertecs.it>

# FIRE

Alberto Quaranta,<sup>1†</sup> Enrico Zanazzi,<sup>1</sup> Matteo Favaro,<sup>1</sup> Andrea Ficorella,<sup>1</sup> Lucio Pancheri,<sup>1</sup> Gian-Franco Dalla Betta,<sup>1</sup> Beatrice Fraboni,<sup>2</sup> Laura Basiricò,<sup>2</sup> Andrea Ciavatti,<sup>2</sup> Ilaria Fratelli,<sup>2</sup> Sara Carturan,<sup>3</sup> Sandra Moretto,<sup>4</sup> Felix Pino<sup>4</sup>

The activity of FIRE project is a CSN5 Call-Project devoted to the development of flexible sensors for the detection of ionizing radiation. Such sensors should be used as dosimeters suitable for the real time monitoring of the dose released in healthy tissues during radiotherapy cancer treatments.

The role of TIFPA unit is the synthesis of flexible scintillators which will be coupled to organic photodetectors for the realization of the first prototypes. In the first year several approaches have been attempted. In general, all the produced scintillators are based on polysiloxane materials doped with either luminescent dye molecules or nanocrystals. Polysiloxanes are characterized by a high chemical and thermal stability with respect to standard aromatic polymers used for the production of commercial scintillators. Moreover, they exhibit a high radiation hardness, can be produced in different shapes with commercial resins, are flexible and can be handled without the formation of cracks maintaining their scintillation yield.

In the first case we realized doped aromatic polysiloxanes capable of discriminating gamma rays from fast neutrons through the pulse discrimination (PD) analysis. (Marchi et al. 2019) In particular, it was demonstrated that with 6% of PPO as primary dye in the matrix good PD properties were obtained, with figure of merit comparable with solid scintillators available in the market. It is worth noting that the primary dye concentration in our samples is much lower with respect to commercial systems, where concentrations up to 30% were realized, owing to local aggregation effects of dye molecules in the polysiloxane matrix. The proximity of dye molecules is on the basis of PD proper-

ties, related to short range triplet-triplet interactions giving rise to the delayed fluorescence phenomenon.

Recently, radiation hardness tests were performed with a 37 MeV proton beam at the APSS facility in Trento. The light yield during irradiation was monitored by collecting the whole scintillation spectrum with a silica optical fiber connected with an OceanOptics QE-65000 spectrometer. The real time recording of the spectra evidenced that the light yield is constant up to 37 Gy under irradiation with a flux of  $2.5 \times 10^7$  p/s (see Fig. 1).

The light intensity, measured with a power meter coupled with optical grease to the scintillator, was in the range from 10 to 25 nW during irradiation. This value is similar to the power detected from the best commercial plastic scintillator, EJ-200, analyzed for comparison during the measurement run.

Flexible scintillators for the detection of thermal neutrons were realized by dispersing <sup>6</sup>LiF nanocrystals and ZnS:Ag powder in a polysiloxane matrix. <sup>6</sup>LiF crystals were synthesized by a co-precipitation process and different crystal dimensions ranging from hundreds of nm to tens of  $\mu$ m were obtained. (Carturan et al. 2019) The tests allowed to choose the best crystal dimension for a good mixing with the scintillator powder, reaching a detection efficiency of 90% with respect to the commercial analogue (EJ-420), with the advantage that the polysiloxane system is flexible and manageable.

Several attempts were carried on for the realization of scintillating systems based on polysiloxane samples containing luminescent quantum dots. Quantum dots have a broad absorption spectrum and a sharp luminescence peak whose position depends on the dot radius.

<sup>†</sup>Contact Author: [alberto.quaranta@unitn.it](mailto:alberto.quaranta@unitn.it)

<sup>1</sup>University of Trento and INFN TIFPA, Trento, Italy

<sup>2</sup>INFN Bologna and University of Bologna, Italy

<sup>3</sup>INFN LNL and University of Padua, Italy

<sup>4</sup>INFN Padua and University of Padua, Italy

Optical analyses on polysiloxane samples doped with core shell CdSe/ZnS QDs, evidenced that the overlap of the QD absorption spectrum with the matrix luminescence band allows a radiative energy transfer between the two systems, while there is no evidence of non-radiative (Förster type) energy transfer. (Zanazzi et al. 2020) Nonetheless the light yield of doped systems gave an increase of the 8% with respect to undoped scintillators owing the higher. This phenomenon was ascribed to the higher energy loss, due to the presence of QDs, experienced by protons. Luminescent QDs were also dis-

persed in polyvinyl alcohol, which is a material quite labile under irradiation. After irradiation the damaged matrix is characterized by luminescence features around 400-450 nm and we demonstrated that an energy transfer process between those emitting centers and QDs grew up, leading to an enhancement of the QD luminescence yield under UV excitation. (Zanazzi et al. 2019) This effect can be exploited for the realization of off-line dosimeters, where the released dose can be measured through the variation of QD luminescence yield.

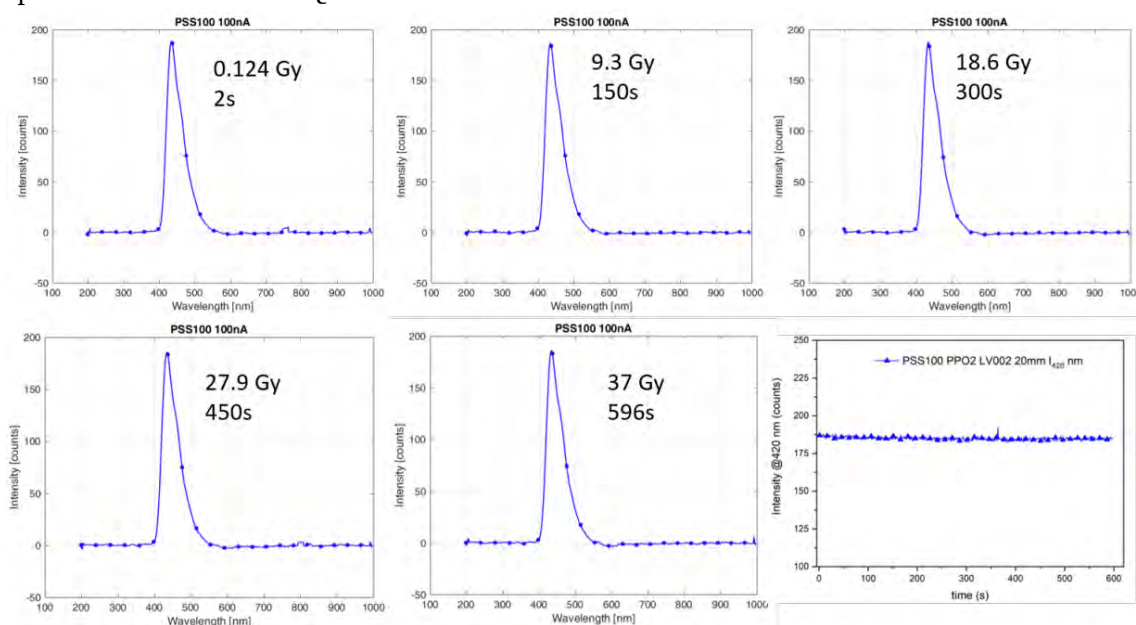


Figure 1: Luminescence spectra of a polysiloxane scintillator under proton irradiation. Each spectrum was collected with 1 s of integration time. The dose (Gy) was calculated from the released energy in the sample. Last figure shows the peak intensity at 420 nm as a function of the irradiation time.

## References

- Carturan, S., Vesco, M., Bonesso, I., Quaranta, A., Maggioni, G., Stevanato, L., Zanazzi, E., Marchi, T., Fabris, D., Cinausero, M., Pino, F., and Gramegna, F. (2019). *Flexible scintillation sensors for the detection of thermal neutrons based on siloxane  ${}^6\text{LiF}$  containing composites: Role of  ${}^6\text{LiF}$  crystals size and dispersion*. *Nuclear Instruments and Methods A* **925**, pp. 109–115.
- Marchi, T., Pino, F., Fontana, C. L., Quaranta, A., Zanazzi, E., Vesco, M., Cinausero, M., Daldosso, N., Paterlini, V., Gramegna, F., Moretto, S., Collazuol, G., Degerlier, M., Fabris, D., and Carturan, S. M. (2019). *Optical properties and pulse shape discrimination in siloxane-based scintillation detectors*. *Scientific Reports* **9**. Art. no.: 9154.
- Zanazzi, E., Favaro, M., Ficorella, A., Pancheri, L., Betta, G. D., and Quaranta, A. (2019). *Photoluminescence enhancement of colloidal CdSe/ZnS quantum dots embedded in polyvinyl alcohol after 2 MeV proton irradiation: crucial role of the embedding medium*. *Optical Materials* **88**, pp. 271–276.
- Zanazzi, E., Favaro, M., Ficorella, A., Pancheri, L., Betta, G. D., and Quaranta, A. (2020). *Real-Time Optical Response of Polysiloxane/Quantum Dot Nanocomposites under 2 MeV Proton Irradiation: Luminescence Enhancement of Polysiloxane Emission through Quantum Dot Sensitization*. *Physica Status solidi a* **217**. Art. no.: 1900586.

# External calibration of the FOOT Drift Chamber detector

Giuseppe Battistoni,<sup>1</sup> Sofia Colombi,<sup>2,3</sup> Benedetto Di Ruzza,<sup>3</sup> Yunsheng Dong,<sup>4,1</sup> Chiara La Tessa,<sup>2,3</sup> Leonello Servoli,<sup>5,6</sup> Gianluigi Silvestre,<sup>5,6</sup> Francesco Tommasino<sup>2,3†</sup>

The main goal of the FOOT (FragmentatiOn Of Target) experiment is to measure the double differential cross sections with respect to kinetic energy and emission angle of fragments produced in nuclear interactions of particles with energies relevant for hadrontherapy and radio-protection in space. These measurements will fill the current gaps at the energies of interest in the nuclear fragmentation cross section databases, allowing the improvement of the current treatment planning systems adopted in particle therapy, the study of possible new particles to be involved in hadrontherapy, the study of spacecraft shields for long-term space missions and the use of the data as benchmark for the Monte Carlo simulation models and tools. Due the low kinetic energy, the target fragments produced by a proton projectile have a range of few microns, therefore they can not be measured directly. This issue is overcome in FOOT with the use of the inverse kinematic approach combined with the technique of subtraction of cross sections as already adopted in (Dudouet et al. 2013b).<sup>1</sup> FOOT will thus measure the fragmentation of different ions beams (e.g. He, C, O) onto targets of C<sub>2</sub>H<sub>4</sub> and C. The final cross sections are evaluated by subtracting the data obtained from the former with the latter targets in order to isolate the contribution of the Hydrogen. By measuring the beam four momentum, it is then possible to recover the direct kinematic information performing a Lorentz transformation. Secondary fragments in the inverse kinematics reference frame can

be detected given their boosted energies and longer ranges. The accuracy required for the cross section data are of 5% with an energy resolution of the order of 1-2 MeV/u and a charge and isotopic identification uncertainty below 3% and 5% respectively. The FOOT experiment consists in two different setups: the emulsion setup, which is based on the emulsion cloud chamber (ECC) capabilities to measure the light charged fragments contribution ( $Z \leq 3$ ),<sup>2</sup> and the electronic setup, which is based on electronic detectors and a magnetic spectrometer to measure fragments heavier than helium. The TIFPA unit of the FOOT experiment is dedicated to the study and the optimization of the performances of two detectors inherited from the FIRST experiment:<sup>3</sup> the Start Counter (SC) and the Beam Monitor (BM). These activities are performed together with the Milano Unit. The SC is a plastic scintillator adopted in the emulsion setup to count the total number of delivered particles, to provide the trigger signal for the acquisition chain and the time reference measurement for the BM hits time measurements. It is a 250  $\mu\text{m}$  thick disk with a radius of 26 mm. The light is collected by 160 optical fibers grouped into four bundles and readout by fast PMT with 40% of quantum efficiency. The BM is a drift chamber adopted in both the experimental setups to reconstruct the direction and the position of the projectile. It consists of twelve layers of alternated horizontal and vertical cells perpendicular with respect to the beam line and staggered by a half of a cell between

<sup>†</sup>Contact Author: francesco.tommasino@unitn.it

<sup>1</sup>INFN Milan, Italy

<sup>2</sup>University of Trento, Italy

<sup>3</sup>INFN TIFPA, Trento, Italy

<sup>4</sup>University of Milan, Italy

<sup>5</sup>University of Perugia, Italy

<sup>6</sup>INFN Perugia, Italy

<sup>1</sup>Dudouet, J. et al. (2013), Phys Rev C **88**, Art.no.: 064615.

<sup>2</sup>Montesi, M. et al. (2019), Open Physics **17**(1), pp. 233–240.

<sup>3</sup>Toppi, M. et al. (2016), Phys Rev C **93**, Art.no.: 064601.

Paoloni, A. et al. (2012), SciVerse ScienceDirect **37**, pp. 1466–1472.

two consecutive layers of the same view. Each layer is made by three rectangular cells (16 mm × 10 mm) with the longer side orthogonal to the beam.

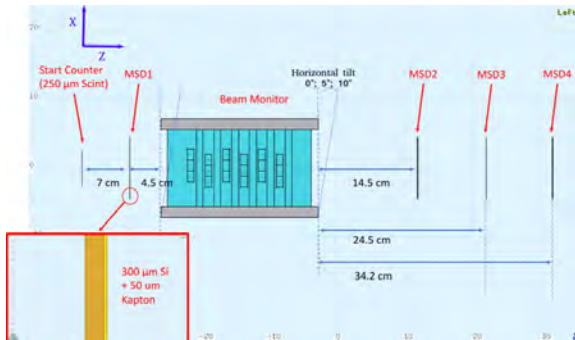


Figure 1: Schematic view of the experimental setup. The insert shows a detail of the MSD detector.

In 2019 two main activities involved the TIFPA and Milano units of the FOOT experiment. The first one consisted in a test beam dedicated to the characterization and the calibration of the space-time relation of the BM has been performed at the Trento Proton Therapy center.<sup>4</sup>

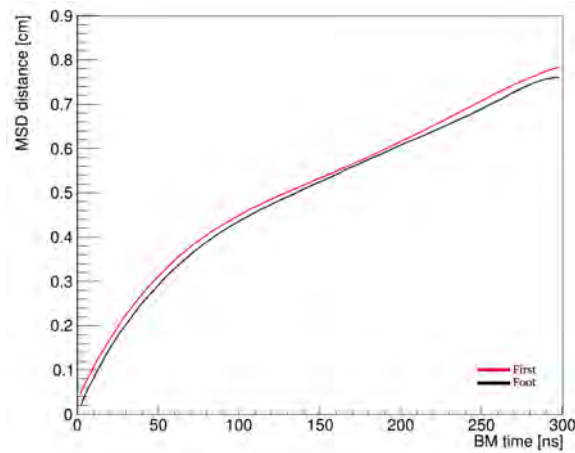


Figure 2: Space-time relations evaluated with the MSD reconstructed tracks (black) and the relations adopted in the FIRST experiment.<sup>3</sup>

The experimental setup includes the SC, the BM and four layers of Microstrip Silicon Detector (MSD) adopted as external tracking detector. The MSD detectors were provided by the Perugia Unit of the FOOT experiment. The SC was placed at the isocenter of the beam, fol-

lowed by one layer of MSD placed between SC and BM, and the other three placed after the BM. A schematic view of the apparatus is shown in Fig. 1.

the BM has been tilted at 0°, 5° and 10° with respect to the X axis in order to irradiate the whole BM cell area. A beam of protons at 228 and 80 MeV has been used in order to minimize the Multiple Coulomb Scattering effect in the former case and to check the detector response and to evaluate the space-time relation differences in the second case. The track reconstructed by the BM and the MSD has been matched to evaluate the space-time relations and the result for the case of 228 MeV protons is shown in Fig. 2. No relevant differences has been found for the case of protons at 80 MeV.

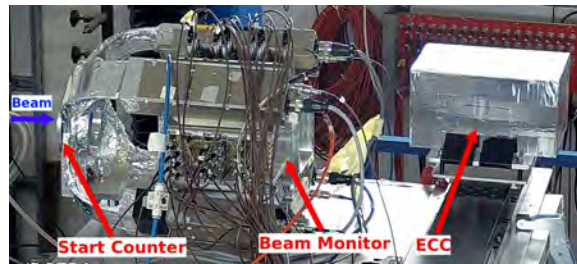


Figure 3: Experimental setup of the FOOT emulsion setup, including the SC, the BM and the ECC

The first data taking of the FOOT experiment took place in 2019 and has been conducted at the GSI accelerator in Germany (Darmstadt). In this case, the BM and the SC have been adopted in the emulsion setup to count the number of delivered particles and to check the irradiation pattern of Oxygen ion beam at 400 and 200 MeV/u. A figure of the experimental setup is shown in Fig. 3.

Furthermore, the BM has been exploited also in the first FOOT electronic setup test together with about 50% of the entire apparatus.

In 2020 the analysis of the BM characterization and performance assessment will be concluded. Two data taking are foreseen at GSI with carbon ion beam at 700 MeV/u and at CNAO (Pavia, Italy) with proton and carbon ion at different energies respectively for the emulsion and the electronic setup.

<sup>4</sup>Tommasino, F. et al. (2017), NIM **869**, pp. 15–20.

# Radiation testing and space qualification for the HERMES project

Riccardo Campana,<sup>1,2†</sup> Irina Rashevskaya,<sup>3</sup> Giuseppe Dilillo,<sup>4</sup> Daniela Cirrincione,<sup>4</sup> Fabio Fuschino,<sup>1,2</sup> Giovanni Pauletta,<sup>4</sup> Filippo Ambrosino,<sup>5</sup> Nicola Zampa,<sup>6</sup> Diego Cauz,<sup>4</sup> Benedetto Di Ruzza,<sup>3</sup> Claudio Labanti,<sup>1,2</sup> Yuri Evangelista,<sup>5,7</sup> Fabrizio Fiore,<sup>8</sup> Andrea Vacchi,<sup>4,6</sup> Francesco Tommasino,<sup>9,3</sup> Enrico Verroi<sup>3</sup>

HERMES (*High Energy Rapid Modular Ensemble of Satellites*) Technological Pathfinder is a Progetto Premiale MIUR led by Italian Space Agency (ASI), with the collaboration of several institutions, and is currently being improved with a Scientific Pathfinder phase, in the framework of a H2020 project. The main objective of these projects is to pave the way for a new generation of high-energy space astrophysical experiments onboard nanosatellites. The scientific objective is the study of high-energy cosmic transients (e.g. Gamma Ray Bursts) with a fast and sensitive X and gamma-ray detector, and to exploit the time delay between the detection of a signal from different nanosatellites to determine their location. Using a nanosatellite platform to carry out these experiments allows for reduced cost, reduced development time, high modularity avoiding single points of failure, and replicability, besides allowing for different orbital locations and therefore large baselines for the signal triangulation. In the framework of both projects, six nanosatellites will be built and launched around 2022 as a piggy-back (secondary payload) mission.

The foreseen detector for this experiment exploits the solid-state Silicon Drift Detectors (SDD) developed by INFN and FBK in the framework of the ReDSOX Collaboration.<sup>1</sup> These devices, being sensitive to both X-ray and optical photons, and characterised by a very low intrinsic electronic noise, can be exploited both as direct X-ray detectors and as photode-

tectors for the scintillation light produced by the absorption of a gamma-ray in an inorganic scintillator crystal. This allows for the realisation a single, compact experiment with a huge sensitivity band ( $\sim 2$  keV up to several MeVs) for X and gamma-rays, and with a high temporal resolution ( $< 1 \mu s$ ). Fig. 1 shows a sketch of the proposed payload (which will fit in a 3U CubeSat platform).

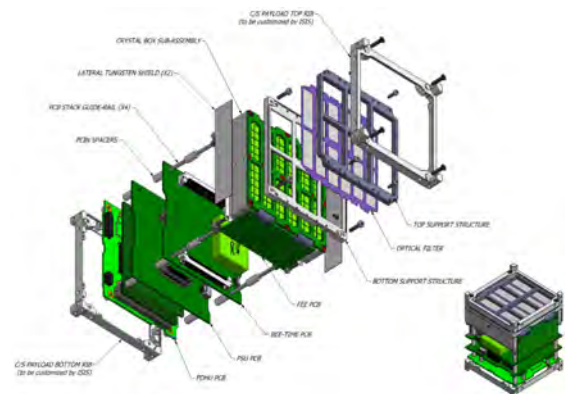


Figure 1: Exploded view the HERMES payload.

Since the nanosatellites will be launched as secondary payloads in a low-Earth orbit, typically at high orbital inclinations, they are subject to a large amount of high-energy radiation fluxes (mostly cosmic-rays and geomagnetically trapped protons). This results in a degradation of the performance of the scintillator crystals (due to e.g. activation and creation of additional luminescence centers) and of the silicon detectors (mainly due to the Non-Ionizing En-

<sup>†</sup>Contact Author: [riccardo.campana@inaf.it](mailto:riccardo.campana@inaf.it)

<sup>1</sup>INAF/OAS, Bologna, Italy

<sup>2</sup>INFN Bologna, Italy

<sup>3</sup>INFN TIFPA, Trento, Italy

<sup>4</sup>University of Udine, Italy

<sup>5</sup>INAF/IAPS, Rome, Italy

<sup>6</sup>INFN Trieste, Italy

<sup>7</sup>INFN Roma Tor Vergata, Rome, Italy

<sup>8</sup>INAF/OATs, Trieste, Italy

<sup>9</sup>University of Trento, Italy

<sup>1</sup><http://redsox.iasfbo.inaf.it>

ergy Loss radiation damage, leading to an increase of the leakage current). The aim of the beam test campaign at the Protontherapy centre was to gain insight on the behaviour of both the proposed scintillator crystal and of the SDD, when exposed to proton doses representative of typical values encountered on orbit during the whole operative life (at least 1–2 years).

**Background and aims** For the HERMES detectors, the choice of the optimal scintillator material required a careful evaluation of several factors, e.g. the maximisation of the light output (photons per unit of absorbed energy), the non-hygroscopicity of the crystal and its high density, average atomic number (stopping power), absence of crystal self-radioactivity (background), good radiation-resistance properties and short light emission characteristic time. Therefore, the choice has fallen on a relatively recent material,  $\text{Gd}_3\text{Al}_2\text{Ga}_3\text{O}_{12}$  or GAGG, that has not yet been extensively investigated with respect to radiation resistance and performance after irradiation, although the published results are very encouraging. However, an issue is the non-negligible amount of afterglow observed after a 100 krad  $^{60}\text{Co}$  irradiation: the crystals exhibit a phenomenon of phosphorescence on a  $\sim 100$  s characteristic time scale, that will lead to a slight transitory worsening of the energy resolution and light output.

The first objective of this campaign was therefore to further investigate these results by a careful evaluation of the afterglow phenomenon and the variations in optical properties of the scintillator with proton doses and at increasing dose steps, representative of the actual in-orbit radiation environment foreseen for HERMES. The second objective was to confirm and extend space-qualification tests on Silicon Drift Detectors. In particular, we aimed to confirm and extend previous results obtained by our group on large-area SDDs, built with a slightly different technology, with single cell SDDs representative of the HERMES sensors ( $\sim 1 \text{ cm}^2$  effective area, where multiple cells can be arranged in a monolithic matrix), by care-

fully monitoring detector temperature and leakage current during and after the irradiation.

**Experimental setup and beam test** The characterization was carried on at the TIFPA-APSS experimental area of the Trento Proton Therapy Center, with irradiated doses chosen to be representative of typical fluxes encountered in the foreseen HERMES low-Earth orbit, at a beam energy of 70 MeV and using several irradiation steps. A GAGG crystal sample ( $1 \times 1 \times 3 \text{ cm}^3$  volume) was optically coupled to a pair of photomultiplier tubes (PMT) through an optical waveguide a few cm long, to ensure the PMT shielding from the proton beam. The afterglow effects were measured immediately after (from 60 s up to  $\sim 1000$  s) the irradiation, by monitoring the amount of current flowing through the PMT anode (proportional to the scintillation light emitted by the crystal and collected by the PMT) by means of a picoammeter and a data logger. Scintillator optical properties such as characteristic emission time, light output and energy resolution were then evaluated by acquiring spectra of single proton events by means of a waveform digitizer, and comparing the results with those obtained before the irradiation. Four SDD samples were irradiated with similar doses, with their leakage current monitored during and up to several weeks after the irradiation.

**Preliminary results** The results of the leakage current measurements on irradiated SDD samples were found to be consistent with the theory, with a temperature-dependent *annealing* effect as expected. Irradiation of the GAGG crystal sample showed afterglow emission after each step. A detailed model of the crystal response, taking into account the dose, the material characteristics, the concurrent process of radio-activation and detector properties has been developed, allowing to derive the expected in-orbit behavior of the HERMES detector. A paper fully outlining the irradiation campaign, beam test and results is in preparation (Dilillo et al., 2020).

# LIDAL

Livio Narici,<sup>1,2†</sup> on behalf of the LIDAL collaboration

LIDAL (Light Ion Detector for ALTEA) is a detector based on scintillators for fast time applications, designed to work paired with three ALTEA Silicon Detector Units (SDU), in order:

- (i) to extend the ALTEA detection capability for the lower Z-part of the radiation spectrum onboard the International Space Station (ISS)
- (ii) to enhance particle discrimination through the measurements of the Time of Flight of the detected ions.

Time of Flight (TOF) measurements, will allow to measure the kinetic energy of the passing-through particle: the possibility to match such information to the  $dE/dx$  measured by ALTEA will help to discriminate the different elemental species.

The different LIDAL subsystems for the Flight Model were realized under ASI-URTV LIDAL contract and the LIDAL-ALTEA FM payload assembled and integrated by KI with the support of URTV for the optical part consisting in the detector units (scintillators plus light guide plus PMTs).

This Report focuses on the activities performed under the responsibility of URTV, in June 2019 at the TIFPA center in Trento.

**Short summary of the tests** The LIDAL Flight Model test campaign with protons was performed in TIFPA to test the detector functionality and calibrate the system.

The LIDAL - FM has been sent to NASA on July 19th.

**The accelerator tests** The test in TIFPA, June 10-15, permitted to test/calibrate the FM with protons. The test has been successful. During these works a few communication glitches emerged. These glitches have been taken care of during de-bugging works which included also visits to Kayser (Livorno).

A total of 28 run in TIFPA have been carried out with protons between 91 and 220 MeV.

Test results are in agreement with the device expected performances. In Table 1 are sum-

TIFPA PROTON BEAM				
Scintillator	Energy (MeV/n)	TOF (ns)	Sigma (ps)	MC TOF (ns)
4	91	4.84	130	4.8
4-5	91	4.83	114	4.8
5	91	-	-	4.8
6	91	4.81	101	4.8
6	219.8	2.85	74	2.95
6	219.8	2.85	71	2.95
4	219.8	2.9	75	2.95
3	219.8	2.85	71	2.95
2	219.8	2.82	70	2.95
2	219.8	2.98	79	2.95
5	219.8	2.86	70	2.95
7	219.8	2.87	74	2.95
8	219.8	2.84	73	2.95
8	219.8	2.85	72	2.95
8	169	3.17	75	3.21
6	169	3.19	74	3.21
2	169	3.17	80	3.21
1	169	3.28	84	3.21
4	169	3.25	78	3.21

Table 1: Time of Flight measurements at TIFPA accelerator. Last column shows the Monte Carlo simulation.

<sup>2</sup>INFN Rome Tor Vergata, Italy

<sup>†</sup>Contact Author: narici@roma2.infn.it

<sup>1</sup>University of Rome Tor Vergata, Italy

marised the measured TOF and the Monte Carlo simulation calculations.

The degree of success of these tests is also illustrated by the preliminary spectra in Fig. 1, showing the sigma's of the ToF measurements.

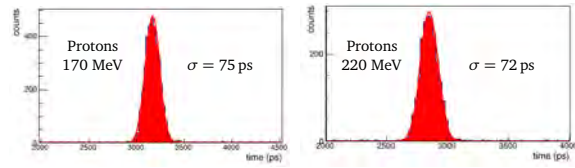


Figure 1: Spectra of the Time of Flight measurements in selected runs. The requirement, well fulfilled, was  $\sigma < 100$  ps.

# MoVeIT-TO

R. Cirio,<sup>1,2</sup> F. Fausti,<sup>2a</sup> S. Giordanengo,<sup>2</sup> O. Hammad Ali,<sup>1,2b</sup> F. Mas Milian,<sup>1,2,3</sup> V. Monaco,<sup>1,2</sup> R. Sacchi,<sup>1,2†</sup> E. Scifoni,<sup>4</sup> A. Staiano,<sup>2</sup> Z. Shakarami,<sup>1,2</sup> F. Tommasino,<sup>5,4</sup>, A. Vignati,<sup>1,2</sup> E. Verroi<sup>4</sup>

Within the MoVeIT project, the INFN - Torino and the University of Torino are developing two detector prototypes based on the UFSD (Ultra Fast Silicon Detector) technology for proton beam monitoring. The first prototype aims at counting the number of beam protons at radiobiological fluxes (up to  $10^8$  p/cm<sup>2</sup>s), while the second one aims at measuring the proton beam energy exploiting Time-of-Flight (ToF) techniques.

**Counter prototype** The beam test at TIFPA was meant for characterizing the strip sensors (specifically designed and produced for the MoVeIT project) in terms of counting rate capability and for studying the time structure of the beam at the ns level. Fig. 1 shows the measured rate in two adjacent detector strips as a function of the estimated rate, obtained using a pinpoint dosimeter, with the TIFPA proton beam.

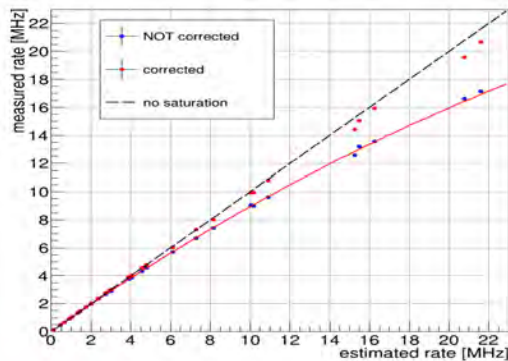


Figure 1: Measured rate in two neighboring strips as a function of the estimated rate before (blue points) and after (red points) pileup correction. The rate to be considered for radiobiological experiments, i.e. the rate of interests for the MoVeIT project, is 2 MHz

The deviation from linearity of measured

rate (blue points) at large rates is caused by signal pileup. Statistical correction methods based on the time correlation between neighboring strips have been developed (red points in Fig. 1) and benchmarked with Montecarlo simulations assuming the beam time structure reported in Fig. 2. When applied to the data they seem to perform well except at the very large rates.

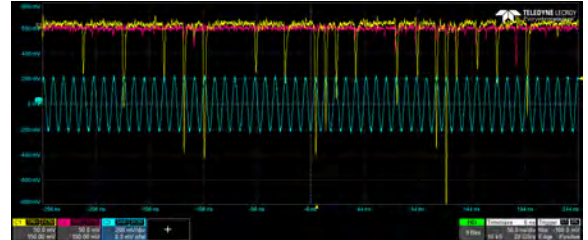


Figure 2: TIFPA beam time structure: proton signals (yellow curve) are synchronous with the 100 MHz radiofrequency of the accelerator (blue curve).

**Energy measurement prototype** UFSD strips sensors specifically designed and produced for the energy measurement prototype of the MoVeIT project were positioned in a telescope configuration. The average Time-of-Flight values at different detector distances for 5 beam energies were used in a global fit where the nominal energies at the isocenter, corrected for energy loss in the sensors and in the air between the two sensors, were used to constrain the distance between the sensors and the time offset between acquisition channels. The residual between nominal and measured energy, reported in Fig. 3 right for the two largest distances, does not show systematic trends and indicates that a statistical uncertainty smaller than 1 MeV can be obtained in the whole energy range.

<sup>†</sup>Contact Author: roberto.sacchi@unito.it

<sup>1</sup>University of Turin, Italy

<sup>2</sup>INFN Torino, Italy

<sup>3</sup>Universidade Estadual de Santa Cruz, Ilheus, Brazil

<sup>4</sup>INFN TIFPA, Trento, Italy

<sup>5</sup>University of Trento, Italy

<sup>a</sup>now at DE.TEC.TOR. Devices & Technologies Torino S.r.l., Torino, Italy

<sup>b</sup>now at FBK, Trento, Italy

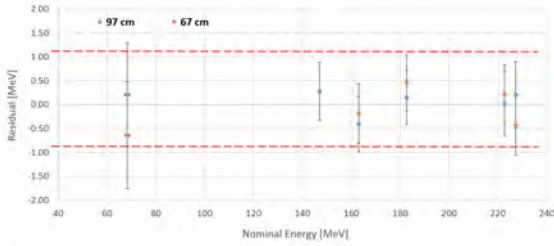


Figure 3: Residuals (nominal-measured) as a function of the beam energy at the two largest beam energies (error bars indicate the statistical uncertainties).

**Front-end electronics and readout** The prototype of the readout chip for the sensors, named TERA10, has been designed and produced in the UMC 110 nm technology through Europractice. It features 24 channels, each composed of preamplifier followed by a discriminator providing a digital signal to be read out by an FPGA implementing the particle counting and the algorithms for pileup correction. Alternative designs, based on a charge sensitive preamplifier and on a differential transimpedance amplifier, were attempted to meet the demanding specifications (pulse-rate counting efficiency up to 100 MHz/channel for pulse charges in the range 4 - 150 fC).

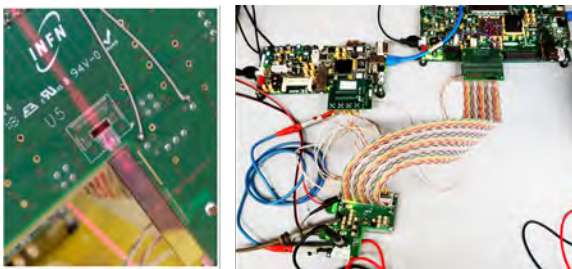


Figure 4: TERA10 on the test board connected to a strip sensor (left) and the acquisition setup showing the two FPGAs.

Fig. 4 (left) shows the chip glued to the dedicated test board and bonded to a MoVeIT strip sensor and (right) the entire acquisition setup including two FPGA for readout and for programming of the chip. The full characterization of the chip + sensor is still ongoing, both with lab measurements and using clinical beams, and is providing promising results. As an example, Fig. 5 shows the amplitude distribution of the measured pulses, obtained by varying the comparator threshold, when the detector is exposed to the TIFPA proton beam of 70 MeV. A clear separation between noise and signal can be observed, proving the good pulse discrimination capability of the system.

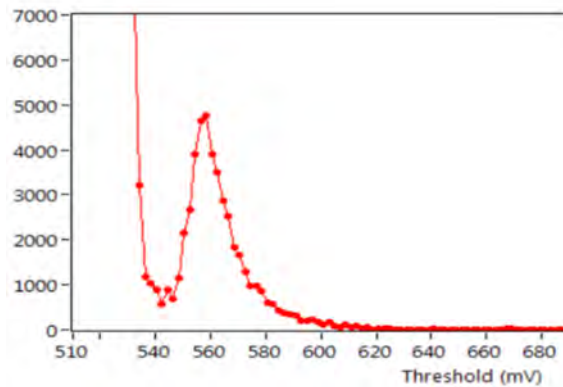


Figure 5: Peak amplitude distribution when the detector is exposed to the TIFPA proton beam of 70 MeV.

# MoVe IT-WP3

Alessandra Bisio,<sup>1,2†</sup> Devid Maniglio,<sup>1</sup> Vittoria D' Avino,<sup>3</sup> Walter Tinganelli,<sup>4</sup> Palma Simoniello,<sup>3,5</sup> Mariagabriella Pugliese,<sup>3,6</sup> Walter Bonani,<sup>7</sup> Francesco Tommasino,<sup>1,2</sup> Stefano Lorentini,<sup>8</sup> Enrico Verroi,<sup>2</sup> and Emanuele Scifoni<sup>2</sup>

The present series of experimental activities based at the TIFPA proton beam lab, in the context of the MoVe IT CSN5 project (see corresponding general report at page 88) were dedicated to developing a novel biological phantom for RBE measurements and to characterize radiobiologically the beamline for an exemplary selection of tissue types.

After initial test irradiations of the first design of biological phantom, a novel protocol for the inclusion of human and/or murine tumoral cells has been established. It is based on Gelatin Methacrylate (GelMA) as an alternative to Alginate, which was selected, at the beginning of the project, as the hydrogel to be used for the generation of the 3D scaffold. GelMA presented different advantages in comparison to the previously used reagents:

- (a) in this hydrogel cells do not become quiescent (blocked in G1 phase of the cell cycle and therefore not able to divide and proliferate) but rather acquire their morphology and maintain the potential of doubling (critical condition to evaluate radiation-induced damages);
- (b) the phantom structure resulted more robust and simplifying the experimental steps post-irradiation.

In a first test, we used murine melanoma-derived B16-F10 cells, a very aggressive cancer model, which were included in 20% GelMa and subsequently, (72 h after inclusion) X-rays irradiated (at the TIFPA X-ray facility) at a dose of 2 Gy. One hour after irradiation, phantoms were fixed in 4% Formaldehyde for 1 h, and we increased their density by incubation in

10% Sucrose over-day followed by 30% Sucrose over-night. The day after, phantoms were included in OCT and were cut at cryostat as longitudinal sections to preserve the 4 cm shape of the whole phantom. These last steps required additional optimization either for the robustness of the structure (with or without sucrose incubation before OCT inclusion) or for the generation of slices with the right thickness and length. The obtained slices were analyzed to measure the radiation-induced DNA damage. We performed immunofluorescence to detect nuclear foci of the phosphorylated form of the histone variant H2AX (a recognized marker to identify DNA damage) in irradiated cells compared to untreated controls. Nuclei were counterstained with Hoechst 33342. The protocol has now proved to be robust and the same experiment will be repeated using a proton beam.

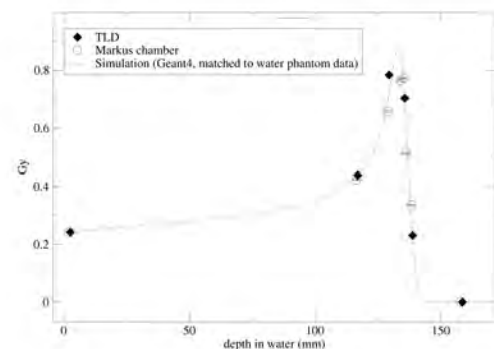


Figure 1: Comparison of TLD measurements, after calibration, and Markus chamber dosimetry as well as simulations, previously tuned with water phantom pin point chamber measurements

In parallel, in the experimental room at the

<sup>†</sup>Contact Author: [alessandra.bisio@unitn.it](mailto:alessandra.bisio@unitn.it)

<sup>1</sup>University of Trento

<sup>2</sup>TIFPA INFN, Trento, Italy

<sup>3</sup>INFN Naples, Italy

<sup>4</sup>GSI, Darmstadt, Germany

<sup>5</sup>University of Naples Parthenope

<sup>6</sup>University of Naples Federico II

<sup>7</sup>EC Joint Research center, Karlsruhe, Germany

<sup>8</sup>APSS, Trento, Italy

Protontherapy Center, we characterized the biology line proton beam (Tommasino et al. 2019f) evaluating the DNA damage response along the proton beam in two different cell lines: MDA-MB-231 and U87. To this aim, we irradiated the cells at a single dose level (0.23 Gy at entrance, corresponding to a peak dose of 0.88 Gy) at six depth positions along the proton beam (entrance channel, Bragg peak, and exit channel). The different dosage delivered to the cells along

the proton beam was also measured using properly calibrated TLD (Liuzzi et al. 2020), which will be used also for the biophantom, positioned in the proximity of the irradiated cells and with Markus chambers for absolute dosimetry (see Fig. 1). DNA damage evaluation was conducted using immunofluorescence to detect  $\gamma$ H<sub>2</sub>AIX phosphorylation; moreover, we considered the recruitment to nuclear foci of 53BP1, a second and delayed DNA damage marker (Figs. 2, 3).

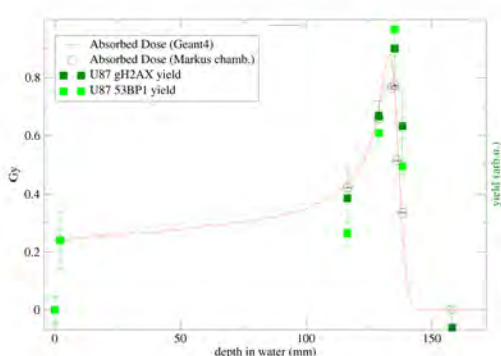


Figure 2: Results of DNA damage assay through  $\gamma$ H<sub>2</sub>AIX and 53BP1 assays for U87 cells superimposed to the dose profile measured and computed for the proton beam used

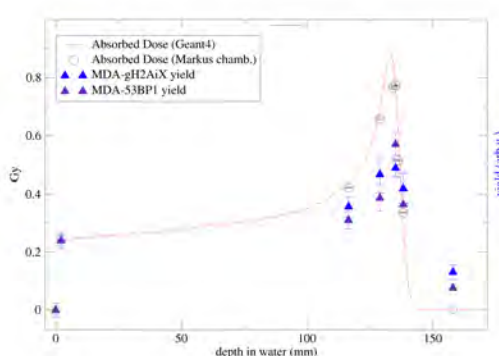


Figure 3: Results of DNA damage assay through  $\gamma$ H<sub>2</sub>AIX and 53BP1 assays for MDA cells superimposed to the dose profile measured and computed for the proton beam used

## References

- Liuzzi, R., Piccolo, C., D'Avino, V., Clemente, S., Oliviero, C., Cella, L., and Pugliese, M. (2020). *Dose-Response of TLD-100 in the Dose Range Useful for Hypofractionated Radiotherapy*. *Dose-Response* **18**(1). Art. no.: 1559325819894081.
- Tommasino, F., Rovituro, M., Bortoli, E., La Tessa, C., Petringa, G., Lorentini, S., Verroi, E., Simonov, Y., Weber, U., Cirrone, P., Schwarz, M., Durante, M., and Scifoni, E. (2019f). *A new facility for proton radiobiology at the Trento proton therapy centre: Design and implementation*. *Physica Medica* **58**, pp. 99–106.

# SEUP

Daniela Calvo,<sup>1†</sup> Paolo De Remigis,<sup>1</sup> Enrico Verroi,<sup>2</sup> Francesco Tommasino,<sup>2,3</sup> Richard Wheadon<sup>1</sup>

The INFN-Torino has developed ASICs for read-out applications of detectors in several different technologies. Among them a commercial 110 nm CMOS technology suitable for small projects due to its relatively low cost, even if it lacks a systematic characterization of its radiation tolerance.

The first ASIC designed at INFN-Torino in this technology was the prototype of Fig. 1 named PASTa (PANDA Strip ASIC) for the read-out of silicon micro-strips devices for the Micro Vertex Detector (MVD) of the PANDA experiment. It was developed by a JLU Gießen, FZ Jülich and INFN Torino collaboration.

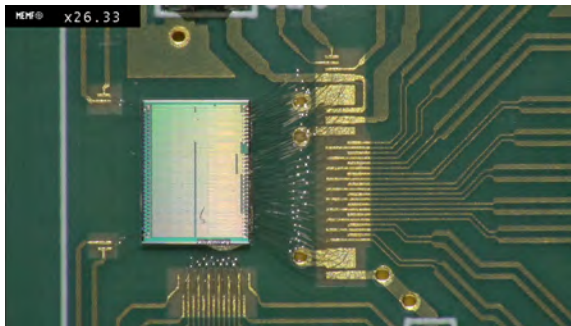


Figure 1: PASTa chip wire bonded to its testing board

Since it implements the two typical methods to mitigate the Single Event Upset (SEU) effects, Triple Modular Redundancy (TMR) technique and Hamming Encoding, it is a good candidate to investigate the behaviour of that commercial 110 nm technology in a radiation environment.

In general, TMR may be preferred when die size and power consuming are not a problem in the project, two requests that are often rather stringent in the electronics for a vertex detector as it is in the case of PASTa circuit.

An assessment was conducted using PASTa as device under test and using proton beams to perform a direct measurements of upset rate in its channel configuration registers.

PASTa implements 64 readout channels and

uses the Time over Threshold (ToT) technique to determine the charge information by a 8 bit resolution measurement (Quagli et al. 2017). Each channel contains three distinct building blocks: an analog front-end, an analog TDC and a digital TDC controller. A global controller merges the data from all the channels and distributes the configuration information.

The analog front-end implements a specific design to cope with micro-strips sensors and consists of four stages:

- the charge sensitive amplifier developed to process signals coming from both p- and n-type silicon strips
- the current buffer to provide a current amplification and an impedance adaptation
- the ToT amplifier to discharge a feedback capacitance with a constant current
- the comparator designed as a dual threshold hysteresis circuit. Its lower threshold secures the leading edge of the signal to get the event timestamp, while the higher threshold works on the signal falling edge to complete the ToT measurement information.

The output signal from the comparator is used by a local controller to drive the TDC with an analog interpolator circuit equipped with a Time to Amplitude converter and a latched comparator.

Several registers are implemented in each channel: 13 single bit registers, additional 29 bits distributed on 8 registers featuring words with different length of bit (2, 4 and 5 bits). To protect these circuits from SEU effects, two different techniques were implemented: TMR on single bit registers and Hamming encoding on multiple bits registers.

The chip prototype is mounted on a dedicated test board (provided by the group from

<sup>†</sup>Contact Author: calvo@to.infn.it

<sup>1</sup>INFN Torino, Italy

<sup>2</sup>INFN TIFPA, Trento, Italy

<sup>3</sup>University of Trento, Italy

JLU Gießen, involved in the PANDA MVD project) and a dedicated DAQ in LABView was developed at INFN-Torino to configure the ASIC registers and acquire data. It is a standalone setup based on a Xilinx Virtex 6 ML605 Evaluation Board.

Each channel requires to be configured with a sequence 42 bit long and for the SEU evaluation a legal sequence balanced in 1 and 0 is sent to the chip to set up each channel. The tests are performed following this procedure: a writing command is followed by a reading phase until an upset is detected showing an inefficiency of the TMR circuit or Hamming Encoding technique, then the cycle starts again from the beginning.

The acquisition program counts the number of times when the bit changes its value (1-0, 0-1), therefore it records the number of errors which have been detected.

The measurements (Calvo et al. 2020) were performed at the experimental room of INFN-TIFPA in the proton-therapy Centre of Trento.

The naked chip was positioned along the proton beam and the proton flux on the device was obtained using wire chambers, with an estimated error of 10 %.

The proton energy was set to 131.3 MeV

and measurements were performed at three different beam current values corresponding to  $2.2 \cdot 10^9$  proton/( $\text{cm}^2 \cdot \text{s}$ ),  $4.4 \cdot 10^9$  proton/( $\text{cm}^2 \cdot \text{s}$ ) and  $6.2 \cdot 10^9$  proton/( $\text{cm}^2 \cdot \text{s}$ ), with the clock frequency of the chip set up to 50 MHz.

No upsets were detected during tests with the first two beam current.

With the last one, upsets were detected and a cross section value for upset effects of  $3.5 \cdot 10^{-16} \text{cm}^2/\text{bit}$  was estimated.

Measurement with a 160 MHz clock frequency set up to the chip and a beam current corresponding to  $4.3 \cdot 10^9$  proton/( $\text{cm}^2 \cdot \text{s}$ ) induces to a cross section value for upset effects of  $9.1 \cdot 10^{-16} \text{cm}^2/\text{bit}$ .

The irradiation of readout circuits with proton beams of 100-200 MeV should give a good information for their application in a hadron environment for what concerns upset effects (Huhtinen and Faccio 2000).

Then the obtained result with PASTA prototype is adequate since the number of upsets expected in the micro-strip detector of PANDA equipped with 3112 electronics readout chips working with a 160 MHz clock frequency, is about 1 bit flip per hour taking into account that an evaluated particle flux of  $5 \cdot 10^4$  hadrons/ $\text{cm}^2$  contribute to upset effects.

## References

- Calvo, D. et al. (2020). *Study of SEU effects in circuits developed in 110 nm CMOS technology*. Proceedings of Science - TWEPP 2019. Submitted.
- Huhtinen, M. and Faccio, F. (2000). *Computational method to estimate Single Event Upset rates in an accelerator environment*. Nuclear Instruments and Methods in Physics Research A **450**, pp. 155–172.
- Quagli, T. et al. (2017). *First results of the front-end ASIC for the strip detector of the PANDA MVD*. JINST **12**. Art. no.: C03063.

# SUN\_MEYER

Iacopo Sardi,<sup>1</sup> Giacomo Casati,<sup>1†</sup> Anna Lisa Iorio,<sup>1</sup> Laura Giunti<sup>1</sup>

Our project will be composed by different steps to test the feasibility of the combinational approach, Doxorubicin (Dox), an anthracycline drug in combination with Proton-Therapy (PT), for GBM therapy. Firstly we evaluated, through Clonigenic Assay, the effect of Proton-Therapy on the growth of T98G and A172, GBM cell lines, obtaining good results that showed how these cell lines were sensitive to Proton-Therapy. The second step will be to evaluate the combined cytotoxic effect between Dox and Proton-Therapy on U87MG, T98G and A172, GBM cell lines.

**Cell lines** The human glioblastoma (GBM) cell lines used in this study were U87MG, T98G and A172. The cells were purchased from the American Type Culture Collection (ATCC, Manassas, Virginia, USA) and grown in a humidified atmosphere at 37 °C with 5% CO<sub>2</sub>. The culture conditions were varied according to the cell type. The U87MG and T98G cell lines were grown in Eagle's Minimum Essential Medium (EMEM) (Cell Biology, Manassas, Virginia, USA) while the A172 cell line was grown in Dulbecco's Modified Eagle Medium (DMEM) (Cell Biology, Manassas, Virginia, USA). 10% of fetal bovine serum (FBS, Euroclone S.P.A, Italy) and 1% of penicillin-streptomycin (Euroclone S.P.A, Italy) were added to the soils, in accordance with the indications of the supplier company.

**Experimental design of the combined Proton Therapy-Doxorubicin treatment** The three GBM lines were sown in small flasks (T25 Culture Flask, Corning Incorporated, New York, USA) 24 hours before treatment with proton-therapy (PT). For each cell line, a flask was prepared for each irradiation condition, quantified in Gray (Gy):

0 Gy (control), 1 Gy, 2 Gy, 4 Gy, 8 Gy, 16 Gy  
 $5 \times 10^5$  cells/flask of T98G and  $7 \times 10^5$  cells/flask of U87MG and A172 were seeded, so as to obtain their subconfluence 24 hours after sowing. Once irradiated, the cells remained in

an overnight incubator in order to allow the decay of the residual radiation. The next day the cells were seeded in 96-well plates (Corning Incorporated, New York, USA):  $5 \times 10^3$  cells of the U87MG line,  $3 \times 10^3$  cells of the T98G line and  $5 \times 10^3$  cells of the A172 line.

After 24h the pharmacological treatment was performed on the three cell lines with Doxorubicin (DOX) at different dosages:

0.5  $\mu\text{g/ml}$ , 0.2  $\mu\text{g/ml}$ , 0.1  $\mu\text{g/ml}$ , 0.05  $\mu\text{g/ml}$

At 24 hours from the administration of the drug, the MTT cell viability test was performed on all plates and, after reading the absorbance at the spectrophotometer, it was possible to an-

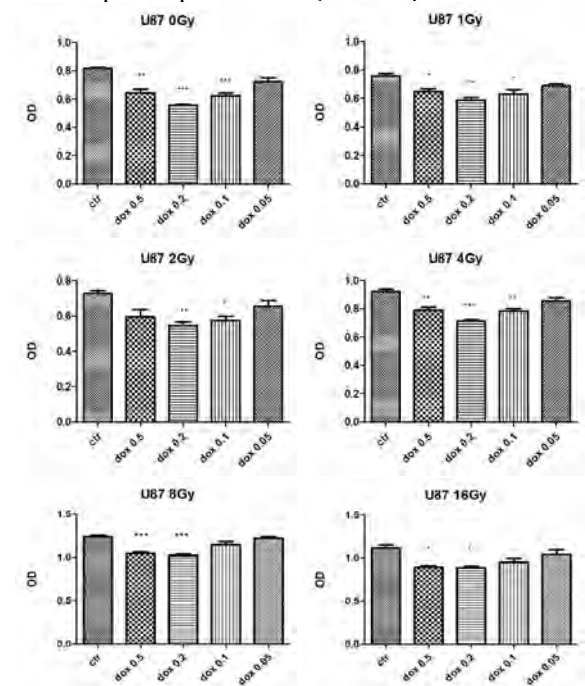


Figure 1: U87MG cell line treated with protontherapy (0 Gy, 1 Gy, 2 Gy, 4 Gy, 8 Gy, 16 Gy) in combination with Doxorubicin (0.5  $\mu\text{g/ml}$ , 0.2  $\mu\text{g/ml}$ , 0.1  $\mu\text{g/ml}$ , 0.05  $\mu\text{g/ml}$ ).

**Results** The results of the MTT cell viability assay, performed on all three GBM cell lines, are preliminary data obtained from a single experiment. The OD (optical density, which is directly proportional to the number of viable cells) of the U87MG cells at 4 Gy, 8 Gy and 16 Gy irradiations are higher compared to the 0 Gy con-

<sup>†</sup>Contact Author: giacomo\_casati@libero.it

<sup>1</sup>Azienda Osped. Univers. Meyer, Florence, Italy

trol. The cells subjected to combined treatment, Proton therapy + Doxorubicin, and the cells subjected only to pharmacological treatment instead always have a lower optical density than the respective control, demonstrating the effectiveness of Doxorubicin on the U87MG cell line, in particular the dosages 0.2 and 0, 5  $\mu\text{g}/\text{ml}$  (see Fig. 1).

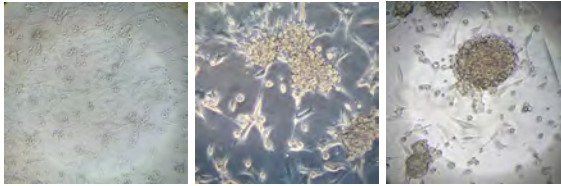


Figure 2: comparison between non-irradiated and irradiated U87MG images.

Morphologically, the U87MGs subjected to irradiation present clusters of cells that are not found in non-irradiated cells, demonstrating a possible cellular stress caused by proton therapy (see Fig. 2).

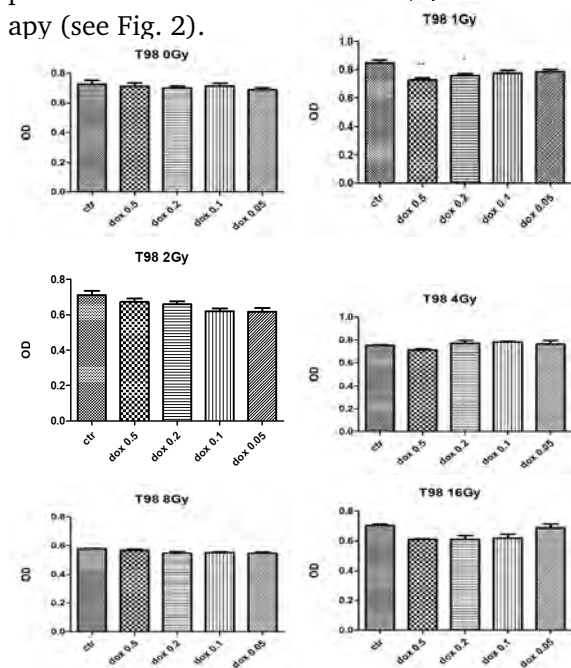


Figure 3: T98G cell line treated with proton therapy (0 Gy, 1 Gy, 2 Gy, 4 Gy, 8 Gy, 16 Gy) in combination with doxorubicin (0.5  $\mu\text{g}/\text{ml}$ , 0.2  $\mu\text{g}/\text{ml}$ , 0.1  $\mu\text{g}/\text{ml}$ , 0.05  $\mu\text{g}/\text{ml}$ ).

With regard to the T98G cell line, cells resistant to Doxorubicin, the OD parameter shows a more or less constant trend in all irradiations compared to the control except the 8Gy which has a reduction in cell viability. Treatment with Doxorubicin, as expected, under all conditions

does not significantly change the optical density values (see Fig 3).

Finally, in the A172 cell line, the optical density decreases from 0 Gy to 16 Gy proportionally with respect to the intensity of the radiation, demonstrating the effectiveness of proton therapy on this cell line. Doxorubicin treatment is significant compared to the respective controls,

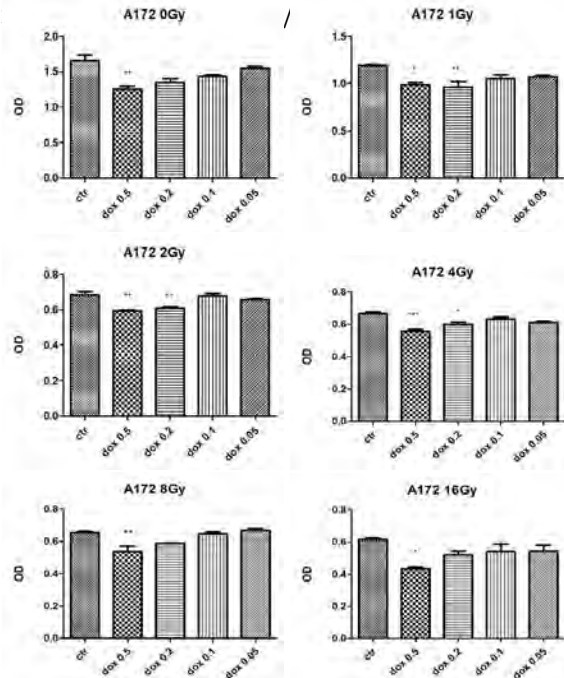


Figure 4: A172 cell line treated with proton therapy (0 Gy, 1 Gy, 2 Gy, 4 Gy, 8 Gy, 16 Gy) in combination with doxorubicin (0.5  $\mu\text{g}/\text{ml}$ , 0.2  $\mu\text{g}/\text{ml}$ , 0.1  $\mu\text{g}/\text{ml}$ , 0.05  $\mu\text{g}/\text{ml}$ ).

**Conclusions** The preliminary data obtained after the MTT test demonstrate that the A172 cell line is sensitive to the treatment with Proton therapy and to the combined treatment, Protontherapy-Doxorubicin, especially in the 16 Gy irradiation at the dose of 0.5  $\mu\text{g}/\text{ml}$  of drug, a significant reduction in cell viability. As for the other two lines, the data obtained partially show an incorrect dose-effect correspondence.

The results obtained so far must be implemented with further cell viability experiments using the Doxorubicin-Temozolomide combination after irradiation. These further tests will be used to validate the preliminary data, increasing the statistics and the number of samples, and to reduce to a minimum variables that can invalidate the accuracy of the data.



**TIFPA**  
publications



# TIFPA Publications

## Virtual Labs

### Sensors and detectors

- Andrä, M., Zhang, J., Bergamaschi, A., Barten, R., Borca, C., Borghi, G., Boscardin, M., Busca, P., Brückner, M., Cartiglia, N., Chiriotti, S., Dalla Betta, G.-F., Dinapoli, R., Fajardo, P., Ferrero, M., Ficorella, F., Fröjdh, E., Greiffenberg, D., Huthwelker, T., Lopez-Cuenca, C., Meyer, M., Mezza, D., Mozzanica, A., Pancheri, L., Paternoster, G., Redford, S., Ruat, M., Ruder, C., Schmitt, B., Shi, X., Sola, V., Thattil, D., Tinti, G., and Vetter, S. (2019). *Development of low-energy X-ray detectors using LGAD sensors*. *Journal Synchrotron Radiation* **26**, pp. 1226–1237.
- Boscardin, M., Ceccarelli, R., Dalla Betta, G., Darbo, G., Dinardo, M., Giacomini, G., Menasce, D., Mendicino, R., Meschini, M., Messineo, A., Moroni, L., Rivera, R., Ronchin, S., Sultan, D., Uplegger, L., Vilianni, L., Zoi, I., and Zuolo, D. (2020). *Performance of new radiation-tolerant thin planar and 3D columnar  $n^+$  on  $p$  silicon pixel sensors up to a maximum fluence of  $\sim 5 \times 10^{15} n_{eq}/cm^2$* . *Nuclear Instruments and Methods in Physics Research Section A: Accelerators, Spectrometers, Detectors and Associated Equipment* **953**. Art. no.: 163222.
- Calderini, G. et al. (2019a). *Active-edge FBK-INFN-LPNHE thin  $n$ -on- $p$  pixel sensors for the upgrade of the ATLAS Inner Tracker*. *Nucl. Instrum. Meth.* **A936**, pp. 638–639.
- (2019b). *Performance of the FBK/INFN/LPNHE thin active edge pixel detectors for the upgrade of the ATLAS Inner Tracker*. *JINST* **14(7)**. Art. no.: C07001.
- Ferrero, M., Arcidiacono, R., Barozzi, M., Boscardin, M., Cartiglia, N., Dalla Betta, G. F., Galloway, Z., Mandurrino, M., Mazza, S., Paternoster, G., Ficorella, F., Pancheri, L., Sadrozinski, H.-F. W., Siviero, F., Sola, V., Staiano, A., Seiden, A., Tornago, M., and Zhao, Y. (2019). *Radiation resistant LGAD design*. *Nuclear Instrum. Methods A* **919**, pp. 16–26.
- Forcolin, G., Mendicino, R., Boscardin, M., Lai, A., Loi, A., Ronchin, S., Vecchi, S., and Betta, G.-F. D. (2019a). *Development of 3D trenched-electrode pixel sensors with improved timing performance*. *Journal of Instrumentation* **14(7)**. Art. no.: C07011.
- Fuschino, F., Campana, R., Labanti, C., Evangelista, Y., Feroci, M., Burderi, L., Fiore, F., Ambrosino, F., Baldazzi, G., Bellutti, P., Bertacin, R., Bertuccio, G., Borghi, G., Cirrincione, D., Cauz, D., Ficorella, F., Fiorini, M., Gandola, M., Grassi, M., Guzman, A., Rosa, G. L., Lavagna, M., Lunghi, P., Malcovati, P., Morgante, G., Negri, B., Pauletta, G., Piazzolla, R., Picciotto, A., Pirrotta, S., Pliego-Caballero, S., Puccetti, S., Rachevski, A., Rashevskaya, I., Rignanese, L., Salatti, M., Santangelo, A., Silvestrini, S., Sottile, G., Tenzer, C., Vacchi, A., Zampa, G., Zampa, N., and Zorzi, N. (2019b). *HERMES: An ultra-wide band X and gamma-ray transient monitor on board a nano-satellite constellation*. *Nuclear Instruments and Methods in Physics Research A* **936**, pp. 199–203.
- Hafizh, I., Bellotti, G., Carminati, M., Utica, G., Gugiatti, M., Balerna, A., Tullio, V., Lepore, G., Borghi, G., Ficorella, F., Picciotto, A., Zorzi, N., Capsoni, A., Coelli, S., Bombelli, L., and Fiorini, C. (2019b). *Characterization of ARDESIA: a 4-channel SDD X-ray spectrometer for synchrotron measurements at high count rates*. *Journal of Instrumentation* **14(6)**. Art. no.: P06027.
- Loi, A., Contu, A., Mendicino, R., Forcolin, G. T., Lai, A., Dalla Betta, G. F., Boscardin, M., and Vecchi, S. (2020). *Timing optimization for 3D silicon sensors*. *Nuclear Instruments and Methods in Physics Research Section A: Accelerators, Spectrometers, Detectors and Associated Equipment* **958**. *Proceedings of the Vienna Conference on Instrumentation 2019*. Art. no.: 162491.
- Mandurrino, M., Arcidiacono, R., Boscardin, M., Cartiglia, N., Dalla Betta, G. F., Ferrero, M., Ficorella, F., Pancheri, L., Paternoster, G., Siviero, F., and Tornago, M. (2019a). *Demonstration of 200-, 100-*

- and 50- $\mu\text{m}$  Pitch Resistive AC-Coupled Silicon Detectors (RSD) With 100% Fill-Factor for 4D Particle Tracking. *IEEE Electron Device Letters* **40**(11), pp. 1780–1783.
- Mandurrino, M., Siviero, F., Cartiglia, N., Tornago, M., Ferrero, M., Boscardin, M., Paternoster, G., Ficorella, F., Dalla Betta, G.-F., and Pancheri, L. (2019b). “High performance 4D tracking with 100% fill-factor and very fine pitch Silicon detectors”. *Proceedings of Science - VERTEX 2019*. Trieste, Italy: SISSA, p. 056.
- Mendicino, R., Forcolin, G. T., Boscardin, M., Ficorella, F., Lai, A., Loi, A., Ronchin, S., Vecchi, S., and Betta, G.-F. D. (2019c). *3D trenched-electrode sensors for charged particle tracking and timing*. *Nuclear Instruments and Methods in Physics Research Section A: Accelerators, Spectrometers, Detectors and Associated Equipment* **927**, pp. 24–30.
- Meschini, M., Ceccarelli, R., Dinardo, M., Gennai, S., Moroni, L., Zuolo, D., Demaria, L., Monteil, E., Gaioni, L., Messineo, A., Currás, E., Duarte, J., Fernández, M., Gómez, G., Garía, A., González, J., Silva, E., Vila, I., Betta, G. D., Mendicino, R., and Boscardin, M. (2019b). *First results on 3D pixel sensors interconnected to the RD53A readout chip after irradiation to  $1 \times 10^{16} n_{eq} \text{ cm}^{-2}$* . *Journal of Instrumentation* **14**(6). Art. no.: C06018.
- Oide, H. et al. (2019a). *INFN-FBK developments of 3D sensors for High-Luminosity LHC*. *Nucl. Instrum. Meth.* **A924**, pp. 73–77.
- Paternoster, G. et al. (2017). *Developments and first measurements of Ultra-Fast Silicon Detectors produced at FBK*. *JINST* **12**(02), p. C02077.
- Sola, V., Arcidiacono, R., Boscardin, M., Cartiglia, N., Dalla Betta, G. F., Ficorella, F., Ferrero, M., Mandurrino, M., Mazza, S., Pancheri, L., Paternoster, G., and Staiano, A. (2019a). *First FBK production of 50  $\mu\text{m}$  ultra-fast silicon detectors*. *Nuclear Instrum. Methods A* **924**, pp. 360–368.

## Particle Physics

### ATLAS

- Aaboud, M. et al., ATLAS (2019a). *Combination of searches for invisible Higgs boson decays with the ATLAS experiment*. *Phys. Rev. Lett.* **122**(23). Art. no.: 231801.
- ATLAS, CMS (2019b). *Combinations of single-top-quark production cross-section measurements and  $|f_{LV}V_{tb}|$  determinations at  $\sqrt{s} = 7$  and 8 TeV with the ATLAS and CMS experiments*. *JHEP* **05**, p. 088.
- ATLAS (2019c). *Comparison of Fragmentation Functions for Jets Dominated by Light Quarks and Gluons from  $pp$  and  $Pb+Pb$  Collisions in ATLAS*. *Phys. Rev. Lett.* **123**(4). Art. no.: 042001.
- ATLAS (2019d). *Constraints on mediator-based dark matter and scalar dark energy models using  $\sqrt{s} = 13$  TeV  $pp$  collision data collected by the ATLAS detector*. *JHEP* **05**, p. 142.
- ATLAS (2019e). *Dijet azimuthal correlations and conditional yields in  $pp$  and  $p+Pb$  collisions at  $s_{NN}=5.02\text{TeV}$  with the ATLAS detector*. *Phys. Rev. C* **100**(3). Art. no.: 034903.
- ATLAS (2019f). *Electron reconstruction and identification in the ATLAS experiment using the 2015 and 2016 LHC proton-proton collision data at  $\sqrt{s} = 13$  TeV*. *Eur. Phys. J. C* **79**(8), p. 639.
- ATLAS (2020a). *Fluctuations of anisotropic flow in  $Pb+Pb$  collisions at  $\sqrt{s_{NN}} = 5.02$  TeV with the ATLAS detector*. *JHEP* **01**, p. 051.
- ATLAS (2019g). *Measurement of fiducial and differential  $W^+W^-$  production cross-sections at  $\sqrt{s} = 13$  TeV with the ATLAS detector*. *Eur. Phys. J. C* **79**(10), p. 884.
- ATLAS (2020b). *Measurement of  $J/\psi$  production in association with a  $W^\pm$  boson with  $pp$  data at 8 TeV*. *JHEP* **01**, p. 095.
- ATLAS (2019h). *Measurement of jet-substructure observables in top quark,  $W$  boson and light jet production in proton-proton collisions at  $\sqrt{s} = 13$  TeV with the ATLAS detector*. *JHEP* **08**, p. 033.

- ATLAS (2020c). *Measurement of long-range two-particle azimuthal correlations in Z-boson tagged pp collisions at  $\sqrt{s}=8$  and 13 TeV.* Eur. Phys. J. C **80**(1), p. 64.
  - ATLAS (2019i). *Measurement of prompt photon production in  $\sqrt{s_{NN}} = 8.16$  TeV p+Pb collisions with ATLAS.* Phys. Lett. B **796**, pp. 230–252.
  - ATLAS (2019j). *Measurement of the four-lepton invariant mass spectrum in 13 TeV proton-proton collisions with the ATLAS detector.* JHEP **04**, p. 048.
  - ATLAS (2019k). *Measurement of the ratio of cross sections for inclusive isolated-photon production in pp collisions at  $\sqrt{s} = 13$  and 8 TeV with the ATLAS detector.* JHEP **04**, p. 093.
  - ATLAS (2019l). *Measurement of the relative  $B_c^\pm/B^\pm$  production cross section with the ATLAS detector at  $\sqrt{s} = 8$  TeV.*
  - ATLAS (2019m). *Measurement of the  $t\bar{t}Z$  and  $t\bar{t}W$  cross sections in proton-proton collisions at  $\sqrt{s} = 13$  TeV with the ATLAS detector.* Phys. Rev. D **99**(7). Art. no.: 072009.
  - ATLAS (2019n). *Measurement of  $VH, H \rightarrow b\bar{b}$  production as a function of the vector-boson transverse momentum in 13 TeV pp collisions with the ATLAS detector.* JHEP **05**, p. 141.
  - ATLAS (2019o). *Measurement of  $W^\pm Z$  production cross sections and gauge boson polarisation in pp collisions at  $\sqrt{s} = 13$  TeV with the ATLAS detector.* Eur. Phys. J. C **79**(6), p. 535.
  - ATLAS (2019p). *Measurement of ZZ production in the  $\ell\ell\nu\nu$  final state with the ATLAS detector in pp collisions at  $\sqrt{s} = 13$  TeV.* JHEP **10**, p. 127.
  - ATLAS (2019q). *Measurements of top-quark pair spin correlations in the  $e\mu$  channel at  $\sqrt{s} = 13$  TeV using pp collisions in the ATLAS detector.*
  - ATLAS (2019r). *Modelling radiation damage to pixel sensors in the ATLAS detector.* JINST **14**(06). Art. no.: P06012.
  - ATLAS (2019s). *Observation of electroweak production of a same-sign W boson pair in association with two jets in pp collisions at  $\sqrt{s} = 13$  TeV with the ATLAS detector.* Phys. Rev. Lett. **123**(16). Art. no.: 161801.
  - ATLAS (2019t). *Search for a right-handed gauge boson decaying into a high-momentum heavy neutrino and a charged lepton in pp collisions with the ATLAS detector at  $\sqrt{s} = 13$  TeV.* Phys. Lett. B **798**. Art. no.: 134942.
  - ATLAS (2019u). *Search for excited electrons singly produced in proton–proton collisions at  $\sqrt{s} = 13$  TeV with the ATLAS experiment at the LHC.* Eur. Phys. J. C **79**(9), p. 803.
  - ATLAS (2019v). *Search for heavy charged long-lived particles in the ATLAS detector in  $36.1\text{ fb}^{-1}$  of proton-proton collision data at  $\sqrt{s} = 13$  TeV.* Phys. Rev. D **99**(9). Art. no.: 092007.
  - ATLAS (2019w). *Search for heavy particles decaying into a top-quark pair in the fully hadronic final state in pp collisions at  $\sqrt{s} = 13$  TeV with the ATLAS detector.* Phys. Rev. D **99**(9). Art. no.: 092004.
  - ATLAS (2019x). *Search for long-lived neutral particles in pp collisions at  $\sqrt{s} = 13$  TeV that decay into displaced hadronic jets in the ATLAS calorimeter.* Eur. Phys. J. C **79**(6), p. 481.
  - ATLAS (2019y). *Search for low-mass resonances decaying into two jets and produced in association with a photon using pp collisions at  $\sqrt{s} = 13$  TeV with the ATLAS detector.* Phys. Lett. B **795**, pp. 56–75.
  - ATLAS (2019z). *Search for scalar resonances decaying into  $\mu^+\mu^-$  in events with and without b-tagged jets produced in proton-proton collisions at  $\sqrt{s} = 13$  TeV with the ATLAS detector.* JHEP **07**, p. 117.
  - ATLAS (2019aa). *Searches for scalar leptoquarks and differential cross-section measurements in dilepton-dijet events in proton-proton collisions at a centre-of-mass energy of  $\sqrt{s} = 13$  TeV with the ATLAS experiment.* Eur. Phys. J. C **79**(9), p. 733.
  - ATLAS (2019ab). *Searches for third-generation scalar leptoquarks in  $\sqrt{s} = 13$  TeV pp collisions with the ATLAS detector.* JHEP **06**, p. 144.
- Aad, G. et al., ATLAS (2019a). *ATLAS b-jet identification performance and efficiency measurement with  $t\bar{t}$  events in pp collisions at  $\sqrt{s} = 13\hat{E}$ TeV.* Eur. Phys. J. C **79**(11), p. 970.

- Aad, G. et al., ATLAS (2020a). *ATLAS data quality operations and performance for 2015-2018 data-taking*. JINST **15**(04). Art. no.: P04003.
- ATLAS (2020b). *Combination of searches for Higgs boson pairs in pp collisions at  $\sqrt{s} = 13$  TeV with the ATLAS detector*. Phys. Lett. B **800**. Art. no.: 135103.
  - ATLAS (2020c). *Combined measurements of Higgs boson production and decay using up to  $80 \text{ fb}^{-1}$  of proton-proton collision data at  $\sqrt{s} = 13$  TeV collected with the ATLAS experiment*. Phys. Rev. D **101**(1). Art. no.: 012002.
  - ATLAS (2019b). *Electron and photon performance measurements with the ATLAS detector using the 2015–2017 LHC proton-proton collision data*. JINST **14**(12). Art. no.: P12006.
  - ATLAS (2020d). *Evidence for electroweak production of two jets in association with a  $Z\gamma$  pair in pp collisions at  $\sqrt{s} = 13$  TeV with the ATLAS detector*. Phys. Lett. B **803**. Art. no.: 135341.
  - ATLAS (2019c). *Evidence for the production of three massive vector bosons with the ATLAS detector*. Phys. Lett. B **798**. Art. no.: 134913.
  - ATLAS (2019d). *Evidence for the production of three massive vector bosons in pp collisions with the ATLAS detector*. PoS **DIS2019**, p. 135.
  - ATLAS (2019e). *Identification of boosted Higgs bosons decaying into b-quark pairs with the ATLAS detector at 13 TeV*. Eur. Phys. J. C **79**(10), p. 836.
  - ATLAS (2019f). *Measurement of angular and momentum distributions of charged particles within and around jets in Pb+Pb and pp collisions at  $\sqrt{s_{NN}} = 5.02$  TeV with the ATLAS detector*. Phys. Rev. C **100**(6). Art. no.: 064901.
  - ATLAS (2020e). *Measurement of azimuthal anisotropy of muons from charm and bottom hadrons in pp collisions at  $\sqrt{s} = 13$  TeV with the ATLAS detector*. Phys. Rev. Lett. **124**(8). Art. no.: 082301.
  - ATLAS (2020f). *Measurement of differential cross sections for single diffractive dissociation in  $\sqrt{s} = 8$  TeV pp collisions using the ATLAS ALFA spectrometer*. JHEP **02**, p. 042.
  - ATLAS (2019g). *Measurement of distributions sensitive to the underlying event in inclusive Z-boson production in pp collisions at  $\sqrt{s} = 13$  TeV with the ATLAS detector*. Eur. Phys. J. C **79**(8), p. 666.
  - ATLAS (2019h). *Measurement of flow harmonics correlations with mean transverse momentum in lead-lead and proton-lead collisions at  $\sqrt{s_{NN}} = 5.02$  TeV with the ATLAS detector*. Eur. Phys. J. C **79**(12), p. 985.
  - ATLAS (2019i). *Measurement of  $K_S^0$  and  $\Lambda^0$  production in  $t\bar{t}$  dileptonic events in pp collisions at  $\sqrt{s} = 7$  TeV with the ATLAS detector*. Eur. Phys. J. C **79**(12), p. 1017.
  - ATLAS (2020g). *Measurement of the azimuthal anisotropy of charged-particle production in Xe+Xe collisions at  $\sqrt{s_{NN}} = 5.44$  TeV with the ATLAS detector*. Phys. Rev. C **101**(2). Art. no.: 024906.
  - ATLAS (2019j). *Measurement of the cross-section and charge asymmetry of W bosons produced in proton-proton collisions at  $\sqrt{s} = 8$  TeV with the ATLAS detector*. Eur. Phys. J. C **79**(9), p. 760.
  - ATLAS (2019k). *Measurement of the inclusive cross-section for the production of jets in association with a Z boson in proton-proton collisions at 8 TeV using the ATLAS detector*. Eur. Phys. J. C **79**(10), p. 847.
  - ATLAS (2019l). *Measurement of the inclusive isolated-photon cross section in pp collisions at  $\sqrt{s} = 13$  TeV using  $36 \text{ fb}^{-1}$  of ATLAS data*. JHEP **10**, p. 203.
  - ATLAS (2019m). *Measurement of the jet mass in high transverse momentum  $Z(\rightarrow b\bar{b})\gamma$  production at  $\sqrt{s} = 13$  TeV using the ATLAS detector*.
  - ATLAS (2019n). *Measurement of the production cross section for a Higgs boson in association with a vector boson in the  $H \rightarrow WW^* \rightarrow \ell \nu \ell \nu$  channel in pp collisions at  $\sqrt{s} = 13$  TeV with the ATLAS detector*. Phys. Lett. B **798**. Art. no.: 134949.
  - ATLAS (2019o). *Measurement of the top-quark mass in  $t\bar{t} + 1$ -jet events collected with the ATLAS detector in pp collisions at  $\sqrt{s} = 8$  TeV*. JHEP **11**, p. 150.
  - ATLAS (2019p). *Measurement of the transverse momentum distribution of Drell-Yan lepton pairs in proton-proton collisions at  $\sqrt{s} = 13$  TeV with the ATLAS detector*.

- ATLAS (2019q). *Measurement of the  $t\bar{t}$  production cross-section and lepton differential distributions in  $e\mu$  dilepton events from  $pp$  collisions at  $\sqrt{s} = 13$  TeV with the ATLAS detector.*
- ATLAS (2020h). *Measurement of the  $Z(\rightarrow \ell^+\ell^-)\gamma$  production cross-section in  $pp$  collisions at  $\sqrt{s} = 13$  TeV with the ATLAS detector.* JHEP **03**, p. 054.
- ATLAS (2019r). *Measurement of  $W^\pm$ -boson and  $Z$ -boson production cross-sections in  $pp$  collisions at  $\sqrt{s} = 2.76$  TeV with the ATLAS detector.* Eur. Phys. J. C **79**(11), p. 901.
- ATLAS (2019s). *Measurement of  $W^\pm$  boson production in  $Pb+Pb$  collisions at  $\sqrt{s_{NN}} = 5.02$  TeV with the ATLAS detector.* Eur. Phys. J. C **79**(11), p. 935.
- ATLAS (2019t). *Measurements of top-quark pair differential and double-differential cross-sections in the  $\ell$ +jets channel with  $pp$  collisions at  $\sqrt{s} = 13$  TeV using the ATLAS detector.* Eur. Phys. J. C **79**(12), p. 1028.
- ATLAS (2019u). *Observation of light-by-light scattering in ultraperipheral  $Pb+Pb$  collisions with the ATLAS detector.* Phys. Rev. Lett. **123**(5). Art. no.: 052001.
- ATLAS (2020i). *Performance of electron and photon triggers in ATLAS during LHC Run 2.* Eur. Phys. J. C **80**(1), p. 47.
- ATLAS (2019v). *Properties of jet fragmentation using charged particles measured with the ATLAS detector in  $pp$  collisions at  $\sqrt{s} = 13$  TeV.* Phys. Rev. D **100**(5). Art. no.: 052011.
- ATLAS (2019w). *Resolution of the ATLAS muon spectrometer monitored drift tubes in LHC Run 2.* JINST **14**(09). Art. no.: P09011.
- ATLAS (2019x). *Search for a heavy charged boson in events with a charged lepton and missing transverse momentum from  $pp$  collisions at  $\sqrt{s} = 13$  TeV with the ATLAS detector.* Phys. Rev. D **100**(5). Art. no.: 052013.
- ATLAS (2019y). *Search for bottom-squark pair production with the ATLAS detector in final states containing Higgs bosons,  $b$ -jets and missing transverse momentum.* JHEP **12**, p. 060.
- ATLAS (2019z). *Search for diboson resonances in hadronic final states in  $139\text{ fb}^{-1}$  of  $pp$  collisions at  $\sqrt{s} = 13$  TeV with the ATLAS detector.* JHEP **09**, p. 091.
- ATLAS (2020j). *Search for direct stau production in events with two hadronic  $\tau$ -leptons in  $\sqrt{s} = 13$  TeV  $pp$  collisions with the ATLAS detector.* Phys. Rev. D **101**(3). Art. no.: 032009.
- ATLAS (2020k). *Search for displaced vertices of oppositely charged leptons from decays of long-lived particles in  $pp$  collisions at  $\sqrt{s} = 13$  TeV with the ATLAS detector.* Phys. Lett. B **801**. Art. no.: 135114.
- ATLAS (2020l). *Search for electroweak production of charginos and sleptons decaying into final states with two leptons and missing transverse momentum in  $\sqrt{s} = 13$  TeV  $pp$  collisions using the ATLAS detector.* Eur. Phys. J. C **80**(2), p. 123.
- ATLAS (2020m). *Search for flavour-changing neutral currents in processes with one top quark and a photon using  $81\text{ fb}^{-1}$  of  $pp$  collisions at  $\sqrt{s} = 13$  TeV with the ATLAS experiment.* Phys. Lett. B **800**. Art. no.: 135082.
- ATLAS (2019aa). *Search for heavy neutral Higgs bosons produced in association with  $b$ -quarks and decaying to  $b$ -quarks at  $\sqrt{s} = 13$  TeV with the ATLAS detector.*
- ATLAS (2019ab). *Search for heavy neutral leptons in decays of  $W$  bosons produced in 13 TeV  $pp$  collisions using prompt and displaced signatures with the ATLAS detector.* JHEP **10**, p. 265.
- ATLAS (2019ac). *Search for high-mass dilepton resonances using  $139\text{ fb}^{-1}$  of  $pp$  collision data collected at  $\sqrt{s} = 13$  TeV with the ATLAS detector.* Phys. Lett. B **796**, pp. 68–87.
- ATLAS (2019ad). *Search for light long-lived neutral particles produced in  $pp$  collisions at  $\sqrt{s} = 13$  TeV and decaying into collimated leptons or light hadrons with the ATLAS detector.* arXiv. 1909.01246.
- ATLAS (2020n). *Search for long-lived neutral particles produced in  $pp$  collisions at  $\sqrt{s} = 13$  TeV decaying into displaced hadronic jets in the ATLAS inner detector and muon spectrometer.* Phys. Rev. D **101**(5). Art. no.: 052013.

- Aad, G. et al., ATLAS (2020o). *Search for Magnetic Monopoles and Stable High-Electric-Charge Objects in 13 TeV Proton-Proton Collisions with the ATLAS Detector*. Phys. Rev. Lett. **124**(3). Art. no.: 031802.
- ATLAS (2020p). *Search for new resonances in mass distributions of jet pairs using  $139\text{ fb}^{-1}$  of pp collisions at  $\sqrt{s} = 13\text{ TeV}$  with the ATLAS detector*. JHEP **03**, p. 145.
- ATLAS (2020q). *Search for non-resonant Higgs boson pair production in the  $bbl\nu\ell\nu$  final state with the ATLAS detector in pp collisions at  $\sqrt{s} = 13\text{ TeV}$* . Phys. Lett. B **801**. Art. no.: 135145.
- ATLAS (2019ae). *Search for squarks and gluinos in final states with same-sign leptons and jets using  $139\text{ fb}^{-1}$  of data collected with the ATLAS detector*.
- ATLAS (2019af). *Search for the electroweak diboson production in association with a high-mass dijet system in semileptonic final states in pp collisions at  $\sqrt{s} = 13\text{ TeV}$  with the ATLAS detector*. Phys. Rev. D **100**(3). Art. no.: 032007.
- ATLAS (2020r). *Search for the Higgs boson decays  $H \rightarrow ee$  and  $H \rightarrow e\mu$  in pp collisions at  $\sqrt{s} = 13\text{ TeV}$  with the ATLAS detector*. Phys. Lett. B **801**. Art. no.: 135148.
- ATLAS (2020s). *Searches for electroweak production of supersymmetric particles with compressed mass spectra in  $\sqrt{s} = 13\text{ TeV}$  pp collisions with the ATLAS detector*. Phys. Rev. D **101**(5). Art. no.: 052005.
- ATLAS (2020t). *Searches for lepton-flavour-violating decays of the Higgs boson in  $\sqrt{s} = 13\text{ TeV}$  pp collisions with the ATLAS detector*. Phys. Lett. B **800**. Art. no.: 135069.
- ATLAS (2020u). *Transverse momentum and process dependent azimuthal anisotropies in  $\sqrt{s_{NN}} = 8.16\text{ TeV}$  p+Pb collisions with the ATLAS detector*. Eur. Phys. J. C **80**(1), p. 73.
- ATLAS (2020v). *Z boson production in Pb+Pb collisions at  $\sqrt{s_{NN}} = 5.02\text{ TeV}$  measured by the ATLAS experiment*. Phys. Lett. B **802**. Art. no.: 135262.

## FASE2\_ATLAS

- Calderini, G., Bomben, M., D’Eramo Ducourthial, A., Luise, I., Marchiori, G., Boscardin, M., Ronchin, S., Zorzi, N., Bosisio, L., Dalla Betta, G. F., Darbo, G., Giacomini, G., Meschini, M., and Messineo, A. (2019c). *Active-edge FBK-INFN-LPNHE thin n-on-p pixel sensors for the upgrade of the ATLAS Inner Tracker*. Nuclear Instrum. Methods A **936**, pp. 638–639.
- Calderini, G., Bomben, M., D’Eramo, L., Luise, I., Marchiori, G., Taibah, R., Boscardin, M., Ronchin, S., Zorzi, N., Bosisio, L., Dalla Betta, G. F., Darbo, G., and Giacomini, G. (2019d). *Performance of the FBK/INFN/LPNHE thin active edge pixel detectors for the upgrade of the ATLAS Inner Tracker*. Journal Instrum. **14**. Art. no.: C07001.
- Duarte-Campderros, J., Curries, E., Fernández, F., Gómez, G., González, J., Silva, E., Vila Jaramillo, R., Meschini, M., Ceccarelli, R., Dinardo, M., Gennai, S., Moroni, L., Zuolo, D., Demaria, L., Monteil, E., Gaioni, L., Messineo Dalla Betta, G.-F., Mendicino, R., Boscardin, M., Hidalgo, S., Pellegrini, G., Quirion, D., and Manna, M. (2019). *Results on proton-irradiated 3D pixel sensors interconnected to RD53A readout ASIC*. Nuclear Instrum. Methods A **944**. Art. no.: 162625.
- Ducourthial, A., Bomben, M., Calderini, G., Camacho, R., D’Eramo, L., Luise, I., Marchiori, G., Boscardin, M., Bosisio, L., Darbo, G., Dalla Betta, G. F., Giacomini, G., Meschini, M., Messineo, A., Ronchin, S., and Zorzi, N. (2019). *Performance of thin planar n-on-p silicon pixels after HL-LHC radiation fluences*. Nuclear Instrum. Methods A **927**, pp. 219–229.
- Medicino, R., Boscardin, M., and Dalla Betta, G.-F. (2019a). *Characterization of FBK small-pitch 3D diodes after neutron irradiation up to  $3.5 \times 10^{16}\text{ n}_{eq}\text{ cm}^{-2}$* . Journal Instrum. **14**. Art. no.: C01005.
- Meschini, M., Ceccarelli, R., Dinardo, M., Gennai, S., Moroni, L., Zuolo, D., Demaria, L., Monteil, E., Gaioni, L., Messineo, A., Curràs, E., Duarte, J., Fernández, F., Gómez, G., Garía, A., González, J., Silva, E., Vila, I., Dalla Betta, G.-F., Mendicino, R., and Boscardin, M. (2019a). *First results on 3D pixel sensors interconnected to the RD53A readout chip after irradiation to  $1 \times 10^{16}\text{ n}_{eq}\text{ cm}^{-2}$* . Journal Instrum. **14**. Art. no.: C06018.

- Moscatelli, F., Morozzi, A., Passeri, D., Mattiazzo, S., Dalla Betta, G. F., Bergauer, T., Dragicevic, M., Konig, A., Hinger, V., and Bilei, G. (2019). *Analysis of surface radiation damage effects at HL-LHC fluences: Comparison of different technology options*. Nuclear Instrum. Methods A **924**, pp. 198–202.
- Oide, H., Alimonti, G., Boscardin, M., Dalla Betta, G., Darbo, G., Ficorella, F., Fumagalli, E., Gariano, G., Gaudiello, A., Gemme, C., Meschini, M., Messineo, A., Mendicino, R., Ronchin, S., Rovani, A., Ruscino, E., Sultan, D., Zorzi, N., and Vazquez Furelos, D. (2019b). *INFN-FBK developments of 3D sensors for High-Luminosity LHC*. Nuclear Instrum. Methods A **924**, pp. 73–77.

## Astroparticle Physics

- Abrescia, M. et al., EEE collaboration (2019). *The new Trigger/GPS module for the extreme energy events project*. Nucl. Instrum. Meth. A. Art. no.: 162358.

### ADHD

- Dimiccoli, F., Nozzoli, F., and Zuccon, P (2019d). “Detectors for antideuteron search in cosmic rays: current status and new ideas”. *15th Topical Seminar on Innovative Particle and Radiation Detectors (in press on JINST)*. IOP Publishing, pp. 1–10.
- Nozzoli, F., Dimiccoli, F., and Zuccon, P (2019). “Perspectives of dark matter indirect search with ADHD in space”. *10th Young Researcher Meeting (in press on JoP)*. IOP Publishing, pp. 1–6.
- von Doetinchem, P et al. (2020). *Cosmic-ray Antinuclei as Messengers of New Physics: Status and Outlook for the New Decade*.

### AMS

- Aguilar, M. et al., AMS collaboration (2019a). *Properties of Cosmic Helium Isotopes Measured by the Alpha Magnetic Spectrometer*. Phys. Rev. Lett. **123**(18). Art. no.: 181102.
- AMS collaboration (2019b). *Towards Understanding the Origin of Cosmic-Ray Electrons*. Phys. Rev. Lett. **122**(10). Art. no.: 101101.
- AMS collaboration (2019c). *Towards Understanding the Origin of Cosmic-Ray Positrons*. Phys. Rev. Lett. **122**(4). Art. no.: 041102.
- Dimiccoli, F., Basara, L., Kanishchev, K., Nozzoli, F., and Zuccon, P (2019a). *Measurement of the D/p ratio in Cosmic rays with the AMS-02 experiment*. Nucl. Part. Phys. Proc. **306-308**, pp. 80–84.
- (2019b). *Measurements of the  $^3\text{He}$  and D components in cosmic rays with the AMS-02 experiment*. Nuovo Cim. **C42**(4), p. 174.
- Dimiccoli, F., Battiston, R., Kanishchev, K., Nozzoli, F., and Zuccon, P (2019c). “Cosmic Ray Isotopes Measured by AMS02”. *Meeting of the Division of Particles and Fields of the American Physical Society (DPF2019) Boston, Massachusetts, July 29-August 2, 2019*.
- Nozzoli, F. (2019). *Properties of Elementary Particle Fluxes in Primary Cosmic Rays Measured with the Alpha Magnetic Spectrometer on the International Space Station*. EPJ Web Conf. **209**. Art. no.: 01007.
- Zuccon, P (2019). *AMS-02 experiment: status and perspectives*. Nucl. Part. Phys. Proc. **306-308**, pp. 74–79.

### DarkSide

- Gola, A. et al. (2019). *NUV-Sensitive Silicon Photomultiplier Technologies Developed at Fondazione Bruno Kessler*. Sensors **19**, p. 308.

## FISH

- Farolfi, A., Trypogeorgos, D., Colzi, G., Fava, E., Lamporesi, G., and Ferrari, G. (2019a). *Design and characterization of a compact magnetic shield for ultracold atomic gas experiments*. Review of Scientific Instruments **90**(11). Art. no.: 115114.
- Farolfi, A., Trypogeorgos, D., Mordini, C., Lamporesi, G., and Ferrari, G. (2019b). *Observation of magnetic solitons in two-component Bose-Einstein condensates*. arXiv:1912.10513.
- Gallemí, A., Pitaevskii, L. P., Stringari, S., and Recati, A. (2019). *Decay of the relative phase domain wall into confined vortex pairs: The case of a coherently coupled bosonic mixture*. Phys. Rev. A **100**(2). Art. no.: 023607.
- Roccuzzo, S. M., Gallemí, A., Recati, A., and Stringari, S. (2020). *Rotating a Supersolid Dipolar Gas*. Phys. Rev. Lett. **124**(4). Art. no.: 045702.
- Tajima, H., Recati, A., and Ohashi, Y. (2020). *Spin-dipole mode in a trapped Fermi gas near unitarity*. Phys. Rev. A **101**(1). Art. no.: 013610.

## HUMOR

- Asjad, M., Abari, N. E., Zippilli, S., and Vitali, D. (2019). *Optomechanical cooling with intracavity squeezed light*. OPTICS EXPRESS **27-22**, pp. 32427–32444.
- Chowdhury, A., Vezio, P., Bonaldi, M., Borrielli, A., Marino, F., Morana, B., Pandraud, G., Pontin, A., Prodi, G., Sarro, M., Serra, E., and Marin, F. (2019). *Calibrated quantum thermometry in cavity optomechanics*. QUANTUM SCIENCE AND TECHNOLOGY **4-2**. Art. no.: 024007.

## LIMADOU

- Marchetti, D. et al. (2020). *Possible Lithosphere-Atmosphere-Ionosphere Coupling effects prior to the 2018  $M_w = 7.5$  Indonesia earthquake from seismic, atmospheric and ionospheric data*. Journal of Asian Earth Sciences **188**, p. 104097.
- Picozza, P. et al. (2019a). *Scientific Goals and In-orbit Performance of the High-energy Particle Detector on Board the CSES*. The Astrophysical Journal Supplement Series **243**(1), p. 16.
- Proc. 15th Topical Seminar on Innovative Particle and Radiation Detectors (Siena, Italy, October 2019) (2020). Vol. C05014. JINST. Trieste, Italy: Sissa.

## LISA Pathfinder

- Armano, M. et al., LISA Pathfinder (2019a). *LISA Pathfinder micronewton cold gas thrusters: In-flight characterization*. Phys. Rev. D **99**(12). Art. no.: 122003.
- LISA Pathfinder (2019b). *LISA Pathfinder Performance Confirmed in an Open-Loop Configuration: Results from the Free-Fall Actuation Mode*. Phys. Rev. Lett. **123**(11). Art. no.: 111101.
- Armano, M. et al., LISA Pathfinder (2019c). *LISA Pathfinder Platform Stability and Drag-free Performance*. Phys. Rev. D **99**(8). Art. no.: 082001.
- Armano, M. et al., LISA Pathfinder (2019d). *Novel methods to measure the gravitational constant in space*. Phys. Rev. D **100**(6). Art. no.: 062003.
- Armano, M. et al., LISA Pathfinder (2019e). *Temperature stability in the sub-milliHertz band with LISA Pathfinder*. Mon. Not. Roy. Astron. Soc. **486**(3), pp. 3368–3379.
- Grimani, C. et al., LISA Pathfinder (2019). *Forbush Decreases and  $< 2$  Day GCR Flux Non-recurrent Variations Studied with LISA Pathfinder*. Astrophys. J. **874**(2), p. 167.
- Thorpe, J. I. et al., LISA Pathfinder, ST7-DRS Operations Team (2019). *Micrometeoroid Events in LISA Pathfinder*. Astrophys. J. **883**, p. 53.

**VIRGO**

- Abbott, B. P. et al., LIGO Scientific, Virgo (2019a). *A gravitational-wave measurement of the Hubble constant following the second observing run of Advanced LIGO and Virgo*. arXiv preprint:1908.06060v2.
- LIGO Scientific, Virgo (2019b). *All-sky search for continuous gravitational waves from isolated neutron stars using Advanced LIGO O2 data*. Phys. Rev. D **100**(2). Art. no.: 024004.
- LIGO Scientific, Virgo (2019c). *All-sky search for long-duration gravitational-wave transients in the second Advanced LIGO observing run*. Phys. Rev. D **99**(10). Art. no.: 104033.
- LIGO Scientific, Virgo (2019d). *All-Sky Search for Short Gravitational-Wave Bursts in the Second Advanced LIGO and Advanced Virgo Run*. Phys. Rev. D **100**(2). Art. no.: 024017.
- LIGO Scientific, Virgo (2020a). *An Optically Targeted Search for Gravitational Waves emitted by Core-Collapse Supernovae during the First and Second Observing Runs of Advanced LIGO and Advanced Virgo*. Phys. Rev. D **101**. Art. no.: 084002.
- LIGO Scientific, Virgo (2019e). *Directional limits on persistent gravitational waves using data from Advanced LIGO's first two observing runs*. Phys. Rev. D **100**(6). Art. no.: 062001.
- LIGO Scientific, Virgo (2019f). *Low-latency Gravitational-wave Alerts for Multimessenger Astronomy during the Second Advanced LIGO and Virgo Observing Run*. Astrophys. J. **875**(2), p. 161.
- LIGO Scientific, Virgo (2020b). *Model comparison from LIGO-Virgo data on GW170817's binary components and consequences for the merger remnant*. CLASSICAL AND QUANTUM GRAVITY **37**.
- LIGO Scientific, Virgo (2019g). *Narrow-band search for gravitational waves from known pulsars using the second LIGO observing run*. Phys. Rev. D **99**(12). Art. no.: 122002.
- LIGO Scientific, Virgo (2019h). *Search for Eccentric Binary Black Hole Mergers with Advanced LIGO and Advanced Virgo during Their First and Second Observing Runs*. The Astrophysical Journal **883**(2), p. 149.
- LIGO Scientific, Virgo (2019i). *Search for gravitational waves from Scorpius X-1 in the second Advanced LIGO observing run with an improved hidden Markov model*. Phys. Rev. D **100**(12). Art. no.: 122002.
- LIGO Scientific, Virgo, IPN (2019j). *Search for gravitational-wave signals associated with gamma-ray bursts during the second observing run of Advanced LIGO and Advanced Virgo*. Astrophys. J. **886**, p. 75.
- LIGO Scientific, Virgo (2019k). *Search for intermediate mass black hole binaries in the first and second observing runs of the Advanced LIGO and Virgo network*. Phys. Rev. D **100**(6). Art. no.: 064064.
- LIGO Scientific, Virgo (2019l). *Search for Subsolar Mass Ultracompact Binaries in Advanced LIGO's Second Observing Run*. Phys. Rev. Lett. **123**(16). Art. no.: 161102.
- LIGO Scientific, Virgo (2019m). *Search for the isotropic stochastic background using data from Advanced LIGO's second observing run*. Phys. Rev. D **100**(6). Art. no.: 061101.
- LIGO Scientific, Virgo (2019n). *Search for Transient Gravitational-wave Signals Associated with Magnetar Bursts during Advanced LIGO's Second Observing Run*. Astrophys. J. **874**(2), p. 163.
- LIGO Scientific, Virgo (2019o). *Searches for Gravitational Waves from Known Pulsars at Two Harmonics in 2015-2017 LIGO Data*. Astrophys. J. **879**(1), p. 10.
- LIGO Scientific, Virgo (2019p). *Tests of General Relativity with the Binary Black Hole Signals from the LIGO-Virgo Catalog GWTC-1*. Phys. Rev. D **100**(10). Art. no.: 104036.
- Acernese, F. et al., Virgo (2019). *Increasing the Astrophysical Reach of the Advanced Virgo Detector via the Application of Squeezed Vacuum States of Light*. Phys. Rev. Lett. **123**(23). Art. no.: 231108.
- Virgo (2020). *The advanced Virgo longitudinal control system for the O2 observing run*. ASTROPARTICLE PHYSICS **116**.
- Salemi, F., Milotti, E., Prodi, G., Vedovato, G., Lazzaro, C., Tiwari, S., Vinciguerra, S., Drago, M., and Klimentko, S. (2019). *Wider look at the gravitational-wave transients from GWTC-1 using an unmodeled reconstruction method*. Physical Review D **100**(4). Art. no.: 042003.

Soares-Santos, M. et al., DES, LIGO Scientific, Virgo (2019). *First Measurement of the Hubble Constant from a Dark Standard Siren using the Dark Energy Survey Galaxies and the LIGO/Virgo Binary-Black-hole Merger GW170814*. *Astrophys. J.* **876**(1), p. L7.

## Nuclear Physics

### AEGIS

Aghion, S., Amsler, C., Bonomi, G., Brusa, R., Caccia, M., Caravita, R., Castelli, F., Cerchiari, G., Comparat, D., Consolati, G., Demetrio, A., Di Noto, L., Doser, M., Evans, C., Fan, M., Ferragut, R., Fesel, J., Fontana, A., Gerber, S., Giammarchi, M., Gligorova, A., Guatieri, F., Haider, S., Hinterberger, A., Holmestad, H., Kellerbauer, A., Khalidova, O., Krasnicky, D., Lagomarsino, V., Lansonneur, P., Lebrun, P., Malbrunot, C., Mariazzi, S., Marton, J., Matveev, V., Mazzotta, Z., Müller, S., Nebbia, G., Nedelec, P., Oberthaler, M., Pacifico, N., Pagano, D., Penasa, L., Petracek, V., Prelz, F., Prevedelli, M., Rienaecker, B., Robert, J., Roehne, O., Rotondi, A., Sandaker, H., Santoro, R., Smestad, L., Sorrentino, F., Testera, G., Tietje, I., Widmann, E., Yzombard, P., Zimmer, C., Zmeskal, J., Zurlo, N., and Antonello, M. (2019). *Correction to: Compression of a mixed antiproton and electron non-neutral plasma to high densities*. *European Physical Journal D* **73**(11). Art. no.: 234.

Amsler, C. et al., AEGIS collaboration (2019a). *A  $\sim 100$   $\mu\text{m}$ -resolution position-sensitive detector for slow positronium*. *NIMB* **457**, pp. 44–48.

— AEGIS collaboration (2019b). *Velocity-selected production of  $2^3\text{S}$  metastable positronium*. *Phys. Rev. A* **99**. Art. no.: 033405.

Antonello, M. et al., AEGIS collaboration (2019). *Efficient  $2^3\text{S}$  positronium production by stimulated decay from the  $3^3\text{P}$  level*. *Phys. Rev. A* **100**. Art. no.: 063414.

Caravita, R., Mariazzi, S., Aghion, S., Amsler, C., Antonello, M., Belov, A., Bonomi, G., Brusa, R., Caccia, M., Camper, A., Castelli, F., Cerchiari, G., Comparat, D., Consolati, G., Demetrio, A., Di Noto, L., Doser, M., Evans, C., Fan, M., Ferragut, R., Fesel, J., Fontana, A., Gerber, S., Giammarchi, M., Gligorova, A., Guatieri, F., Hackstock, P., Haider, S., Hinterberger, A., Holmestad, H., Kellerbauer, A., Khalidova, O., Krasnicky, D., Lagomarsino, V., Lansonneur, P., Lebrun, P., Malbrunot, C., Marton, J., Matveev, V., Müller, S., Nebbia, G., Nedelec, P., Oberthaler, M., Pagano, D., Penasa, L., Petracek, V., Prelz, F., Prevedelli, M., Rienaecker, B., Robert, J., Roehne, O., Rotondi, A., Sandaker, H., Santoro, R., Smestad, L., Sorrentino, F., Testera, G., Tietje, I., Vujanovic, M., Widmann, E., Yzombard, P., Zimmer, C., Zmeskal, J., and Zurlo, N. (2019). “Positronium Rydberg excitation diagnostic in a 1T cryogenic environment”. *AIP Conference Proceedings*. Vol. 2182. Art. no.: 030002.

Khalidova, O., Aghion, S., Amsler, C., Antonello, M., Belov, A., Bonomi, G., Brusa, R., Caccia, M., Camper, A., Caravita, R., Castelli, F., Cerchiari, G., Comparat, D., Consolati, G., Demetrio, A., Di Noto, L., Doser, M., Evans, C., Fani, M., Ferragut, R., Fesel, J., Fontana, A., Gerber, S., Giammarchi, M., Gligorova, A., Guatieri, F., Hackstock, P., Haider, S., Hinterberger, A., Holmestad, H., Kellerbauer, A., Krasnicky, D., Lagomarsino, V., Lansonneur, P., Lebrun, P., Malbrunot, C., Mariazzi, S., Marton, J., Matveev, V., Müller, S., Nebbia, G., Nedelec, P., Oberthaler, M., Pagano, D., Penasa, L., Petracek, V., Prelz, F., Prevedelli, M., Rienaecker, B., Robert, J., Roehne, O., Rotondi, A., Sandaker, H., Santoro, R., Smestad, L., Sorrentino, F., Testera, G., Tietje, I., Vujanovic, M., Widmann, E., Yzombard, P., Zimmer, C., Zmeskal, J., and Zurlo, N. (2019). “The AEGIS experiment: Towards antimatter gravity measurements”. *Journal of Physics: Conference Series*. Vol. 1390. 1. Art. no.: 012104.

Mariazzi, S., Caravita, R., Aghion, S., Amsler, C., Antonello, M., Belov, A., Bonomi, G., Brusa, R., Caccia, M., Camper, A., Castelli, F., Cerchiari, G., Comparat, D., Consolati, G., Demetrio, A., Di Noto,

- L., Doser, M., Evans, C., Fan, M., Ferragut, R., Fesel, J., Fontana, A., Gerber, S., Giammarchi, M., Gligorova, A., Guatieri, F., Hackstock, P., Haider, S., Hinterberger, A., Holmestad, H., Kellerbauer, A., Khalidova, O., Krasnicky, D., Lagomarsino, V., Lansonneur, P., Lebrun, P., Malbrunot, C., Matveev, V., Mueller, S., Nebbia, G., Nedelec, P., Oberthaler, M., Pagano, D., Penasa, L., Petracek, V., Prelz, F., Prevedelli, M., Rienaecker, B., Robert, J., Roehne, O., Rotondi, A., Sandaker, H., Santoro, R., Smestad, L., Sorrentino, F., Testera, G., Tietje, I., Widmann, E., Yzombard, P., Zimmer, C., and Zurlo, N. (2019). “Production of long-lived positronium states via laser excitation to 33P level”. *AIP Conference Proceedings*. Vol. 2182. Art. no.: 030004.
- Pino, F., Fontana, C., Lunardon, M., Moretto, S., Stevanato, L., Brusa, R., Caravita, R., Mariazzi, S., Penasa, L., Povolo, L., and Nebbia, G. (2019). *A low cost 2/3 of 4π detector for the study of Ps decay*. Nuclear Instruments and Methods in Physics Research, Section A: Accelerators, Spectrometers, Detectors and Associated Equipment **942**. Art. no.: 162416.
- Zurlo, N., Aghion, S., Amsler, C., Antonello, M., Belov, A., Bonomi, G., Brusa, R., Caccia, M., Camper, A., Caravita, R., Castelli, F., Cerchiari, G., Comparat, D., Consolati, G., Demetrio, A., Di Noto, L., Doser, M., Evans, C., Fan, M., Ferragut, R., Fesel, J., Fontana, A., Gerber, S., Giammarchi, M., Gligorova, A., Guatieri, F., Hackstock, P., Haider, S., Hinterberger, A., Holmestad, H., Kellerbauer, A., Khalidova, O., Krasnicky, D., Lagomarsino, V., Lansonneur, P., Lebrun, P., Malbrunot, C., Mariazzi, S., Marton, J., Matveev, V., Müller, S., Nebbia, G., Nedelec, P., Oberthaler, M., Pagano, D., Penasa, L., Petracek, V., Prelz, F., Prevedelli, M., Rienaecker, B., Robert, J., Roehne, O., Rotondi, A., Sacerdoti, M., Sandaker, H., Santoro, R., Smestad, L., Sorrentino, F., Testera, G., Tietje, I., Vujanovic, M., Widmann, E., Yzombard, P., Zimmer, C., and Zmeskal, J. (2019). *Monte-Carlo simulation of positronium laser excitation and anti-hydrogen formation via charge exchange*. Hyperfine Interactions **240**(1). Art. no.: 18.

## FOOT

- Montesi, M. et al. (2019a). *Ion charge separation with new generation of nuclear emulsion films*. Open Physics **17**(1), pp. 233–240.
- Morrocchi, M. et al. (2019). *Development and characterization of a ΔE-TOF detector prototype for the FOOT experiment*. NIM-A **916**, pp. 116–124.

## Theoretical Physics

- Traini, M. C. and Blaizot, J.-P. (2019). *Diffractive incoherent vector meson production off protons: a quark model approach to gluon fluctuation effects*. The European Physical Journal C **79**(4), p. 327.
- Vento, V. and Traini, M. (2020). *Scattering of charged particles off monopole–anti-monopole pairs*. The European Physical Journal C **80**(1), p. 62.

## BELL

- Albeverio, S., Mazzucchi, S., and Cangiotti, N. (2020). *A rigorous mathematical construction of Feynman path integrals for the Schrödinger equation with magnetic field*. Commun. Math. Phys. **374**.
- Blanzieri, E. and Pastorello, D. (2019). *Quantum Annealing Learning Search for solving QUBO problems*. Quantum Information Processing **18**, p. 303.
- Drago, N. and Moretti, V. (2020). *The notion of observable and the moment problem for \*-algebras and their GNS representations*. Lett. Math. Phys.
- Landsman, K., Moretti, V., and Ven, C. van de (2020). *A Strict Deformation Quantization Map on the state space of  $M_k(\mathbb{C})$  and the Classical Limit of the Curie-Weiss model*. Reviews in Mathematical Physics **32**. Art. no.: 1950013.

## BIOPHYS

- Borsatto, A., Marino, V., Abrusci, G., Lattanzi, G., and Dell'Orco, D. (2019). *Effects of Membrane and Biological Target on the Structural and Allosteric Properties of Recoverin: A Computational Approach*. International Journal of Molecular Sciences **20**, pp. 5009–5023.
- Carli, M., Turelli, M., and Faccioli, P. (2019). *Microscopic calculation of absorption spectra of macromolecules: An analytic approach*. journal of chemical physics **150**. Art. no.: 144103.
- Erban, R., Harris, S., and Potestio, R. (2019). *Multi-resolution simulations of intracellular processes*. Interface Focus **9**(3). Art. no.: 20190028.
- Giulini, M. and Potestio, R. (2019). *A deep learning approach to the structural analysis of proteins*. Interface Focus **9**(3). Art. no.: 20190003.
- Perego, C. and Potestio, R. (2019). *Computational methods in the study of self-entangled proteins: a critical appraisal*. Journal of Physics: Condensed Matter.
- Potestio, R. (2019). *Searching the Optimal Folding Routes of a Complex Lasso Protein*. Biophysical Journal.
- Potestio, R., Heidari, M., Cortes-Huerto, R., Potestio, R., and Kremer, K. (2019). *Steering a solute between coexisting solvation states: Revisiting nonequilibrium work relations and the calculation of free energy differences*. The Journal of Chemical Physics.
- Riccardi, E., Pantano, S., and Potestio, R. (2019). *Envisioning data sharing for the biocomputing community*. Interface Focus **9**(3). Art. no.: 20190005.
- Rigoli, M., Spagnolli, G., Faccioli, P., Requena, J. R., and Biasini, E. (2019). *Ok google, how could I design therapeutics against prion diseases*. Current opinion in pharmacology **44**, pp. 39–45.
- Spagnolli, G. et al. (2019). *Full atomistic model of prion structure and conversion*. PLoS Pathogens **15**. Art. no.: e1007864.
- Tarenzi, T., Calandrini, V., Potestio, R., and Carloni, P. (2019). *Open-Boundary Molecular Mechanics / Coarse-Grained Framework for Simulations of Low-Resolution G-Protein-Coupled Receptor–Ligand Complexes*. Journal of Chemical Theory and Computation **15**(3), pp. 2101–2109.
- Wodak, S. et al. (2019). *Allostery in its many disguises: from theory to applications*. Structure **27**, pp. 566–578.

## FBS

- Efros, V. D., Leidemann, W., and Shalamova, V. Y. (2019). *On Calculating Response Functions Via Their Lorentz Integral Transforms*. Few-Body Systems **60**, 35a–35g.
- Filandri, E., Andreatta, P., Manzata, C. A., Ji, C., Leidemann, W., and Orlandini, G. (2020). *Beryllium-9 in cluster effective field theory*. SCiPost Phys. Proc. **3**, pp. 34.1–34.9.

## FLAG

- Casalino, A. and Rinaldi, M. (2019). *Testing Horndeski gravity as dark matter with hi-class*. Phys. Dark Univ. **23**. Art. no.: 100243.
- Casalino, A., Rinaldi, M., Sebastiani, L., and Vagnozzi, S. (2019). *Alive and well: mimetic gravity and a higher-order extension in light of GW170817*. Class. Quant. Gravity **36**. Art. no.: 017001.
- Rinaldi, M., Vanzo, L., and Vicentini, S. (2019). *Scale-invariant inflation with 1-loop quantum corrections*. PHYS. REV. D **D99**. Art. no.: 103516.
- Sebastiani, L., Vanzo, L., and Zerbini, S. (2019). *On a WKB formula for echoes*. Int. J. of Geom. Methods in Physics **16**. Art. no.: 1950181-1.

**MANYBODY**

- Andreoli, L., Cirigliano, V., Gandolfi, S., and Pederiva, F. (2019). *Quantum Monte Carlo calculations of dark matter scattering off light nuclei*. PHYSICAL REVIEW C **99**(2). Art. no.: 025501.
- Lovato, A., Rocco, N., and Schiavilla, R. (2019). *Muon capture in nuclei: An ab initio approach based on Green's function Monte Carlo methods*. PHYSICAL REVIEW C **100**(3). Art. no.: 035502.
- Lynn, J. E., Tews, I., Gandolfi, S., and Lovato, A. (2019). "Quantum Monte Carlo Methods in Nuclear Physics: Recent Advances". ANNUAL REVIEW OF NUCLEAR AND PARTICLE SCIENCE, VOL 69. Ed. by Holstein, BR. Vol. 69. Annual Review of Nuclear and Particle Science. 4139 EL CAMINO WAY, PO BOX 10139, PALO ALTO, CA 94303-0897 USA: ANNUAL REVIEWS, 279–305.
- Maass, B., Huether, T., König, K., Kraemer, J., Krause, J., Lovato, A., Mueller, P., Pachucki, K., Puchalski, M., Roth, R., Sanchez, R., Sommer, F., Wiringa, R. B., and Noertershaeuser, W. (2019). *Nuclear Charge Radii of 10,11(B)*. PHYSICAL REVIEW LETTERS **122**(18). Art. no.: 182501.
- Rocco, N., Barbieri, C., Benhar, O., De Pace, A., and Lovato, A. (2019[a]). *Neutrino-nucleus cross section within the extended factorization scheme*. PHYSICAL REVIEW C **99**(2). Art. no.: 025502.
- Rocco, N., Nakamura, S. X., Lee, T.-S. H., and Lovato, A. (2019[b]). *Electroweak pion production on nuclei within the extended factorization scheme*. PHYSICAL REVIEW C **100**(4). Art. no.: 045503.
- Schiavilla, R., Baroni, A., Pastore, S., Piarulli, M., Girlanda, L., Kievsky, A., Lovato, A., Marcucci, L. E., Pieper, S. C., Viviani, M., and Wiringa, R. B. (2019). *Local chiral interactions and magnetic structure of few-nucleon systems*. PHYSICAL REVIEW C **99**(3). Art. no.: 034005.
- Sobczyk, J. E., Rocco, N., Lovato, A., and Nieves, J. (2019). *Weak production of strange and charmed ground-state baryons in nuclei*. PHYSICAL REVIEW C **99**(6). Art. no.: 065503.

**NEMESYS**

- Abrams, K., Dapor, M., Stehling, N., Azzolini, M., Kyle, S., Schäfer, J. A., Quade, A., Mika, F., Kratky, S., Pokorna, Z., Konvalina, I., Mehta, D., Black, K., and Rodenburg, C. *Making Sense of Complex Carbon and Metal/Carbon Systems by Secondary Electron Hyperspectral Imaging*. Advanced Science **6**. Art. no.: 1900719.
- Azzolini, M., Ridzel, O. Y., Kaplya, P. S., Afanas'ev, V., Pugno, N. M., Taioli, S., and Dapor, M. (2020). *A comparison between Monte Carlo method and the numerical solution of the Ambartsumian-Chandrasekhar equations to unravel the dielectric response of metals*. Computational Materials Science **173**. Art. no.: 109420.
- Masters, R., Stehling, N., Abrams, K., Kumar, V., Azzolini, M., Pugno, N., Dapor, M., Andreas, H., Schäfer, P., Lidzey, D., and Rodenburg, C. *Mapping Polymer Molecular Order in the SEM with Secondary Electron Hyperspectral Imaging*. Advanced Science **6**. Art. no.: 1801752.
- Morresi, T., Binosi, D., Simonucci, S., Piergallini, R., Roche, S., Pugno, N. M., and Taioli, S. (2019). *Exploring Event Horizons and Hawking Radiation through Deformed Graphene Membranes*. arXiv preprint:1907.08960.
- Morresi, T., Pedrielli, A., Beccara, S., Gabbrielli, R., Pugno, N. M., and Taioli, S. (2020). *Structural, electronic and mechanical properties of all-sp<sup>2</sup> carbon allotropes with density lower than graphene*. Carbon **159**, pp. 512–526.
- Vescovi, D., Piersanti, L., Cristallo, S., Busso, M., Vissani, F., Palmerini, S., Simonucci, S., and Taioli, S. (2019a). *The effects of a revised <sup>7</sup>Be e<sup>-</sup>-capture rate on solar neutrino fluxes*. Astronomy & Astrophysics **623**(A126), p. 7.
- (2019b). *VizieR Online Data Catalog: Effects of a revised <sup>7</sup>Be e-capture rate*. VizieR Online Data Catalog **362**.

## TEONGRAV

- Ciolfi, R., Kastaun, W., Kalinani, J. V., and Giacomazzo, B. (2019). *First 100 ms of a long-lived magnetized neutron star formed in a binary neutron star merger*. Phys. Rev. D **100**(2). Art. no.: 023005.
- Cipolletta, F., Vijay Kalinani, J., Giacomazzo, B., and Ciolfi, R. (2019). *Spritz: a new fully general-relativistic magnetohydrodynamic code*. preprint, arXiv:1912.04794.
- Endrizzi, A., Perego, A., Fabbri, F. M., Branca, L., Radice, D., Bernuzzi, S., Giacomazzo, B., Pederiva, F., and Lovato, A. (2020). *Thermodynamics conditions of matter in the neutrino decoupling region during neutron star mergers*. Eur. Phys. J. A **56**(1), p. 15.

## Technological and Interdisciplinary Physics

- Dionisi, F., Fiorica, F., D'Angelo, E., Maddalo, M., Giacomelli, I., Tornari, E., Rosca, A., Vigo, F., Romanello, D., Cianchetti, M., Tommasino, F., Massaccesi, M., and Orlandi, E. (2019). *Organs at risk's tolerance and dose limits for head and neck cancer re-irradiation: A literature review*. Oral Oncology **98**, pp. 35–47.
- Fellin, F., Iacco, M., D'Avino, V., Tommasino, F., Farace, P., Palma, G., Conson, M., Giacomelli, I., Zucchetti, C., Falcinelli, L., Amichetti, M., Aristei, C., and Cella, L. (2019). *Potential skin morbidity reduction with intensity-modulated proton therapy for breast cancer with nodal involvement*. Acta Oncologica **58**, pp. 934–942.
- Morone, M., Berucci, C., Cipollone, P., De Donato, C., Di Fino, L., Iannilli, M., La Tessa, C., Manea, C., Masciantonio, G., Messi, R., Narici, L., Nobili, G., Pecchi, D., Picozza, P., Reali, E., Rizzo, A., Rovituro, M., Tommasino, F., and Vitali, G. (2019). *A compact Time-Of-Flight detector for radiation measurements in a space habitat: LIDAL-ALTEA*. Nuclear Instruments and Methods in Physics Research Section A: Accelerators, Spectrometers, Detectors and Associated Equipment **936**, pp. 222–223.
- Tommasino, F., Cella, L., and Farace, P. (2019a). *In regards to DeCesaris et al.* International Journal of Radiation Oncology Biology Physics **105**, pp. 676–677.
- Tommasino, F., Rovituro, M., Bortoli, E., La Tessa, C., Petringa, G., Lorentini, S., Verroi, E., Simonov, Y., Weber, U., Cirrone, P., Schwarz, M., Durante, M., and Scifoni, E. (2019b). *A new facility for proton radiobiology at the Trento proton therapy centre: Design and implementation*. Physica Medica **58**, pp. 99–106.
- Tommasino, F., Rovituro, M., Lorentini, S., La Tessa, C., Petringa, G., Cirrone, P., Romano, F., Scifoni, E., Schwarz, M., and Durante, M. (2019c). *STUDY FOR A PASSIVE SCATTERING LINE DEDICATED TO RADIOBIOLOGY EXPERIMENTS AT THE TRENTO PROTON THERAPY CENTER*. Radiation Protection Dosimetry **183**, pp. 274–279.

## 3DSIAM

- Menichelli, M. et al. (2020). *Hydrogenated amorphous silicon detectors for particle detection, beam flux monitoring and dosimetry in high-dose radiation environment*.

## ARCADIA

- Pancheri, L., Olave, J., Panati, S., Rivetti, A., Cossio, F., Rolo, M., Demaria, N., Giubilato, P., Pantano, D., and Mattiazzo, S. (2019). *A 110 nm CMOS process for fully-depleted pixel sensors*. Journal of Instrumentation **14**. Art. no.: C06016.

**ARDESIA**

- Hafizh, I., Bellotti, G., Carminati, M., Utica, G., Gugiatti, M., Balerna, A., Tullio, V., Borghi, G., Picciotto, A., Ficorella, F., Zorzi, N., Capsoni, A., Coelli, S., Bombelli, L., and Fiorini, C. (2019a). *ARDESIA: a Fast SDD X-ray Spectrometer for Synchrotron Applications*. *X-Ray Spectrometry* **48**(5), pp. 382–386.
- Hafizh, I., Bellotti, G., Carminati, M., Utica, G., Gugiatti, M., Balerna, A., Tullio, V., Lepore, G., Borghi, G., Ficorella, F., Picciotto, A., Zorzi, N., Capsoni, A., Coelli, S., Bombelli, L., and Fiorini, C. (2019c). *Characterization of ARDESIA: a 4-channel SDD X-ray spectrometer for synchrotron measurements at high count rates*. *Journal of Instrumentation* **14**(6). Art. no.: P06027.
- Utica, G., Fabbrica, E., Gugiatti, M., Hafizh, I., Carminati, M., Balerna, A., Borghi, G., Ficorella, F., Zorzi, N., Capsoni, A., Coelli, S., and Fiorini, C. (To be published). “Towards Efficiency and Count-Rate Enhancement of X-ray ARDESIA Spectrometer”. *Conference Record of the 2019 IEEE Nuclear Science Symposium and Medical Imaging Conference*. IEEE.

**ASAP**

- Musacci, M., Bigongiari, G., Brogi, P., Checchia, C., Collazuol, G., Dalla Betta, G.-F., Ficorella, A., Marrocchesi, P., Mattiazzo, S., Morsani, F., Noli, S., Pancheri, L., Ratti, L., Savoy Navarro, A., Silvestrin, L., Stolzi, F., Suh, J., Sulaj, A., Vacchi, C., and Zarghami, M. (2019). *Radiation tolerance characterization of Geiger-mode CMOS avalanche diodes for a dual-layer particle detector*. *Nuclear Instruments and Methods in Physics Research, Section A* **936**, pp. 695–696.
- Ratti, L., Brogi, P., Collazuol, G., Dalla Betta, G.-F., Ficorella, A., Lodola, L., Marrocchesi, P., Mattiazzo, S., Morsani, F., Musacci, M., Pancheri, L., and Vacchi, C. (2019a). *Dark Count Rate Degradation in CMOS SPADs Exposed to X-Rays and Neutrons*. *IEEE Transactions on Nuclear Science* **66**(2).
- Ratti, L., Brogi, P., Collazuol, G., Dalla Betta, G.-F., Ficorella, A., Marrocchesi, P., Pancheri, L., and Vacchi, C. (2019b). *Dark Count Rate Distribution in Neutron-Irradiated CMOS SPADs*. *IEEE Transactions on Electron Devices* **66**(12), pp. 5230–5237.

**DRAGoN**

- Facinelli, D., Larcher, M., Brunelli, D., and Fontanelli, D. (2019). “Cooperative UAVs Gas Monitoring using Distributed Consensus”. *2019 IEEE 43rd Annual Computer Software and Applications Conference (COMPSAC)*. Vol. 1, pp. 463–468.
- Tosato, P., Facinelli, D., Prada, M., Gemma, L., Rossi, M., and Brunelli, D. (2019). “An Autonomous Swarm of Drones for Industrial Gas Sensing Applications”. *2019 IEEE 20th International Symposium on "A World of Wireless, Mobile and Multimedia Networks" (WoWMoM)*, pp. 1–6.

**FIRE**

- Carturan, S., Vesco, M., Bonesso, I., Quaranta, A., Maggioni, G., Stevanato, L., Zanazzi, E., Marchi, T., Fabris, D., Cinausero, M., Pino, F., and Gramegna, F. (2019). *Flexible scintillation sensors for the detection of thermal neutrons based on siloxane 6LiF containing composites: Role of 6LiF crystals size and dispersion*. *Nuclear Instruments and Methods A* **925**, pp. 109–115.
- Marchi, T., Pino, F., Fontana, C. L., Quaranta, A., Zanazzi, E., Vesco, M., Cinausero, M., Daldosso, N., Paterlini, V., Gramegna, F., Moretto, S., Collazuol, G., Degerlier, M., Fabris, D., and Carturan, S. M. (2019). *Optical properties and pulse shape discrimination in siloxane-based scintillation detectors*. *Scientific Reports* **9**. Art. no.: 9154.

- Zanazzi, E., Favaro, M., Ficorella, A., Pancheri, L., Betta, G. D., and Quaranta, A. (2019). *Photoluminescence enhancement of colloidal CdSe/ZnS quantum dots embedded in polyvinyl alcohol after 2 MeV proton irradiation: crucial role of the embedding medium*. *Optical Materials* **88**, pp. 271–276.
- Zanazzi, E., Favaro, M., Ficorella, A., Pancheri, L., Betta, G. D., and Quaranta, A. (2020). *Real-Time Optical Response of Polysiloxane/Quantum Dot Nanocomposites under 2 MeV Proton Irradiation: Luminescence Enhancement of Polysiloxane Emission through Quantum Dot Sensitization*. *Physica Status solidi a* **217**. Art. no.: 1900586.

## GLARE-X

- Battocchio, P et al. (2020). *Ballistic measurements of laser ablation generated impulse*. *Measurement Science and Technology*. submitted.
- Panarella, D. (2018/2019). “Laser Ablation Propulsion: synthesis of target materials and thrust measurement”. Supervisor: Prof. Antonio Miotello. Master’s Degree in Physics.

## KIDS\_RD

- Faverzani, M., Ferri, E., Giachero, A., Giordano, C., Margesin, B., Mezzena, R., Nucciotti, A., and Puiu, A. (2020). *Characterization of the low temperature behavior of thin Titanium/Titanium Nitride multilayer films*. *Supercond. Sci. Technol* **33**. Art. no.: 045009.
- Mezzena, R., Faverzani, M., Ferri, E., Giachero, A., Margesin, B., Nucciotti, A., Puiu, A., and Vinante, A. (2019). *Development of Microwave Kinetic Inductance Detectors for IR Single-Photon Counting*. *J. Low Temp. Phys.* DOI: 10.1007/s10909-019-02251-1.

## MoVe IT

- Catalano, R., Petringa, G., Cuttone, G., Bonanno, V., Chiappara, D., Musumeci, M., Puglia, S., Stella, G., Scifoni, E., Tommasino, F., and Cirrone, P (2020). *Transversal dose profile reconstruction for clinical proton beams: A detectors inter-comparison*. *Physica Medica* **70**, pp. 133–138.
- Garbacz, M., Battistoni, G., Durante, M., Gajewski, J., Krah, N., Patera, V., Rinaldi, I., Schiavi, A., Scifoni, E., Skrzypek, A., et al. (2019). “Proton therapy treatment plan verification in CCB Krakow using fred Monte Carlo TPS tool”. *World Congress on Medical Physics and Biomedical Engineering 2018*. Springer, pp. 783–787.
- Hespeels, F., Heuskin, A.-C., Tabarrant, T., Scifoni, E., Kraemer, M., Chêne, G., Strivay, D., and Lucas, S. (2019a). *Backscattered electron emission after proton impact on gold nanoparticles with and without polymer shell coating*. *Physics in Medicine & Biology* **64**(12). Art. no.: 125007.
- Hespeels, F., Lucas, S., Tabarrant, T., Scifoni, E., Kraemer, M., Chêne, G., Strivay, D., Tran, H. N., and Heuskin, A.-C. (2019b). *Experimental measurements validate the use of the binary encounter approximation model to accurately compute proton induced dose and radiolysis enhancement from gold nanoparticles*. *Physics in Medicine & Biology* **64**(6). Art. no.: 065014.
- Palma, G., Monti, S., Xu, T., Scifoni, E., Yang, P., Hahn, S., Durante, M., Mohan, R., Liao, Z., and Cella, L. (2019a). *OC-0613 Spatial dose patterns of radiation pneumonitis in lung cancer patients treated by photons or protons*. *Radiotherapy and Oncology* **133**, S324–S325.
- Palma, G., Monti, S., Xu, T., Scifoni, E., Yang, P., Hahn, S., Durante, M., Mohan, R., Liao, Z., and Cella, L. (2019b). *The Low-Dose Bath Paradox: Do Spatial Irradiation Patterns Play a Role in the Incidence of Radiation Pneumonitis Following PSPT or IMRT?* *International Journal of Radiation Oncology \* Biology \* Physics* **105**(1), S6–S7.

- Palma, G., Monti, S., Xu, T., Scifoni, E., Yang, P., Hahn, S. M., Durante, M., Mohan, R., Liao, Z., and Cella, L. (2019c). *Spatial dose patterns associated with radiation pneumonitis in a randomized trial comparing intensity-modulated photon therapy with passive scattering proton therapy for locally advanced non-small cell lung cancer*. *International Journal of Radiation Oncology\* Biology\* Physics* **104**(5), pp. 1124–1132.
- Palma, G., Taffelli, A., Fellin, F., D'Avino, V., Scartoni, D., Tommasino, F., Scifoni, E., Durante, M., Amichetti, M., Schwarz, M., and Cella, L. (2020). *Modelling the risk of radiation induced alopecia in brain tumor patients treated with scanned proton beams*. *Radiotherapy and Oncology* **144**, pp. 127–134.
- Palma, G., Taffelli, A., Fellin, F., D'Avino, V., Scartoni, D., Tommasino, F., Scifoni, E., Durante, M., Amichetti, M., Schwarz, M., et al. (2019d). *NTCP Models for Permanent Radiation Induced Alopecia in Brain Tumor Patients Treated with Scanned Proton Beams*. *International Journal of Radiation Oncology \* Biology \* Physics* **105**(1), S168.
- Sokol, O., Kraemer, M., Hild, S., Durante, M., and Scifoni, E. (2019). *Kill painting of hypoxic tumors with multiple ion beams*. *Physics in medicine and biology* **64**. Art. no.: 045008.
- Tommasino, F., Rovituso, M., Lorentini, S., La Tessa, C., Petringa, G., Cirrone, P., Romano, F., Scifoni, E., Schwarz, M., and Durante, M. (2019d). *Study for a passive scattering line dedicated to radiobiology experiments at the Trento proton therapy center*. *Radiation protection dosimetry* **183**(1-2), pp. 274–279.
- Tommasino, F., Rovituso, M., Bortoli, E., La Tessa, C., Petringa, G., Lorentini, S., Verroi, E., Simonov, Y., Weber, U., Cirrone, P., Schwarz, M., Durante, M., and Scifoni, E. (2019e). *A new facility for proton radiobiology at the Trento proton therapy centre: Design and implementation*. *Physica Medica* **58**, pp. 99–106.
- Tommasino, F., Widesott, L., Fracchiolla, F., Lorentini, S., Righetto, R., Algranati, C., Scifoni, E., Dionisi, F., Scartoni, D., Amelio, D., et al. (2019g). *EP-1837 A new hybrid approach to allow robust Monte Carlo-based multi-field optimization in proton therapy*. *Radiotherapy and Oncology* **133**, S996–S997.
- Williart, A., Munoz, A., Boscolo, D., Scifoni, E., Krämer, M., and Garcia, G. (2019). *Study on Tl-204 simultaneous electron and photon emission spectra and their interaction with gold absorbers. Experimental results and Monte Carlo simulations*. *Nuclear Instruments and Methods in Physics Research Section A: Accelerators, Spectrometers, Detectors and Associated Equipment* **927**, pp. 435–442.

## Redsox2

- Cirrincone, D., Ahangarianabhari, M., Ambrosino, F., Bajnati, I., Bellutti, P., Bertuccio, G., Borghi, G., Bufon, J., Cautero, G., Ceraudo, F., Evangelista, Y., Fabiani, S., Feroci, M., Ficorella, F., Gandola, M., Mele, F., Orzan, G., Picciotto, A., Sammartini, M., Rachevski, A., Rashevskaya, I., Schillani, S., Zampa, G., Zampa, N., Zorzi, N., and Vacchi, A. (2019). *High precision mapping of single-pixel Silicon Drift Detector for applications in astrophysics and advanced light source*. *Nuclear Instruments and Methods in Physics Research Section A: Accelerators, Spectrometers, Detectors and Associated Equipment* **936**. *Frontier Detectors for Frontier Physics: 14th Pisa Meeting on Advanced Detectors*, pp. 239–241.
- Halder, S. et al., Belle II SVD Group (2019). *Spatial Resolution of the Belle II Silicon Vertex Detector*. *PoS VERTEX2018*, p. 054.
- Kodyš, P. et al., Belle-II DEPFET, PXD, SVD (2019). *The Belle II vertex detector integration*. *Nucl. Instrum. Meth. A* **936**, pp. 616–620.
- Kourousias, G., Billè, F., Cautero, G., Bufon, J., Rachevski, A., Schillani, S., Cirrincone, D., Altissimo, M., Menk, R., Zampa, G., Zampa, N., Rashevskaya, I., Borghes, R., Gandola, M., Picciotto, A.,

- Borghi, G., Ficorella, F., Zorzi, N., Bellutti, P., Bertuccio, G., Vacchi, A., and Gianoncelli, A. (2019). *XRF topography information: Simulations and data from a novel silicon drift detector system*. Nuclear Instruments and Methods in Physics Research Section A: Accelerators, Spectrometers, Detectors and Associated Equipment **936**. Frontier Detectors for Frontier Physics: 14th Pisa Meeting on Advanced Detectors, pp. 80–81.
- Lalwani, K. et al. (2019a). *Performance of the Belle II SVD*. Springer Proc. Phys. **234**, pp. 87–92.
- Belle II SVD Group (2019b). *Performance Studies of the Belle II Silicon Vertex Detector*. PoS **VERTEX2018**, p. 052.
- Picozza, P., Battiston, R., Ambrosi, G., Bartocci, S., Basara, L., Burger, W. J., Campana, D., Carfora, L., Casolino, M., Castellini, G., Cipollone, P., Conti, L., Contin, A., Donato, C. D., Santis, C. D., Follega, F. M., Guandalini, C., Ionica, M., Iuppa, R., Laurenti, G., Lazzizzera, I., Lolli, M., Manea, C., Marcelli, L., Martucci, M., Masciantonio, G., Mergé, M., Osteria, G., Pacini, L., Palma, F., Palmonari, F., Panico, B., Parmentier, A., Patrizii, L., Perfetto, F., Piersanti, M., Pozzato, M., Puel, M., Rashevskaya, I., Ricci, E., Ricci, M., Ricciarini, S., Scotti, V., Sotgiu, A., Sparvoli, R., Spataro, B., Vitale, V., Zuccon, P., and Zoffoli, S. (2019b). *Scientific Goals and In-orbit Performance of the High-energy Particle Detector on Board the CSES*. The Astrophysical Journal Supplement Series **243**(1), p. 16.
- Rachevski, A., Ahangarianabhari, M., Aquilanti, G., Bellutti, P., Bertuccio, G., Borghi, G., Bufon, J., Cautero, G., Ciano, S., Cicuttin, A., Cirrincione, D., Crespo, M., Fabiani, S., Ficorella, F., Gandola, M., Giuressi, D., Mannatunga, K., Mele, F., Menk, R., Olivi, L., Orzan, G., Picciotto, A., Rashevskaya, I., Sammartini, M., Schillani, S., Zampa, G., Zampa, N., Zorzi, N., and Vacchi, A. (2019b). *The XAFS fluorescence detector system based on 64 silicon drift detectors for the SESAME synchrotron light source*. Nuclear Instruments and Methods in Physics Research Section A: Accelerators, Spectrometers, Detectors and Associated Equipment **936**. Frontier Detectors for Frontier Physics: 14th Pisa Meeting on Advanced Detectors, pp. 719–721.
- Resmi, P. et al., Belle II SVD (2019). *Construction and quality assurance of the Belle II Silicon Vertex Detector*. PoS **VERTEX2018**, p. 051.
- Ricci, E., Di Ruzza, B., Iuppa, R., Serra, E., Manea, C., and Rashevskaya, I. (2019). *ALPIDE for space applications: Power consumption*. Nuovo Cim. C **42**(4), p. 209.
- Thalmeier, R. et al., Belle-II SVD (2019a). *The Belle II silicon vertex detector: Assembly and initial results*. Nucl. Instrum. Meth. A **936**, pp. 712–714.
- Thalmeier, R. et al., Belle II SVD (2019b). *Machine learning: hit time finding with a neural network*. PoS **TWEPP2018**, p. 065.
- Zhang, S., Santangelo, A., Feroci, M., Xu, Y., Lu, F., Chen, Y., Feng, H., Zhang, S., Brandt, S., Hernandez, M., et al. (2018b). *The enhanced X-ray Timing and Polarimetry mission eXTP*. Science China Physics, Mechanics Astronomy **62**(2).

## SICILIA

- Ciampi, C., Pasquali, G., Altana, C., Bini, M., Boscardin, M., Calcagno, L., Casini, G., Cirrone, G., Fazzi, A., Giove, D., Gorini, G., Labate, L., Via, F. L., Lanzalone, G., Litrico, G., Muoio, A., Ottanelli, P., Poggi, G., Puglia, S., Rebai, M., Ronchin, S., Santangelo, A., Stefanini, A., Trifirù, A., Tudisco, S., and Zimbone, M. (2019). *Nuclear fragment identification with  $\Delta E$ -E telescopes exploiting silicon carbide detectors*. Nuclear Instruments and Methods in Physics Research Section A: Accelerators, Spectrometers, Detectors and Associated Equipment **925**, pp. 60–69.
- Rebai, M., Rigamonti, D., Cancelli, S., Croci, G., Gorini, G., Cippo, E. P., Putignano, O., Tardocchi, M., Altana, C., Angelone, M., Borghi, G., Boscardin, M., Ciampi, C., Cirrone, G., Fazzi, A., Giove, D., Labate, L., Lanzalone, G., Via, F. L., Loreti, S., Muoio, A., Ottanelli, P., Pasquali, G., Pillon, M., Puglia, S., Santangelo, A., Trifiro, A., and Tudisco, S. (2019). *New thick silicon carbide detectors:*

*Response to 14 MeV neutrons and comparison with single-crystal diamonds.* Nuclear Instruments and Methods in Physics Research Section A: Accelerators, Spectrometers, Detectors and Associated Equipment **946**. Art. no.: 162637.

Tudisco, S. et al. (2019). *Silicon carbide for future intense luminosity nuclear physics investigations.* Nuovo Cim. **C42**(2-3-3), p. 74.

Tudisco, S., La Via, F., Agodi, C., Altana, C., Borghi, G., Boscardin, M., Bussolino, G., Calcagno, L., Camarda, M., Cappuzzello, F., Carbone, D., Cascino, S., Casini, G., Cavallaro, M., Ciampi, C., Cirrone, G., Cuttone, G., Fazzi, A., Giove, D., Gorini, G., Labate, L., Lanzalone, G., Litrico, G., Longo, G., Lo Presti, D., Mauceri, M., Modica, R., Moschetti, M., Muoio, A., Musumeci, F., Pasquali, G., Petringa, G., Piluso, N., Poggi, G., Privitera, S., Puglia, S., Puglisi, V., Rebai, M., Ronchin, S., Santangelo, A., Stefanini, A., Trifirù, A., and Zimbone, M. (2018). *SiCILIA - Silicon Carbide Detectors for Intense Luminosity Investigations and Applications.* Sensors **18**(7). Art. no.: 2289.

## SIMP

Faverzani, M., Cruciani, A., D'Addabbo, A., Day, P.K., Di Domizio, S., Ferri, E., Fresch, P., Giachero, A., Margesin, B., Mezzena, R., Minutolo, L., Nucciotti, A., Puiu, A., and Vignati, M. (2019). *Thermal kinetic inductance detectors for soft X-ray spectroscopy.* NUCLEAR INSTRUMENTS & METHODS IN PHYSICS RESEARCH SECTION A-ACCELERATORS SPECTROMETERS DETECTORS AND ASSOCIATED EQUIPMENT **936**, 197–198.

Mezzena, R., Faverzani, M., Ferri, E., Giachero, A., Margesin, B., Nucciotti, A., Puiu, A., and Vinante, A. *Development of Microwave Kinetic Inductance Detectors for IR Single-Photon Counting.* JOURNAL OF LOW TEMPERATURE PHYSICS.

## THEEOM-RD

Haghighi, I. M., Malossi, N., Natali, R., Di Giuseppe, G., and Vitali, D. (2018). *Sensitivity-Bandwidth Limit in a Multimode Optoelectromechanical Transducer.* Phys. Rev. Appl. **9**. Art. no.: 034031.

Malossi, N., Haghighi, I. M., Natali, R., Di Giuseppe, G., and Vitali, D. (2019). “Multimode Opto-Electro-Mechanical Transducer for Non-Reciprocal Conversion of Radio-Frequency and Optical Signals”. *2019 Conference on Lasers and Electro-Optics Europe & European Quantum Electronics Conference (CLEO Europe-EQEC).* IEEE, pp. 1–1.

## TIMESPOT

Forcolin, G., Mendicino, R., Boscardin, M., Lai, A., Loi, A., Ronchin, S., Vecchi, S., and Dalla Betta, G.-F. (2019b). *Development of 3D trenched-electrode pixel sensors with improved timing performance.* Journal Instrum. **14**. Art. no.: C07011.

Loi, A., Dalla Betta, G.-F., Lai, A., Mendicino, R., and Vecchi, S. (2019a). “Design and simulation of 3D-silicon sensors for future vertex detectors”. *2018 IEEE NSS-MIC Conference Record.* Piscataway, NJ, USA: IEEE, p. 1.

Loi, A., Lai, A., Dalla Betta, G.-F., Mendicino, and Vecchi, S. (2019b). *Simulation of 3D-Silicon sensors for the TIMESPOT project.* Nuclear Instrum. Methods A **936**, pp. 701–702.

Mendicino, R., Boscardin, M., Ficorella, F., Forcolin, G., Lai, A., Loi, A., Ronchin, S., Vecchi, S., and Dalla Betta, G.-F. (2019b). *3D Trenched-Electrode Sensors for Charged Particle Tracking and Timing.* Nuclear Instrum. Methods A **927**, pp. 24–30.



# Seminars

## TIFPA Guest Seminars

- Ihor Tymchuk, Bogolyubov Institute for Theoretical Physics, Kiev, Ukraine, *Energy Physics tracking detector modules based on aluminium-polyimide adhesiveless dielectrics and SpTAB process*, Feb. 5, 2019.
- Maksym Protsenko, Bogolyubov Institute for Theoretical Physics, Kiev, Ukraine, *SpTAB process for Space and Terrestrial photovoltaics*, Feb. 5, 2019.
- Cisterna Adolfo Roa, Universidad Austral de Chile y Universidad de Concepción, Valdivia, Chile, *Homogenous anti-de Sitter black strings in GR and Lovelock gravities*, Feb. 20, 2019.
- Federico Urban, CEICO Central European Institute for Cosmology and Fundamental Physics, Czech Republic, *Testing fuzzy Dark Matter and fifth forces with binary pulsars*, Apr. 3, 2019.
- Antonio Racioppi, NICPB National Institute of Chemical Physics and Biophysics, Tallinn, Estonia, *The Palatini side of inflationary attractor*, May 7, 2019.
- Fabrizio Ferrari Ruffino, University of Udine, Italy, *Hyperspherical Harmonics with particle excitations degrees of freedom*, July 16, 2019.
- Francesco Guatieri, TUM Technische Universität München, Munich, Germany, *Upgrading of the control system and the data acquisition system of the positron beam*, Sept. 19, 2019.
- Cecilia Giavoni, Arnold Sommerfeld Center for Theoretical Physics, LMU, Munich, Germany, *Dynamical Horizons and Hawking Effect*, Nov. 12, 2019.

## Particle Physics

### FASE2\_ATLAS

- Gian-Franco Dalla Betta, *Feasibility Study of Charge Multiplication by Design in Thin Silicon 3D Sensors*, At: 2019 IEEE Nuclear Science Symposium and Medical Imaging Conference (NSS - MIC'19), Manchester, UK, Oct. 2019.
- Roberto Mendicino, *Characterisation of FBK small-pitch 3D sensors after irradiation up to  $3.5 \times 10^{16} n_{eq} cm^{-2}$* , At: 2019 IEEE Nuclear Science Symposium and Medical Imaging Conference (NSS - MIC'19), Manchester, UK, Oct. 2019.

## Astroparticle Physics

- Francesco Nozzoli, *Investigazione dei processi di decadimento  $2\beta$  in  $^{146}\text{Nd}$ ,  $^{144}\text{Sm}$  e negli altri isotopi finora inesplorati*, At: 105° Congresso Nazionale Società Italiana di Fisica, Gran Sasso Science Institute, L'Aquila, Italy, Sept. 2019.
- Francesco Nozzoli, invited talk: *Detection of high-energy particles from the Universe: basic concepts, methods, and challenges*, At: PHYSICS and ASTROPHYSICS of COSMIC RAYS, Vith CNRS thematic School of Astroparticle Physics, OHP Saint Michel l'Observatoire, France, Nov. 2019.

### ADHD

- Francesco Dimiccoli, *Prospettive per la ricerca di Anti-Deuterio nei raggi cosmici con ADHD*, At: IFAE 2019 - Incontri di Fisica delle Alte Energie, Università Federico II, Napoli, Italy, Apr. 2019.

Francesco Dimiccoli, *Detectors for antideuteron search in cosmic rays: current status and new ideas*, At: 15th Topical Seminar on Innovative Particle and Radiation Detectors (IPRD19), Università di Siena, Siena, Italy, Oct. 2019.

Francesco Nozzoli, *Status of the Anti Deuteron Helium Detector (ADHD) project*, At: Antideuteron 2019, University of California, Los Angeles, USA, Mar. 2019.

Francesco Nozzoli, *Perspectives of dark matter indirect search with ADHD in space*, At: 10th Young Researcher Meeting, Università degli Studi di Roma Tor Vergata, Roma, Italy, June 2019.

Francesco Nozzoli, *Perspectives for Anti-Deuteron identification in cosmic rays with an Helium-based detector*, At: Light Anti-Nuclei as a Probe for New Physics (LAN2019), Lorentz Center, Leiden, The Netherlands, Oct. 2019.

## AMS

Francesco Dimiccoli, *Misure del flusso di deuterio nei raggi cosmici con l'esperimento AMS-02*, At: IFAE 2019 - Incontri di Fisica delle Alte Energie, Università Federico II, Napoli, Italy, Apr. 2019.

Francesco Dimiccoli, *Measurement of Cosmic Deuteron Flux with the AMS-02 Detector*, At: 10th Young Researcher Meeting, Università degli Studi di Roma Tor Vergata, Roma, Italy, June 2019.

Francesco Dimiccoli, *Cosmic Ray isotopes measured by AMS02*, At: 2019 Meeting of the Division of Particles & Fields of the American Physical Society (DPF2019), NorthEastern University, Boston, USA, July 2019.

Francesco Dimiccoli, *Misure del flusso di Deuterio nei raggi cosmici con l'esperimento AMS-02*, At: 105° Congresso Nazionale Società Italiana di Fisica, Gran Sasso Science Institute, L'Aquila, Italy, Sept. 2019.

Paolo Zuccon, invited talk: *Measuring cross sections for anti-p and anti-d production with COMPASS++/AMBER*, At: Antideuteron 2019, University of California, Los Angeles, USA, Mar. 2019.

Paolo Zuccon, invited talk: *Antiproton Flux in Primary Cosmic Rays Measured with the Alpha Magnetic Spectrometer on the ISS*, At: Antideuteron 2019, University of California, Los Angeles, USA, Mar. 2019.

Paolo Zuccon, invited talk: *Status and perspective of the AMS-02 Experiment*, At: 19th Lomonosov Conference on High Energy Particles, Moscow State University, Moscow, Russia, Aug. 2019.

Paolo Zuccon, invited talk: *The COMPASS++/AMBER program for cross-sections measurements*, At: Light Anti-Nuclei as a Probe for New Physics (LAN2019), Lorentz Center, Leiden, The Netherlands, Oct. 2019.

Paolo Zuccon, invited talk: *The COMPASS++/AMBER program for p-bar production cross-sections measurements*, At: XSCRC2019: Cross sections for Cosmic Rays at CERN, CERN, Meyrin, Switzerland, Nov. 2019.

## DarkSide

Alberto Mazzi, *Cryogenic SiPM technology for a direct dark matter detection experiment (DarkSide 20k)*, At: IEEE NSS-MIC 2019, Manchester, UK, Oct. 2019.

## FISH

Gabriele Ferrari, invited talk: *Towards topological excitations in Rabi-coupled spinor BECs*, At: international workshop "Vortex Dynamics, Turbulence and Related Phenomena In Quantum Fluids", International Institute of Physics, Natal, Brazil, July 2019.

Gabriele Ferrari, invited talk: *Towards the production of vortices in coherently coupled condensates*, At: International workshop on Quantum Mixtures, Trento, Italy, July 2019.

Gabriele Ferrari, invited talk: *Towards the production of vortices in coherently-coupled spin binary BECs*, At: Bose-Einstein Condensation 2019 International Conference, Sant Feliu de Guixols, Spain, Sept. 2019.

Giacomo Lamporesi, invited talk: *Magnetic solitons in two-component superfluid mixtures*, ICFO, Barcelona, Spain, Nov. 2019.

### LISA Pathfinder

Bortoluzzi Daniele, *Analysis of the in-flight injection of the LISA Pathfinder test masses*, At: ESMATS2019, Munich, Germany, 2019.

Castelli Eleonora, *LISA Pathfinder nal noise performance: Effect of disturbances on the low frequency*, At: 22nd International Conference on General Relativity, Valencia, Spain, 2019.

Dal Bosco Davide, poster: *On-ground Torsion Pendulum Testing for LISA: Force Noise Performance*, At: 22nd International Conference on General Relativity, Valencia, Spain, 2019.

Dolesi Rita, invited talk: *LISA PathFinder results*, At: Rencontres de Moriond-Gravitation, La Thuille, Italy, 2019.

Ferroni Valerio, invited talk: *LASER Interferometer Space Antenna*, At: IEEE NSS-MIC 2019, Manchester, UK, 2019.

Muratore Martina, poster: *Accuracy on Time Delay Interferometry computation*, At: 22nd International Conference on General Relativity, Valencia, Spain, 2019.

Russano Giuliana, *LISA Charge Management System, discussion and on-ground testing results*, At: 22nd International Conference on General Relativity, Valencia, Spain, 2019.

Vetruugno Daniele, invited talk: *From LISA Pathfinder to LISA a gravitational waves space-based observatory*, At: Gravitation Waves Advanced Detector Workshop, Elba, Italy, 2019.

Vitale Stefano, plenary: *LISA Pathfinder*, At: 649th XianShang Conference, Beijing, China, 2019.

Vitale Stefano, plenary: *Space Borne Gravitational Wave Observatories*, At: Gravitational Wave Science and Technology, Padua, Italy, 2019.

Weber William, plenary: *From LISA Pathfinder to LISA: preparing for gravitational wave observation*, At: 22nd International Conference on General Relativity, Valencia, Spain, 2019.

### QUAX

Caterina Braggio, invited talk: *Probing the axion-electron coupling in cm-scale atomic targets*, At: HighRR Workshop “Vistas on Detector Physics”, Physikalisches Institut, Heidelberg, Germany, Sept. 2019.

Nicolò Crescini, invited talk: *QUAX: a ferromagnetic axion haloscope*, At: 13th LCN Workshop, Nizhny Novgorod State Technical University, Nizni Novgorod, Russia, Jan. 2019.

Nicolò Crescini, invited talk: *Towards the development of the ferromagnetic haloscope: status report of QUAX*, At: 15th Patras workshop on axions, wimps and wisps, Insitute of Physics of the Albert-Ludwigs University Freiburg, Freiburg, Germany, June 2019.

Nicolò Crescini, invited talk: *Towards the development of the Ferromagnetic Axion Haloscope*, At: Axions detectors in Germany, Goettingen, Germany, Aug. 2019.

Raffaele Di Vora, *Preliminary results of the QUAX- $\alpha\gamma$  experiment and future perspectives*, At: 105° Congresso Nazionale SIF, Gran Sasso Science Institute, L'Aquila, Italy, Sept. 2019.

Claudio Gatti, invited talk: *Galactic axions search with a superconducting resonant cavity*, At: 15th Patras workshop on axions, wimps and wisps, Insitute of Physics of the Albert-Ludwigs University Freiburg, Freiburg, Germany, June 2019.

Alessio Rettaroli, *First QUAX galactic axion search with a SC resonant cavity*, At: IFAE - Incontri di Fisica delle Alte Energie, Sezione INFN di Napoli e Dipartimento di Fisica “Ettore Pancini” dell’Università di Napoli Federico II, Naples, Italy, Apr. 2019.

Alessio Rettaroli, *First QUAX galactic axion search with a superconducting cavity*, At: INVISIBLES '19 Workshop Neutrinos, Dark Matter and Dark Energy, University of Valencia, Valencia, Spain, June 2019.

## Nuclear Physics

### AEGIS

Ruggero Caravita, *Progressed towards measuring the gravitational interaction on antimatter in the AEGIS experiment*, At: Rencontres de Moriond: gravitation, La Thuile, Italy, Mar. 2019.

Ruggero Caravita, invited talk: *Experiments and Perspectives with Metastable  $2^3S$  Positronium Beams*, At: POSMOL, International Workshop on Low-Energy Positron and Positronium Physics, Belgrade, Serbia, July 2019.

Ruggero Caravita, invited talk: *Long-lived Positronium for pulsed antihydrogen production*, At: SLOPOS, International Workshop on Slow Positron Beam Techniques & Applications, Prague, Czech Republic, Sept. 2019.

Sebastiano Mariazzi, invited talk: *Techniques for production and detection of a  $2^3S$  positronium beam*, At: SLOPOS, International Workshop on Slow Positron Beam Techniques & Applications, Prague, Czech Republic, Sept. 2019.

Roberto S. Brusa, invited talk: *Positronium for fundamental studies*, At: 3rd Jagiellonian Symposium on Fundamental and Applied Subatomic Physics, Krakow, Poland, June 2019.

Roberto S. Brusa, invited talk: *Open volumes structure and molecular transport in polymer and biopolymer nanocomposites*, At: SLOPOS, International Workshop on Slow Positron Beam Techniques & Applications, Prague, Czech Republic, Sept. 2019.

### FOOT

Sofia Colombi, *The FOOT experiment: enhancing the understanding of fragmentation processes in hadrontherapy and space radiation protection*, At: NUSPRASEN Workshop on Nuclear Science Applications, Helsinki, Finland, Nov. 2019.

## Theoretical Physics

### BELL

Sonia Mazzucchi, invited talk: *Open problems in the mathematical definition of Feynman path integrals*. At: AMS Special Session on Mathematical Physics Some Open Problems for the 21st Century, Denver, USA, Jan. 2020.

Valter Moretti, invited talk: *Spectral measures of functions of non commuting observables*, At: Operator algebras in quantum field theory and quantum probability, Università Roma II, Rome, Italy, Dec. 2019.

Davide Pastorello, *Quantum Annealing Learning Search for solving QUBO problems*, At: Quantum Computing and High Performance Computing, CINECA, Bologna, Italy, Dec. 2019.

### BIOPHYS

Pietro Faccioli, invited talk: *Challenges in Large Scale Molecular Simulations 2019: Bridging Theory and Experiment*, At: CECAM Workshop on Challenges in Large Scale Molecular Simulations 2019: Bridging Theory and Experiment, Cargese Conference Centre, Cargese, France, May 2019.

- Pietro Faccioli, invited talk: *Connecting Atomistic Models to Time-Resolved Spectroscopy Data for Protein Folding*, At: CECAM Workshop on Challenges in Large Scale Molecular Simulations 2019: Bridging Theory and Experiment, Cargese Conference Centre, Cargese, France, May 2019.
- Pietro Faccioli, *Challenges in Large Scale Molecular Simulations 2019: Bridging Theory and Experiment*, At: Workshop: Open Quantum Systems: From Atomic Nuclei to Ultracold Atoms and Quantum Optics, ECT\*, Villazzano (Trento), Italy, Oct. 2019.
- Pietro Faccioli, invited talk: *From Nuclear Theory to Drug Discovery*, At: ITA-USA Innovation Forum, Stanford University, Palo Alto, CA, USA, Nov. 2019.
- Gianluca Lattanzi, invited talk: *Challenges in Computational Biophysics: simulations meet experiments*, At: MD2meeting2019, University of Bologna, Bologna, Italy, Mar. 2019.
- Gianluca Lattanzi, invited talk: *Computational Biophysics in Trento: Challenges and Opportunities*, At: Current Advances and Challenges in Computational Modeling of Materials, Technical University of Eindhoven, Eindhoven, the Netherlands, May 2019.
- Gianluca Lattanzi, invited talk: *Computational Biophysics in Trento: Challenges and Opportunities*, At: CECAM Summer School on Classical Molecular Dynamics for Material Science, Nanotechnology and Biophysics, International School of Advanced Studies (SISSA), Trieste, Italy, June 2019.
- Raffaello Potestio, invited talk: *Systematic and non-uniform coarse-graining of biomolecules*, At: XV International Workshop on Complex Systems, Andalo, Italy, Mar. 2019.
- Raffaello Potestio, invited talk: *Uniform-resolution and multiple-resolution coarse-graining of soft matter*, At: First meeting of the EUREGIO project Joint Computational Physics Initiative, Free University of Bozen, Bozen, Italy, Apr. 2019.
- Raffaello Potestio, invited talk: *Searching the optimal folding routes of a complex lasso protein*, At: Integrative Approaches to Protein Folding & Aggregation, University of Lisbon, Lisbon, Portugal, June 2019.
- Raffaello Potestio, invited talk: *On the algorithmic identification of optimal coarse-grained representations of biomolecular structures*, At: X Brazilian Meeting on Simulational Physics, Ouro Preto, Brazil, July 2019.
- Raffaello Potestio, invited talk: *Variable resolution models for multi-scale simulations of complex biomolecules*, At: Photonic reservoir computing and information processing in complex networks, University of Trento, Trento, Italy, Dec. 2019.

## FBS

- Winfried Leidemann, invited talk: *Reactions with Lorentz Integral Transform (LIT) method*, At: Symposium on "Nuclear Structure and Reactions: The Next Significant Breakthroughs", GANIL, Caen, France, Mar. 2019.
- Winfried Leidemann, parallel: *On the determination of response functions obtained from their Lorentz integral transforms*, At: 24th European Conference on Few-Body Problems in Physics (EFB24), University of Surrey, Guildford, Great Britain, Sept. 2019.
- Giuseppina Orlandini, invited talk: *Recent developments in integral transform approaches*, At: ECT\* Workshop on Neutrini and nuclei, challenges and opportunities for nuclear theory, ECT\*, Trento, Italy, May 2019.
- Giuseppina Orlandini, invited talk: *From Sum Rules to Integral Transform*, At: TNPI 2019-XVII Conference in Theoretical Nuclear Physics in Italy, Cortona, Italy, Oct. 2019.

## MANYBODY

- Alessandro Lovato, invited talk: *Neutrino-nucleus interactions at low (and moderate) momentum transfer*, At: First Nuclear and Particle Theory Meeting, St. Louis, MO, United States, Mar. 2019.

- Alessandro Lovato, invited talk: *Spectral functions from quantum Monte Carlo*, At: Second Workshop on quantitative challenges in SRC and EMC Research, Boston, MA, United States, Mar. 2019.
- Alessandro Lovato, invited talk: *Ab-initio calculations of neutrino-nucleus interactions*, At: APS April Meeting 2019, Denver, CO, United States, Apr. 2019.
- Alessandro Lovato, invited talk: *Lepton-nucleus interactions from quantum Monte Carlo*, At: Nuclear and Particle Theory for Accelerator Neutrino Experiments, Fermilab, Batavia, IL, United States, May 2019.
- Alessandro Lovato, invited talk: *Overview of electron/neutrino scattering*, At: 2019 NUCLEI meeting, Santa Fe, NM, United States, May 2019.
- Alessandro Lovato, invited talk: *Current status and prospects of QMC calculations of lepton-nucleus interactions*, At: ECT\* Workshop Testing and Improving Models of Neutrino Nucleus Interactions in Generators, ECT\*, Trento, Italy, June 2019.
- Alessandro Lovato, invited talk: *Low- (and high-) energy  $^{12}\text{C}$  electroweak responses*, At: ELBA 2019 – Lepton Interaction with Nucleons and Nuclei, EIPC, Marciana Marina, Italy, June 2019.
- Alessandro Lovato, invited talk: *Lepton-nucleus interactions from quantum Monte Carlo*, At: XXth International Conference "Recent Progress in Many Body Theories", Toulouse, France, Sept. 2019.
- Alessandro Lovato, parallel: *Modelling neutrino-nucleus interactions*, At: NuMu2019 Workshop, Paul Scherrer Institut, Villigen, Switzerland, Oct. 2019.
- Francesco Pederiva, invited talk: *First steps towards simulating quantum dynamics of nucleons on a quantum chip*, At: Ab initio Nuclear Theory, from Breakthroughs to Applications, University of Surrey, Guildford, United Kingdom, July 2019.
- Francesco Pederiva, invited talk: *Quantum computing of nuclear dynamics*, At: Open Quantum Systems: From atomic nuclei to ultracold atoms and quantum optics, ECT\*, Trento, Italy, Oct. 2019.

## NEMESYS

- Simone Taioli, invited talk: *Relativistic Theory and Ab Initio Simulations of Electroweak Decay Spectra in Medium? Heavy Nuclei*, At: Precise beta decay calculations for searches for new physics, ECT\*, Italy, Apr. 2019.
- Simone Taioli, invited talk: *Enabling materials by dimensionality: from 0D to 3D carbon-based nanostructures*, At: 15th International Conference of Computational Methods in Sciences and Engineering (ICCMSE 2019), Rhodos, Greece, May 2019.
- Simone Taioli, invited talk: *Relativistic Approaches to beta-decays in stellar plasmas*, At: PANDORA: Measuring beta-decays in plasmas, Perugia, Italy, Oct. 2019.

## TEONGRAV

- Federico Cipolletta, *Spritz: a new fully general relativistic magnetohydrodynamic code*, At: APS April Meeting 2019, American Physical Society, Sheraton Denver Downtown Hotel, Denver, CO, United States, Apr. 2019.
- Federico Cipolletta, *Spritz: a new fully general relativistic magnetohydrodynamic code*, At: North American Einstein Toolkit workshop 2019, Rochester Institute of Technology, Rochester, NY, United States, June 2019.
- Federico Cipolletta, *Spritz: a new fully general relativistic magnetohydrodynamic code*, At: TCAN "Advancing Computational Methods to Understand the Dynamics of Ejection, Accretion, Winds and Jets in Neutron Star Mergers" Workshop, Rochester Institute of Technology, Rochester, NY, United States, June 2019.
- Bruno Giacomazzo, invited talk: *BNS mergers with modern microscopic nuclear EOS*, At: Workshop "GWEOS-2019", Pisa, Italy, Feb. 2019.

- Bruno Giacomazzo, *Effects of Chiral Effective Field Theory Equation of State on Binary Neutron Star Mergers*, At: PHAROS Conference 2019, Platja D'Aro - Girona, Spain, Apr. 2019.
- Bruno Giacomazzo, invited talk: *Binary Neutron Star Mergers with WhiskyMHD*, At: Workshop "North American Einstein Toolkit workshop 2019", Rochester Institute of Technology, Rochester, NY, USA, June 2019.
- Bruno Giacomazzo, invited talk: *Binary Neutron Star Mergers: Numerical Simulations and Observations*, At: Workshop "3rd FLAG Meeting: the Quantum and Gravity", Catania, Italy, June 2019.
- Bruno Giacomazzo, *TEONGRAV: HPC Simulations of Gravitational Wave Sources*, At: SM & FT 2019, University of Bari, Italy, Dec. 2019.

## Technological and Interdisciplinary Physics

- Chiara La Tessa, *Microdosimetry as a tool for radiation risk assessment*, At: 1st International Biophysics Collaboration Meeting, GSI Helmholtzzentrum für Schwerionenforschung GmbH, Darmstadt, Germany, May 2019.
- Chiara La Tessa, invited talk: *What do cancer radiotherapy and Mars exploration have in common?*, At: African Nuclear Physics Conference ANPC, iThemba Lab, Kruger National Park, South Africa, July 2019.

### 3DSIAM

- J. Davis, invited talk: *Modelling a thick hydrogenated amorphous silicon substrate for ionising radiation detectors*, At: IEEE-NSS-2019, Manchester, UK, 2019.
- Mauro Menichelli, invited talk: *The development of a 3D detector on a hydrogenated amorphous silicon substrate*, At: 14th Trento Workshop on Advance Silicon Radiation Detectors, Trento, Italy, Feb. 2019.
- Mauro Menichelli, *3D detectors on Hydrogenated Amorphous Silicon for particle tracking in High radiation environment*, At: DeSyT-2019, Messina, Italy, Sept. 2019.
- Mauro Menichelli, invited talk: *Hydrogenated amorphous silicon detectors for particle detection, beam flux monitoring and dosimetry in high-dose radiation environment*, At: IPRD19, Bologna, Italy, Oct. 2019.
- Mauro Menichelli, invited talk: *Development of a 3D detector on a hydrogenated amorphous silicon substrate*, At: CPAD Instrumentation Frontier Workshop, Madison, USA, Dec. 2019.

### ARCADIA

- Lucio Pancheri, invited talk: *CMOS Pixel Sensors on Thick Fully-depleted Silicon Substrates for NIR Imaging*, At: PhotonIcs & Electromagnetics Research Symposium (PIERS 2019), Rome, Italy, June 2019.

### ASAP

- Lucio Pancheri, invited talk: *Two-tier Geiger-mode avalanche pixel sensors for charged particle detection*, At: VIII International Course "Detectors and Electronics for High Energy Physics, Astrophysics, Space and Medical Physics", INFN, Legnaro (PD), Italy, Apr. 2019.
- Lucio Pancheri, *A 48×48 pixel two-tier avalanche sensor for charged particle detection*, At: 2019 IEEE NSS-MIC, Manchester, UK, Oct. 2019.

## MoVe IT

Emanuele Scifoni, invited talk: *Research and Development for Hadrontherapy in Italy*, At: VIII International Course “Detectors and Electronics for High Energy Physics, Astrophysics, Space and Medical Applications”, LNL, Legnaro, Italy, Apr. 2019.

Emanuele Scifoni, *MoVe IT Modeling and verification for ion beam treatment planning. New insights from Fair Beams?*, At: 1st International Biophysics Collaboration Meeting, GSI, Darmstadt, Germany, May 2019.

Emanuele Scifoni, invited talk: *The MoVe-IT project*, At: SIF 2019, GSSI, l’Aquila, Italy, Sept. 2019.

Emanuele Scifoni, invited talk: *Particle track radiolysis with TRAX-CHEM: impact of oxygenation and nanoparticle enhancement*, At: RRS 2019, Radiation Research Society, San Diego, USA, Nov. 2019.

## SIMP

Paolo Falferi, *Status of the SIMP project: Towards the Single Microwave Photon Detection*, At: 18th International Workshop on Low Temperature Detectors, University of Milano-Bicocca and Istituto Nazionale di Fisica Nucleare, Milan, Italy, July 2019.

Eugenio Monticone, *Status of the SIMP project: Towards the Single Microwave Photon Detection*, At: Single-Photon Workshop 2019, Politecnico di Milano, Milan, Italy, Oct. 2019.

Sergio Pagano, *Josephson junction based single photon microwave detector for axion detection*, At: 14th European Conference on Applied Superconductivity, UK Superconductivity community, Glasgow, UK, Sept. 2019.

## TIMESPOT

Giulio Tiziano Forcolin, *Development of 3D Trenched-Electrode Pixel Sensors with Improved Timing performance*, At: 2019 IEEE Nuclear Science Symposium and Medical Imaging Conference (NSS - MIC’19), Manchester, UK, Oct. 2019.

Giulio Tiziano Forcolin, *3D Trenched-Electrode Pixel Sensors: design, technology and initial results*, At: HSTD12 - 12th International “Hiroshima” Symposium on the Development and Application of Semiconductor Tracking Detectors, Hiroshima, Japan, Dec. 2019.

Roberto Mendicino, *Characterization of SINTEF 3D diodes with trenched-electrode geometry before and after neutron irradiation*, At: 21st International Workshop on Radiation Imaging Detectors (IWORID2019), Crete, Greece, July 2019.





Trento Institute for  
Fundamental Physics  
and Applications

**TIFPA - INFN**

c/o Dipartimento di Fisica  
Università di Trento  
Via Sommarive, 14  
38123 Povo (Trento), Italy  
tel.: +39 0461 281500  
fax: +39 0461 282000  
email: [info@tifpa.infn.it](mailto:info@tifpa.infn.it)  
[www.tifpa.infn.it](http://www.tifpa.infn.it)